frontiers | Research Topics

Research advances of modification and nutrition properties of food carbohydrates, volume I

Edited by
Yanjun Zhang, Jianhua Xie, Bin Li and Srinivas Janaswamy

Published in
Frontiers in Nutrition

ISSN 1664-8714
ISBN 978-2-8325-3206-5
DOI 10.3389/978-2-8325-3206-5

About Frontiers

Frontiers is more than just an open access publisher of scholarly articles: it is a pioneering approach to the world of academia, radically improving the way scholarly research is managed. The grand vision of Frontiers is a world where all people have an equal opportunity to seek, share and generate knowledge. Frontiers provides immediate and permanent online open access to all its publications, but this alone is not enough to realize our grand goals.

Frontiers journal series

The Frontiers journal series is a multi-tier and interdisciplinary set of open-access, online journals, promising a paradigm shift from the current review, selection and dissemination processes in academic publishing. All Frontiers journals are driven by researchers for researchers; therefore, they constitute a service to the scholarly community. At the same time, the *Frontiers journal series* operates on a revolutionary invention, the tiered publishing system, initially addressing specific communities of scholars, and gradually climbing up to broader public understanding, thus serving the interests of the lay society, too.

Dedication to quality

Each Frontiers article is a landmark of the highest quality, thanks to genuinely collaborative interactions between authors and review editors, who include some of the world's best academicians. Research must be certified by peers before entering a stream of knowledge that may eventually reach the public - and shape society; therefore, Frontiers only applies the most rigorous and unbiased reviews. Frontiers revolutionizes research publishing by freely delivering the most outstanding research, evaluated with no bias from both the academic and social point of view. By applying the most advanced information technologies, Frontiers is catapulting scholarly publishing into a new generation.

What are Frontiers Research Topics?

Frontiers Research Topics are very popular trademarks of the *Frontiers journals series*: they are collections of at least ten articles, all centered on a particular subject. With their unique mix of varied contributions from Original Research to Review Articles, Frontiers Research Topics unify the most influential researchers, the latest key findings and historical advances in a hot research area.

Find out more on how to host your own Frontiers Research Topic or contribute to one as an author by contacting the Frontiers editorial office: frontiersin.org/about/contact

Research advances of modification and nutrition properties of food carbohydrates, volume I

Topic editors

Yanjun Zhang — Chinese Academy of Tropical Agricultural Sciences, China
Jianhua Xie — Nanchang University, China
Bin Li — Shenyang Agricultural University, China
Srinivas Janaswamy — South Dakota State University, United States

Citation

Zhang, Y., Xie, J., Li, B., Janaswamy, S., eds. (2023). *Research advances of modification and nutrition properties of food carbohydrates, volume I*. Lausanne: Frontiers Media SA. doi: 10.3389/978-2-8325-3206-5

Table of contents

frontiers | Frontiers in Nutrition

TYPE Editorial
PUBLISHED 04 October 2023
DOI 10.3389/fnut.2023.1270049

OPEN ACCESS

EDITED AND REVIEWED BY
Ken Ng,
The University of Melbourne, Australia

*CORRESPONDENCE
Yanjun Zhang
✉ zhangyanjun0305@163.com

RECEIVED 31 July 2023
ACCEPTED 28 August 2023
PUBLISHED 04 October 2023

CITATION
Zhang Y, Xie J, Li B and Janaswamy S (2023) Editorial: Research advances of modification and nutrition properties of food carbohydrates, volume I. *Front. Nutr.* 10:1270049. doi: 10.3389/fnut.2023.1270049

Editorial: Research advances of modification and nutrition properties of food carbohydrates, volume I

Yanjun Zhang[1,2]*, Jianhua Xie[3], Bin Li[4] and Srinivas Janaswamy[5]

[1]Spice and Beverage Research Institute, Chinese Academy of Tropical Agricultural Sciences, Wanning, China, [2]Key Laboratory of Processing Suitability and Quality Control of the Special Tropical Crops of Hainan Province, Wanning, Hainan, China, [3]Department of Food Nutrition, State Key Laboratory of Food Science and Resources, Nanchang University, Nanchang, China, [4]Department of Food Processing, College of Food Science and Engineering, Shenyang Agricultural University, Shenyang, China, [5]Department of Dairy and Food Science, South Dakota State University, Brookings, SD, United States

KEYWORDS

starch, non-starch polysaccharides, dietary fiber, cellulose, hemicellulose

Editorial on the Research Topic
Research advances of modification and nutrition properties of food carbohydrates, volume I

1. Introduction

As a group of essential biopolymers, carbohydrates exist widely in living organisms and play many known and unknown biological roles in life activities via different pathways. Carbohydrates are widely used in foodstuffs, pharmaceuticals, biofuels, and biomaterials, to name a few. Parallelly, a growing understanding and deeper investigation drive the development of natural carbohydrates for novel applications, especially for treating chronic diseases, e.g., hyperlipidemia, obesity, and diabetes. The emerging evidence indicates that carbohydrates are effective for modulating gut microbiota, a vital organ in health and diseases. In addition, modifying carbohydrates alters and/or enhances nutrition properties, further expanding their application potential. Notably, the nutritional properties of carbohydrates depend on their chemical structures and chain conformations. Thus, structural identification of carbohydrates and their derivatives helps expand their food, pharmaceutical, and related applications. To this end, a Research Topic entitled "*Research Advances of Modification and Nutrition Properties of Food Carbohydrates*" was launched by Frontiers in Nutrition, Food Chemistry (Frontiers) to provide a forum for researchers to disseminate their latest research findings on starch, non-starch polysaccharides, dietary fiber, pectin, cellulose, hemicellulose, and other food components. A total of 16 manuscripts from various countries were submitted, of which 12 were accepted for publication after the peer review, including two reviews and 10 research articles.

2. Starch

There were many studies on the modification and nutritional properties of food carbohydrates. In this set, starch is widely used in the food industry for bakery items, noodles, instant foods, and snacks. However, poor solubility, instability during pasting, undesired consistency, and retrogradation of native starches limit their widespread utility. To address these issues, physical, chemical, and enzymatic modifications and their combinations have been employed to enhance the physicochemical properties of starch. These modifications improve solubility, stability, and consistency and reduce retrogradation, making starch more suitable for various food applications. Gao et al. isolated and purified Lanzhou Lily (*Lilium davidii* var. unicolor) by polyethylene glycol-based ultrasonic-assisted enzymatic extraction method (PEG-UAEE). Single-factor experiments and response surface methodology (RSM) established the most effective process conditions. Subsequently, the preliminary structure of the low-molecular-weight polysaccharides (LLPs) was characterized using HPLC, FT-IR, and SEM, and their antioxidant activities were assessed. The findings demonstrated that the optimized conditions resulted in an LLPs yield of 14.75%: enzyme-to-substrate (E/S) ratio of 1,400 U/g; pH of 5.0; ultrasonic time of 30 min; and ultrasonic temperature of 50°C. The LLPs exhibited a pyranose ring, uronic acid, and characteristic absorption peaks of –OH, C=O, and C–H. Scanning electron microscopy revealed irregular distribution, dispersed structure, and numerous pores in the LLPs. HPLC analysis indicated that the LLPs were heteropolysaccharides consisting of galactose (6.36%), glucose (76.03%), rhamnose (2.02%), and arabinose (7.09%). Furthermore, *in vitro* testing demonstrated significant antioxidant effects of the LLPs. These results suggest that LLPs hold potential for applications as natural antioxidants and functional food ingredients. Yan et al. provided an overview of the production strategies employed for xylooligosaccharides (XOS) and discussed the raw materials, preparation methods, and purification techniques. Additionally, they presented the biological characteristics and applications of XOS. The most commonly recommended approach for XOS production is the two-stage method involving alkaline pre-treatment and enzymatic hydrolysis, with subsequent membrane filtration for enhanced yield and prebiotic functionality. Furthermore, novel strategies and technologies such as hydrothermal and steam explosion methods have also been explored, combined with enzymatic hydrolysis to produce XOS. It exhibits various significant physiological activities, particularly regulating blood glucose, reducing blood lipid levels, and improving the host intestinal flora structure. Furthermore, an additional study examined the correlation between glycemic release characteristics and the fine supramolecular structure of starches derived from cassava (ECS), potato (EPS), jackfruit seed (EJFSS), maize (EMS), wheat (EWS), and rice (ERS). These starches were prepared using an improved extrusion modification technology (IEMS). The results revealed that the extruded cooking starches transitioned from the A-type to V-type crystal structure. Specifically, IEMS-treated cassava, potato, and rice starches displayed broken α-1,6-glycosidic amylopectin (long chains), while the others exhibited sheared α-1,4-glycosidic amylopectin. The molecular weight, medium and long chain counts, and relative crystallinity decreased while the number of amylopectin short chains increased. ECS, EPS, EJFSS, and EWS demonstrated improved glycemic index (GI) and digestive speed rate constant (k) compared to raw starch. Although EMS and ERS exhibited degraded molecular structures, their particle morphology transformed from looser polyhedral shapes to more compact ones with fewer enzymolysis channels due to the rearrangement of side chain clusters of amylopectin, resulting in enhanced enzyme resistance. Notably, the IEMS-treated samples exhibited significant variations in starch characteristics. EPS had the highest amylose content, medium chains, long chains, and molecular weight but with the lowest GI, relative crystallinity, and k. Conversely, ERS displayed an opposite trend. Consequently, IEMS impacts starches with variable GIs. This investigation provides a foundation for broader applications of conventional crop starches in the food industry catering to diverse nutritional needs (Li, Zhang, et al.). Li L. et al. investigated the structural properties and physicochemical characteristics of lotus seed cross-linked resistant starches (LSCSs). Various concentrations of crosslinking agents were used to produce eight samples LS-0CS, LS-1CS, LS-2CS, LS-4CS, LS-6CS, LS-8CS, LS-10CS, and LS-12CS. The degree of crosslinking increased with higher crosslinking, leading to greater LSCS granular agglomeration. As observed in FT-IR analysis the P=O vibration at 1,250 cm^{-1} confirmed the crosslinking reaction. The covalent bonds formed by the phosphate groups were primarily composed of distarch monophosphate (DMSP), as determined by ^{31}P NMR. As the degree of crosslinking increased, the peak strength of DMSP became stronger, and the specific gravity increased. Among the eight samples, LS-12CS exhibited the highest degree of crosslinking and the greatest specific gravity. Additionally, the solubility of LSCSs decreased, while thermal stability and resistance to digestion improved with increasing crosslinking, which correlated with the degree of agglomeration and the presence of DMSP. LS-12CS displayed a resistant starch (RS) content of 48.95 ± 0.86%. With its low solubility, heat resistance, and high RS content, LS-12CS demonstrates potential as a prebiotic ingredient for the food industry. Zeng et al. summarized the effects of various dietary compounds, including cell walls, proteins, lipids, non-starchy polysaccharides, and polyphenols, on the enzymatic digestion of starch. These compounds were found to have distinct impacts on the digestion process. Cell walls, proteins, and non-starchy polysaccharides hindered starch disruption during hydrothermal treatment, preserving ordered structures that limited enzymatic binding. Additionally, these compounds encapsulated starch granules and acted as physical barriers, preventing enzymes from accessing the starch. Proteins, non-starchy polysaccharides, lipids, and polyphenols interacted with starch and formed organized assemblies. Furthermore, non-starchy polysaccharides and polyphenols exhibited a strong ability to reduce the activities of α-amylase and α-glucosidase. Based on these findings, it can be concluded that dietary compounds play a role in reducing starch digestion through three main mechanisms: (i) preservation of ordered structures and formation of organized assemblies with dietary compounds; (ii) creation of physical barriers that prevent enzyme access and binding to starch; and (iii) inhibition of enzyme activities. Modulating starch enzymatic digestion by dietary compounds holds significant potential in

regulating postprandial glucose response to food and preventing or treating type II diabetes. Li, Xie, et al. isolated starches from Chinese mutant *Musa acuminata* Colla acuminata and double balbisiana (MA), Musa double acuminata cv. Pisang Mas (MAM), *Musa acuminata* cv. Pisang Awak (MAA), Musa Basjoo Siebold (MBS), Musa double acuminata and balbisiana-Prata (MAP). The results showed that all the starches had a high amylose content, ranging from 34.04 to 42.59%. Based on particle size, the starches were categorized into two groups: medium-sized (MA, MAM) with particle sizes ranging from 14.54 to 17.71 μm, and large-sizes (MAA, MBS, and MAP) from 23.01 to 23.82 μm. The medium-sized starches exhibited A-type crystallization, higher peak viscosity, final viscosity, gel fracturability, and gel hardness. On the other hand, the large-sized starches presented B-type crystallization, compact particle morphology, a higher degree of crystallinity, short-range order, gelatinization enthalpy, pasting temperature, lower porosity, and higher water absorption capacity (WAC), and oil absorption capacity. The medium-sized starches with higher peak viscosity and gel hardness were found suitable as food thickening or gelling agents. The large-sized starches, with their unique characteristics such as higher degree of crystallinity, lower porosity, and WAC, showed potential as materials for resistant starch production. The study highlighted the significant influence of amylose content on the microstructure and physicochemical properties of starch samples. Overall, these findings suggested that the amylose content plays a crucial role in determining the microstructure and properties of starches, and provide opportunities for utilization in various food applications.

3. Non-starch polysaccharides

Non-starch polysaccharides find extensive application in various foods, including candies, pastries, and dairy products. They offer nutritional benefits and enhance the quality and texture of these foods through gelation, water holding, binding, foaming, stability, solubility, emulsification, and other properties. However, functional properties often fall short of expectations. Several methods, such as physical, chemical, and enzymatic modifications, are handy to improve the functional properties. He et al. summarized an overview of the chemical structures and probiotic potential of polysaccharides (LPs) extracted from fermented litchi pulp using *Lactobacillus fermentum* for different durations (ranging from 0 to 72 h, corresponding to LP-0 through LP-72, respectively). The fermentation time impacted the yields, total sugar content, uronic acid content, molecular weight, and monosaccharide composition of LPs. The LPs' yields and uronic acid content displayed irregular trends with fermentation time, while the total sugar content decreased and the molecular weight increased. Notably, LP-6 exhibited the highest extraction yield (2.67%), lowest uronic acid content, and smallest average molecular weight (104 kDa; $p < 0.05$). Analysis of the monosaccharide composition in the fermented LPs indicated decreased glucose proportions, whereas arabinose and galacturonic acid proportions increased compared to unfermented LP-0. Furthermore, LP-6 demonstrated the highest growth stimulation for Bifidobacterium compared to LP-0, while other fermentation durations exhibited comparable or inferior probiotic-promoting activities. These findings suggest that fermentation by lactic acid bacteria alters the physicochemical properties of litchi polysaccharides, and selecting an appropriate fermentation duration can enhance their probiotic activities. They further indicate that a proper fermentation time by lactic acid bacteria for litchi pulp might facilitate the probiotic properties of its polysaccharides. Wei et al. evaluated the relationship between the characteristics of regional rice as raw material and the resulting quality of rice noodles. Four commonly used rice cultivars for noodle production in Guangxi were examined. The findings revealed that the composition of rice flour significantly influenced gelatinization and retrogradation, which in turn affected the textural and sensory properties of rice noodles. The amylose content exhibited a strong positive correlation with the peak viscosity (PV) and trough viscosity (TV) of rice flour ($p < 0.01$). PV and TV showed strong negative correlations with adhesive strength ($p < 0.01$) and positive correlations with chewiness ($p < 0.05$), hardness, peak load, and deformation at the peak of rice noodles ($p < 0.01$). The protein content demonstrated a positive correlation with the setback of rice flour ($p < 0.05$), which is known to influence retrogradation. Additionally, solubility exhibited positive correlations with cooking loss ($p < 0.01$) and broken rate ($p < 0.05$) of rice noodles and a strong negative correlation with springiness ($p < 0.01$). Swelling power negatively correlated with the broken rate ($p < 0.05$). As the sensory score of rice noodles was negatively correlated with the broken rate ($p < 0.05$) and cooking loss ($p < 0.01$) and positively correlated with springiness ($p < 0.01$), it can be inferred that the solubility and swelling power of rice flours are useful indicators for predicting consumer acceptability of rice noodles. Ji et al. isolated a new polysaccharide (PZMP3-1) from *Ziziphus Jujuba* cv. Muzao fruit, and composition, molecular weight, and principal structural components were examined. It contains 2.56 rhamnose, 7.70 arabinose, 3.73 galactose, and 6.73 galactose, with an average molecular weight of 241 kDa. Methylation and nuclear magnetic resonance spectroscopy (NMR) analyses identified the key structural components, including 1,2,4 and 1,4-linked GalpA, 1,4-linked Galp, 1,3 and 1,5-linked Araf, and 1-linked Rhap. Structural analysis using X-ray diffraction (XRD), Fourier transform infrared spectroscopy (FT-IR), atomic force microscopy (AFM), and scanning electron microscopy (SEM) revealed a tangled and branching pattern. Overall, PZMP3-1 possesses unique bioactivities and potential for wide applications in nutritional supplements. Yang et al. conducted an extraction of polysaccharides from *Sibiraea laexigata* (L.) Maxim (SLM) and purified two fractions of SLM polysaccharides (SLMPs) named SLMPs-1-1 and SLMPs-2-1 using DEAE Cellulose-52 and Sephadex G-100 chromatography. The preliminary structure of these two fractions was established through various analyses such as chemical composition, molecular weight measurement, UVS, HPLC-PMP, FTIR, nuclear magnetic resonance (NMR) spectroscopy, and SEM. The results revealed that the two fractions had different molecular weights of 1.03 and 1.02 kDa composed of glucose (46.76 and 46.79%, respectively). The structural characterization using FT-IR, 1H NMR, and SEM indicated that SLMPs-1-1 and SLMPs-2-1 exhibited typical pyranose polysaccharide characteristics with α-glycosidic and β-glycosidic bonds. Additionally, it was observed that SLMPs-1-1 could increase the levels of tumor necrosis

factor-alpha (TNF-α) and interleukin-2 (IL-2) while mitigating immune organ tissue damage in cyclophosphamide (Cy)-treated mice. The results from RT-qPCR and Western blot analysis showed that SLMPs-1-1 significantly upregulated the levels of NF-kB and TLR4, indicating its potential involvement in the immunosuppressive protection of Cy-treated mice. These findings suggest that SLMPs-1-1 has the potential to serve as an alternative immunostimulatory and could find applications in the food and pharmaceutical industries. Zeng et al. examined the effects of polysaccharides from *Artocarpus heterophyllus* Lam. pulp (jackfruit, JFP-Ps) on intestinal barrier function. The researchers investigated the impact of JFP-Ps on intestinal health by performing H&E staining and biochemical analysis to assess the pathological and inflammatory state of the intestine, as well as oxidative damage. They also analyzed the expression of genes and proteins associated with intestinal health and inflammation using RT-qPCR and western blotting. The results demonstrated that JFP-Ps had several beneficial effects on intestinal barrier function. Firstly, JFP-Ps promoted bowel movement and modified the physiochemical environment of the intestine by reducing fecal pH and increasing fecal water content. Additionally, they alleviated oxidative damage in the colon, relieved intestinal colonic inflammation, and regulated blood glucose transport in the small intestine. They further repaired intestinal mucosal damage, increased the thickness of the mucus layer, and improved intestinal physiological status. Furthermore, they downregulated the expression of inflammatory genes such as TNF-α and IL-6, while upregulating the expression of free fatty acid receptors (GPR41 and GPR43) and tight junction protein (occludin). These findings suggest that JFP-Ps exert a protective effect on intestinal function by enhancing the intestine's biological, mucosal, immune, and mechanical barrier functions. JFP-Ps also activate signaling pathways related to short-chain fatty acids (SCFAs) and GPR41/GPR43. Based on these results, JFP-Ps show promise as a natural compound for improving human intestinal health and may be used as a potential phytochemical for this purpose. Gao et al. (1) extracted polysaccharides (ALPs) from *Arctium lappa* L. using an optimized aqueous two-phase system with specific conditions: polyethylene glycol (PEG) relative molecular weight of 6,000, PEG quality fraction of 25%, $(NH_4)_2SO_4$ quality fraction of 18%, and extraction temperature of 80°C. The extraction rate reached 28.83%. FTIR, SEM, and HPLC analyses revealed that ALPs were acidic heteropolysaccharides with uneven particle size distribution, irregular shape, and rough surface. The composition of ALPs consisted primarily of glucose, rhamnose, arabinose, and galactose, with molar ratios of 70.19:10.95:11.16:6.90, respectively. Additionally, ALPs exhibited strong *in vitro* antioxidant activity, effectively scavenging hydroxyl radicals (·OH), DPPH radicals, and superoxide anions, with IC50 values of 1.732 mg/ml, 0.29 mg/ml, and 0.15 mglmL, respectively. These findings highlight the potent antioxidant properties of ALPs and their potential as functional food ingredients.

4. Dietary fiber, cellulose and hemicellulose

Dietary fiber, a non-digestible polysaccharide, is considered a crucial nutrient by the nutritional community. It cannot be absorbed by the gastrointestinal tract, making it unique among nutrients. Enhancing insoluble dietary fiber's quality and functional properties through physical, chemical, and biological methods is essential for its extensive use in the food industry. These approaches aim to improve its characteristics and make it more suitable for various food applications. Wang et al. utilized tigernut to synthesize soluble dietary fiber-manganize complex [SDF-Mn(II)]. Comprehensive microscopic and structural analyses were conducted, including scanning electron microscopy, Fourier infrared spectroscopy, UV full-band scanning, X-ray diffraction, thermal analysis, gel permeation chromatography, and nuclear magnetic resonance. The *in vitro* hypoglycemic activity of SDF-Mn(II) was also investigated. The results revealed that the interaction between Mn(II) and SDF primarily involved hydroxyl and carbonyl groups. Nuclear magnetic resonance analysis demonstrated specific covalent bonding and substitution primarily occurring at the C6 position. Compared to SDF alone, the SDF-Mn(II) complex exhibited a porous structure, induced a red-shift and enhanced color intensity in UV characteristic peaks, displayed increased crystallinity, reduced molecular weight, and improved thermal stability. Furthermore, SDF-Mn(II) demonstrated significantly enhanced inhibition of α-amylase and α-glucosidase, indicating potent *in vitro* digestive enzyme inhibition activity.

Cellulose and hemicellulose, like non-starch polysaccharides, are widely utilized in various food applications. They contribute not only to the nutritional value but also to the quality and texture of foods due to their gelation, water retention, binding, foaming, stability, solubility, emulsification, and other functional properties. However, the inherent functional limitations of cellulose and hemicellulose often necessitate improvements. Various methods, including physical, chemical, and enzymatic modifications, have been employed to enhance the functional properties of cellulose and hemicellulose, allowing for their broader utilization in the food industry. Su et al. (2) found that cellulose and hemicellulose edible films with 10% microcapsule content showed the best overall performance, improving mechanical properties, thermal stability, and barrier properties. The films effectively inhibited *Listeria monocytogenes* (93.69%) and *Escherichia coli* (95.55%) and suppressed the growth of *Staphylococcus griseus*. When used for blueberry preservation, the ClO_2 self-releasing films delayed quality decline and prevented mold contamination during a 14-day storage period. Additionally, the antibacterial film group exhibited higher anthocyanin accumulation. These findings suggest that films containing ClO_2 microcapsules hold promise for future fruit and vegetable packaging.

5. Conclusions

The articles in this Research Topic encompass a wide range of topics, including enhancing the physical properties of key food components, investigations into biological activities, and applications in food preservation. Pursuing desirable food texture and taste, as well as the increasing demand for safe, environmentally friendly, and efficient food materials, are the main motivations driving ongoing research in this field. We hope these

novel research findings find practical and more useful applications in food and related applications.

Author contributions

YZ: Writing—original draft, Writing—review and editing. JX: Writing—review and editing. BL: Writing—review and editing. SJ: Writing—review and editing.

Funding

This work was supported from the Key Research and Development Program of Hainan Province (ZDYF2022SHFZ122), Chinese Central Public Interest Scientific Institution Basal Research Fund (1630142022007), Yunnan Academician and Tan Lehe Expert Workstation (202205AF150037), and USDA National Institute of Food and Agriculture (SD00H772-22) is highly appreciated.

Conflict of interest

The authors declare that the research was conducted in the absence of any commercial or financial relationships that could be construed as a potential conflict of interest.

The author(s) declared that they were an editorial board member of Frontiers, at the time of submission. This had no impact on the peer review process and the final decision.

Publisher's note

References

1. Gao D, Chen H, Li H, Yang X, Guo X, Zhang Y, et al. Extraction, structural characterization, and antioxidant activity of polysaccharides derived from *Arctium lappa* L. *Front Nutr.* (2023) 10:1149137. doi: 10.3389/fnut.2023.1149137

2. Su H, Chen Z, Zhao Y, An J, Huang H, Liu R, et al. Polyvinyl alcohol film with chlorine dioxide microcapsules can be used for blueberry preservation by slow-release of chlorine dioxide gas. *Front Nutr.* (2023) 10:1177950. doi: 10.3389/fnut.2023.1177950

frontiers | Frontiers in Nutrition

TYPE Original Research
PUBLISHED 05 August 2022
DOI 10.3389/fnut.2022.976607

OPEN ACCESS

EDITED BY
Yanjun Zhang,
Chinese Academy of Tropical Agricultural Sciences, China

REVIEWED BY
Ping Li,
Zhejiang Gongshang University, China
Hang Xiao,
University of Massachusetts Amherst, United States
Jianhua Xie,
Nanchang University, China

*CORRESPONDENCE
Jutian Yang
jutianyang988@163.com

†These authors have contributed equally to this work

SPECIALTY SECTION
This article was submitted to Food Chemistry, a section of the journal Frontiers in Nutrition

RECEIVED 23 June 2022
ACCEPTED 19 July 2022
PUBLISHED 05 August 2022

CITATION
Gao D, Chen H, Liu H, Yang X, Guo P, Cao X, Cai Y, Xu H and Yang J (2022) Structure characterization and antioxidant activity analysis of polysaccharides from Lanzhou Lily. *Front. Nutr.* 9:976607. doi: 10.3389/fnut.2022.976607

Structure characterization and antioxidant activity analysis of polysaccharides from Lanzhou Lily

Dandan Gao[1†], Hong Chen[1†], Honghai Liu[2], Xuhua Yang[1], Penghui Guo[1], Xin Cao[1], Yong Cai[1], Hongwei Xu[1] and Jutian Yang[1*]

[1]College of Life Sciences and Engineering, Northwest Minzu University, Lanzhou, China, [2]Technology Research and Development Center, Gansu Tobacco Industry Co. Ltd, Lanzhou, China

Lanzhou Lily (*Lilium davidii var. unicolor*) is a traditional medicinal plant and popular edible vegetable bulb in China. In this study, the polysaccharides of Lanzhou Lily (LLPs) were extracted by polyethylene glycol-based ultrasonic-assisted enzymatic extraction method (PEG-UAEE). The optimum process conditions were obtained by single-factor experiments and response surface methodology (RSM). Then, the preliminarily structure of LLPs was characterized by HPLC, FT-IR, and SEM, and its antioxidant activities were evaluated. The results showed that LLPs yield reached 14.75% under the optimized conditions: E/S ratio 1,400 U/g; pH 5.0, ultrasonic time 30 min; and ultrasonic temperature 50 °C. The LLPs has pyranoid ring, uronic acid, and the characteristic absorption peaks of -OH, C = O, and C-H. The results of scanning electron microscope indicated that the LLPs had irregular distribution, dispersed structure, and many holes. The HPLC analysis showed that the LLPs were heteropolysaccharide containing galactose (6.36%), glucose (76.03%), rhamnose (2.02%), and arabinose (7.09%). Moreover, the LLPs showed obvious antioxidant effect *in vitro*.

KEYWORDS

Lanzhou Lily, polysaccharide, extraction, structural characteristic, antioxidant activity

Introduction

Lanzhou Lily is a plant of morningstar lily bulb, called "sweet lily." It is the only sweet and edible lily in China with white color and sweet taste (1). Modern researches have shown that Lanzhou Lily has high edible, medicinal and ornamental value, and has further development and application potential (2). Lanzhou Lily contains massive pectin, alkaline elements and natural phospholipids, as well as abundant plant protein and cellulose. Lanzhou Lily has the functions of strengthening the spleen, nourishing the stomach, delaying aging and preventing gout. Lanzhou Lily also has many biological activities, including antioxidant, antitumor, hypoglycemic, immunomodulatory, and other pharmacological effects (3, 4), thus protecting human spleen, lung, and other organs, is beneficial to human body.

Polysaccharide is a natural high polymer linked by aldose or ketose through glycosidic bonds, and widely exists in plants. It is an important macromolecular substance in organisms and a basic substance maintaining normal life activities. Polysaccharides are mostly polymerized by several monosaccharides in a certain proportion. Polysaccharides vary in the molecular composition and weight (5). The content of polysaccharides in Lanzhou Lily is about 14.58 mg/g, which exert pharmacological effects such as antioxidant, hypoglycemic, anti-tumor, anti-fatigue and immune regulation (6). The principle of extracting Lanzhou Lily polysaccharide is to obtain the maximum extraction rate and reserve the active structure. It is of great significance to select an appropriate extraction method for polysaccharides.

The commonly used extraction methods of lily polysaccharide include hot water extraction, ultrasonic extraction, microwave extraction, and enzymatic extraction (7). Hot water extraction method is easy to operate and realize, but the cost is high and the yield is low. Ultrasonic extraction method can dramatically shorten the extraction time and improve the extraction efficiency, but it has high requirements on the container and large noise. Microwave extraction has the advantages of short time and simple equipment, but it is easy to be affected by external factors. Enzymatic extraction reaction conditions mild, less side reaction, but it needs a long time.

PEG can be used as solvent and cosolvent due to the good water solubility and low relative molecular weight (8). In this work, we developed an ultrasonic assisted enzymatic extraction method to obtain LLPs using PEG as the solvent. The method has developed a kind of efficient extraction technique to extract polysaccharides from various biomaterials. As expected, compared to ultrasonic assisted, PEG reagent provides -OH groups to enhance the interaction of polysaccharides which could improve polysaccharides yield. The optimal extraction process of LLPs was obtained by single-factor experiments and RSM with box-behnken design. Then, FT-IR, SEM, and HPLC were used to analyze the compositions and structural characteristic of LLPs. Moreover, antioxidant activities of LLPs were also evaluated.

Materials and methods

Materials and reagents

Fresh Lanzhou Lily at the mature stage of commercial was purchased from the local markets at Lanzhou city (Gansu, China). Cellulose and pectinase were obtained from Solarbio Biological Reagent Co., Ltd. (Beijing, China). 1,1-diphenyl-2-trinitrophenylhydrazine (DPPH), Trifluoroacetic acid (TFA) and monosaccharide standard products were from Sigma-Aldrich Chemical Co., Ltd. (Louis, USA). PEG and other reagents were all analytically pure and purchased from Sinopharm Chemical Reagent Co., Ltd. (Beijing, China).

Extraction of LLPs

Fresh Lanzhou Lily was cleaned, and then was frozen-dried by a vacuum freeze dryer (LGJ-100F, Thermo Co., USA). The dried lily powder was crushed and collected through an 80 mesh sieve. Then the power was degreased twice with n-hexane (M: V = 1:3) for 6 h every time, dried and collected for further use. Three gram defatted lily powder was accurately weighed, 45 mL 30% PEG-400 solution was added at the ratio of material to liquid of 1:15, and a mixed enzyme (cellulose: pectase = 1:2) was added. After pH adjustment, ultrasonic cleaning machine (SB-500DTY, Ningbo Xinzhi Biotechnology Co., China) was used for extracting under a ultrasonic power of 250 W. Repeated the above process 3 times. The extracts were mixed, centrifuged at 5,000 rpm for 10 min (Heraeus Multifuge X1R, Thermo, America), and the supernatant was taken. Sevage reagent (n-butanol: chloroform = 1: 5, v/v) was added to the supernatant to remove proteins. The solution was centrifuged (5,000 r/min, 10 min) and the upper layer solution was collected. Then 3 times (v/v) anhydrous ethyl alcohol was added for alcohol precipitation, and precipitate was formed after standing at 4°C for 24 h. The precipitate was recovered by centrifugation at 5,000 r/min for 10 min, and was successively washed by ethanol, petroleum ether and diethyl ether. The precipitate was dried in a DHG-9030A oven (Shanghai Grows Instrument Co., Ltd., China) to obtain LLPs. The extraction rate (%) of LLPs was calculated as follows:

$$R = \frac{m_1}{m_0} \times 100 \quad (1)$$

Where R is the extraction rate of LLPs (%); m_1 is the weight of lily polysaccharide extracted (g); m_0: the weight of the extracted lily powder (g).

Experimental design of optimization of extraction conditions

The effects of E/S ratio (700, 1,400, 2,100, 2,800, and 3,500 U/g), pH (3.0, 4.0, 5.0, 6.0, and 7.0), ultrasound time (10, 20, 30, 40, and 50 min), and ultrasound temperature (30, 40, 50, 60, and 70°C), on the extraction rate of LLPs were investigated. The experiments were conducted in triplicate.

According to the results of the single-factor experiments, X_1 (E/S ratio), X_2 (pH value), X_3 (ultrasound time), X_4 (ultrasound temperature) were selected as the independent variable, and Y (crude polysaccharide extraction rate) was used as the response value. A four-factor three-level Box-Behnken response surface

TABLE 1 The process parameters setting for LLPs extraction, according to Box-Benkhen design.

Factor	Level		
	−1	0	1
X_1-E/S ratio /(U/g)	700	1,400	2,100
X_2-Extraction pH value	4.0	5.0	6.0
X_3-ultrasound times/min	20	30	40
X_4-ultrasonic temperature/ °C	40	50	60

experimental design (BBD) was carried out. Three levels (−1, 0, and 1) were designed for each independent variable, the influencing factors and level design were shown in Table 1. Each experiment was repeated 3 times. By analyzing the results, a linear quadratic model was obtained as follow:

$$Y = B_0 + \sum_{i=1}^{k=3} B_i X_i + \sum_{i=1}^{k=3} B_{ii} X_i^2 + \sum_{i=1}^{k=3} B_{ii} X_i Y_i \quad (2)$$

Where Y is the response variable (LLPs extraction yield, %); B_0, B_i, B_{ii}, and B_{ij} are the regression coefficients of variables for the intercept, linear, quadratic, and interaction terms, respectively; X_i and X_j are the independent variables ($i \neq j$).

FT-IR spectrometric analysis of LLPs

A sample pellet was prepared by mixing 1 mg LLPs with 500 mg KBr, mortared, and pressed 5 min by a HYP-15 machine (Tianjin Port East Technology Co., Ltd, China). The sample was scanned for 20 min between 4,000 and 400 cm^{-1} using a Fourier infrared spectrometer (FTIR-650, Tianjin Port East Technology Co., Ltd, China) to analyze the chemical bonds and functional groups of LLPs (9).

SEM analysis of LLPs

LLPs were fixed on the sample table with conductive adhesive, and the samples coated with gold sputtering were scanned at 20 kV with Zeiss tungsten filament scanning electron microscope (ZEISS EVO18, Carl Zeiss AG, Bruker Co., Germany) to observe the sample morphology under different multiples (10).

Monosaccharide composition analysis

The monosaccharide components of LLPs were determined by HPLC (Agilent1260, USA) coupled with 3-methyl-1-phenyl-2-pyrazolin-5-one (PMP) pre-column derivatization (4.6 × 250 mm, 5 μm, Agilent Co., USA) (9, 11). 10.00 mg crude LLPs sample was precisely weighed and 5 mL of 2 M trifluoroacetic acid (TFA) solution was added. Then the sample was hydrolyzed in water bath at 100°C for 5 h. After cooling, the pH was adjusted to 7.0 using 3 M NaOH, then centrifuged at 5,000 r/min for 10 min. 0.2 mL of 0.5 M PMP/methanol solution and 0.3 M NaOH were added into 0.2 mL polysaccharide hydrolysate. After swirling mixing, water bath at 70°C for 1 h was performed. Then, 1 mL chloroform and 0.2 mL HCL (0.3 M) were mixed, centrifuged to get the supernatant and filtered through 0.22 μm membrane for monosaccharide composition analysis. Monosaccharide standards (rhamnose, glucose, galactose, fructose, and arabinose) were treated as same as described above.

HPLC analysis was performed using an Agilent 1260 HPLC system with a diode array UV-Vis detector (DVD), and an Agilent ZORBAX Eclipse XDB-C18 analytical HPLC column (4.6 × 250 mm, 5 μm). The mobile phase consisted of 20.0 mM phosphate buffer (pH 6.8) (A) and acetonitrile (B) in a ratio of 81: 19 (v/v). The column temperature was 28°C and the flow rate was 1 mL/min. The injection volume was 5 μL and the detection wavelength was 250 nm.

In vitro antioxidant activity assay

·OH radical scavenging assay

The ·OH radical scavenging activity of LLPs were determined by the method of Zhou et al. (12). The solutions of LLPs were prepared at concentrations of 0.0, 0.2, 0.4, 0.6, 0.8, and 1.0 mg/mL, respectively. An aliquot of 1.0 mL sample solution, 1.0 mL o-phenanthroline ethanol solution (0.75 mM) and 1.0 mL $FeSO_4$ (0.75 mM) were mixed, and placed in a water bath at 37°C for 30 min. After that, 1.0 mL H_2O_2 (0.01%) and 2.0 mL PBS (pH 7.4) were added to the mixture. When the mixture was evenly mixed, incubated it in a water bath at 37°C for 15 min. After cooling, the absorbance value A_x of the sample solution was determined at 510 nm, and distilled water was used as blank control. V_C (0.0, 0.2, 0.4, 0.6, 0.8, and 1.0 mg/mL) was used as positive control. The ·OH radical scavenging activity was calculated by the following formula:

$$E = (1 - \frac{A_x - A_{xo}}{A_o}) \times 100 \quad (3)$$

Where E is ·OH radical scavenging activity (%); A_o is the absorbance value of blank control; A_x is the absorbance value of

the samples; A_{xo} is the absorbance value of the sample without ·OH radical.

DPPH radical scavenging assay

The DPPH radical scavenging activity of LLPs was measured by the method of Liu et al. with slight modification (13). 2 mL LLPs samples at different concentrations (0.0, 0.2, 0.4, 0.6, 0.8, 1.0 mg/mL) were mixed with 2 mL DPPH solution (0.2 mM), reacted at room temperature for 30 min in a dark environment. And the absorbance value of the mixed solution was measured at 517 nm. The control 1 was composed by 2.0 mL DPPH and 2.0 mL distilled water, the control 2 was composed by 2.0 mL sample solution and 2.0 mL distilled water, and V_C group was used as positive control. The DPPH radical scavenging ability was calculated according to the following equation (14):

$$E = (1 - \frac{A_a - A_c}{A_b}) \times 100 \quad (4)$$

Where A_a is the absorbance of the samples; A_b is the absorbance of the control 1; A_c is the absorbance of the control 2.

$\cdot O_2^-$ radical scavenging assay

The $\cdot O_2^-$ radical scavenging activity of LLPs was determined according to the method described previously (15, 16). The LLPs samples and V_C were formulated into solutions with concentration gradients of 0.0, 0.2, 0.4, 0.6, 0.8, and 1.0 mg/mL, respectively. After adding 1.0 mL LLPs solution and 4.5 mL Tris-HCl buffer (pH 8.2), the mixture was incubated at 25°C water bath for 10 min. Then 0.4 mL of 25 mM catechol solution was added and fully mixed, and incubated at 25°C water bath for 5 min. Finally, 1 mL of 8 M hydrochloric acid was added to terminate the reaction, and the absorbance values were measured at 320 nm. Distilled water instead of polysaccharide solution was used as blank control and V_C group as positive control. The scavenging activity was calculated as follows:

$$E = \frac{A_{ii} - A_i}{A_{ii}} \times 100 \quad (5)$$

Where A_i is the absorbance of the control; A_{ii} is the absorbance of the samples.

Statistical analysis

SPSS 25.0 software was used to analyze the data, and the results were expressed as mean ± standard deviation. An ANOVA analysis was performed. The design expert software (Version 8.0.6, Stat-Ease, Inc., Minneapolis, MN, USA) was used for the experiment design. All the experiments or analyses were carried out in triplicate. The 50% inhibitory concentrations (IC_{50} values) were calculated by Probit analysis method using the SPSS software.

Results and discussion

Effects of E/S ratio, pH, ultrasonic time, and ultrasonic temperature on the extraction yield of LLPs

Cellulase and pectinase are normally able to degrade cellulose and pectin in plant cell walls, which could improve the extraction yield of LLPs (17). The cellulase and pectinase amounts can markedly affect the extraction yield of the LLPs. As a consequence, E/S ratio (700, 1,400, 2,100, 2,800, 3,500 U/g) on the extraction yield were investigated with enzymolysis pH of 5.0, ultrasonic time of 30 min, and ultrasonic temperature of 50°C. As shown in Figure 1A, the extraction ratio of LLPs increased from 10.95 to 13.42%, and then fall solely as E/S ratio increased from 1,400 to 3,500 U/g. The possible reason for this is the increase of cellulase and pectinase can effectively destroy the lily cells, resulting in more polysaccharide overflow and higher polysaccharide yield. However, when the E/S ratio was large, the polysaccharide glycosidic bond was partially hydrolyzed due to substrate saturation, and the extraction decreases (18). Considering the cost, E/S ratio of 1,400 U/g was selected as the center point of RSM.

It has been shown that the same type of enzymes from different origins have different activities and different pH optimums. PH value will affect the degree of dissociation of the essential groups on the enzyme activity center. The enzyme shows different activities under different pH conditions, and too high or too low pH value will reduce the enzymatic hydrolysis efficiency. Hence, pH values (3.0, 4.0, 5.0, 6.0, and 7.0) were selected as a univariate variable. As Figure 1B showed that the extraction ratio of LLPs increased with pH from 3.0 to 5.0, reaching a maximum value of 14.05 ± 0.09% at pH 5.0, and then decreased continuously with pH from 5.0 to 7.0 (17). The results could be that cellulase enzyme achieved only limited solubilization (19). Based on our results, a pH value of 5.0 was chosen as the RSM central point.

Ultrasound treatment could improve the efficiency of LLPs extraction, because of high pressure, temperature and shear force generated by the ultrasonic wave may break chemical bonds of polysaccharide in cell walls (20). The increase of ultrasonic time provides the conditions for ultrasonic wave to destroy more lily cells, so that more polysaccharides can be dissolved in PEG solution. As a result, the effect of ultrasonic time (10, 20, 30, 40, 50 min) on the extraction yield were investigated when the others extraction parameters were set as follows: E/S ratio 5.0, pH 5.0, and ultrasonic temperature 50°C. Figure 1C shows that polysaccharide yield reached the

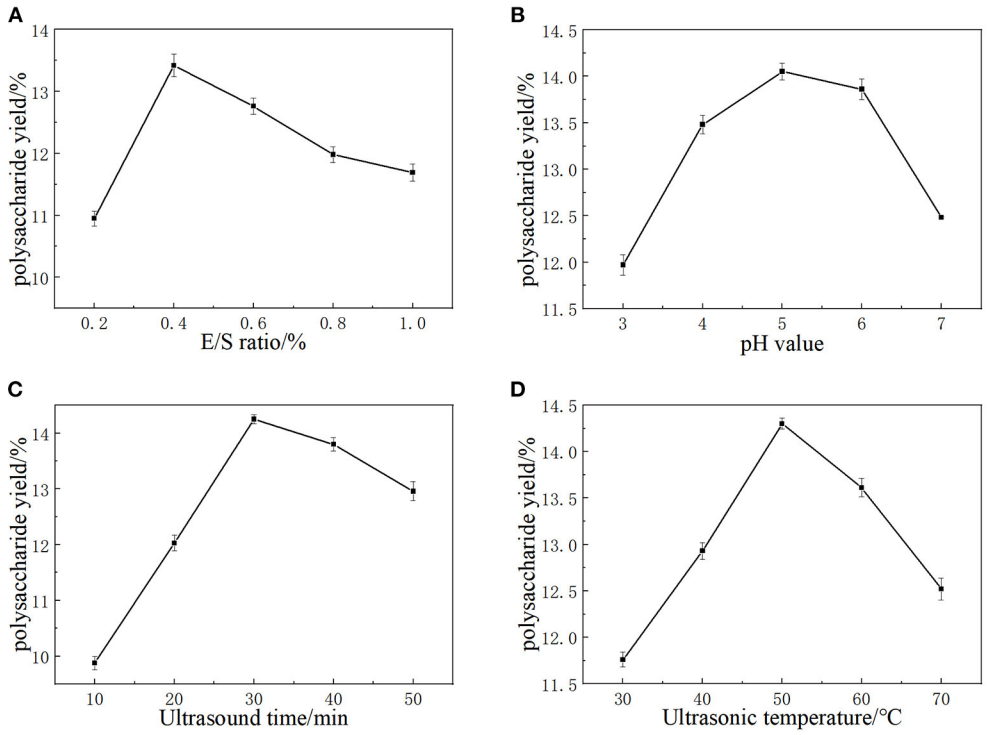

FIGURE 1
The effects of E/S ratio **(A)**, extraction pH **(B)**, Ultrasound time **(C)**, and Ultrasonic temperature **(D)** on the yield of LLPs.

maximum value of 14.25 ± 0.04% when ultrasonic time was 30 min. If the ultrasonic time exceeded 30 min, the LLPs extraction rate decreased significantly. When the ultrasonic time was <30 min, more polysaccharides had enough time to dissolve in the container with the extension of time, so the yield of polysaccharides increased. When the ultrasonic time exceeded 30 min, the high pressure, temperature and shear force generated by ultrasonic may destroy the chemical bonds of polysaccharides, leading to the hydrolysis of some polysaccharides, and the extraction rate of LLPs decreased significantly. Cai et al. (21) reported that with extended ultrasonic times, strong mechanical shock damages the dissolved ingredients and leads to the hydrolysis of some polysaccharides, which is consistent with our findings. Hence, 30 min was chosen as the optimal ultrasonic time and the RSM central point.

Temperature is also an important factor in the extraction of polysaccharides. The diffusion coefficient and solubility of polysaccharide in the extracting solvent was enhanced at a higher temperature, is possibly caused by the increase of the extraction rate of polysaccharides (22). Therefore, ultrasonic temperature (30, 40, 50, 60, 70°C) was studied under the conditions of fixed E/S ratio 5.0, pH 5.0, ultrasonic time 30 min. According to Figure 1D, the yield of LLPs increased with temperature in the range of 30–50°C, and reached the maximum value of 14.30 ± 0.02% at 50°C. After that, the yield of LLPs decreased with the increase of temperature (50–70°C). The main reason for this phenomenon was that the solubility and diffusion coefficient of polysaccharides in the extraction solvent increase at higher temperature, so that the amount of polysaccharides dissolved in the solution increases. When the temperature was too high, the biological potential of the enzyme was destroyed and lost activity, and irreversible changes occurred. Meanwhile, the polysaccharide structure was damaged and degraded in the high temperature environment, so the extraction rate of polysaccharide decreased. Cai et al. (21) reported that the mild conditions are beneficial to maintain the biological potential of enzyme, while a higher temperature will destroy the biological potential of enzyme (23). In conclusion, the optimal ultrasonic temperature was 50°C, which was used as the center point of RSM.

Analysis of the response surface

Statistical analysis and the model fitting

According to the principle of BBD central combined test, 29 groups were designed by Design-expert 8.0.6 software. The experimental Design level and experimental results of independent variables were summarized in Table 2. The extraction rate varied from 9.28 to 14.75%, with the maximum

TABLE 2 Box-Benkhen design of the independent variables and experimental values of LLPs yield (Y).

No.	Factor				Y (LLPs yield)/%
	X_1-E/S ratio/(U/g)	X_2-pH value	X_3-ultrasonic times/min	X_4-ultrasonic temperature)/°C	
1	700	4.00	30.00	50.00	11.05
2	2,100	4.00	30.00	50.00	11.88
3	700	6.00	30.00	50.00	12.91
4	2,100	6.00	30.00	50.00	11.50
5	1,400	5.00	20.00	40.00	10.27
6	1,400	5.00	40.00	40.00	9.69
7	1,400	5.00	20.00	60.00	10.61
8	1,400	5.00	40.00	60.00	10.10
9	700	5.00	30.00	40.00	11.76
10	2,100	5.00	30.00	40.00	10.28
11	700	5.00	30.00	60.00	11.31
12	2,100	5.00	30.00	60.00	11.56
13	1,400	4.00	20.00	50.00	10.88
14	1,400	6.00	20.00	50.00	11.24
15	1,400	4.00	40.00	50.00	9.38
16	1,400	6.00	40.00	50.00	11.62
17	700	5.00	20.00	50.00	12.87
18	2,100	5.00	20.00	50.00	9.98
19	700	5.00	40.00	50.00	9.28
20	2,100	5.00	40.00	50.00	12.39
21	1,400	4.00	30.00	40.00	9.89
22	1,400	6.00	30.00	40.00	11.48
23	1,400	4.00	30.00	60.00	10.95
24	1,400	6.00	30.00	60.00	11.49
25	1,400	5.00	30.00	50.00	14.75
26	1,400	5.00	30.00	50.00	13.97
27	1,400	5.00	30.00	50.00	14.18
28	1,400	5.00	30.00	50.00	14.64
29	1,400	5.00	30.00	50.00	14.43

value being obtained under the conditions of E/S ratio 1,400 U/g, pH 5.0, ultrasonic time 30 min, and ultrasonic temperature 50°C. The second-order polynomial equation of the influence of the three test variables on the response variables was obtained as follows:

$$Y = 14.39 - 0.13X_1 + 0.52X_2 - 0.28X_3 + 0.22X_4 - 0.56X_1X_2 + 1.50X_1X_3 + 0.43X_1X_4 + 0.47X_2X_3 - 0.26X_2X_4 + 0.017X_3X_4 - 1.12X_1^2 - 1.43X_2^2 - 2.17X_3^2 - 2.04X_4^2 \quad (6)$$

Where Y is the LLPs yield (%); X_1, X_2, X_3, and X_4 are the coded values of the tested E/S ratio (%), extraction pH value, ultrasonic times (min), and ultrasonic temperature (°C), respectively.

The results of analysis of variance (ANONA) analysis were shown in Table 3. The model had a high F value (81.95) and a low P-value (<0.0001), indicating that the model was statistically significant and effective. Where $R^2 = 0.9879$, indicating that 98.79% of the results can be explained by this model adjustment coefficient, and 1.21% of the results can't be explained. The $R^2_{adj} = 0.9759$, closed to R^2, indicating that the model has a good fit with the actual, the correlation between the observed value and the predicted value is good (13). The low coefficient of variation (C.V. = 2.14%) showed high accuracy of the model. The significance of each coefficient was listed in Table 3. The major factor (X_2, X_3, and X_4), minor factor (X_1^2, X_2^2, X_3^2, and X_4^2) and interaction item (X_1X_2, X_1X_3, X_1X_4, and X_2X_3) had significant effects on the yield of LLPs ($P < 0.01$). However, the interaction term (X_2X_4 and X_3X_4) of the main factor (X_1) had not a significant influence ($P > 0.05$). It can be seen that

TABLE 3 Analysis of variance and results of regression equation.

Source	Sum of square	Df	Mean square	F value	*P*-value
Model	70.39	14	5.03	81.95	<0.0001**
X_1	0.21	1	0.21	3.43	0.0851
X_2	3.21	1	3.21	52.38	<0.0001**
X_3	0.96	1	0.96	15.61	0.0014**
X_4	0.59	1	0.59	9.54	0.008**
X_1X_2	1.25	1	1.25	20.44	0.0005**
X_1 X_3	9	1	9	146.69	<0.0001**
X_1 X_4	0.75	1	0.75	12.2	0.0036**
X_2 X_3	0.88	1	0.88	14.4	0.002**
X_2 X_4	0.28	1	0.28	4.49	0.0524
X_3 X_4	0.001	1	0.001	0.02	0.8896
X_1^2	8.08	1	8.08	131.71	<0.0001**
X_2^2	13.24	1	13.24	215.79	<0.0001**
X_3^2	30.65	1	30.65	499.51	<0.0001**
X_4^2	26.96	1	26.96	439.39	<0.0001**
Model	0.86	14	0.061		
Lack of Fit	0.44	10	0.044	0.43	0.8729
Pure Error	0.41	4	0.1		
Cor total	71.25	28			
	$R^2 = 0.9879$		C.V. = 2.14%	$R^2_{Adj} = 0.9759$	

*represents significant difference ($P < 0.05$), **represents extremely significant difference ($P < 0.01$).

the influencing factors of the four variables were in the order of $X_2 > X_3 > X_4 > X_1$, and the pH value had the greatest influence on the extraction rate.

Response surface plot and contour plot analyses of the extracted LLPs

The three-dimensional response surface and contour diagram are shown in Figure 2. Each sub-figure shows the response surface and contour map of two factors to LLPs extraction rate, respectively. The influence of various factors on the response surface is staggered, and the degree of influence can be clearly reflected by the strength of the isoline in the contour map and the steep inclination of the response surface. Dense contour lines indicate steeper response surface and higher impact. The larger the distance between contour lines, the smaller the influence (24). Figures 2A–C showed that when pH value, ultrasonic time and ultrasonic temperature were fixed at the median value (level 0), the extraction rate reached the highest with the increase of E/S ratio. When the E/S ratio remained level 0, the extraction rate increased first with the increase of pH value, ultrasonic time and ultrasonic temperature, and then decreased. The results indicated that long ultrasonic time or high extraction temperature would increase the solubility rate of LLPs, but excessive ultrasonic time and extraction temperature would result in the hydrolysis of polysaccharides. A moderate high pH increased the activity of the enzyme, but a higher pH inhibited the activity of the enzyme. Figures 2D,E showed that when ultrasonic time and temperature were fixed at level 0, the highest extraction yield was observed with the increase of pH. The extraction rate increased first and then decreased with the increase of pH value, ultrasonic time and ultrasonic temperature. The interaction between ultrasonic time and ultrasonic temperature was shown in Figure 2F, when the ultrasonic time and temperature were fixed at level 0, the extraction rate was maximal. During the experiment, when E/S ratio, pH value, sonication time, and sonication temperature closed to 1,400 U/g, 5.00, 30 min, and 50°C, respectively, the polysaccharide extraction rate was maximized. The graphs of X_1 and X_2, X_1 and X_3, X_1 and X_4, X_2 and X_3 were steeper, and their contour lines can be seen to be ellipses. The graphs of X_2 and X_4, X_3 and X_4 were gentler, and their contour lines were circles. This result was consistent with the results of the ANOVE.

Validation of the predictive model

According to the mathematical prediction of the BBD, the optimal PEG-based UAEE conditions with the maximum LLPs yield (Y) obtained by the Design Expert software were: E/S ratio (X_1) of 1,295 U/g, extraction pH value (X_2) of 5.20, ultrasonic times (X_3) of 28.95 min

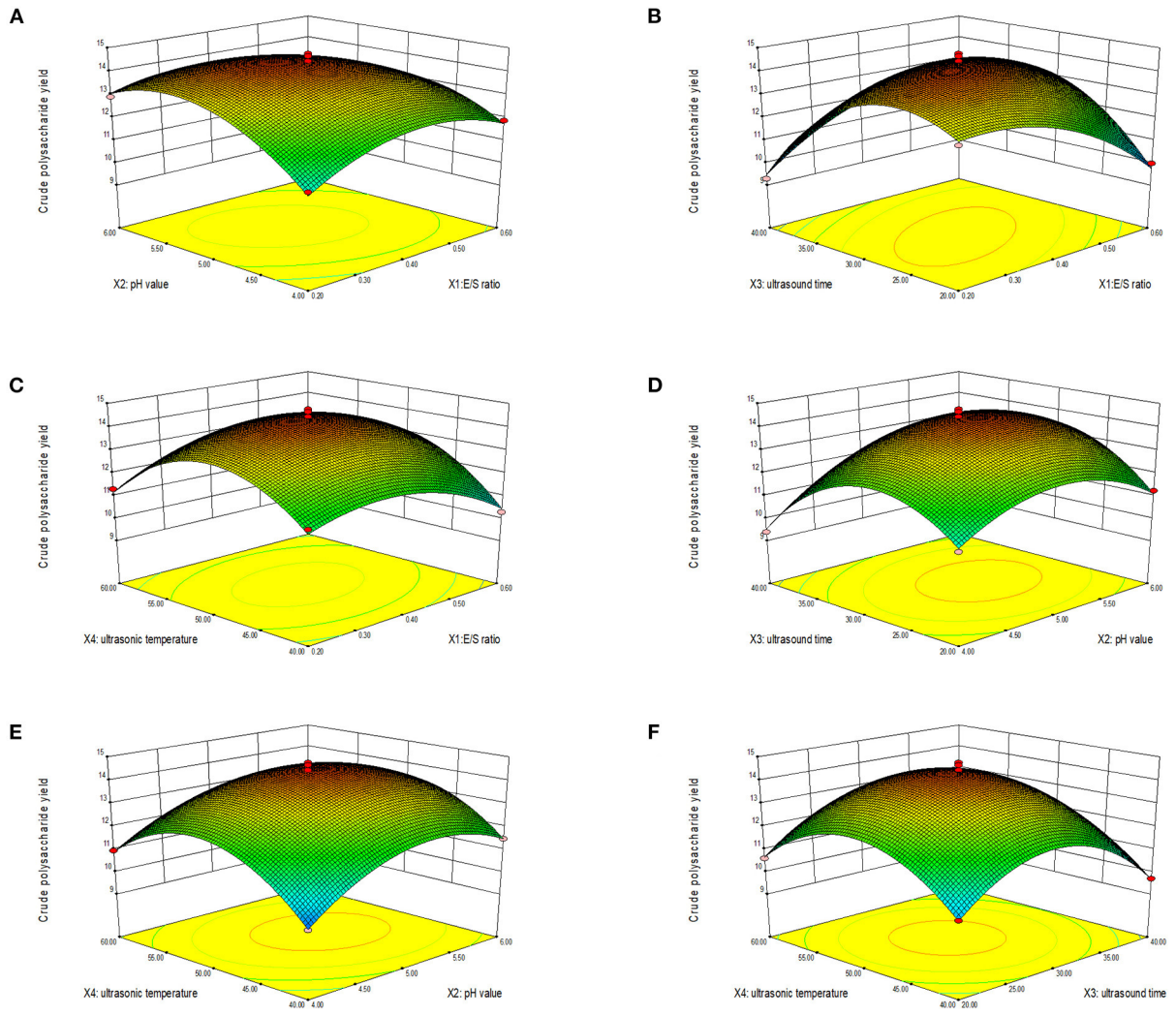

FIGURE 2
Response surface (3D) showing the effect of E/S ratio and pH value **(A)**, E/S ratio and ultrasonic time **(B)**, E/S ratio and ultrasonic temperature **(C)**, pH value and ultrasonic time **(D)**, pH value and ultrasonic temperature **(E)**, and ultrasonic time and ultrasonic temperature **(F)** on extraction yield of LLPs.

and ultrasonic temperature (X_4) of 50.22°C. Under the optimal conditions, the extraction yield reached 14.75%, close to the predicted value of 14.39% by response surface. The ultrasound-assisted enzymatic extraction (25) showed a low extraction rate (9.62%) compared to our method, indicating the PEG-UAEE extraction of LLPs is effective.

FT-IR spectrum of LLPs

Figure 3 shows the Fourier infrared spectrum of LLPs. According to the spectrogram, the characteristic absorption peak at 3379.6 cm^{-1} was assigned to the O-H stretching vibration (26), the 2999.7 cm^{-1} peak was relegated to C-H stretching vibration. The rough absorption peak at 1540.5 cm^{-1} were caused by C=O stretching vibration of the carboxyl products in the polysaccharide, and suggested the existence of uronic acid (26). The broader band of LLPs at 1540.5 cm^{-1} indicated higher content of uronic acid. There was also an absorption peak at 1 080.6 cm^{-1}, suggesting the LLPs has pyranose rings. The absorption peak at 773.5 cm^{-1} indicated that LLPs was α -D-glucan (25). This conclusion is generally consistent with Chen et al. (27) that the polysaccharide of tiger lily has the characteristics of pyranose.

Microstructure of LLPs

The data of SEM were presented in Figure 4. Sub-Figures 4A,B were 500X and 1000X images amplified under scanning electron microscopy. LLPs showed a fragmented and irregularly shaped morphology at magnifications of 500X (28). LLPs were composed of many small particles and clay-like clusters with irregular shapes and sizes. Most of the particles were massive, with irregular size and cracks (29, 30). The surface of LLPs when observed at magnifications of 1000X appeared to be relatively smooth, with some honeycombed cavities. LLPs presented irregular distribution, structure scattered, with many holes. Compared with the results of Hou et al. (31), the smooth surface of LLPs and the far difference in other characteristics may be due to the different treatment methods affecting the sample structure.

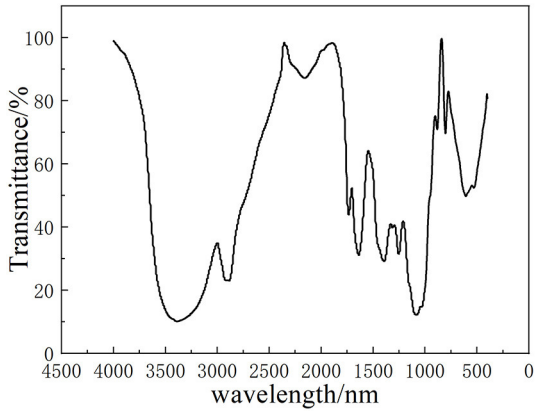

FIGURE 3
Infrared spectra of LLPs.

Monosaccharide composition of LLPs

The chromatogram of standards (rhamnose, glucose, galactose, fructose, and arabinose) and the LLPs are shown in Figure 5. The results showed that the LLPs was mainly composed of galactose, glucose, rhamnose, and arabinose, with a molar ratio of 6.36: 76.03: 2.02: 7.09. Chen et al. (27) found that LLPs-3, a purified component of lily water-soluble polysaccharide, was mainly composed of arabinose, galactose, glucose and mannose, with a molar ratio of 2:2:2:1. Gao et al. inferred that l-rhamnopyranose, d-arabinofuranose, d-glucopyranose, and d-galactopyranose in the molar ratio of 1.88:2.13:1.00:2.50 were main monosaccharide type of a novel polysaccharide fraction (LP2-1) from the edible bulbs of Lilium lancifolium Thunb (32). The two results indicated that the main monosaccharide compositions of LLPs were similar.

Antioxidant activity analysis

Scavenging hydroxyl radical

Hydroxyl radicals are a kind of compound harmful to organisms, and have a very high reactivity and can essentially attack and destroy living cells (33). Polysaccharides can be used as electron or hydrogen donors to remove hydroxyl radicals. Polysaccharides not only inhibit the production of ·OH, but also remove existing ·OH, indicating important antioxidant effects (34). The ·OH radical scavenging ability of LLPs was shown in Figure 6A, the scavenging ability of LLPs increased in the range of 0.2–1.0 mg/mL. Particularly, LLPs reached the highest values of 65.5% when the concentration was at 1.0 mg/mL, indicating that the scavenging ability of LLPs on ·OH free radical was concentration-dependent. At the same time, the semi-inhibitory concentration IC_{50} of LLPs was 0.63 mg/mL. The IC_{50} of V_C was 0.51 mg/mL. LLPs owe their scavenging ability of ·OH free radical to either the ·OH group possibly existing in their structure or the influence imposed by the density of electrons around heterocyclic carbon (35).

DPPH radical scavenging

Polysaccharides have many hydroxyl groups and most of them can donate hydrogen to reduce the DPPH radical (36). DPPH radical scavenging model is widely used in quantitative analysis of antioxidant ability. The Figure 6B showed the DPPH scavenging activity of LLPs increased from 23.3 to 65.5% with the concentration ranging from 0.0 to 1.0 mg/mL, indicating that the scavenging DPPH free radical of LLPs in a concentration-dependent manner (29). The concentration in the range of 0.0–0.4 mg/mL had a greater effect on DPPH radical scavenging ability, while the concentration had a smaller effect in the range of 0.4–1.0 mg/mL. LLPs at 1.0 mg/mL showed the highest DPPH radical scavenging ability of 86.1%. The scavenging ability of V_C at the same concentration was 95.1%. Moreover, the IC_{50} of LLPs was 0.32 mg/mL. Results showed that LLPs had a significant scavenging effect on DPPH free radicals, which was similar to results from a previous study (25).

Scavenging superoxide anion radicals

Superoxide radical can be found in the numerous biological and photochemical reactions. Although the superoxide radical is less reactive, it can reproduce other reactive oxygen species to cause the tissue damage and various diseases. As shown in Figure 6C, LLPs had significant scavenging activity on $\cdot O_2^-$ radical. The scavenging value of LLPs reached 83.4%

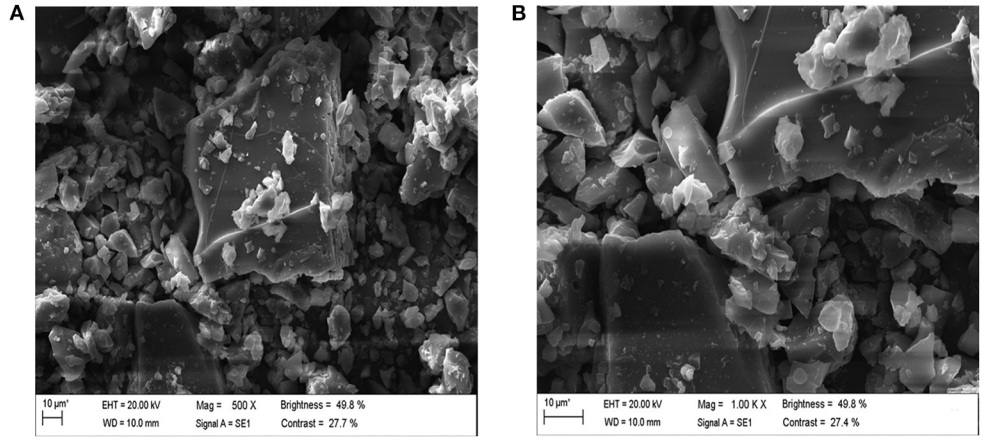

FIGURE 4
Scanning electron microscopy of LLPs [**(A)**: 500 X, **(B)**: 1.00 KX].

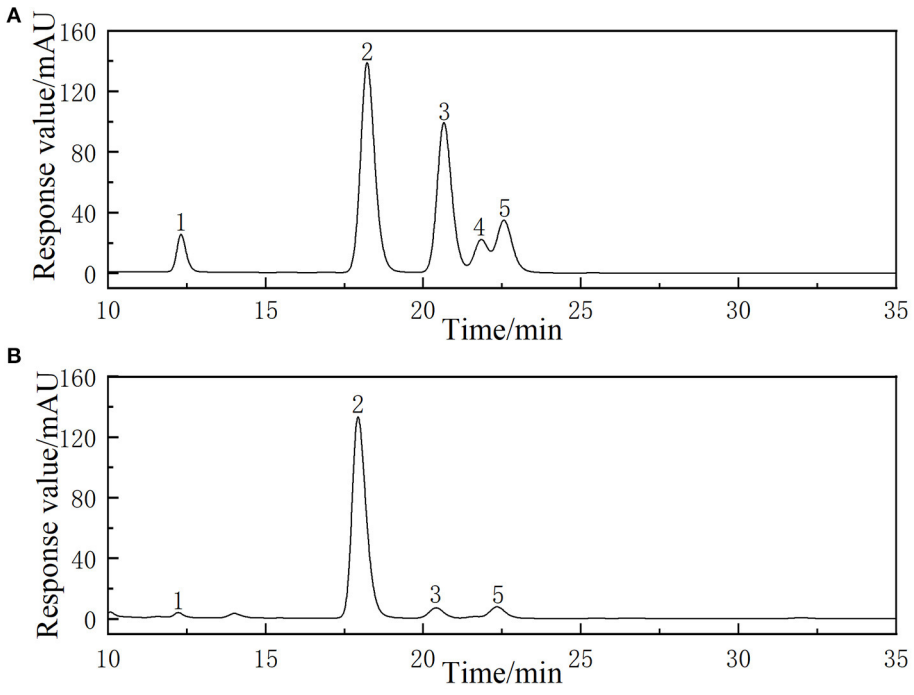

FIGURE 5
HPLC chromatogram of reference monosaccharides **(A)** and monosaccharides composition of LLPs **(B)**.

at 0.2 mg/mL, increased slowly in the range of 0.2–1.0 mg/mL. Particularly, the clearance rates of V_C and LLPs at 1.0 mg/mL were 99.5 and 88.9%, respectively. Although the superoxide radical scavenging activity of LLPs was a little weaker than those of V_C, LLPs could be used as the superoxide radical inhibitors to reduce oxidative damage (37). In addition, the IC_{50} of LLPs was 0.30 mg/mL. Xu et al. reported that the scavenging activities of LLPs (LLP-1, LLP-2, LLP-3) were 93.20, 91.49, 96.83% when the concentration was 1.0 mg/mL (38).

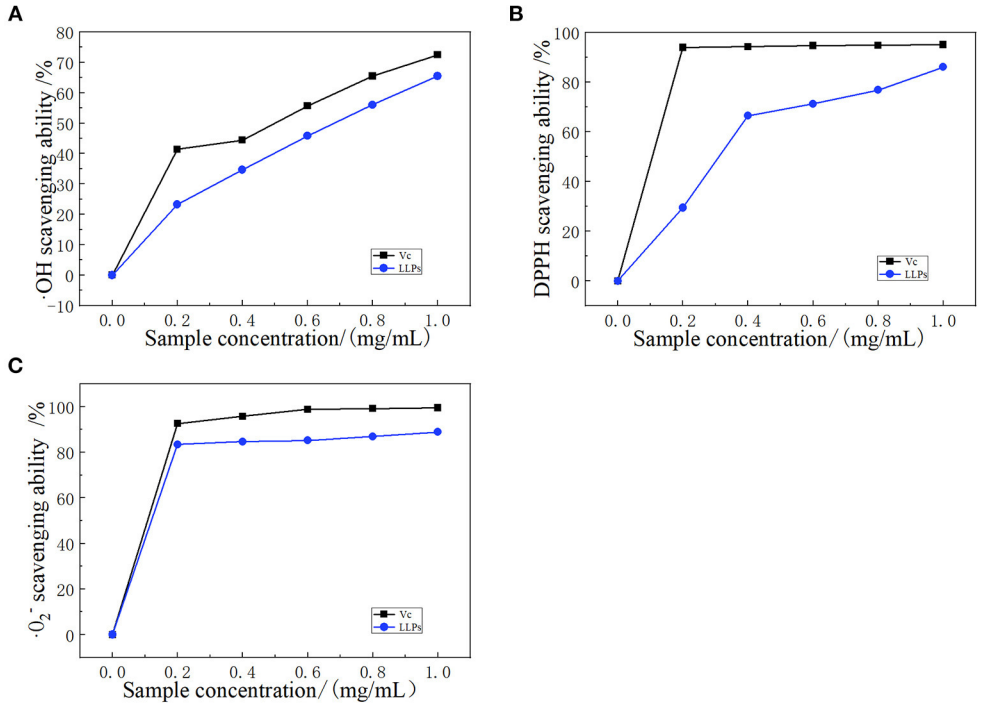

FIGURE 6
Scavenging effect of LLPs on **(A)** ·OH radicals compared with V_C, **(B)** DPPH radicals compared with V_C, and **(C)** $\cdot O_2^-$ radicals compared with V_C.

Conclusions

LLPs were extracted by ultrasonic assisted enzymatic method with polyethylene glycol. A LLPs yield of 14.75% was obtained at the optimized conditions: E/S ratio 1,400 U/g, pH 5.0, ultrasonic temperature 50 °C, ultrasonic time 30 min. The LLPs was mainly composed of galactose, glucose, rhamnose, and arabinose, with a ratio of 6.36: 76.03: 2.02: 7.09. LLPs were a α-d-glucan and pyranoid polysaccharide with characteristic absorption peaks of -OH, C=O, and C-H. The LLPs product had irregular distribution, dispersed structure and many holes. The LLPs showed a high ·OH radical scavenging activity, DPPH radical scavenging activity, and $\cdot O_2^-$ radical scavenging activity of 62.1, 65.5, and 88.9%, with IC_{50} values of 0.63, 0.32, and 0.30 mg/mL, respectively. The results suggested that LLPs have potential application as natural antioxidant and food ingredients in functional food.

Data availability statement

The raw data supporting the conclusions of this article will be made available by the authors, without undue reservation.

Author contributions

The initiative for this work was from JY and DG designed experiments. DG and PG did experimental design of antioxidant. XY and HC prepared LLPs. XC and HX did the determination of purified LLPs structural. DG and HC wrote the manuscript. All authors read and approved the final manuscript.

Funding

This work was supported by the Natural Science Foundation of China (No. 31960461); The Fundamental Research Funds for the Central Universities of Northwest Minzu University (31920220045 and BELTY201901); The Young Doctor Fund of Gansu Province (2021QB-147).

Conflict of interest

Author HL was employed by Gansu Tobacco Industry Co. Ltd.

The remaining authors declare that the research was conducted in the absence of any commercial or financial relationships that could be construed as a potential conflict of interest.

Publisher's note

References

1. Ahmad A, Rehman MU, Wali AF, El-Serehy HA, Al-Misned FA, Maodaa SN, et al. Box-Behnken response surface design of polysaccharide extraction from *Rhododendron arboreum* and the evaluation of its antioxidant potential. *Molecules.* (2020) 25:3835. doi: 10.3390/molecules25173835

2. Zhang Xf, Zhang Q, Xue H, Zhang J, Wang X. A green and highly efficient method of extracting polyphenols from *Lilium davidii* var. unicolor Salisb using deep eutectic solvents. *Chem Eng Commun.* (2021) 209:271–80. doi: 10.1080/00986445.2020.1864625

3. Berkani F, Dahmoune F, Achat S, Dairi S, Kadri N, Zeghichi-Hamri S, et al. Response surface methodology optimization of microwave-assisted polysaccharide extraction from Algerian jujube (*Zizyphus lotus* L.) pulp and peel. *J Pharm Innov.* (2020) 16:630–42. doi: 10.1007/s12247-020-09475-9

4. Alboofetileh M, Rezaei M, Tabarsa M, You S. Ultrasound-assisted extraction of sulfated polysaccharide from *Nizamuddinia zanardinii*: process optimization, structural characterization, and biological properties. *J Food Proc Eng.* (2018) 42:1–13. doi: 10.1111/jfpe.12979

5. Soumya RS, Vineetha VP, Reshma PL, Raghu KG. Preparation and characterization of selenium incorporated guar gum nanoparticle and its interaction with H9c2 cells. *PLoS ONE.* (2013) 8:e74411. doi: 10.1371/journal.pone.0074411

6. Yu Y, Zhu H, Shen MY, Yu Q, Chen Y, Xie JH. Sulfation modification enhances the intestinal regulation of Cyclocarya paliurus polysaccharides in cyclophosphamide-treated mice via restoring intestinal mucosal barrier function and modulating gut microbiota. *Food Funct.* (2021) 12:12278–90. doi: 10.1039/D1FO03042F

7. Wang B, Liu Q, Huang Y, Yuan Y, Ma Q, Du M, et al. Extraction of polysaccharide from spirulina and evaluation of its activities. *Evid Based Complement Alternat Med.* (2018) 2018:3425615. doi: 10.1155/2018/3425615

8. Chang J, Yang Z, Li J, Jin Y, Gao Y, Sun Y, et al. Preparation and *in vitro* and *in vivo* antitumor effects of VEGF targeting micelles. *Technol Cancer Res Treat.* (2020) 19:5–190. doi: 10.1177/1533033820957022

9. Do TH, Nguyen VT, Dung NQ, Chu MN, Van Kiet D, Ngan TTK, et al. Study on methylene blue adsorption of activated carbon made from *Moringa oleifera* leaf. *Mater Today Proc.* (2021) 38:3405–13. doi: 10.1016/j.matpr.2020.10.834

10. Zhang X, Teng G, Zhang J. Ethanol/salt aqueous two-phase system based ultrasonically assisted extraction of polysaccharides from *Lilium davidiivar*. unicolor Salisb: physicochemical characterization and antiglycation properties. *J Mol Liquids.* (2018) 256:497–506. doi: 10.1016/j.molliq.2018.02.059

11. Ma XL, Song FF, Zhang H, Huan X, Li SY. Compositional monosaccharide analysis of *Morus nigra* Linn by HPLC and HPCE quantitative determination and comparison of polysaccharide from *Morus nigra* Linn by HPCE and HPLC. *Curr Pharm Anal.* (2017) 13:433–7. doi: 10.2174/1573412913666170330150807

12. Zhou S, Huang G, Chen G. Extraction, structural analysis, derivatization and antioxidant activity of polysaccharide from Chinese yam. *Food Chem.* (2021) 361:130089. doi: 10.1016/j.foodchem.2021.130089

13. Liu H, Li F, Luo P. Effect of carboxymethylation and phosphorylation on the properties of polysaccharides from *Sepia esculenta* Ink: antioxidation and anticoagulation *in vitro*. *Mar Drugs.* (2019) 17:626. doi: 10.3390/md17110626

14. Xie JH, Wang ZJ, Shen MY, Nie SP, Gong B, Li HS, et al. Sulfated modification, characterization and antioxidant activities of polysaccharide from *Cyclocarya paliurus*. *Food Hydrocolloids.* (2016) 53:7–15. doi: 10.1016/j.foodhyd.2015.02.018

15. Tu JQ, Liu HP, Wen YH, Chen P, Liu ZT. A novel polysaccharide from *Hericium erinaceus*: preparation, structural characteristics, thermal stabilities, and antioxidant activities *in vitro*. *J Food Biochem.* (2021) 45:e13871. doi: 10.1111/jfbc.13871

16. Li G, Chen P, Zhao Y, Zeng Q, Ou S, Zhang Y, et al. Isolation, structural characterization and anti-oxidant activity of a novel polysaccharide from garlic bolt. *Carbohydr Polym.* (2021) 267:118194. doi: 10.1016/j.carbpol.2021.118194

17. Mirzaeinia S, Pazhang M, Imani M, Chaparzadeh N, Amani-Ghadim AR. Improving the stability of uricase from *Aspergillus flavus* by osmolytes: use of response surface methodology for optimization of the enzyme stability. *Process Biochem.* (2020) 94:86–98. doi: 10.1016/j.procbio.2020.04.020

18. Yang S, Xiao H, Yu S, Xie Z, Yu S, Sun W, et al. Optimization for the extraction of polysaccharide from walnut (*Juglans regia* L.) leaves: antioxidant activities *in vitro*. *Am J Biochem Biotechnol.* (2019) 15:163–78. doi: 10.3844/ajbbsp.2019.163.178

19. Wang F, Jiang Y, Guo W, Niu K, Zhang R, Hou S, et al. An environmentally friendly and productive process for bioethanol production from potato waste. *Biotechnol Biofuels.* (2016) 9:50. doi: 10.1186/s13068-016-0464-7

20. Zhang Y, Li Y, Li S, Zhang H, Ma H. *In situ* monitoring of the effect of ultrasound on the sulfhydryl groups and disulfide bonds of wheat gluten. *Molecules.* (2018) 23:1376. doi: 10.3390/molecules23061376

21. Cai C, Ma J, Han C, Jin Y, Zhao G, He X. Extraction and antioxidant activity of total triterpenoids in the mycelium of a medicinal fungus, *Sanghuangporus sanghuang*. *Sci Rep.* (2019) 9:7418. doi: 10.1038/s41598-019-43886-0

22. Yuan X, Zeng Y, Nie K, Luo D, Wang Z. Extraction optimization, characterization and bioactivities of a major polysaccharide from *Sargassum thunbergii*. *PLoS ONE.* (2015) 10:e0144773. doi: 10.1371/journal.pone.0144773

23. Chen G, Bu F, Chen X, Li C, Wang S, Kan J. Ultrasonic extraction, structural characterization, physicochemical properties and antioxidant activities of polysaccharides from bamboo shoots (*Chimonobambusa quadrangularis*) processing by-products. *Int J Biol Macromol.* (2018) 112:656–66. doi: 10.1016/j.ijbiomac.2018.02.013

24. Yuan S, Xu CY, Xia J, Feng YN, Zhang XF, Yan YY. Extraction of polysaccharides from *Codonopsis pilosula* by fermentation with response surface methodology. *Food Sci Nutr.* (2020) 8:6660–9. doi: 10.1002/fsn3.1958

25. Li W, Wang Y, Wei H, Zhang Y, Guo Z, Qiu Y, et al. Structural characterization of Lanzhou lily (*Lilium davidii* var. unicolor) polysaccharides and determination of their associated antioxidant activity. *J Sci Food Agric.* (2020) 100:5603–16. doi: 10.1002/jsfa.10613

26. Chen QY, Wang RF, Wang Y, An XP, Liu N, Song M, et al. Characterization and antioxidant activity of wheat bran polysaccharides modified by *Saccharomyces cerevisiae* and *Bacillus subtilis* fermentation. *J Cereal Sci.* (2021) 97:103157. doi: 10.1016/j.jcs.2020.103157

27. Chen ZG, Zhang DN, Zhu Q, Yang QH, Han YB. Purification, preliminary characterization and *in vitro* immunomodulatory activity of tiger lily polysaccharide. *Carbohydr Polym.* (2014) 106:217–22. doi: 10.1016/j.carbpol.2014.02.004

28. Liu YJ, Mo XL.Tang XZ, Li JH, Hu MB, Yan D, et al. Extraction optimization, characterization, and bioactivities of polysaccharides from Pinelliae Rhizoma Praeparatum Cum Alumine Employing Ultrasound-Assisted. *Molecules.* (2017) 22:965. doi: 10.3390/molecules22060965

29. Hui H, Li X, Jin H, Yang X, Xin A, Zhao R, et al. Structural characterization, antioxidant and antibacterial activities of two heteropolysaccharides purified from the bulbs of *Lilium davidii* var. unicolor Cotton. *Int J Biol Macromol.* (2019) 133:306–15. doi: 10.1016/j.ijbiomac.2019.04.082

30. Zhang W, Xiang Q, Zhao J, Mao G, Feng W, Chen Y, et al. Purification, structural elucidation and physicochemical properties of a polysaccharide from *Abelmoschus esculentus* L (okra) flowers. *Int J Biol Macromol.* (2020) 155:740–50. doi: 10.1016/j.ijbiomac.2020.03.235

31. Hou R, Chen J, Yue C, Li X, Liu J, Gao Z, et al. Modification of lily polysaccharide by selenylation and the immune-enhancing activity. *Carbohydr Polym.* (2016) 142:73–81. doi: 10.1016/j.carbpol.2016.01.032

32. Gao J, Zhang T, Jin ZY, Xu XM, Wang JH, Zha XQ, et al. Structural characterisation, physicochemical properties and antioxidant activity of polysaccharide from *Lilium lancifolium* Thunb. *Food Chem.* (2015) 169:430–8. doi: 10.1016/j.foodchem.2014.08.016

33. Gong T, Liu S, Wang H, Zhang M. Supercritical CO_2 fluid extraction, physicochemical properties, antioxidant activities and hypoglycemic activity of polysaccharides derived from fallen Ginkgo leaves. *Food Biosci.* (2021) 42:101153. doi: 10.1016/j.fbio.2021.101153

34. Dong Y, Qi Y, Liu M, Song X, Zhang C, Jiao X, et al. Antioxidant, anti-hyperlipidemia and hepatic protection of enzyme-assisted *Morehella esculenta* polysaccharide. *Int J Biol Macromol.* (2018) 120(Pt. B):1490–9. doi: 10.1016/j.ijbiomac.2018.09.134

35. Hamid N, Dong ZY, Yin XS, Liu SL, Zhang TH, Ren H, et al. Ultrasonic-assisted extraction, antioxidant activity and structural characterization of polysaccharides from *Oenothera Biennis* L. leaves. *E3S Web Conf.* (2020) 189:2025–31. doi: 10.1051/e3sconf/202018902025

36. Hoseiniyan Benvidi SM, Jahanbin K. A new water-soluble polysaccharide from *Echinops pungens* Trautv roots. Part I. Isolation, purification, characterization and antioxidant activity. *Int J Biol Macromol.* (2020) 161:909–16. doi: 10.1016/j.ijbiomac.2020.06.128

37. Zhang L, Cheng Z, Zhao Q, Wang M. Green and efficient PEG-based ultrasound-assisted extraction of polysaccharides from superfine ground lotus plumule to investigate their antioxidant activities. *Industrial Crops Prod.* (2017) 109:320–6. doi: 10.1016/j.indcrop.2017.08.018

38. Xu Z, Wang H, Wang B, Fu L, Yuan M, Liu J, et al. Characterization and antioxidant activities of polysaccharides from the leaves of *Lilium lancifolium* Thunb. *Int J Biol Macromol.* (2016) 92:148–55. doi: 10.1016/j.ijbiomac.2016.07.028

frontiers | Frontiers in Nutrition

TYPE Original Research
PUBLISHED 09 August 2022
DOI 10.3389/fnut.2022.989042

OPEN ACCESS

EDITED BY
Yanjun Zhang,
Chinese Academy of Tropical Agricultural Sciences, China

REVIEWED BY
Chao Li,
South China University of Technology, China
Zihao Wei,
Ocean University of China, China
Junfu Ji,
China Agricultural University, China

*CORRESPONDENCE
Yi Zhang
zyifst@163.com
Hongliang Zeng
zhlfst@fafu.edu.cn

SPECIALTY SECTION
This article was submitted to Food Chemistry, a section of the journal Frontiers in Nutrition

RECEIVED 08 July 2022
ACCEPTED 26 July 2022
PUBLISHED 09 August 2022

CITATION
Li L, He S, Lin Y, Zheng B, Zhang Y and Zeng H (2022) A novel lotus seed cross-linked resistant starch: Structural, physicochemical and digestive properties. *Front. Nutr.* 9:989042. doi: 10.3389/fnut.2022.989042

A novel lotus seed cross-linked resistant starch: Structural, physicochemical and digestive properties

Lanxin Li[1,2], Shuqi He[1,2], Yongjie Lin[1,2], Baodong Zheng[1,2,3], Yi Zhang[1,2,3]* and Hongliang Zeng[1,2,3]*

[1]College of Food Science, Fujian Agriculture and Forestry University, Fuzhou, China, [2]Fujian Provincial Key Laboratory of Quality Science and Processing Technology in Special Starch, Fujian Agriculture and Forestry University, Fuzhou, China, [3]China-Ireland International Cooperation Center for Food Material Science and Structure Design, Fujian Agriculture and Forestry University, Fuzhou, China

The structural properties and physicochemical characteristics of lotus seed cross-linked resistant starches (LSCSs; LS-0CS, LS-1CS, LS-2CS, LS-4CS, LS-6CS, LS-8CS, LS-10CS, and LS-12CS) with different concentrations of cross-linking agents were investigated. The degrees of cross-linking of LSCSs increased along with the amount of cross-linking agent. The higher the degree of cross-linking, the greater the degree of LSCSs granule agglomeration. The occurrence of the cross-linking reaction was confirmed by the appearance of P = O at 1,250 cm^{-1} as assessed by FT-IR, and the covalent bonds formed by the phosphate group in LSCSs were mainly composed of distarch monophosphate (DMSP) as determined by ^{31}P NMR. As the crosslinking degree increased, the peak strength of DMSP in starch was stronger and the specific gravity of DMSP was larger. Among the samples, LS-12CS had the highest cross-linking degree, with a greater specific gravity of DMSP. Moreover, the solubility levels of LSCSs decreased and the thermal stability and anti-digestive properties improved as the cross-linking degree increased, which was correlated with the degree of agglomeration and DMSP in LSCSs. The RS content of LS-12CS was 48.95 ± 0.86%.

KEYWORDS

lotus seed cross-linked resistant starch, cross-linking, structural properties, physicochemical properties, *in vitro* digestion

Introduction

Lotus seeds are an economically important specialty product in China, with a greater than 2,000-year history of cultivation. Starch, the main constituent of lotus seeds, represents approximately 50% of the dry basis and is abundant in raw material resources, especially during the processing of lotus seed milk drinks that produce numerous

lotus seed starch by-products (1). Natural starches are susceptible to reconstitution and dehydration during storage, low resistant to pH, temperature changes and mechanical treatment and have unstable functional properties. However, these inherent functional limitations can be overcome by starch modification. Resistant starch (RS) is divided into five types: physically trapped starch (RS1), natural resistant starch granules (RS2), retrograded starch (RS3), chemically modified starch (RS4) and a complex of amylose and lipids (RS5). They all require modifications to form, except for RS1 and RS2 (2). These starches are prepared using three main methods: physical, chemical and enzymatic modifications.

RS4 is currently being widely studied and applied in routine food products. It is formed using chemical modification methods, such as etherification, esterification and cross-linking reactions. Cross-linking treatments are usually used in the chemical modification of starch. During the cross-linking reaction, cross-linking agents are introduced into the intermolecular bridges between biopolymer layers to undergo chemical reactions, such as esterification reaction and etherification, which may change the overall structural properties and surface chemistry of the polymer backbone (3). The cross-linking agents commonly used in this reaction are sodium trimetaphosphate (STMP), sodium tripolyphosphate (STPP), epichlorohydrin and phosphoryl chloride (4). Phosphoryl chloride reacts violently with water and poses certain safety hazards.Although epichlorohydrin has the advantages of mild reaction, easy control and excellent cross-linking effect, it is toxic by oral and nasal inhalation and skin absorption. STMP and STPP are nontoxic and safe with low costs, controllable degrees of substitution, ability to change physical and chemical properties even at low substitution, and small structural changes of starch chain bases. The cross-linking reaction results in the starch structure being strong and dense, reduces the transparency of the paste, increases the resistance of the starch granules to acid, heat and shear, and reduces their tendency to dissolve and swell (5). Sandhu et al. (6) prepared cross-linked sorghum starch with different doses (0.1–1.0%) of epichlorohydrin as cross-linker and showed that its amylose content, swelling power and solubility decreased as the amount of cross-linker increased compared with raw starch. The surface of cross-linked sorghum starch is rough, with cavities and cracks. Broad bean starch with different concentrations (1, 3, and 5%) STMP as a cross-linking agent was formed by Sharma et al. (7). The cross-linked starch has a higher phase transition temperature and enthalpy of pasting (ΔH) compared with the raw starch, indicating a denser internal structure of the starch granules. The content of RS increases along with the concentration of cross-linking agent, indicating limitations in the actions of digestive enzymes.

Although much research has been conducted on the preparation and characterization of cross-linked starches, it is meaningful to study their structure-phosphorylation-function relationships in depth. No studies on the modification of lotus seed starch by cross-linking have been performed. Thus, here, lotus seed starch was reacted with different doses of cross-linking agents (STMP/STPP) in an alkaline environment to form lotus seed cross-linked resistant starches (LSCSs) with different degrees of cross-linking. The aim was to characterize their structural properties and to investigate the physicochemical properties as well as *in vitro* digestibility of LSCSs prepared by the addition of different cross-linking agents.

Materials and methods

Materials

Lotus seed starch (Green Field Food Co., Ltd., Fujian, China) was isolated as described previously (8). Sodium trimetaphosphate (STMP) and sodium tripolyphosphate (STPP) were obtained from China National Pharmaceutical Group Chemical Reagent Co. The α-amylase and glucose amylase for *in vitro* digestibility studies were provided by Shanghai Yuanye Biotechnology Co.

Preparation of lotus seed cross-linked resistant starch

LSCSs was prepared using the methodology of Carmona-Garcia et al. (9) with slight modifications. Lotus seed starch (20 g) was dispersed in water (30 mL), mixed with Na_2SO_4 (2 g), and the pH adjusted to 11.5 using NaOH (1 mol/L). Then, 0%, 1%, 2%, 4%, 6%, 8%, 10%, and 12% (w/w) of mixed cross-linking reagents (STMP/STPP, 99:1) were added independently, and stirred at 50°C for 4 h in a water bath. Then, HCl (1 mol/L) was used to adjust the pH to 6.5, and the starch slurry was washed with distilled water until neutralization. Samples were centrifuged two to three times at 3,000 × *g*, then hot air-dried at 45°C for 24 h. These samples were designated as LS-(0, 1, 2, 4, 6, 8, 10, and 12) CS, respectively.

Degree of cross-linking

The total phosphorous content of each cross-linked starch was determined as previously described (10). The samples (0.5 mg) were digested with a mixture of concentrated nitric acid and concentrated sulfuric acid. The absorbance of the solution at 825 nm was determined spectrophotometrically. The absorbance of the measured solution was compared with the calibration curve to determine the phosphorous content, and the phosphorous content was calculated using Eq. (1). The

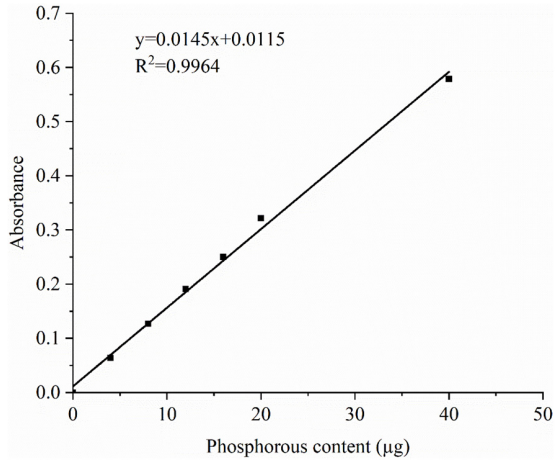

FIGURE 1
Standard curve of the phosphorus content.

phosphorous content was used to express the degree of cross-linking. Standard curve of the phosphorus content is shown in **Figure 1**

$$Phosphorous\ content\ (\%) = \frac{M_1 \times V_0 \times 100}{M_0 \times V_1 \times 10^6} \quad (1)$$

where M_1 (μg) represents the phosphorus content of the sample solution determined from the standard curve, V_0 (mL) represents the volume of the sample solution, M_0 (g) represents the mass of the test sample and V_1 (mL) represents an equal volume of sample solution for determination.

Scanning electron microscopy (SEM)

Scanning electron micrographs of starch samples were obtained by SEM (PHILIPS = XL30 ESEM, Philips-FEI, Netherlands) with a magnification of 5,000× operating at an accelerating voltage of 6.0 kV, as described by Lin et al. (11) with some modifications. A small amount of sample was uniformly distributed on the conductive adhesive metal platform and gold sprayed.

X-ray diffraction

X-ray diffraction patterns and relative crystallinities of the samples were determined using an X-ray diffractometer (Xpert 3; Analyx Corp. Ltd., Boston, MA, United States), as described by Zhang et al. (1), with some modifications. The diffraction angle was scanned from 5°to 50°at a scanning rate of 5°/min, with a target voltage of 40 kV and a current of 200 mA. The degrees of crystallinity were calculated by Eq. (2).

$$Crystallinity(\%)\ \frac{Ac}{Aa+Ac} \times 100\% \quad (2)$$

where *Ac* represents the crystalline area on the X-ray diffractogram, and *Aa* represents the amorphous area on the X-ray diffractogram.

Fourier transform infrared (FT-IR) spectroscopy

The FT-IR spectra of the samples were measured using an FT-IR spectrometer (Avatar 360, Thermo Nicolet Corporation Ltd., Madison, WI, United States). The starch samples were mixed well with dried KBr at a ratio of 1:100, ground in an agate mortar under an IR lamp and pressed into round thin slices. The scanning wave number range was 400–4,000 cm^{-1} with a resolution of 4 cm^{-1} and 32 scans.

^{31}P NMR spectroscopy

^{31}P NMR spectra were obtained using an NMR spectrometer (Avance III 500, Bruker Ltd., Karlsruhe, Germany) by solid state resonance, as described by Dong & Vasanthan (2), with some modifications. Pure solid samples were analyzed without any treatment. The spectrometer was configured for a frequency analysis of 161.67 MHz at room temperature, using a double-resonance probe with a CP/MAS detection system.

Swelling power and solubility

Swelling power and solubility were measured in accordance with a modified method of Miaomiao (12). The samples (0.4 g) were mixed with water (40 mL), heated, and stirred in a 95°C water bath for 30 min. They were then cooled to room temperature, centrifuged at 3,000 × *g* for 30 min, and the weights of the dissolved pellet and the supernatant after complete evaporation were directly measured. Swelling power and solubility were calculated using Eqs. (3) and (4), respectively.

$$\text{Solubility}(\%) = \frac{A}{W} \times 100\% \quad (3)$$

$$\text{Swelling power}(g/g) = \frac{P}{W}(1 - \text{Solubility}) \quad (4)$$

where *W* (g) represents the weight of a starch sample; and *A* and *P*(g) represent the weights of the dried supernatants and swollen granules respectively

Differential scanning calorimetry (DSC)

The thermal properties of the samples were measured using a differential scanning calorimeter (DSC-Q2000 TA Instruments, New Castle, DE, United States), as described previously (13). Thermal parameters, including melting enthalpy (ΔH), onset temperature (T_o), peak temperature (T_p) and conclusion temperature (T_c), were recorded.

In vitro starch digestibility

The *in vitro* digestibility of starch was analyzed in accordance with the method of Zheng et al. (14) with some modifications. The samples (0.2 g) were dispersed in sodium acetate buffer (10 mL, pH = 5.2) and incubated at 37°C for 20 min. Then, a mixture (10 mL) of α-amylase (200 U/mL) and amyloglucosidase (160 U/mL) was added and incubation continued in a 37°C water bath with shaking (100 rpm/min). At different time points (0, 20, 40, 60, 90, 120, 150, and 180 min) starch digest (0.5 mL) was aspirated and mixed with 2 mL of anhydrous ethanol to inactivate the enzymes, followed by the addition of distilled water (4 mL) and dilution to 5 mL for the determination of sugar content using the glucose oxidase method. The hydrolysis rate, rapidly digestible starch (RDS), slowly digestible starch (SDS) and resistant starch (RS) contents were calculated using Eqs. (5), (6), (7), and (8), respectively.

$$Hydrolysis\ rate(\%) = \frac{\mathrm{Gt}}{\mathrm{TS}} \times 0.9 \times 100\% \quad (5)$$

$$RSD(\%) = \frac{G_{20\mathrm{min}} - G_{0\mathrm{min}}}{\mathrm{TS}} \times 0.9 \times 100\% \quad (6)$$

$$SDS(\%) = \frac{G_{120\mathrm{min}} - G_{20\mathrm{min}}}{\mathrm{TS}} \times 0.9 \times 100\% \quad (7)$$

$$RS(\%) = (1 - \mathrm{RDS} - \mathrm{SDS}) \times 100\% \quad (8)$$

where Gt represents the glucose release from hydrolysis at time t, G_{0min} represents the free glucose content at 0 min of digestion, G_{20min} represents the glucose release at 20 min of digestion, G_{120min} represents the glucose release at 120 min of digestion, and TS represents the weight of the starch sample.

Statistical analysis

All the experiments were repeated at least three times. Experimental graphics were processed using Origin 9.0 (OriginLab Corporation, Northampton, MA, United States). Data were analyzed and statistical significances were determined using DPS 9.5 (Science Press, Beijing, China) ($p < 0.05$).

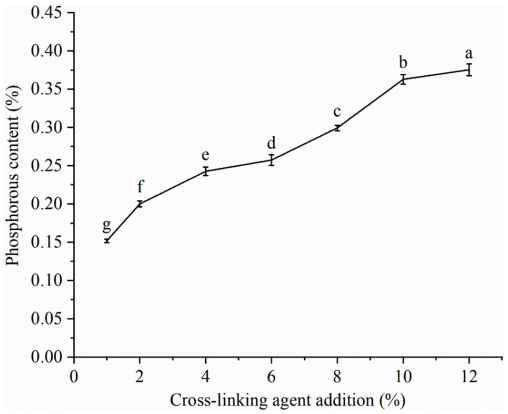

FIGURE 2
Phosphorous content of lotus seed cross-linked resistant starch. Different lowercase letters represent significant differences ($p < 0.05$).

Results and discussion

Crosslinking degree of lotus seed cross-linked resistant starch

The effect of cross-linking agent (STMP/STPP) addition on the degree of cross-linking of LSCSs is shown in Figure 2. The combined phosphorous content showed an obvious increasing trend along with the increased addition of cross-linking agent. When the cross-linking agent content was 12%, the amount of combined phosphorus in the starch was 0.38% ± 0.008%, which did not exceed the upper limit for food safety (0.4%) (15). The effects of different cross-linking agent additions on the crosslinking degree in three crystal forms (A, B and C) of starch have been investigated by Kou and Gao (16). They demonstrated that the phosphate group of STMP/STPP molecules covalently bound with the ionized hydroxyl group of the anhydroglucose unit of starch. The phosphorus content is a value that indirectly indicates the degree of cross-linking. This is because as the amount of cross-linking agent added increases, the more phosphate groups of STMP/STPP molecules involved in the cross-linking reaction, the more phosphorus content in the generated products (17). LSCSs had the highest degree of cross-linking when the cross-linking agent content was 12%. This was in agreement with the results of Sharma et al. (7). They cross-linked broad bean starch at different levels (1, 3, and 5%) using STMP as a cross-linking agent and found that the degree of cross-linking increases along with the cross-linking agent's level.

Scanning electron microscope of lotus seed cross-linked resistant starch

Scanning electron micrographs of LSCSs are shown in Figure 3. The starch granule structure of LS-0CS was

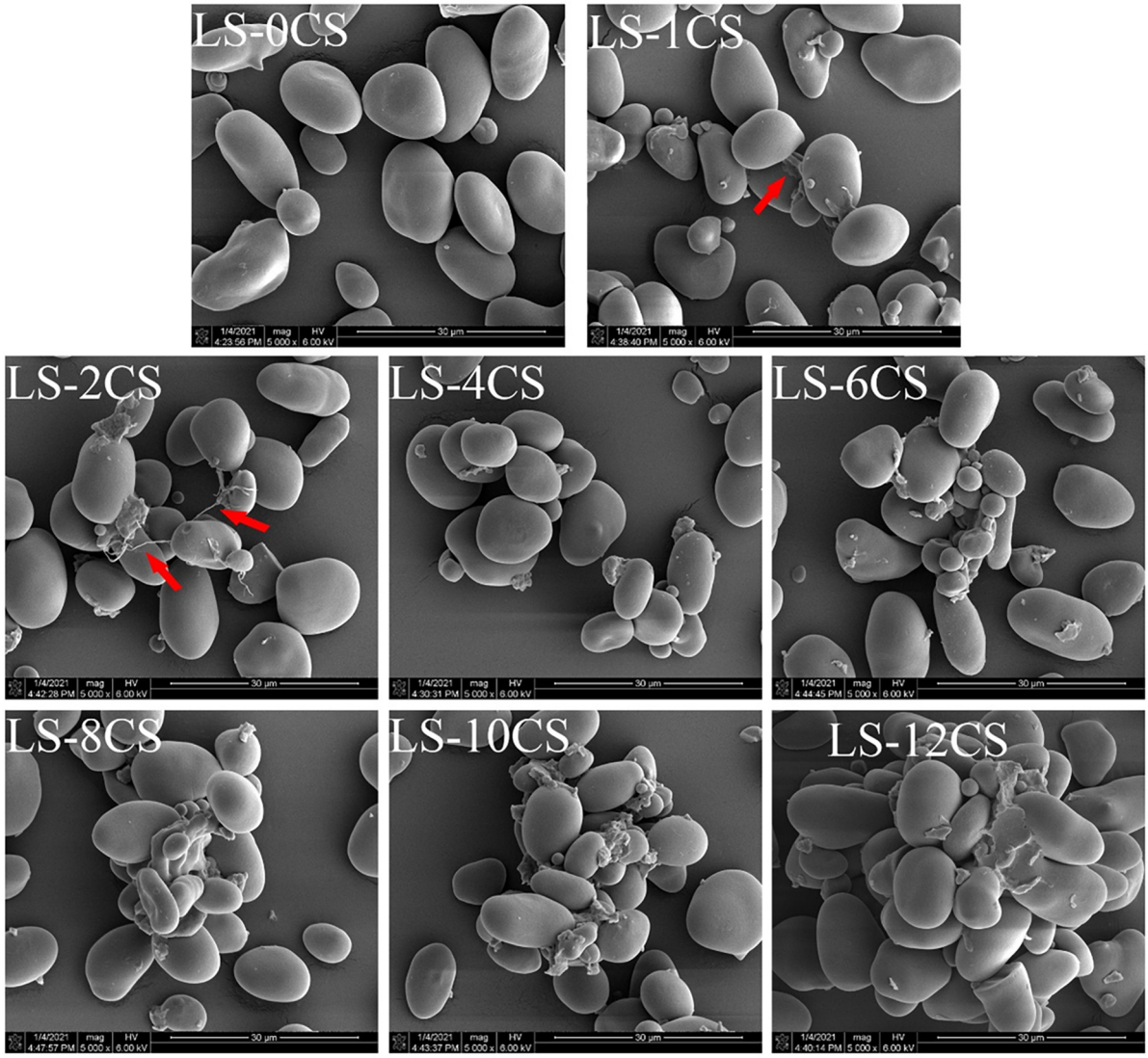

FIGURE 3
Scanning electron microscope images of lotus seed cross-linked resistant starch samples.

complete, circular or oval in shape, with a smooth surface, whereas those of other LSCSs did not change, which indicated that the cross-linking reaction did not change their granular morphology. The granular morphology of LS-0CS was consistent with that of natural lotus seed starch (1). However, adhesion between the starch granules of LS-1CS and LS-2CS was clearly observed owing to the crosslinking reaction between the starch and the cross-linking agent (See the arrow), which resulted in the formation of a "bridge", and promoted adhesion, between the starch molecules. The phenomenon in the present study was consistent with the results reported by Chen et al. (18), in which cross-linked starches were prepared by cross-linking kudzu starch with STMP. They found that starches with different degrees of cross-linking were all similar to the raw starch in terms of granular morphology, and granular adhesion was also observed. Here, the starch granules of LS-4CS started to agglomerate owing to the adhesion phenomenon, and the degree of agglomeration between LSCSs starch granules became stronger as the degree of cross-linking increased, which may result from the introduction of cross-linking agent. Functional groups change the intermolecular interactions between starch chains and connect starch molecules to form spatial network structures. More functional groups were introduced as the cross-linking degree increased, which resulted in more starch molecules being connected and a tighter spatial network structure. Consequently, the degree of agglomeration was greater.

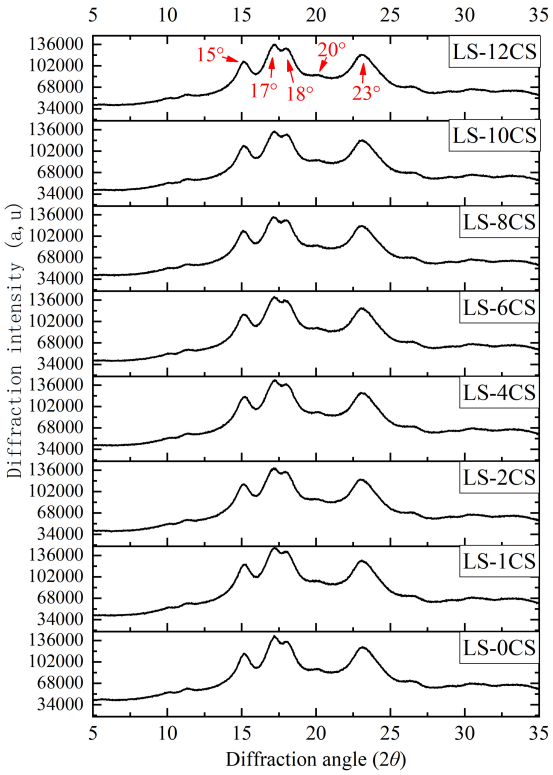

FIGURE 4
X-ray diffraction patterns of lotus seed cross-linked resistant starch samples.

Crystal structure analysis of lotus seed cross-linked resistant starch

On the basis of the source, a natural starch crystal structure is categorized as A, B, C or V type. The characteristic diffraction peaks of the crystalline structure of A-type are at 15°, 17°, 17.8°, and 23°(2θ), and the characteristic diffraction peaks of the crystalline structure of B-type are at 5.6°, 17°, 19.5°, 22°, and 24° (2θ) (19). The crystalline structure of C-type is a mixture of A-and B-crystalline structures, containing characteristic peaks of both crystalline structures (20). Previous studies have shown that natural lotus seed starch is a C-type crystal structure with main diffraction peaks at 14.93°, 17.03°, and 23.02° (2θ) (1).

The X-ray diffraction pattern of LSCSs is shown in **Figure 4**. All the starch samples had obvious diffraction peaks near 15°, 17°, 18°, and 23° (2θ), and a weak diffraction peak at 20° (2θ), which indicated that all the starch samples contained characteristic peaks of the crystalline structures of A- and B-types, making them C-types. This was in accordance with the results of a previous study (1). The positions of the main X-ray diffraction peaks of LSCSs were not affected by the cross-linking reaction compared with LS-0CS, which did not change with increasing degree of cross-linking, because the cross-linking agent acted as a bridge to shorten the distance between starch molecules without changing the crystallization structure within the starch granules. Additionally, the cross-linking reaction mainly occurred in the amorphous regions on the starch granules that were easily exposed to the cross-linking agent. Thus, the cross-linking reaction did not change the crystal type of the starch granule. This conclusion is consistent with a previous report by Yang et al. (21). Moreover, Falsafi et al. (22) prepared cross-linked starches at different pH values (9–12), different cross-linker concentrations (STMP/STPP 99:1, 5–15%) and under sonication and conventional treatment conditions. They found that the cross-linking reaction did not affect the crystal type of the corn starch compared with the raw starch, which was further evidence that the cross-linking reaction occurred mainly in the amorphous region of the granule structure.

The relative crystallinity of LSCSs samples are shown in **Table 1**. Compared with LS-0CS, the crystallinity of the rest of LSCSs was significantly reduced. The crystallinity levels of LS-10CS and LS-12CS were the lowest, which indicated that the crystallinity decreased as the cross-linking increased, presumably due to chemical modifications, and that crystal structure changes occurred during the cross-linking process. The disorder of chain arrangements was caused by substituting the hydroxyl group of starch with phosphate, but the disruption of the crystalline region was not great enough to change the crystalline shape of starch because of the low cross-linking degree. These results were consistent with the previous results reported by Chen et al. (18), which showed that compared with the native starch, the crystallinity of cross-linked starch decreased.

Fourier transform infrared (FT-IR) spectroscopic analysis of lotus seed cross-linked resistant starch

The variations in helical structures, chain conformations and crystal forms of starches alter their absorption of infrared energy. Therefore, the changes in the molecular structure of different LSCSs were analyzed using FT-IR spectroscopy, as shown in **Figure 5**. The extreme broad band at approximately 3,300–3,500 cm^{-1}, which was attributed to inner- and intro-hydroxyl group stretching vibration, was observed in all the starches. The band at 2,930 cm^{-1}, which was strong and sharp, represents the anti-symmetry stretching vibration of the carbon-hydrogen bond (23). Because of the H_2O bending vibration, and given that the hydroxyl groups in water molecules were absorbed by starch, the absorption at 1,640 cm^{-1} is a characteristic absorption band of starch. The shapes and positions of the spectral peaks of all the LSCSs were almost the same. The molecular structures of the samples remained unchanged after the cross-linking treatment, but further observations revealed that the degree of O-H stretching

TABLE 1 Relative crystallinity levels of lotus seed cross-linked resistant starch samples.

Sample	LS-0CS	LS-1CS	LS-2CS	LS-4CS	LS-6CS	LS-8CS	LS-10CS	LS-12CS
Relative crystallinity (%)	32.80 ± 1.13^{a}	30.03 ± 0.95^{b}	29.73 ± 1.12^{bc}	29.63 ± 0.64^{bc}	29.47 ± 0.55^{bc}	29.10 ± 0.42^{bc}	28.20 ± 0.57^{c}	28.15 ± 0.21^{c}

Different superscript letters indicate significant differences ($p < 0.05$).

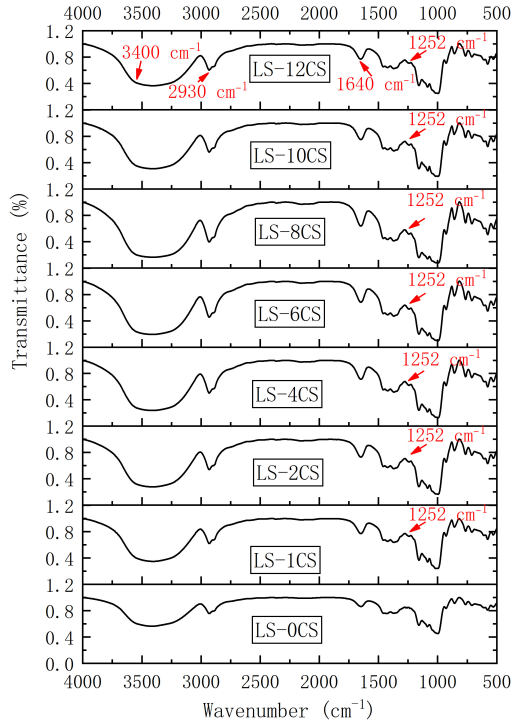

FIGURE 5
FT-IR spectroscopy of lotus seed cross-linked resistant starch samples.

vibration near 3,400 cm^{-1} of the LSCSs changed and the intensity of the peak weakened compared with LS-0CS. This indicated that the alcoholic hydroxyl group of the starch was covalently bound to the phosphate group of the crosslinking agent. This result was in accordance with the reports of Xie et al. (4). A new peak at 1,250 cm^{-1} appeared in the LSCSs, and it was characteristic of P = O bonds in crosslinked starch, which confirmed that the starch samples had reacted with STMP/STPP. This was consistent with the results reported by Shalviri et al. (24). Moreover, when Ashwar et al. (23) prepared rice crosslinked starch, the appearance of P = O at 1,244 cm^{-1} was also observed by FT-IR spectroscopy.

^{31}P NMR of lotus seed cross-linked resistant starch

During the reaction of starch with cross-linking agents, the starch phosphate is formed (25). The starch phosphate content was adjusted by controlling the degrees of starch esterification and crosslinking, which in turn improved the functional properties of the starch. The ^{31}P NMR spectra of lotus seed cross-linked resistant starches are shown in **Figure 6**. The signal peaks at -10 ppm to -5 ppm, -5 ppm to 1 ppm, and 3.6 ppm to 5.2 ppm were attributed to the structures of monostarch diphosphate (MSDP), distarch monophosphate (DSMP) and monostarch monophosphate (MSMP), respectively, as studied previously (5).

The LSCSs had different signal peaks compared with LS-0CS, indicating phosphate starch ester generation, which further confirmed the occurrence of the cross-linking reaction. This was consistent with the results of the FT-IR spectroscopy. LS-1CS and LS-2CS had weak signals at 4.7 ppm, and LS-4CS, LS-6CS and LS-8CS had weak signals at 3.6 ppm. The signal peak of MSMP was hardly observed in LS-10CS and LS-12CS. In the other LSCSs, a small amount of MSMP production occurred. Moreover, the MSMP signals at 4.7 ppm, 4.4 ppm, and 3.6 ppm correspond to the phosphorylation of hydroxyl groups at C-2, C-3, and C-6, respectively (26). Therefore, the MSMP produced in LSCSs was mainly located at C-6 and C-3 of the glucose unit. This indicated that most of the cross-linkages formed in MSMP were between two glucose residues located on different starch chains, and a small portion of cross-linkages may have formed between two glucose residues in the same starch chain. Presumably, because MSMP was unstable, LS-10CS and LS-12CS did not produce signal peaks in the range of 3.6 ppm to 5.2 ppm, which was consistent with the previous results reported by Sang et al. (27), who found that after stirring wheat 10.5 in a slurry at pH 11.5 for 3 h at 45°C, MSMP signal peaks of wheat starch with a high degree of cross-linking disappeared completely.

The LSCSs, except LS-1CS and LS-2CS, generated weak signals in the range of -10 ppm to -5 ppm, indicating that a small amount of MSDP was generated. During the reaction of starch with cross-linker (STMP/STTP) under alkaline conditions, the ring-opening attack of starch alcoholate ions on the cross-linker first formed mono-amyl triphosphate, which was unstable during the synthesis reaction. It had four negatively charged ionized hydrogens, and all three phosphoryl groups on its triphosphoryl chain had a strong ionizable acidic OH. When hydroxide or starch alcoholate ions react with monostarch triphosphate, pyrophosphate is more likely to detach from the group than orthophosphate, which leads to the reaction of an RO- or OH- ion with the α-phosphorous of the triphosphonyl group to form DSMP or MSMP, respectively. With a further

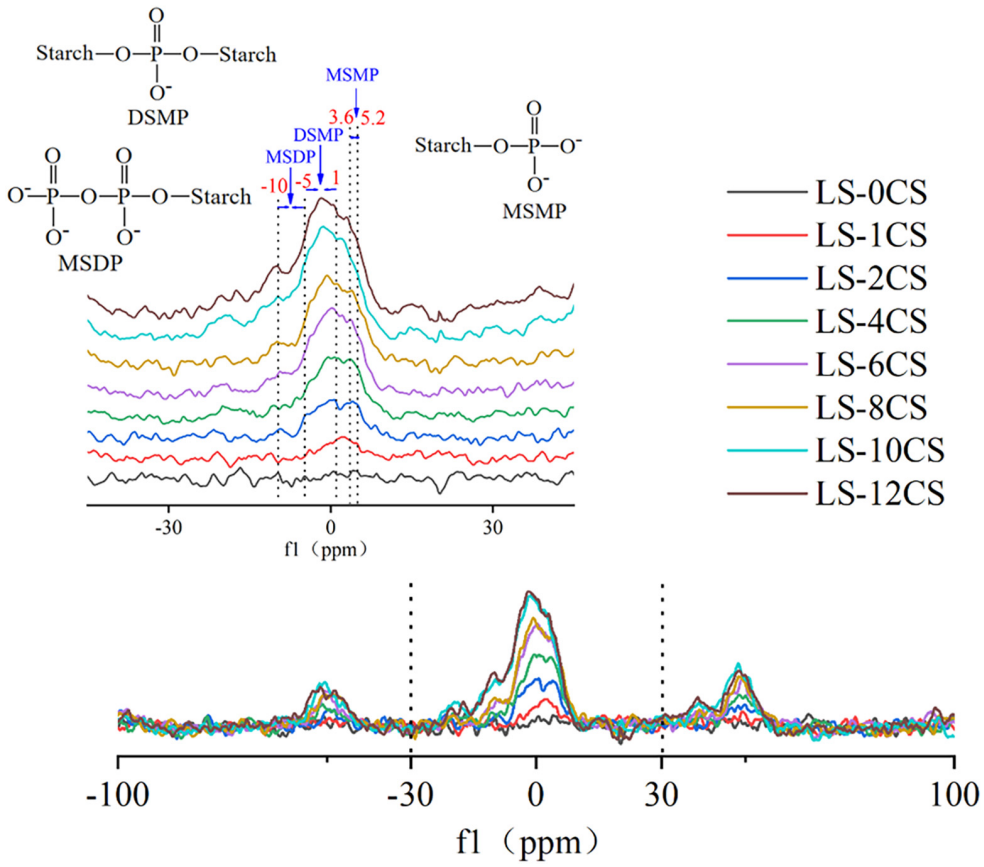

FIGURE 6
^{31}P NMR of lotus seed cross-linked resistant starch samples.

reaction, the γ-phosphate group exfoliates, which in turn generates MSDP. Thus, when a small amount the cross-linking agent was added, the cross-linking reaction was not strong enough to generate MSDP.

The LSCSs had strong signals in the range of -1 to 0 ppm and a weak signal in the range of 0 to 1 ppm, which indicated that the cross-linking reaction mainly produced DSMP. A stronger signal in the -1 to 0 ppm range occurred as the degree of cross-linking increased, leading to a greater content of DSMP. Because the hydroxyl groups at C-6 and C-3 were more reactive to the cross-linking reagent than those at C-2, DMSP may only occur within the hydroxyl groups at C-6 and C-3. Lack et al. (28) found that the DSMP signal in the range of -1 to 0 ppm indicated a cross-linking reaction between two different starch molecules, and the DSMP signal in the range of 0 to 1 ppm was a cross-linking reaction within the starch molecule, meaning between the hydroxyl groups of the glucose part of the same chain. This indicated that the generation of DMSP in this study was mainly a cross-linking reaction between the lotus starch molecules. Thus, the cross-linking reaction under alkaline conditions could induce the existing MSDP and MSMP to form new cross-linked ester bonds with hydroxyl groups, increasing the DSMP level. Moreover, as shown in Figure 5, as the crosslinking degree increased, the peak strength of DMSP in starch was stronger and the specific gravity of DMSP was larger. The covalent bonds formed by phosphate groups are mainly composed of DMSP (29), and combined with the phosphorous spectral analysis in this study, DMSP was presumably closely related to the physicochemical and digestive properties of the LSCSs.

Swelling power and solubility of lotus seed cross-linked resistant starch

The swelling power and solubility indicate the magnitude of starch chain interactions within the amorphous and crystalline regions, respectively (30). The swelling power of starch granules is the characteristic of a disordered crystalline region and consequent association between hydroxyl groups and water molecules via hydrogen bonding. The solubility levels and swelling powers of the LCSCs under heating treatment are shown in Figure 7. Compared with LS-0CS, the solubility of the LSCSs were all significantly lower, with

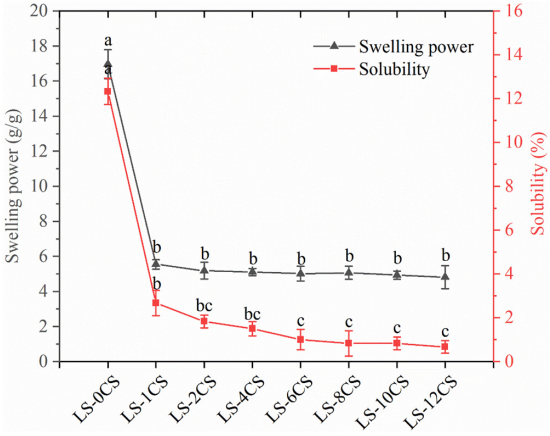

FIGURE 7
Swelling powers and solubility levels of lotus seed cross-linked resistant starch samples. Different lowercase letters represent significant differences ($p < 0.05$).

LS-6CS, LS-8CS, LS-10CS, and LS-12CS having significantly lower solubility levels than LS-1CS. Compared with LS-0CS, the crystallinity of the LSCSs were also all significantly lower. This indicated that the decrease in solubility was related to crystallinity. These results were consistent with the previous results reported by Chen et al. (18) in which the decrease in crystallinity contributes to the decrease in starch granule solubility. According to the ^{31}P NMR analysis, the higher cross-linked LSCSs contained more phosphate groups forming covalent bonds, and the specific gravity of DMSP was greater. Additionally, the starch molecules were strengthened by covalent bonding, which caused a significant decrease in solubility. Shi et al. (12) prepared pea cross-linked starch using different concentrations of cross-linking agents (STMP/STPP, 99:1, w/w). They found that the solubility of pea cross-linked starch was lower than that of natural starch and that it decreased as the amount of cross-linking agent added increased.

The swelling power of LSCS was also significantly lower than that of LS-0CS because the cross-linking reaction enhanced the intra- and intermolecular bonds between amylose and amylopectin, increasing the density of starch by binding the starch chains together, decreasing the mobility of the macromolecular chains and the degree of decomposition of starch granules during pasting, which limited the expansion of starch granules. However, there were no significant differences among the swelling powers of the LSCSs, indicating that within a certain range, the leaching of starch molecules from the starch granules was not significantly affected owing to the increase in cross-linking. Because the hydrogen bond in starch was broken during the pasting process and replaced by hydrogen bond with water, the FT-IR spectroscopy showed that the peak of LS-0CS located at 3,400 cm^{-1} was related to the hydroxyl stretching vibration of free and hydrogen-bonded hydroxyl groups, and the cross-linking reaction weakened the hydrogen bond during the pasting process, which was not easily replaced by the hydrogen bond of water. Thus, the starch granules remained stable and did not easily swell. These results agreed with that of Chen et al. (18). They cross-linked kudzu starch with STMP at different temperatures to obtain cross-linked kudzu starches with different degrees of cross-linking, and the resulting starches' swelling powers were significantly lower than that of the original starch. Additionally, the swelling power did not change significantly as the degree of cross-linking increased.

Thermal stability of lotus seed cross-linked resistant starch

The thermodynamic parameters of the LCSCs are shown in Table 2. Compared with LS-0CS, the phase transition temperatures of the LSCSs increased, with the T_0 of LS-12CS being significantly higher than those of LS-1CS, LS-2CS, LS-4CS, and LS-6CS, and the T_c and T_p values of LS-6CS, LS-8CS, LS-10CS, and LS-12CS being significantly higher than those of LS-1CS, LS-2CS, and LS-4CS. This indicated that higher temperatures were required for LSCSs pasting owing to the covalent bonds formed by phosphate groups in the LSCSs that strengthened the bonding between starch molecules to different degrees. Additionally, the cross-linking treatment inhibited the melting of crystals in starch granules and tightened their lattice structures, which increased the pasting temperature. As indicated by the ^{31}P NMR analysis, the covalent bonds formed by phosphate groups were mainly composed of DMSP (29). The specific gravity of DMSP increased along with the degree of cross-linking; therefore, LS-12CS had the highest phase transition temperature and required the highest pasting temperature. The transition temperature range of starch (T_c–T_0) is a measure of the integrity of the microcrystalline structure of amylopectin. The higher the values of T_c–T_0, the wider the heat absorption peak (31). Compared with LS-0CS, the T_c–T_0 values of the LSCSs were significantly higher, with the T_c–T_0 values of LS-12CS being significantly higher than those of LS-1CS and LS-2CS, which implied that the amylopectin microcrystals were more uniform after cross-linking treatment. These results were consistent with the study of Dong and Vasanthan (32), in which broad bean cross-linked and pea cross-linked starches were prepared, and the DSC showed that the T_0, T_p, T_c, and T_c–T_0 values of the natural bean starch were significantly lower than those of the cross-linked starch.

The energy required for the dissociation of the crystalline double helix is represented as ΔH. Compared with LS-0CS and LS-1CS, the ΔH values of the remaining LSCSs were significantly lower and the ΔH decreased significantly as the degree of cross-linking increased. This indicated that less thermal energy was required to melt the double helixes of the

TABLE 2 Thermal stability levels of lotus seed cross-linked resistant starch samples.

Sample	T_o (°C)	T_p (°C)	T_c (°C)	T_c-T_o (°C)	Δ H_1 (J/g)
LS-0CS	67.71 ± 0.16^{d}	74.58 ± 0.10^{e}	79.40 ± 0.21^{c}	11.70 ± 0.37^{c}	16.41 ± 0.03^{a}
LS-1CS	68.12 ± 0.18^{cd}	76.29 ± 0.14^{d}	81.70 ± 0.16^{b}	13.59 ± 0.02^{b}	16.28 ± 0.04^{a}
LS-2CS	68.27 ± 0.11^{bcd}	76.57 ± 0.11^{c}	81.90 ± 0.16^{b}	13.63 ± 0.04^{b}	14.36 ± 0.07^{b}
LS-4CS	68.42 ± 0.15^{bc}	76.96 ± 0.07^{b}	82.11 ± 0.10^{b}	13.70 ± 0.05^{ab}	13.71 ± 0.06^{c}
LS-6CS	68.51 ± 0.21^{bc}	77.38 ± 0.13^{a}	83.04 ± 0.22^{a}	14.23 ± 0.01^{ab}	13.18 ± 0.05^{d}
LS-8CS	68.72 ± 0.42^{abc}	77.41 ± 0.08^{a}	83.09 ± 0.23^{a}	14.37 ± 0.65^{ab}	10.65 ± 0.06^{e}
LS-10CS	68.82 ± 0.40^{ab}	77.51 ± 0.12^{a}	83.20 ± 0.17^{a}	14.38 ± 0.57^{ab}	10.59 ± 0.04^{e}
LS-12CS	69.19 ± 0.25^{a}	77.52 ± 0.16^{a}	83.42 ± 0.13^{a}	14.53 ± 0.27^{a}	10.31 ± 0.10^{f}

Different superscript letters in the same column indicate significant differences ($p < 0.05$).

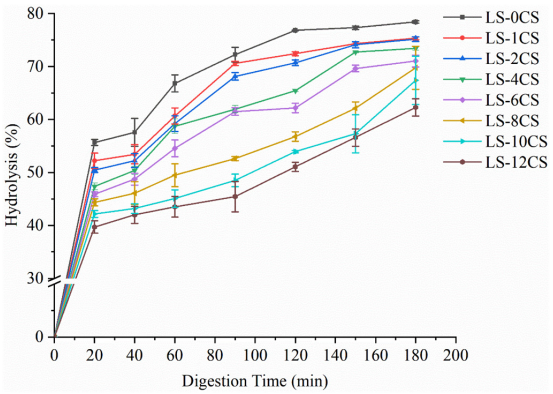

FIGURE 8
Hydrolysis rates of lotus seed cross-linked resistant starch samples.

LSCSs, probably due to the more complex and amorphous internal structures of cross-linked starches. These starch samples were not only connected by hydrogen bonding but also molecularly connected by cross-linking reactions, which was consistent with the change in the relative crystallinity calculated by X-ray diffraction. Similar findings were determined in cross-linked starches from common maize, broad beans and field peas (32), in which the cross-linking reaction increased the thermal stability, broadened the value of T_c–T_0 and decreased the ΔH value to varying degrees compared with natural starches.

In vitro digestion characteristics of lotus seed cross-linked resistant starch

The hydrolysis curves and digestion properties of the LSCSs are shown in Figure 8. Under the same digestion conditions, the hydrolysis rates of the LSCSs were lower than that of LS-0CS, with the most significant effect on LS-12CS after 120 min of digestion. This indicated that the hydrolysis effect of digestive enzymes on starch granules was significantly reduced by the cross-linking reaction, resulting in their lower digestibility levels. The hydrolysis patterns of the LSCSs per unit time showed that their digestibility decreased to different degrees with the length of the cross-linking reaction. This indicated that some of the hydroxyl groups of starch were replaced by phosphate ester bonds generated by the cross-linking reaction, and the presence of phosphate groups on the starch chains sterically hindered the formation of starch-amylase complexes. The abilities of digestive enzymes to enter the internal structures of starches were enhanced by the swelling of starch granules; consequently, the limited swelling of cross-linked starch inhibited its hydrolysis rate. Moreover, the SEM analysis revealed that the higher the degree of cross-linking, the stronger the agglomeration of starch granules, which to a certain extent inhibited the digestive enzymes. This was consistent with the results of Shi et al. (12), who cross-linked starch with different concentrations of STMP and STPP (99:1, w/w) and showed that the higher the degree of cross-linking, the more resistant the starch was to digestion by enzymes. This may also be related to various other factors, such as solubility and swelling power.

The starch fractions of the LSCSs are shown in Figure 9. According to a component availability study of the *in vitro* digestion of starch, starch can be classified into RDS (< 20 min), SDS (20–120 min) and RS (> 120 min) in accordance with the time of starch digestion (33). The modulating effect of the cross-linking reaction on the digestive fraction of lotus seed starch may be clarified by measuring and calculating the variation in the difference between the contents of each fraction of the starch samples. As observed in the Figure 8, the RS content was significantly increased in the LSCSs compared with LS-0CS, and the RDS and SDS contents of the LSCSs decreased with the length of the cross-linking reaction, whereas the RS content increased accordingly. In the cross-linking reaction, the amorphous region was preferentially bound by the phosphorylating reagent, resulting in a change in the starch structure, decreases in the RDS and SDS contents and a corresponding increase in the RS content. Among the various cross-linking reaction products of starch, DSMP

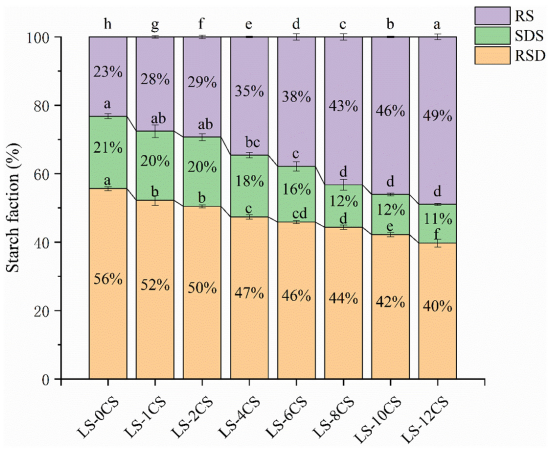

FIGURE 9
RDS, SDS, and RS contents of lotus seed cross-linked resistant starch samples. Different lowercase letters represent significant differences ($p < 0.05$).

was reported to limit the enzymatic action of starch in the presence of a limited number of combined phosphorous and contributed to the formation of indigestible starch fractions (2). According to the phosphorous spectral analysis, the specific gravity of DMSP increased along with the degree of cross-linking. Consequently, the RS content of LS-12CS was the greatest among the samples. In summary, the enzymatic resistance of cross-linked RS of lotus seeds was influenced not only by solubility and swelling power, but also by structural properties, such as starch granule morphology and crystal structure.

Conclusions

Different concentrations of cross-linking agents had significant effects on the structural properties and physicochemical properties of LSCSs, and the degree of cross-linking of LSCSs increased along with the addition of cross-linking agents. The cross-linked starches all exhibited appearances similar to the original starch, but the cross-linking agent played a "bridging" role, causing the granules to gradually aggregate, which resulted in more starch chains being "bound" together by the covalent bonds formed by the phosphate groups. The covalent bonds formed by the phosphate groups in the LSCSs were mainly composed of DMSP. The level of DMSP formed was correlated with the physicochemical properties of the LSCSs. Moreover, the cross-linking reaction mainly occurred in the amorphous regions. Compared with LS-0CS, the more complex and amorphous internal structures of LSCSs allowed the cross-linking reaction to raise the transition temperature, but lowered ΔH and the solubility, which was also related to the degree of LSCSs agglomeration. The RS increased along with the level of cross-linking, indicating a limitation for the digestive enzymes. The higher resistance of LS-12CS to digestion was not only related to its crystallinity, high DSMP specific gravity and other structural properties, but also to its low solubility. Based on its low solubility, heat resistance and high RS content, LS-12CS is a potential prebiotic for the food industry.

Data availability statement

The original contributions presented in this study are included in the article/supplementary material, further inquiries can be directed to the corresponding authors.

Author contributions

LL: writing the original draft, investigation, and methodology. SH and YL: conceptualization and software. BZ, YZ, and HZ: writing – review and editing and formal analysis. All authors contributed to the article and approved the submitted version.

Funding

This work was supported by the National Natural Science Foundation of China (grant number: 31972076), the National Science Foundation for Distinguished Young Scholars of Fujian Province (grant number: 2019J06012), and the Program for Leading Talent in Fujian Provincial University (grant number: 660160190).

Conflict of interest

The authors declare that the research was conducted in the absence of any commercial or financial relationships that could be construed as a potential conflict of interest.

Publisher's note

All claims expressed in this article are solely those of the authors and do not necessarily represent those of their affiliated organizations, or those of the publisher, the editors and the reviewers. Any product that may be evaluated in this article, or claim that may be made by its manufacturer, is not guaranteed or endorsed by the publisher.

References

1. Zhang Y, Zeng H, Wang Y, Zeng S, Zheng B. Structural characteristics and crystalline properties of lotus seed resistant starch and its prebiotic effects. *Food Chem.* (2014) 155:311–8. doi: 10.1016/j.foodchem.2014.01.036

2. Dong H, Vasanthan T. Amylase resistance of corn, faba bean, and field pea starches as influenced by three different phosphorylation (cross-linking) techniques. *Food Hydrocoll.* (2020) 101:105506. doi: 10.1016/j.foodhyd.2019.105506

3. Han X, Wen H, Luo Y, Yang J, Xiao W, Xie J. Effects of chitosan modification, cross-linking, and oxidation on the structure, thermal stability, and adsorption properties of porous maize starch. *Food Hydrocoll.* (2022) 124:107288. doi: 10.1016/j.foodhyd.2021.107288

4. Xie Y, Zhang B, Li M-N, Chen H-Q. Effects of cross-linking with sodium trimetaphosphate on structural and adsorptive properties of porous wheat starches. *Food Chem.* (2019) 289:187–94. doi: 10.1016/j.foodchem.2019.03.023

5. Miranda Sechi NDS, Marques PT. Preparation and physicochemical, structural and morphological characterization of phosphorylated starch. *Mater Res.* (2017) 20:174–80. doi: 10.1590/1980-5373-mr-2016-1008

6. Sandhu KS, Siroha AK, Punia S, Sangwan L, Nehra M, Purewal SS. Effect of degree of cross linking on physicochemical, rheological and morphological properties of Sorghum starch. *Carbohydr Polym Technol Appl.* (2021) 2:100073. doi: 10.1016/j.carpta.2021.100073

7. Sharma V, Kaur M, Sandhu KS, Godara SK. Effect of cross-linking on physico-chemical, thermal, pasting, in vitro digestibility and film forming properties of Faba bean (*Vicia faba L.*) starch. *Int J Biol Macromol.* (2020) 159:243–9. doi: 10.1016/j.ijbiomac.2020.05.014

8. Guo Z-B, Liu W-T, Zeng S-X, Zheng B-D. Effect of ultra high pressure processing on the particle characteristics of lotus-seed starch. *Chin J Struct Chem.* (2013) 32:525–32.

9. Carmona-Garcia R, Sanchez-Rivera MM, Mendez-Montealvo G, Garza-Montoya B, Bello-Perez LA. Effect of the cross-linked reagent type on some morphological, physicochemical and functional characteristics of banana starch (*Musa paradisiaca*). *Carbohydr Polym.* (2009) 76:117–22. doi: 10.1016/j.carbpol.2008.09.029

10. Wang S, Zhang B, Chen T, Li C, Fu X, Huang Q. Chemical cross-linking controls in vitro fecal fermentation rate of high-amylose maize starches and regulates gut microbiota composition. *J Agric Food Chem.* (2019) 67:13728–36. doi: 10.1021/acs.jafc.9b04410

11. Lin Y, Liu L, Li L, Xu Y, Zhang Y, Zeng H. Properties and digestibility of a novel porous starch from lotus seed prepared via synergistic enzymatic treatment. *Int J Biol Macromol.* (2022) 194:144–52. doi: 10.1016/j.ijbiomac.2021.11.196

12. Shi M, Gu F, Wu J, Yu S, Gao Q. Preparation, physicochemical properties, and in vitro digestibility of cross-linked resistant starch from pea starch. *Starch Starke.* (2013) 65:947–53. doi: 10.1002/star.201300008

13. Wang J, Jiang X, Guo Z, Zheng B, Zhang Y. Long-term retrogradation behavior of lotus seed starch-chlorogenic acid mixtures after microwave treatment. *Food Hydrocoll.* (2021) 121:106994. doi: 10.1016/j.foodhyd.2021.106994

14. Zheng Y, Zhang C, Tian Y, Zhang Y, Zheng B, Zeng H, et al. Effects of freeze–thaw pretreatment on the structural properties and digestibility of lotus seed starch–glycerin monostearin complexes. *Food Chem.* (2021) 350:129231. doi: 10.1016/j.foodchem.2021.129231

15. Herwick RP. Food and drug administration, journal of the American pharmaceutical association. *Am Pharm Assoc.* (1947) 8:157–60. doi: 10.1016/S0095-9561(16)31207-5

16. Kou T, Gao Q. New insight in crosslinking degree determination for crosslinked starch. *Carbohydr Res.* (2018) 458:13–8. doi: 10.1016/j.carres.2018.01.009

17. Lemos PVF, Opretzka LCF, Almeida LS, Cardoso LG, Silva JBAD, Souza COD, et al. Preparation and characterization of C-phycocyanin coated with STMP/STPP cross-linked starches from different botanical sources. *Int J Biol Macromol.* (2020) 159:739–50. doi: 10.1016/j.ijbiomac.2020.05.111

18. Chen B, Dang L, Zhang X, Fang W, Hou M, Liu T, et al. Physicochemical properties and micro-structural characteristics in starch from kudzu root as affected by cross-linking. *Food Chem.* (2017) 219:93–101. doi: 10.1016/j.foodchem.2016.09.128

19. Kong L, Lee C, Kim SH, Ziegler GR. Characterization of starch polymorphic structures using vibrational sum frequency generation spectroscopy. *J Phys Chem B.* (2014) 118:1775–83. doi: 10.1021/jp411130n

20. Man J, Cai J, Cai C, Xu B, Huai H, Wei C. Comparison of physicochemical properties of starches from seed and rhizome of lotus. *Carbohydr Polym.* (2012) 88:676–83. doi: 10.1016/j.carbpol.2012.01.016

21. Yang L, Zhou Y, Wu Y, Meng X, Jiang Y, Zhang H, et al. Preparation and physicochemical properties of three types of modified glutinous rice starches. *Carbohydr Polym.* (2016) 137:305–13. doi: 10.1016/j.carbpol.2015.10.065

22. Falsafi SR, Maghsoudlou Y, Aalami M, Jafari SM, Raeisi M. Physicochemical and morphological properties of resistant starch type 4 prepared under ultrasound and conventional conditions and their in-vitro and in-vivo digestibilities. *Ultrason Sonochem.* (2019) 53:110–9. doi: 10.1016/j.ultsonch.2018.12.039

23. Ashwar BA, Gani A, Gani A, Shah A, Masoodi FA. Production of RS4 from rice starch and its utilization as an encapsulating agent for targeted delivery of probiotics. *Food Chem.* (2018) 239:287–94. doi: 10.1016/j.foodchem.2017.06.110

24. Shalviri A, Liu Q, Abdekhodaie MJ, Wu XY. Novel modified starch–xanthan gum hydrogels for controlled drug delivery: synthesis and characterization. *Carbohydr Polym.* (2010) 79:898–907. doi: 10.1016/j.carbpol.2009.10.016

25. Zhao J, Chen Z, Jin Z, de Waard P, Buwalda P, Gruppen H, et al. Level and position of substituents in cross-linked and hydroxypropylated sweet potato starches using nuclear magnetic resonance spectroscopy. *Carbohydr Polym.* (2015) 131:424–31. doi: 10.1016/j.carbpol.2015.06.005

26. Sang Y, Seib PA, Herrera AI, Prakash O, Shi Y-C. Effects of alkaline treatment on the structure of phosphorylated wheat starch and its digestibility. *Food Chem.* (2010) 118:323–7. doi: 10.1016/j.foodchem.2009.04.121

27. Sang Y, Prakash O, Seib PA. Characterization of phosphorylated cross-linked resistant starch by 31P nuclear magnetic resonance (31P NMR) spectroscopy. *Carbohydr Polym.* (2007) 67:201–12. doi: 10.1016/j.carbpol.2006.05.009

28. Lack S, Dulong V, Picton L, Le Cerf D, Condamine E. High-resolution nuclear magnetic resonance spectroscopy studies of polysaccharides crosslinked by sodium trimetaphosphate: a proposal for the reaction mechanism. *Carbohydr Res.* (2007) 342:943–53. doi: 10.1016/j.carres.2007.01.011

29. Hong JS, Gomand SV, Delcour JA. Preparation of cross-linked maize (*Zea mays L.*) starch in different reaction media. *Carbohydr Polym.* (2015) 124:302–10. doi: 10.1016/j.carbpol.2015.02.022

30. Mehboob S, Ali TM, Sheikh M, Hasnain A. Effects of cross linking and/or acetylation on sorghum starch and film characteristics. *Int J Biol Macromol.* (2020) 155:786–94. doi: 10.1016/j.ijbiomac.2020.03.144

31. Vamadevan V, Bertoft E. Structure-function relationships of starch components. *Starch Starke.* (2015) 67:55–68. doi: 10.1002/star.201400188

32. Dong H, Vasanthan T. Effect of phosphorylation techniques on structural, thermal, and pasting properties of pulse starches in comparison with corn starch. *Food Hydrocoll.* (2020) 109:106078. doi: 10.1016/j.foodhyd.2020.106078

33. Tufvesson F, Wahlgren M, Eliasson AC. Formation of amylose-lipid complexes and effects of temperature treatment. Part 1. Monoglycerides. *Starch Starke.* (2003) 55:61–71. doi: 10.1002/star.200390018

frontiers | Frontiers in Nutrition

TYPE Original Research
PUBLISHED 15 August 2022
DOI 10.3389/fnut.2022.985929

OPEN ACCESS

EDITED BY
Yanjun Zhang,
Chinese Academy of Tropical Agricultural Sciences, China

REVIEWED BY
Yue Li,
Jiangnan University, China
Jiangping Ye,
Nanchang University, China
Xu Lu,
Fujian Agriculture and Forestry University, China

*CORRESPONDENCE
Chongxing Huang
huangcx21@163.com

†These authors have contributed equally to this work and share first authorship

SPECIALTY SECTION
This article was submitted to Food Chemistry, a section of the journal Frontiers in Nutrition

RECEIVED 04 July 2022
ACCEPTED 29 July 2022
PUBLISHED 15 August 2022

CITATION
Li B, Zhang Y, Luo W, Liu J and Huang C (2022) Effect of new type extrusion modification technology on supramolecular structure and *in vitro* glycemic release characteristics of starches with various estimated glycemic indices.
Front. Nutr. 9:985929.
doi: 10.3389/fnut.2022.985929

Effect of new type extrusion modification technology on supramolecular structure and *in vitro* glycemic release characteristics of starches with various estimated glycemic indices

Bo Li[1,2,3†], Yanjun Zhang[2,3†], Wanru Luo[1], Jin Liu[4] and Chongxing Huang[1*]

[1]College of Light Industry and Food Engineering, Guangxi University, Nanning, China, [2]Spice and Beverage Research Institute, Chinese Academy of Tropical Agricultural Sciences, Wanning, China, [3]Key Laboratory of Processing Suitability and Quality Control of the Special Tropical Crops of Hainan Province, Wanning, China, [4]Women's and Children's Hospital of Wanning, Wanning, China

Nowadays, the highly effective modified technology to starch with various digestibility is gaining interest in food science. Here, the interactions between glycemic release characteristics and fine supramolecular structure of cassava (ECS), potato (EPS), jackfruit seed (EJFSS), maize (EMS), wheat (EWS), and rice starches (ERS) prepared with improved extrusion modification technology (IEMS) were investigated. The crystalline structures of all extruded cooking starches changed from the A-type to V-type. IEMS-treated cassava, potato, and rice starches had broken α-1.6-glycosidic amylopectin (long chains). The others sheared α-1.4-glycosidic amylopectin. The molecular weight, medium and long chain counts, and relative crystallinity decreased, whereas the number of amylopectin short chains increased. The glycemic index (GI) and digestive speed rate constant (k) of ECS, EPS, EJFSS, and EWS were improved compared to those of raw starch. Although EMS and ERS had degraded molecular structures, their particle morphology changed from looser polyhedral to more compact with less enzymolysis channels due to the rearrangement of side chain clusters of amylopectin, leading to enzyme resistance. The starch characteristics of IEMS-treated samples significantly differed. EPS had the highest amylose content, medium chains, long chains, and molecular weight but lowest GI, relative crystallinity, and k. ERS showed the opposite results. Thus, IEMS may affect starches with different GIs to varying degrees. In this investigation, we provide a basis for wider applications of conventional crop starch in the food industry corresponding to different nutrition audience.

KEYWORDS

glycemic release rate, improved extrusion cooking technology, staple crop starch, fine supramolecular structure, principal component analysis

Highlights

- Various glycemic indices (GI) starches were treated by new extrusion cooking (IEMT).
- GI of IECT rice, maize starch was lower than the native, that differed with others.
- Crystal structure of IECT starches became V-type from A-type after IECT treatment.
- The degraded mode of amylose glycosidic bond was associated with amylose content.
- IECT starches showed lower molecular weight, fraction of long chain than the native.

Introduction

Starch is a major macronutrient required by humans and is frequently extracted from unripe fruit pulp, seeds, roots, tubers, stems, and grains of crops such as jackfruit, cassava, rice, wheat, potato, and maize. Because different starch sources have various molecular encapsulation reaction of glucan chains of amylopectin and amylose, starches are defined as $C_{A/B}$-types, A-types, and B-types based on their crystal structure (1). The Va, Vh and B+V-type crystal structure is usually characteristic of modified starch (2). Starches from different crops have unique supramolecular structures causing such foods to have variable digestibility (3). According to Li et al. (4), jackfruit seed and cassava starches are medium-level blood glucose foods, potato starch is a low-level blood glucose food, and starches of common staple crops such as rice starch are high-level blood glucose foods. This probably produced distinct modification mechanisms between them. However, most native starches are difficult to digest in the initial digestion stage because of their low rate of enzymatic hydrolysis (k), preventing timely nutrient release from native starches in the human body. Furthermore, native starches have a high weight-average molar mass (Mw), high amylopectin long-chain distribution, and high relative crystallinity (Rc), leading to a slow glycemic release. And it is difficult to maintain the necessary nutrition of the human body (2). Therefore, native starches should be modified to improve their digestion rate in the human intestine. The various glycemic release characteristic of cassava, potato, jackfruit seed, maize, wheat, and rice starches were due to the significantly different amylose content, crystalline structures, chain length distribution, molecule weight and particle morphology. This probably also might produce the distinct modification mechanisms between them (1, 4). In addition, based on Zhang et al. (2), extrusion modification could be used to prepare a pregelatinized starch. This kind of starch could use directly as an edible food to provide essential nutrients.

The supramolecular structures and digestibility characteristics of native starches can be changed during extrusion cooking, high-pressure microfluidization, hydrothermal treatment, and annealing treatment (5, 6). Extrusion cooking have been becoming a common modification technology, which was a continuously elevated temperature process with a fast-heating rate. During extrusion cooking process, the moistened expandable starch is physically swelled through an extremely high shear stress, temperature and pressure compared with those of other modification methods. Moreover, the improved extrusion modification technology was initially mentioned by Zhang et al. (7). It can alter the molecular structure of starch by using more mild extrusion cooking conditions (lower shear stress and temperature) and higher intensity of pressure than those of a common extrude. We previously developed an improved extrusion modification (IEMS) system as a gel-modification pattern for changing starch digestibility. This method can alter the molecular structure of starch because it uses a lower shear stress and temperature and higher pressure compared to that of many other approaches (1). According to Al-Rabadi et al. and Zhang et al., as the starch is sourced from diverse plant varieties, the changes of supramolecular structure, *in vitro* glycemic release rate, and estimated glycemic level of starch samples could vary greatly after treated by extrusion cooking. In our previous study, we used IEMS to explore the digestion mechanism of the resistant starch content in JFSS (5). However, the supramolecular structures and *in vitro* digestive kinetics of extruded cooking staple crop starch with various estimated glycemic indices have not been compared, limiting the exploitation and utilization of starch resources from staple crops. Based on the various digestibilities of extrusion cooking starch with various estimated glycemic indices, starch can be produced as an excellent base for thickeners, stabilizers, and potential wall materials for microencapsulation in starch-basis processing industries., to improve the rate of nutrient release from food.

Therefore, jackfruit seed (JFSS) and cassava, rice, wheat, potato, and maize starches were extracted and used to measure the molecular weight distribution, branching chain distribution of amylopectin, crystallization characteristics, amylose content, digestive kinetics, and estimated glycemic index after IEMS treatment. The possibly distinct *in vitro* digestive mechanism of starch with various glycemic indices prepared by IEMS was further analyzed. This study provides a basis for comprehensive

Abbreviations: ECS, extrusion cooking cassava starch; EPS, extrusion cooking potato starch; EJFSS, extrusion cooking jackfruit seed starch; EMS, extrusion cooking maize starch; EWS, extrusion cooking wheat starch; ERS, extrusion cooking rice starches; IEMS, improved extrusion cooking technology; DMSO, dimethyl sulfoxide; HI, hydrolysis index; GI, glycemic index; RDS rapidly digestible starch; SDS slowly digestible starch; RS, resistant starch; SDI, starch digestible index; C_{∞}, equilibrium concentration; k, enzymatic hydrolysis speed rate; Mw, weight-average molar mass; Mn, number-average molar mass; Rg, radius of gyration; Rc, relative crystallinity; PCA, principal component analysis.

application of starches of various digestibility levels in the food industry.

Materials and methods

Materials

Fruits of the Malaysia 1 jackfruit cultivar were collected in 2019 from the Xinglong Tropical Botanical plantation (Wanning, Hainan, China) and assigned voucher number 202009. Cassava, maize, potato, wheat, and rice were purchased from a local market (Nanning, Guangxi, China).

Preparation of different starches

Jackfruit seeds, cassava, maize, potato, wheat, and rice were pre-treated quickly after drying in a drying cabinet at 50°C. The pre-treated samples were milled with distilled water (1:3 w/w) for 2 min in a colloid grinder. Then pH of starch slurry was adjusted to 7.0, mixed with neutral protease solution (0.015% w/w) (Alphalase NP, 240,000 U/g, Sigma, St. Louis, MO, USA), and transferred into a constant-temperature shaking bed (60°C, 9 h and 150 rpm). The mixed solution was filtered through a filter cloth (200 mesh) and centrifuged (3,000 $\times g$, 5 min) to remove residual brown impurities. After repeated washing with distilled water, the sediment was collected. The centrifuged sediments were repeatedly cleaned and collected. The resulting wet starch was dried under vacuum (50°C) until the moisture content was lower than 13 g/100 g. After passing through a 200-mesh sieve, the dry starch was stored in a vacuum dryer until use (8).

Modification of different starches with IEMS

Extrusion modification experiments were conducted in a twin-screw extruder equipped with a barrel with self-adapting multiple-region temperature system (7). The length-width ratio of the extruder screw was approximately 19.5:1, and the diameter was 100 mm. The self-adapting multiple-region temperatures were adjusted to 50, 65, 85, 95, and 100°C, respectively. The starch samples with 30% w/v water prepared by that calculated water and the raw starch with certain quality (dry basis) were added to a flour mixing machine within the extrusion equipment (13 rpm, 5 min). The screw speed range was 25 rpm. The starch was filled into a revolving feed system at 13 rpm. The extrudates were cut with a rotary cutter at 6 rpm, dried under vacuum, and stored in a vacuum dryer. The extrusion-cooked JFSS, cassava, maize, potato, wheat, and rice starches were named as EJFSS, ECS, EMS, EPS, EWS, and ERS, respectively.

In vitro digestibility of extrusion-cooked starches of various estimated glycemic levels

The proportions of resistant starch (RS), slowly digestible starch (SDS), and rapidly digestible starch (RDS) were determined as described by Englyst et al. (9) with slight modifications. The mixed enzyme solution, which contained ≥225 U/mL of amyl-glucosidase and 20 U/mL of porcine pancreas α-amylase (Megazyme, Wicklow, Ireland), was transferred to 20 mL sodium acetate buffer (0.1 M, pH 5.2) with 1 g of starch. The mixed liquids were incubated in a constant temperature water bath (36.5–37°C, 180 rpm). The enzymes were inactivated by adding 70% ethanol (20 mL) to the supernatant (0.5 mL) at 20- and 120-min intervals. This solution was centrifuged (4,000 $\times g$, 10 min), and the supernatant was collected to determine the glucose content using a glucose oxidase-peroxidase method (Megazyme) and a spectrophotometer (UV-2700, Shimadzu, Kyoto, Japan) at 510 nm. The RDS, SDS and RS contents in extrusion-cooked starches were calculated as follows:

$$RDS\,(\%) = \frac{(G_{20} - G_F) \times 0.9}{TS}$$
$$SDS\,(\%) = \frac{(G_{120} - G_{20}) \times 0.9}{TS}$$
$$RS\,(\%) = \frac{[TS - (RDS + SDS)]}{TS}$$

where G_{20} (%) is the released content of glucose within 20 min, G_{120} (%) is the released content of glucose at 120 min, G_F (%) is the free glucose content, and TS (%) is the total starch content.

Characteristics of *in vitro* digestibility kinetics of starch

The *in vitro* digestibility kinetics of starch was determined as described by Goñi et al. (10) with slight modifications. 15-mL sodium acetate buffer solution was mixed with 200 mg starch (dry basis). Then Amyloglucosidase (15 U/mL) and porcine pancreatic α-amylase (290 U/mL) (total 10 mL) (Megazyme) and seven glass were added to that solution. The mixed liquids were reacted in a shaking bed (37°C, 150 rpm). At 10-, 20-, 30-, 60-, 90-, 120- and 180-min, absolute ethanol (4 mL) was added to the supernatant (0.5 mL). This solution was centrifuged at 6,000 $\times g$ for 15 min at 10°C, and the supernatant was transferred to glucose oxidase-peroxidase to analyze the glucose content. The percentage of enzymatic hydrolysis was calculated as follows (11):

$$Percentage\ of\ hydrolyzed\ starch\ (\%) = \frac{G_t \times 25 \times 0.9}{200} \times 100$$

where 0.9 is the transformation coefficient from starch to glucose (162/180 w/w), 25 is the dilution factor, and glucose concentration within t min was defined as G_t.

The equilibrium concentration (C_∞) and speed rate constant (k) (h^{-1}) were obtained from the enzyme hydrolysis curves, and the first-order formulas were as follows:

$$C = C_\infty \left(1 - e^{-kt}\right),\ C_\infty \leq 100\%$$
$$AUC = C_\infty \left(t_f - t_o\right) - \left(\frac{C_\infty}{k}\right)\left[1 - exp - k\left(t_f - t_0\right)\right]$$

where AUC is the area under the fitted curve, t_0 and t_f are the initial and final times of hydrolysis, and t is the time of *in vitro* digestibility kinetics (min).

Predictive glycemic index of starch

The area of the *in vitro* digestibility kinetics curve was calculated as the hydrolysis index (HI) and estimated glycemic index (GI) corresponding to white bread as a reference using the following equation (12):

$$HI = \frac{AUC\ (sample)}{AUC\ (white\ bread)}$$
$$GI = 39.71 + (0.549HI)$$

Granule morphology analysis

As described by Zhang et al. (8), a scanning electron microscope was used to observe the granule morphology of starch samples (Quanta-200, FEI Company, Hillsboro, OR, USA). The accelerating voltage was set to 15 kV and magnification was 60× and 500×.

Fine structure of starch samples

According to Bi et al. (13), the fine structure was generally analyzed by determining the debranched chain length distributions. Pullulanase (10 μL; 1,000 NPUN/g, 50 mM, pH 6, Sigma-Aldrich) was mixed with 40 mg starch for debranching. Short chains [A chains, degree of polymerization (DP): 6–12], middle short chains (B1 chains, DP: 13–24), middle long chains (B2 chains, DP 25–36) and long chains (B3+ chains, DP: ≥ 37) of starch samples were analyzed in a Cabopac PA200 column (3 × 250 mm, Dionex Corporation, Sunnyvale, CA, USA) using high-performance anion-exchange chromatography with pulsed amperometric detection (ICS-5000, Dionex Corporation) connected to a ED50 electrochemical detector.

Molecular structure analysis

As described by Zhang et al. (14), the molecular structure was analyzed by determining the molecular weight distribution. Completely dissolved solution (starch samples/dimethyl sulfoxide was 2 mg/mL, 90°C, 24 h) was evaluated with an absolute molecular weight analysis system including multi-angle laser light-scattering detector (Wyatt Technology Corporation, Santa Barbara, CA, USA), refractive index detector (Wyatt Technologies), and high-performance size-exclusion chromatography (Wyatt Technology Corporation). The guard column, Shodex OHpak SB-804 HQ and Shodex OHpak SB-806 HQ (Showa Denko K.K., Tokyo, Japan) Phenogel columns were used. The column temperature was 60°C, and flow rate of the dimethyl sulfoxide mobile phase was 0.3 mL/min. The sample injection consisted of 100 μL. Data obtained using this system were analyzed with Astra software (version 5.3.4, Wyatt Technology).

Crystal structure and degree of gelatinization analysis

For crystal structure analysis, an X-ray diffractometer (Bede XRD Di System, Durham, UK) operated at 40 kV, 4 to 40°, 200 mA, and 0.154 nm CuKα radiation was used. Relative crystallinity (Rc) was calculated using MDI Jade v6.5 (15). It was measured by that the ratio of peak cell area to total area.

The degree of gelatinization (DG) was defined as the glucose content of per gram of gelatinized starch sample after enzymolysis. Therefore, DG could be carried out based on method of enzymatic detection. 100 mg starch sample were passed 200 mesh sieve and hydrolyzed by amyloglucosidase (50 U, 37°C, 30 min). The glucose oxidase-peroxidase method used to detect glucose content. The DG was measured by the ratio of starch samples to fully gelatinized starch standard.

Proportions of amylose and amylopectin

According to Chen et al. (1), a mixed liquor composed of 1 mL absolute alcohol and 9 mL of 1 M sodium hydroxide was prepared, which was mixed with 100 mg samples (dry basis) and boiled in a water bath for 15 min. This solution was diluted to 100 mL using distilled water. Next, 2.5 mL of the diluent were further diluted to 50 mL using distilled water. The 0.50 mL of acetic acid solution (1 M) and 1 mL of iodide and iodine (0.0025 M I_2, and 0.0065 M KI) was used to react with that diluent, then stewing 20 min for Color reaction. The absorbance was measured in an ultraviolet spectrophotometer at 620 nm (SPECORD 250 plus, Analytik Jena, Germany). The standard curve of potato amylose (Alphalase NP, Sigma) was used to

TABLE 1 *In vitro* nutritionally starch fractions, kinetic equation characteristics of enzymatic hydrolysis and glycemic index of test material.

Starch samples	RDS (%)	SDS (%)	RS (%)	C_∞ (%)	k (h^{-1})	HI	GI
EJFSS	46.28 ± 6.41^{de}	34.60 ± 3.86^{de}	19.11 ± 2.56^{b}	82.52 ± 1.44^{e}	1.88 ± 0.10^{bc}	96.50 ± 1.70^{e}	92.69 ± 0.93^{e}
ECS	53.99 ± 1.74^{ab}	30.75 ± 1.33^{f}	15.26 ± 0.40^{c}	85.28 ± 3.49^{d}	1.61 ± 0.20^{d}	99.69 ± 4.11^{d}	94.43 ± 2.26^{d}
EPS	28.32 ± 0.80^{f}	42.13 ± 4.25^{b}	29.55 ± 5.05^{a}	79.23 ± 1.69^{f}	1.43 ± 0.09^{f}	92.22 ± 1.62^{f}	90.34 ± 0.89^{f}
EMS	50.03 ± 5.18^{cd}	36.83 ± 1.28^{d}	13.13 ± 3.90^{cd}	90.42 ± 2.51^{b}	1.55 ± 0.13^{de}	105.69 ± 2.96^{bc}	97.73 ± 1.62^{bc}
EWS	55.22 ± 1.79^{a}	41.80 ± 1.11^{bc}	2.98 ± 0.27^{e}	92.25 ± 2.02^{a}	1.90 ± 0.13^{b}	107.88 ± 2.38^{a}	98.93 ± 1.30^{a}
ERS	50.44 ± 0.52^{c}	47.66 ± 0.75^{a}	1.90 ± 1.26^{f}	90.78 ± 2.45^{b}	2.06 ± 0.18^{a}	105.17 ± 2.88^{ab}	98.00 ± 1.58^{ab}

RDS, SDS and RS were rapidly digestible starch, slowly digestible starch, and resistant starch. C_∞ and k represented equilibrium concentration and first-order kinetics constant. HI and GI were predictive hydrolysis index and glycaemic index. Samples with different letters in the same column are significantly different at $P < 0.05$.

calculate the amylose and amylopectin contents.

$$Amylopectin\ (\%) = (1 - amylose(\%)) \times 100$$

Statistical analysis

The means, standard deviations, and principal component analysis (PCA) performed using SPSS (version 20.0; SPSS, Inc., Chicago, IL, USA) were used to determine the interaction between the glycemic release rate characteristics and fine supramolecular structure. The data was analyzed by one-way ANOVA at 5% level of significance. The significance of differences between parameters (at $p < 0.05$) was determined using Duncan's multiple.

Results and discussion

In vitro nutrition fractions

The *in vitro* nutrition fragments (RDS, SDS, and RS) of EJFSS, ECS, EPS, ERS, EWS, and EMS were shown in Table 1. The RDS, SDS, and RS showed obvious diversities among the six sample types ($p < 0.05$). EPS showed the maximum proportion of RS but minimum RDS values. ERS showed the maximum SDS and lowest RS. The highest RDS content was observed in EWS and lowest SDS content was observed in ECS. Therefore, EPS showed the strongest enzyme resistance, followed by EJFSS, ECS, EMS, and EWS. ERS was also susceptible to enzymolysis. Moreover, according to Zhang et al. (3), cassava, maize, potato, wheat, and rice starches have an A-type crystalline structure, whereas potato starch has a B-type crystalline structure. Wang et al. (16) also found that cooked some mung bean starch and sago starch with B-type crystalline structure also showed significantly gelatinization characteristics at a molecular level, compared with A-type crystalline corn, oats and barley starch. This phenominon might be exlpained by that the diversities of ishort chain aggregates, isolated single helices rregularly and packed structures between B-type crystalline starch and A-type crystalline satrch (16, 17). Therefore, the highest RS in EPS may be explained by that although extrusion cooking starch might all show V-type crystal structure, the different crystal types between native potato starch and other raw samples still have different modification mechanisms, leading to the various relative crystallinity and repetition distance of semicrystalline lamellar. According to Ma et al. (17), for the extruded A-type crystalline starch samples, different nutrition fragments were produced, possibly because of the responsiveness of α-amylase to the hyperfine structure of starch pellets. Our results were similar to those of hull-less barley starch, which showed an RS content of 17–56% after extrusion cooking (18). The RDS content of the extrusion-cooked starch samples (28.32–55.22%) was consistent with that of extruded high-amylose maize flour (RDS 19.32–66.83%); however, the SDS content (30.75–47.66%) was broadly higher than that of extruded high-amylose maize flour (SDS 2.70–36.51%) (19). These differences may be ascribed to the higher degree of amylopectin polymerization in our samples compared to that in extruded high-amylose maize flour.

The RDS contents of all extruded cooking samples were notably higher compared to those in the corresponding raw samples, whereas the RS content was much lower ($p < 0.05$) (Table 1, Supplementary Table S2). After IEMT treatment, the SDS contents of the JFSS and potato starch were significantly higher, while those of the other native starches were significantly lower ($P < 0.05$). These results indicate that most RS and SDS in ECS, ERS, EWS, and EMS were converted into RDS, whereas the RS in EJFSS and EPS was converted to both RDS and SDS. According to Zhang et al. (19), extrusion promotes the formation of defective crystalline regions and disordered semi-crystalline lamellae. This may lead to improved digestibility of starch samples after extrusion cooking. In addition, based on Li et al. (4), the different conversion abilities of nutrition fragments between JFSS and potato starch compared to other kinds of starch, may be related to the higher amylose content in JFSS (27.01%) and potato starch (24.82%) than in the other starch samples (3.25–21.65%). This led to higher formation of nearly perfect crystals and better short-range order structures for JFSS and potato starch, resulting in different levels of digestibility after extrusion. Changes in the *in vitro* nutrition fraction contents of the six types of starch during extrusion cooking were

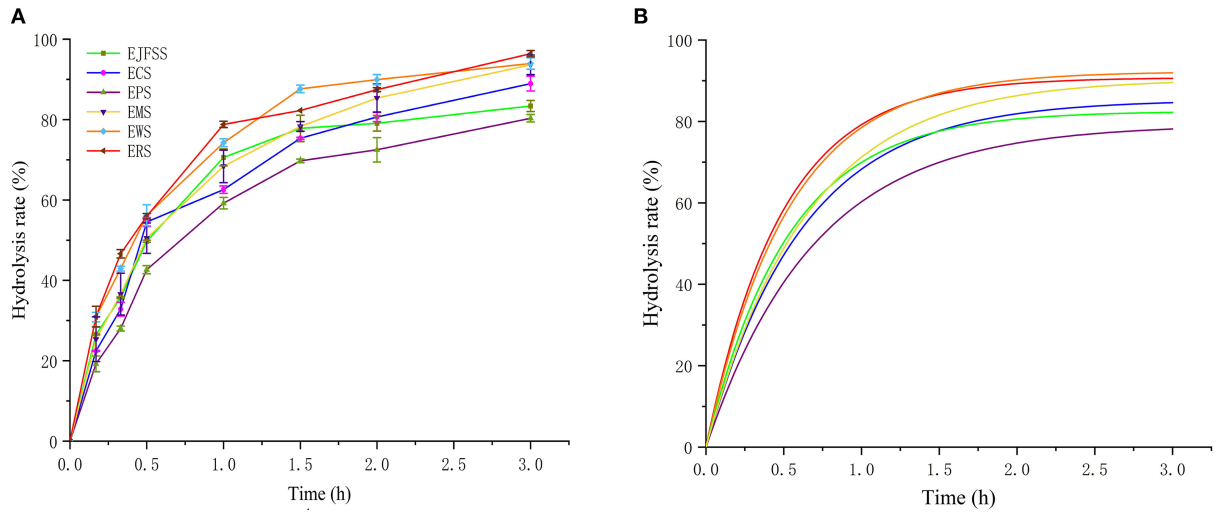

FIGURE 1
Primitive curve **(A)** and forecast curve **(B)** of *in vitro* hydrolysis of different extrusion-cooked starch samples.

similar to those of extruded waxy rice flour, in which the RDS increased from 50.50% to 78.88%, RS decreased from 14.74 to 2.36%, and SDS decreased from 34.77 to 6.84% (20).

However, the *in vitro* nutrition fractions contents suggested by Englyst et al. (9) were not confirmed in accurate enzymolysis studies (21). Hence, the *in vitro* glycemic release rate and estimated glycemic level should be analyzed to assess the digestibility of native starch extrudates.

In vitro digestive kinetics of IEMS starches

As shown in the primary and fitted digestive curves in Figures 1A,B, the enzymatic hydrolysis rates followed the order: ERS > EWS > EMS > ECS > EJFSS > EPS. Le Corre et al. (22) reported that starch digestion mainly occurs in the amorphous region formed by amylose in the entangled state and branch points of low DP amylopectin. Therefore, the various extrudate digestion rates may be explained by their distinct distribution patterns of entangled state amylose, which forms a differently compacted amorphous structure. The hydrolysis curve of extrudates showed a rapid increase from 0–75 min, after which the hydrolysis curve increased slowly to a maximum over 75–180 min (Figures 1A,B, Supplementary Table S1). Zhang et al. (8) also reported that extrusion-cooked JFSS undergoes faster hydrolysis in 0–60 min compared to that in 90–180 min. The digestion rates of the starch extrudates were 59.21–78.80%, 72.49–89.95%, and 80.33–96.39% at 60, 120, and 180 min, respectively. This result indicates that all extrudates were weakly resistant to digestion. Furthermore, the hydrolysis curves of extrudates samples were notably higher compared to those of the corresponding native samples ($p < 0.05$) (Figures 1A,B, Supplementary Tables S1, S2). This occurred possibly because the fragments of amylose and amylopectin reassociated, and the polymers were reconstituted with weak intermolecular forces during the retrogradation stage of extrusion cooking starch based on Zhang et al. (19, 20). Zhang et al. (8) reported similar results; at all time intervals, the hydrolysis ratio of extrusion-cooked JFSS (0–91.68%) exceeded the corresponding hydrolysis ratio of native starch (0–31.84%).

The C_∞ values were in the following order: EWS > ERS ≈ EMS > ECS > EJFSS > EPS (Figure 1B, Table 1). The starch sample extrudates had significantly increased C_∞ values compared with those of the native starches (Table 1 and S1 $p < 0.05$), whereas ERS and EMS showed the opposite trend. The C_∞ values of ERS (90.78%) and EMS (90.42%) were considerably lower than those of raw rice starch (91.06%) and maize starch (92.05%), respectively; these results differed from those of enzymatic hydrolysis curve analysis. C_∞ is significantly correlated with the enzymatic hydrolysis time intervals (12) and k (5). C_∞ represents the predicted final glycemic release content after the digestive reaction. The difference may be attributed to the various k values among EJFSS, ECS, EPS, ERS, EWS, and EMS, resulting in different C_∞ values. To determine the mechanism of the change in C_∞ during extrusion cooking and explain the differences among the results, the k of native starch extrudates was analyzed.

ERS and EWS had higher k values than EJFSS, ECS, EPS, and EMS, indicating faster glycemic release in ERS and EWS and leading to higher C_∞ than that in the other extrudates. This may have led to a notably lower C_∞ of ERS and EWS compared to those of raw starches, whereas the others were higher (Table 1, Supplementary Table S2). Based on previous studies (17, 23), the branching chain distribution properties of

amylopectin and crystallization characteristics may have caused differences in k among the extrudate samples. Furthermore, k of extrusion cooked starches (1.55–2.06 h^{-1}) exceeded that of raw starches (Table 1, Supplementary Table S1). This may be because the enzymatic hydrolysis site transforms from the amorphous region near the particle surface into the amorphous structure near the center in starch particles, as reported by Jiang et al. (24). AlRabadi et al. (25) reported similar results, where the k value of sorghum starch extrudates (2.12 h^{-1}) was higher than that of raw starch (0.20 h^{-1}).

Glycemic index analysis

According to Goñi and Valentín-Gamazo (11), a high blood glucose level was considered as GI $\geq$ 70. A GI value between 55 and 69 is considered as a medium glycemic index level and <55 indicates a low glycemic index level (10). The HI and GI values are shown in Table 1. All extrusion cooking samples had high blood glucose levels (GI: 90.34–98.93, HI: 92.22–107.88). The HI and GI values were in the following order: EWS > ERS $\approx$ EMS > ECS > EJFSS > EPS, possibly because of the various quantities of more ordered mass fractal structure of the extrudates (1). The HI and GI values of the extrusion-modified samples remarkably surpassed those of raw starches ($p < 0.05$), except for ERS and EMS (Table 1, Supplementary Table S2), possibly because the numerous branch linkages in the crystallites caused a higher k but a lower C_∞ in ERS and EMS than in the other samples, as reported by Li et al. (5). The GI of amaranth starch extrudates showed a similar result; the GI value (91.2) of extrusion cooked starches significantly exceed that of native starch (87.2) (26).

Granule morphology

SEM and the supramolecular structure can be used to investigate the *in vitro* glycemic release mechanism of particles after IEMS treatment. Therefore, we examined the granule morphology of starch extrudates. All extrudate samples showed irregular shape (Figure 2). The EPS granules had more compact surfaces with fewer pits compared to those of EJFSS, ECS, ERS, EWS, and EMS granules. EWS had the loosest and most void-distributed granule surfaces. EWS molecules may break more easily during the hydrolysis of amyl-glucosidase and α-amylase than the other samples, whereas EPS showed significant opposite trend (27). Similarly, Faraj et al. (18) showed that the degree of damage to the extrudate granule morphology of different types of barley flour significantly differed. Moreover, the EJFSS, ECS, EPS, and EWS granule morphology exhibited numerous large emulsion bumps with concave holes (Figure 2), in contrast to the smoother, smaller, and round or bell-shaped native starch granule surfaces observed previously (4). Thus, the extrudate granules may have been seriously damaged after IEMS treatment, leading to superior digestibility compared to that of their raw starches (28). The ERS and EMS granules had concave holes and large sizes, whereas their native starches had abundant small pores randomly distributed on the rough surface. Therefore, ERS and EMS had a poor GI value compared with that of their raw starches. Román et al. (29) also found a high degree of granule morphology disruption in extruded maize flour.

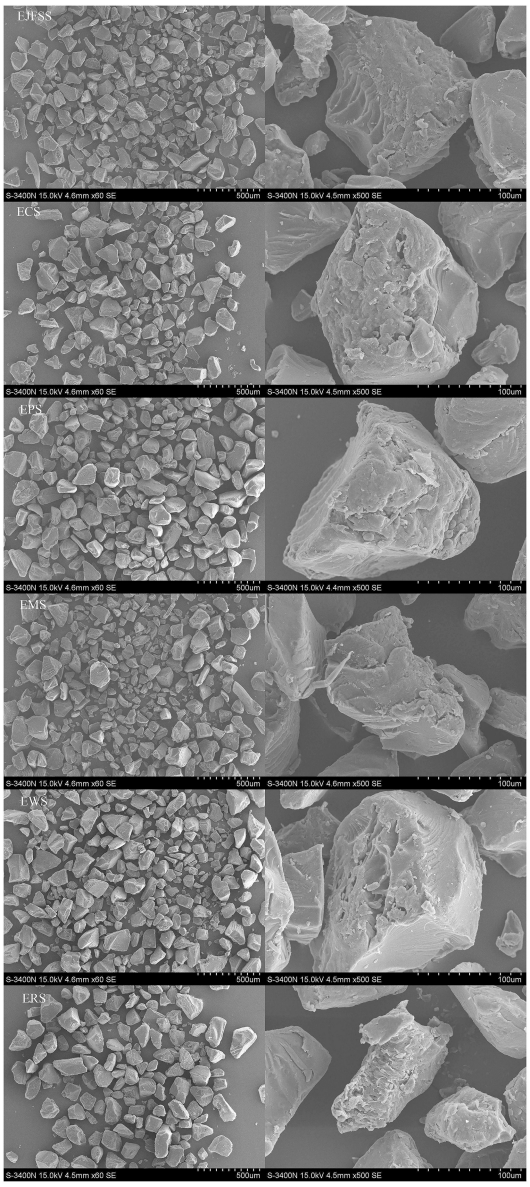

FIGURE 2
Micrographs of different types of starch extrudates at 60× (left) and 500× (right) magnification.

10.3389/fnut.2022.985929

Supramolecular structure

Absolute molecular weight distribution of starch samples

The absolute molecular weight parameters of EJFSS, ECS, EPS, ERS, EWS, and EMS were 0.30–1.31 × 10^7 g/mol (Mw), 0.26–1.13 × 10^7 g/mol (Mn), 53.9–125.4 nm (Rg), and 1.06–2.24 (PI), respectively, and all absolute molecular weight parameters of EPS, EJSS, and ECS were higher than those of EMS, EWS, and ERS (Table 2, Figure 3). This indicates that EMS, EWS, and ERS had looser molecular structures, a weaker force between molecules, and lower molecular weight dispersion compared to those of EPS, EJSS, and ECS (30). The higher Rg, PI, and average molar mass of EPS, EJSS, and ECS may be associated with their relatively lower digestion rates than those of EMS, EWS, and ERS. In addition, Mw chromatogram of starch samples in this study only displayed a single-peak elution curve, that differed with the report of Liu et al. (31) who found the doublet-peak elution curve including amylose and amylopectin curve. This difference might be attributed to the diversity of sensitivity of the MALLS-RI system, the different analysis conditions or variations in the data evaluation techniques.A similar study reported that the Mw of extrusion-cooked waxy maize starch was 40–336 × 10^6 g/mol (32).

In contrast, the Mw and Mn of EJFSS, ECS, EPS, ERS, EWS, and EMS were significantly decreased compared to those of their raw starches (Table 2, Supplementary Table S2). Rg and PI slightly differed between the extrudate samples and raw starch samples. The different Mw and its distribution between the extrudates and native starch samples may be explained by rupture of the internal intermolecular hydrogen bonds during extrusion (19). This results in complete destruction of the amylopectin double helix backbone, leading to crystallization of semicrystalline lamella degradation of starch molecules. Hence, raw starch showed weaker resistance to digestion after extrusion (27). However, ERS and EMS showed lower Mw and Mn but higher resistance to digestion than their native starches. Based on previous reports (13, 30), the shear degradation of unconjugated side-chain branch points of amylopectin outside the starch microcrystal molecule generally resulted in decreased GI, which differed from amylopectin backbone degradation. These contrasting results for ERS and EMS may be explained by the varied degradation approaches. Liu et al. (33) found that granular molecules in rice starch are significantly degraded after extrusion cooking, which is consistent with our results.

Fine molecular structure of modified starch

As shown in Table 2 and Figure 4, the A, B1, B2, and B3+ chain values of EJFSS, ECS, EPS, ERS, EWS, and EMS were 32.06–43.09%, 44.37–48.61%, 10–15.81%, and 2.54–7.46%, respectively. There was notable diversity between the

TABLE 2 The fine supramolecular structures of different types of extrusion modification starches.

Starch sample	DP 6-12	DP 13-24	DP 25-36	DP ≥ 37	Mn (×10^7)	Mw (×10^7)	Rag (nm)	PI	Amylose (%)	Amylopectin (%)	Ratio (%)	Rc (%)
EJFSS	35.47^{b}	44.91^{d}	12.67^{cde}	6.95^{b}	0.36^{c}	0.81^{b}	73.7^{c}	2.24^{a}	26.98 ± 1.50^{b}	73.02 ± 1.50^{e}	36.98 ± 2.81^{b}	16.22^{a}
ECS	32.66^{de}	47.09^{b}	13.48^{bc}	6.77^{bc}	0.61^{b}	0.79^{bc}	68.3^{d}	1.29^{b}	24.08 ± 0.94^{cd}	75.93 ± 0.94^{d}	31.72 ± 1.63^{cd}	15.10^{b}
EPS	32.06^{ef}	44.67^{de}	15.81^{a}	7.46^{a}	1.13^{a}	1.31^{a}	125.4^{a}	1.21^{bcd}	31.34 ± 0.40^{a}	68.66 ± 0.40^{f}	45.65 ± 0.83^{a}	9.28^{f}
EMS	34.49^{bc}	48.61^{a}	12.67^{cde}	4.23^{e}	0.35^{cd}	0.43^{d}	62.3^{e}	1.17^{de}	20.56 ± 0.25^{e}	79.44 ± 0.25^{b}	25.87 ± 0.39^{e}	12.29^{cde}
EWS	43.09^{a}	44.37^{ef}	10.00^{f}	2.54^{f}	0.26^{ef}	0.30^{f}	53.9^{f}	1.20^{bc}	22.50 ± 1.20^{d}	77.50 ± 1.20^{c}	29.05 ± 2.00^{d}	12.62^{cd}
ERS	33.65^{cd}	46.01^{c}	14.08^{b}	6.26^{cd}	0.33^{cde}	0.35^{de}	115.7^{b}	1.06^{f}	9.63 ± 1.40^{f}	90.37 ± 1.40^{a}	10.67 ± 1.71^{f}	13.92^{c}

DP represented the chains degree of polymerization. Mn and Mw were weight-average and number-average molar mass molar mass. Rg and PI were radius of gyration and Mw/ Mn. Rc represented relative crystallinity of starch molecular. Ratio was Amylopectin content/Amylose content. Samples with different letters in the same column are significantly different at $P < 0.05$.

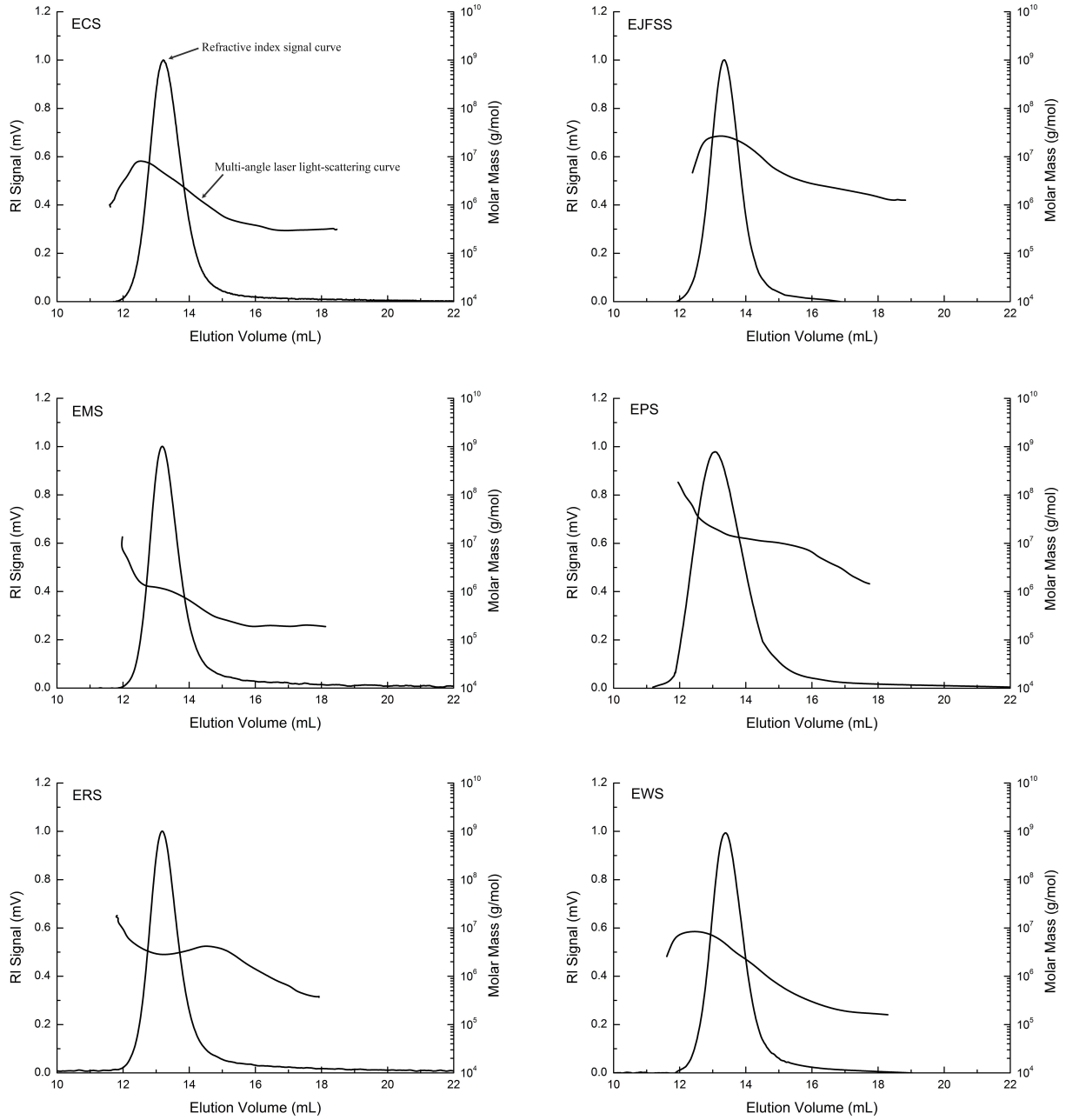

FIGURE 3
Molecular weight and distribution curve of starch samples.

debranched chain length distributions of the extrudate samples ($p < 0.05$). EWS, with the longest A chain lengths, had the shortest medium (B1 chains), medium-long (B2 chains), and long chains (B3+ chains) compared with that of the other extrudates. EPS showed the opposite trend, resulting in EWS having the highest GI and EPS having the lowest GI as described by Bi et al. (13). According to previous studies (2, 13), part of the medium and short chains forms a flawed crystal and amorphous layer, and both medium-long and long chains constitute a defective and perfect crystal layer in the starch semi-crystalline structure. Therefore, the different results of chain length distributions of extrudate samples resulted in diverse structures within crystallized and amorphous layers, leading to their various GI. Similarly, Lee and Moon (34) found that the A chains content in potato starch was 21.1%, proportion of B1 chains was 49.1%, and values of

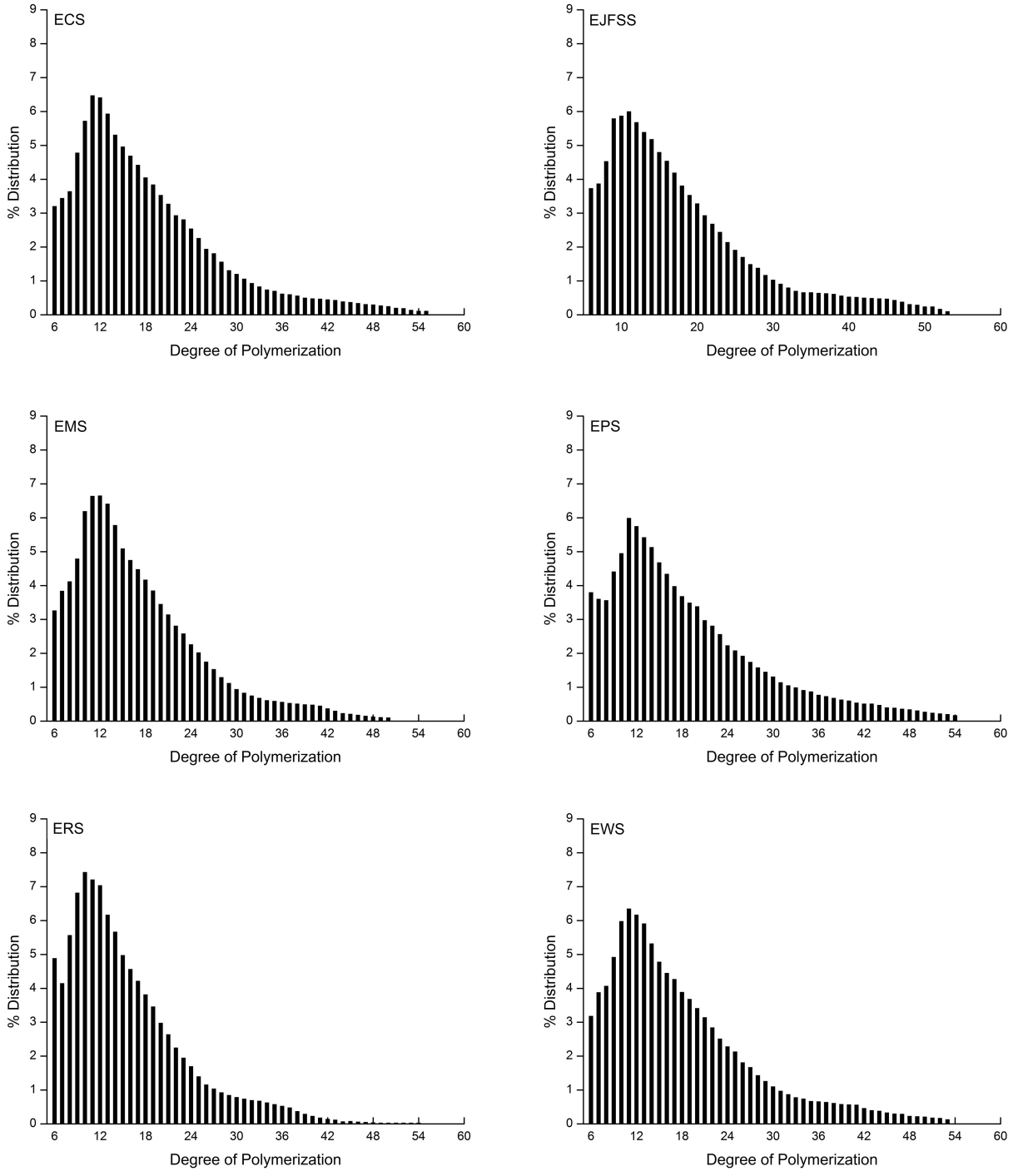

FIGURE 4
Branched chain length distributions of starch samples.

middle-long chains and long chains were 12.0% and 11.6% after heat-moisture treatment.

The proportion of A chains in all extrudate samples was notably increased and those of B2 and B3+ chains were notably decreased compared with those of raw samples (Table 2, Supplementary Table S1). The proportion of B1 chains in EPS, EJFSS, ECS, ERS, and EMS was higher than that in the corresponding native starches, whereas the proportion of B1 chains in EWS showed the opposite tendency. These results indicate that the B2 and B3+ chains of all native starches were

transformed into A and B1 chains. For wheat starch, B1, B2, and B3+ were converted into short chains. These trends caused notable decreases in the Mw of all extrusion modified starches, which is attributed to the significant correlation between the long chains of amylopectin, Mw, and GI (35, 36). According to Zhu (35), for the Mw, fine structure, and digestibility results of raw and extrusion-cooked starches, the long helix with strong hydrogen-bonding interactions in the ordered crystal layer was clearly destroyed. This led to formation of abundant incomplete double-helix chains in the disorder phase of the semi-crystalline structure during IEMS (2, 37). However, compared to native starches, rice and maize extrudates showed a decreased order degree of crystallizing layer arrangement but an increased anti-enzymatic ability. According to Ren et al. (38), this result may be explained by the formation of abundant amylose and more stable α-1,4 glucosidic bonds units within the defective crystallizing layers of IEMS-transformed rice and maize starch. Nakazawa and Wang (37) similarly reported that the A chains value increased and values of B1, B2 and B3+ chains of maize starch decreased during extrusion cooking.

Crystallinity characteristic and DG analysis of starches

As shown in Figure 5 and Table 2, Rc values were in the order EJSS (16.22%) > ECS (15.10%) > ERS (13.92%) > EWS (12.62%) > EMS (12.29%) > EPS (9.28%). According to Liu et al. (33), the differences between samples can be explained by the number of amylose lipid complex, the different degrees of close packing mode of the double-helix structure and double helix orientation within crystal lamellae, leading to various perfect crystallite numbers and sizes of each extrudate. In addition, EPS had a lower Rc but lower digestibility than that of the other starches, possibly because EPS has a larger number of superhelix structure formed by linear amylose and amylopectin compared to that of the other samples (27). A similar study reported that the Rc of extruded rice starch was 4.4–6.5% (33).

The Rc values of starch extrudates (9.28–16.22%) were notably decreased compared to those of the corresponding native samples (15.91–29.39%) (Table 2, Supplementary Table S2), indicating that the crystallization region was degraded after IEMS. The fine supramolecular structures showed that B3+ chains transformed into A, B1, and B2 chains, causing a decrease in Mw and Rc values. Therefore, molecular degradation occurred in most crystalline structures within the crystalline regions, altering the digestive rate between the raw starch and extrudates (39). Similarly, the Rc values decreased from 31.63% and 28.58% to 12.68% and 13.67% in extrusion cooked rice starch and JFSS (2, 7). Diffraction peaks of the extrudates were observed at 15, 13, 17, 18, 20, and 23° (EJFSS) or at 13 and 20° (ECS, EPS, EMS, EWS, and ERS), indicating that A- or B-type crystallinity feature changed to the V-type compared with our previous results

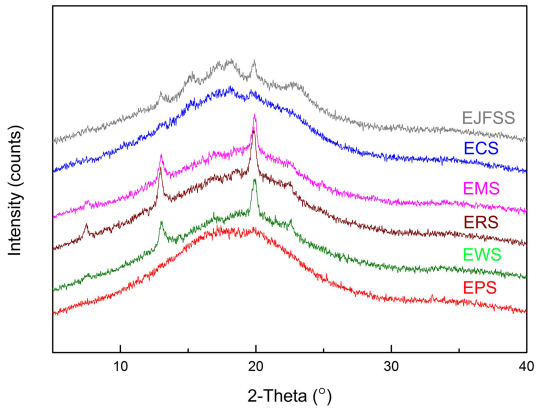

FIGURE 5
X-ray diffraction patterns of different types of starches.

(4). These results may be ascribed to the change in stacking modes of the open packing of helices and array of inter-helical crystal water structures in each hexagonal crystal unit (38). Similarly, Sarawong et al. (40) reported that the A-, B-, or C-type crystalline structures of green banana flour were converted into V-type structures after extrusion cooking.

In addition, the DG values of extrudates followed the order of EPS (98.84%) > EJFSS (98.05%) > ECS (97.63%) > EMS (97.11%) > ERS (96.57%) > EWS (96.08%). The different DG values of extrusion cooking samples might be the diversities of rigidity degree of native starch molecular crosslinking network formed by ordered helices and amorphous single chains. Based on Ren et al. (38), it was found that there was a small impact for DG values to digestibility of starch extrudates when DG values higher than 95%. DG values of extrusion cooking samples was higher than that of cooking foxtail millet starch (<90%) published by Ren et al. (38). This phenomenon might can be due to the high gelatinization efficiency produced by instantaneous high temperature, high pressure and high sheer force of IEMS technology, compared with traditional gelatinization technology.

Amylose content

The proportions of amylose and its proportional relationships with amylopectin of starch followed the order EPS (31.34 and 45.65%) > EJFSS (26.98 and 36.98%) > ECS (24.08 and 31.72%) > EWS (22.50 and 29.05%) > EMS (20.56 and 25.87%) > ERS (9.63 and 10.67%) (Table 2). The amylopectin content followed the order of ERS (90.37%) > EMS (79.44%) > EWS (77.50%) > ECS (75.93%) > EJFSS (73.02%) > EPS (68.66%). The amylose content of the extrudates nearly agreed with the results for the Mw, Rs, and long chains (B2 and B3)

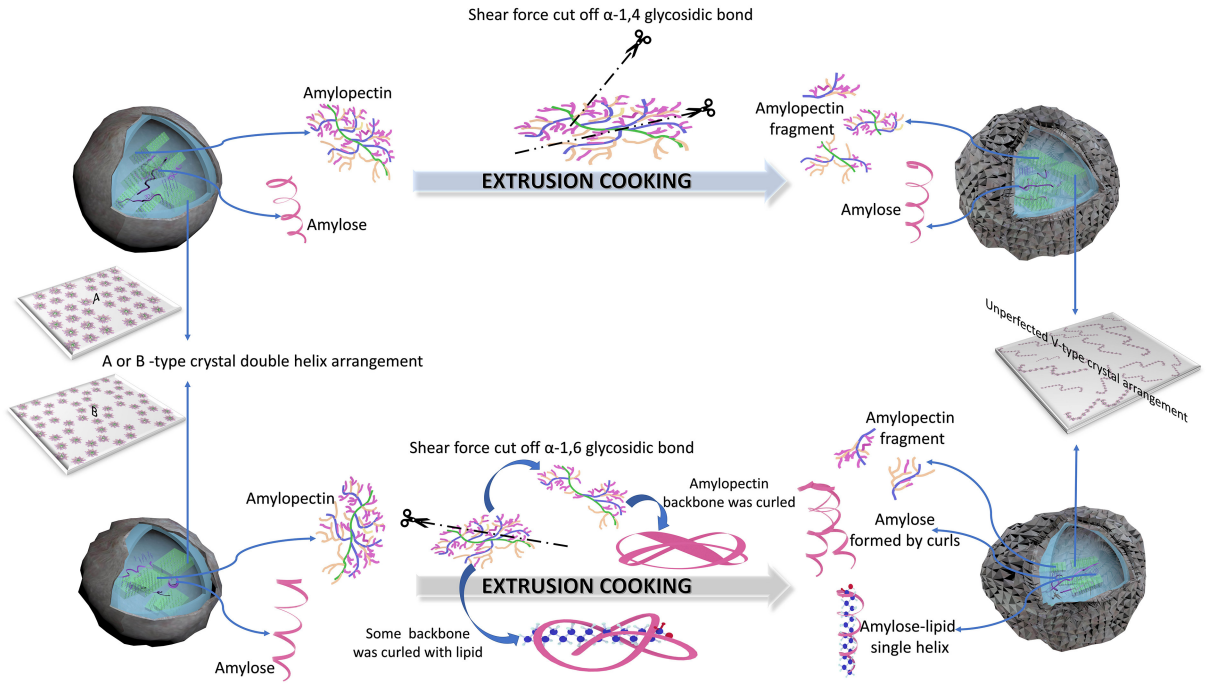

FIGURE 6
Mechanisms of improved extrusion cooking technology (IEMS) treatment of different types of starches.

of amylopectin. These results indicate that higher proportions of amylose, a lower value of amylopectin, and higher values of their ratios can cause higher tensile forces between adjacent amylose conformations, causing shrinkage of the amorphous regions (13, 38). Thus, the fine structures of EPS, EJFSS, and ECS were compact, indicating that these starches were digested more slowly compared to those of EWS, EMS, and ERS, which had a higher proportion of amylose. The proportions of amylose in extrusion cooked samples were similar to those previously reported for extrusion-cooked green banana starch (17.96–33.49%) (40).

The amylose contents and amylose/amylopectin ratios of ECS, EPS, and ERS were notably increased compared to those of the corresponding native samples (Table 2, Supplementary Table S3); the amylopectin contents of ECS, EPS, and ERS showed contrasting results. Sarawong et al. (40) found similar results, where the proportion of amylose in extrusion-cooked banana starch improved from 16.20 to 33.49%. The proportions of amylose and amylose/amylopectin content obtained from EJFSS, EMS, and EWS slightly differed from those of their native starches. Our results were similar to those of previous findings on the amylopectin content of amaranth flour, which changed slightly from 68.8% (native) to 69.4–69.7% (extrudates) (41). During IEMS treatment, the diverse changes in amylose and amylopectin contents between ECS, EPS, and ERS compared to the others, may be ascribed to differences in plant origins and the number of entanglements between amylose chains (19, 35). Additionally, the weight average molar mass of amylopectin accounts for more than 90% of the whole starch molecules (31). The Mw of all different types of starches was decreased during extrusion cooking, indicating that amylopectin (long chains) is degraded into amylose/amylose was sheared into amylose fragments or integral amylopectin sheared into incomplete amylopectin fragments (41). Therefore, the two different mechanisms of IEMS treatment of starch samples require further analysis.

Mechanisms of starch samples treated using IEMS

Figure 6 shows the possible degradation mechanisms of IEMS treatment of different kinds of starches. For cassava, potato, and rice starches, most amylopectin α-1,6-glycosidic bonds linked to the backbone were cut off because of their increasing amylose content, decreasing the Mw and Rc in the presence of the strong shear force generated during IEMS (Figure 6, Table 2, Supplementary Table S2). According to Liu et al. (33) and Le Corre et al. (22), these residual amylopectin backbones with few short side chains may have been entangled and curled by stronger conjugation effects of non-reducing or reducing terminal glucosyl residues, converting into a spiral

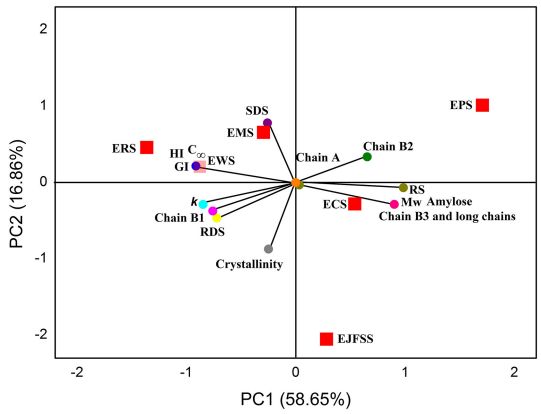

FIGURE 7
Principal component analysis (PCA) score and loading plots (PC1 and PC2) of starches.

amylose fragment. Additionally, numerous branched chains of cleaved α-1,6-glycosidic bonds of amylopectin were converted into amylopectin fragments with a lower Mw, rather than being converted into amylose. Moreover, according to Menegassi et al. (41), few amylose-lipid complexes were generated by amylose formed from the curled amylopectin molecule, which partly slowed digestibility and stabilized few crystalline structures of ECS, EPS, and ERS. Our results agree with published results for wheat and rice starch (31, 40) but contrasted with those of jackfruit seed starch (5).

However, another degradation mechanism was observed in EJFSS, EMS, and EWS during IEMS. As shown in Figure 6, Table 2, Supplementary Table S2, the shear force produced in the extruder mainly acted on α-1,4-glycosidic bonds of long amylopectin chains by degrading them into many amylopectin fragments with lower Mw. This may be explained by their insignificant change in the amylose content, decreasing Mw, and long chains of amylopectin in all starch samples were degraded to middle and short chains during extrusion cooking (Figure 6, Table 2, Supplementary Table S2). According to Chen et al. (1) and Li et al. (42), the higher branch density of amylopectin fragments caused a stronger van der Waals force between each side chain and the corresponding backbones, preventing the amylopectin fragments from curling into amylose through a squeezing conjugation action. Therefore, amylopectin transformed into amylopectin fragments rather than amylose during IEMS. Although EMS showed a degradation pattern opposite to that of ERS, EMS also had a lower digestion rate compared to that of raw maize starch. According to Zhang et al. (3), a different superhelix formed by linear amylose and amylopectin fragments during IEMS treatment may explain this result. The degradation mechanism in EJFSS agreed with that observed previously (5).

Previous studies (2, 27, 43), found that when different types of native starches show distinct amylose values, the hydrogen-bonding forces of the amylopectin branches are significantly different owing to the dissimilar patterns in amylose and amylopectin that are self-assembled by granule-bound starch synthase I or IIa enzymes (GBSSI and SSIIa). Consequently, the higher amylose content of starch resulted in weak intermolecular hydrogen bonding within the side-chains of α-1,4-glycosidic bond of amylopectin than that of the α-1,6-glycosidic bond compared with starch of a lower amylose content (43, 44). Therefore, the different molecular degradation mechanisms during IEMT treatment between cassava, potato, and rice starches and jackfruit seed, maize, and wheat starches may be induced by various amylose contents as well as by the unraveling structural disassembly and reassembly actions of starch molecules grown from distinct plant sources. Moreover, based on the same degradation mechanism, amylopectin was cut off, and B3+ chains of amylopectin in all starch samples were degraded to B1, B2 and A chains. The declining Mw and Rc caused the broken morphology of the native starches. The mechanism of the IEMT treatment of starch samples agreed with that observed by Ji et al. (44), whose conclusion suggested that raw corn starch with a different amylose/amylopectin ratio presented a distinct mechanism of extrusion cooking.

Interaction between glycemic release speed characteristics and fine supramolecular structure

The PCA results are shown in Figure 7, and the results were further analyzed to determine the interaction between glycemic release characteristics and fine supramolecular structure of IEMT treated samples. ERS, EMS, EWS, ECS, EJFSS, and EPS was broadly distributed in the PCA figure, indicating that differed genotypes of the native starches significantly influenced the supramolecular structures and in vitro glycemic release characteristics during IEMT treatment (13). ECS, EJFSS, and EPS were scattered in PC1, and ERS, EMS, and EWS existed in PC2. These results indicate that ECS, EJFSS, and EPS have more similar characteristics than do ERS, EMS, and EWS. Moreover, PC1 mainly included the short chain (A chain), middle-long chain (B2 chain), long chain (B3+ chain), RS, Mw, and proportion of amylose. SDS, C_∞, HI, GI, k, middle-short chain, RDS, and Rc was displayed in PC2 part. A highly remarkably positive relationship was shown among the short chain, middle-long chain, long chain, RS, Mw, and proportion of amylose in PC1 ($p < 0.05$). C_∞, HI, GI, k, middle-short chain, and RDS also showed a significant positive relationship ($p < 0.05$). Zabidi et al. (12) similarly reported that the C_∞ of chempedak seed flour swelled to 15.48% from 14.19%, k swelled to to 0.09 h^{-1} to 0.07 h^{-1}, and GI increased from

61.10 to 63.44. Short chain, middle-long chain, long chain, RS, Mw, and proportion of amylose showed a negative correlation with C_∞, HI, GI, *k*, middle-short chain, and RDS ($p < 0.05$). SDS had a significantly negative relationship with long chain, RS, Mw, proportion of amylose, and Rc ($p < 0.05$). Lee and Moon (34) showed a similar result with present research, who found that a strong negative relationship was observed between the B3+ chain and RDS when waxy potato starch underwent heat–moisture treatment. Rc and RS had a significant negative correlation ($p < 0.05$), which agreed with a published report (13), whose investigation showed that the value RS increased from 19.04 g to 46.42 g/100 g, however, the Rc decreased to 31.41% from 41.66% for cooked banana starch. Rc had a weak correlation with the B3+ chain, Mw, and amylose content, which was similar with a previous report (33), who showed that Rc was closely associated with the molecular weight distribution of extrusion-cooked rice starch. These dissimilarities might be due to dissimilarities in the degree of stability of the chain segment conformations of starch amylopectin molecules (13). The outcomes obtained from PCA indicated that the supramolecular structure plays an important role in affecting the *in vitro* glycemic release characteristics during IEMT treatment. Furthermore, the supramolecular structures of cassava, jackfruit seed, maize, potato, rice, and wheat starches were broken, as observed from the cleavage of the α-1,4, or 1,6-glycosidic bonds of amylopectin fine structure. Accordingly, morphologies of cassava, jackfruit seed, potato, and wheat starches granules were changed from smooth and compact surfaces to looser polyhedrals with many pits and hollows; this transformation resulted in enhanced digestibility. Although the glycosidic bonds of rice and maize starch were broken and the supramolecular structures were degraded during IEMT treatment, the granule morphology had smaller and less concave holes than did that of the native starches as a result of decreased digestibility. The distinct results between ERS and EMS and the other extrudate samples can be ascribed to the lower proportion of amylose and larger pores on the surface fissures, and channels within raw rice and maize starch granules compared to those of cassava, jackfruit seed, corn, potato, and wheat starches (3, 4). Moreover, ordered chain alignment and cross-linking of ERS and EMS amylopectin might have been formed after IEMT (20, 33). Therefore, the ordered and tight cross-linking of long chains with high DP caused the formation of a rigid macromolecular network, resulting in lower *in vitro* glycemic release characteristics in extruded starch than in raw starch.

Conclusion

The glycemic release characteristics and fine supramolecular structure for jackfruit seed, cassava, rice, wheat, potato, and maize starches modified by IEMS were evaluated. ECS, EJFSS, EPS, and EWS showed higher *in vitro* glycemic release compared to that of the corresponding native starches, whereas EMS and ERS showed the opposite trend. The A chains in the extrudates were transformed into B2 and B3+ chains, and Rc and Mw were notably decreased after extrusion cooking ($p < 0.05$). The original crystallization structure of all starch samples was altered to V-type from A-type crystallization. The amylose contents in ECS, EPS, and ERS were remarkably higher than those in corresponding native starches ($p < 0.05$), whereas changes in the amylose content of EMS, EJFSS, and EWS were minimal ($p > 0.05$). In summary, it was demonstrated that, during IEMT treatment, the α-1,4-glycosidic bonds of maize, jackfruit seed, and wheat starch amylopectin were disrupted because of the high amylose content. The lower amylose content observed for cassava, potato, and rice starches was degraded through α-1,6-glycosidic bonds. Consequently, the van der Waals forces between the branched chains were weakened, and abundant unlinear amylose and amylopectin fragments with side chains were generated. After degradation, the various reassembly patterns of amylose and amylopectin molecules resulted in improved digestibility for ECS, EJFSS, EPS, and EWS and stronger enzyme-resistance capacity for EMS and ERS. PCA further revealed the association between the supramolecular structure and *in vitro* glycemic release characteristics. Moreover, ECS, EJFSS, and EPS had a more ordered molecular structure and compact granule morphology compared to those of EWS, EMS, and ERS, resulting in lower digestibility because of the higher Mw, proportion of amylose, and long chains of amylopectin in the EWS, EMS, and ERS granules. These results may improve the utilization of starches with various GIs of different food fields for people who require different nutritional adaptations.

Data availability statement

The original contributions presented in the study are included in the article/Supplementary material, further inquiries can be directed to the corresponding author.

Author contributions

Conceptualization, software, and validation: CH. Formal analysis, investigation, resources, data curation, and writing-original draft preparation: BL. Writing-original draft preparation, writing-review and editing, and methodology: YZ. Visualization and supervision: WL. Project administration and funding acquisition: JL. All authors have read and agreed to the published version of the manuscript.

Funding

This work was supported by the College of Light Industry and Food Engineering, Guangxi University, and Spice and Beverage Research Institute, Chinese Academy of Tropical Agricultural Sciences. This study was financially supported by National Key Research and Development Program (2020YFD1001204), Key Research and Development Program of Hainan Province (ZDYF2019069, ZDYF2020049), Natural Science Foundation of Guangxi Province (2019JJD120012), and Key Research and Development Plan of Guangxi (AB18221126).

Conflict of interest

The authors declare that the research was conducted in the absence of any commercial or financial relationships that could be construed as a potential conflict of interest.

Publisher's note

Supplementary material

The Supplementary Material for this article can be found online at: https://www.frontiersin.org/articles/10.3389/fnut.2022.985929/full#supplementary-material

References

1. Chen J, Liang Y, Li X, Chen L, Xie F. Supramolecular structure of jackfruit seed starch and its relationship with digestibility and physicochemical properties. *Carbohydr Polym.* (2016) 150:269–77. doi: 10.1016/j.carbpol.2016.05.030

2. Zhang Y, Zuo H, Xu F, Zhu K, Tan L, Dong W, et al. The digestion mechanism of jackfruit seed starch using improved extrusion cooking technology. *Food Hydrocoll.* (2021) 110:106154. doi: 10.1016/j.foodhyd.2020.106154

3. Zhang Y, Li B, Xu F, He S, Zhang Y, Sun L, et al. Jackfruit starch: composition, structure, functional properties, modifications and applications. *Trends Food Sci Technol.* (2021) 107:268–83. doi: 10.1016/j.tifs.2020.10.041

4. Li B, Wang H, Wang X, Zhang Y, Tan Y, Zhang Y, et al. Prediction of the postprandial blood sugar response estimated by enzymatic kinetics of in vitro digestive and fine molecular structure of artocarpus heterophyllus lam seed starch and several staple crop starches. *Starch/Staerke.* (2019) 71:1800351. doi: 10.1002/star.201800351

5. Li B, Zhang Y, Xu F, Khan MR, Zhang Y, Huang C, et al. Supramolecular structure of Artocarpus heterophyllus Lam seed starch prepared by improved extrusion cooking technology and its relationship with in vitro digestibility. *Food Chem.* (2021) 336:127716. doi: 10.1016/j.foodchem.2020.127716

6. Wang S, Chao C, Cai J, Niu B, Copeland L, Wang S. Starch–lipid and starch–lipid–protein complexes: a comprehensive review. *Compr Rev Food Sci Food Saf.* (2020) 19:1056–79. doi: 10.1111/1541-4337.12550

7. Zhang Y, Liu W, Liu C, Luo S, Li T, Liu Y, et al. Retrogradation behaviour of high-amylose rice starch prepared by improved extrusion cooking technology. *Food Chem.* (2014) 158:255–61. doi: 10.1016/j.foodchem.2014.02.072

8. Zhang Y, Zhang Y, Li B, Wang X, Xu F, Zhu K, et al. In vitro hydrolysis and estimated glycemic index of jackfruit seed starch prepared by improved extrusion cooking technology. *Int J Biol Macromol.* (2019) 121:1109–17. doi: 10.1016/j.ijbiomac.2018.10.075

9. Englyst HN, Kingman SM, Cummings JH. Classification and measurement of nutritionally important starch fractions. *Eur J Clin Nutr.* (1992) 46:S33–50.

10. Goñi I, Garcia-Alonso A, Saura-Calixto F. A starch hydrolysis procedure to estimate glycemic index. *Nutr Res.* (1997) 17:427–37. doi: 10.1016/S0271-5317(97)00010-9

11. Goñi I, Valentín-Gamazo C. Chickpea flour ingredient slows glycemic response to pasta in healthy volunteers. *Food Chem.* (2003) 81:511–5. doi: 10.1016/S0308-8146(02)00480-6

12. Zabidi MA, Aziz NAA. In vitro starch hydrolysis and estimated glycaemic index of bread substituted with different percentage of chempedak (Artocarpus integer) seed flour. *Food Chem.* (2009) 117:64–8. doi: 10.1016/j.foodchem.2009.03.077

13. Bi Y, Zhang Y, Jiang H, Hong Y, Gu Z, Cheng L, et al. Molecular structure and digestibility of banana flour and starch. *Food Hydrocoll.* (2017) 72:219–27. doi: 10.1016/j.foodhyd.2017.06.003

14. Zhang Y, Zhang Y, Xu F, Wu G, Tan L. Molecular structure of starch isolated from jackfruit and its relationship with physicochemical properties. *Sci Rep.* (2017) 7:13423. doi: 10.1038/s41598-017-13435-8

15. Ren Y, Guo K, Zhang B, Wei C. Comparison of physicochemical properties of very small granule starches from endosperms of dicotyledon plants. *Int J Biol Macromol.* (2020) 154:818–25. doi: 10.1016/j.ijbiomac.2020.03.147

16. Wang S, Li C, Copeland L, Niu Q, Wang S. Starch retrogradation: a comprehensive review. *Compr Rev Food Sci Food Saf.* (2015) 14:568–85. doi: 10.1111/1541-4337.12143

17. Ma M, Wang Y, Wang M, Jane J-l, Du S-k. Physicochemical properties and in vitro digestibility of legume starches. *Food Hydrocoll.* (2017) 63:249–55. doi: 10.1016/j.foodhyd.2016.09.004

18. Faraj A, Vasanthan T, Hoover R. The effect of extrusion cooking on resistant starch formation in waxy and regular barley flours. *Food Res Int.* (2004) 37:517–25. doi: 10.1016/j.foodres.2003.09.015

19. Zhang X, Chen Y, Zhang R, Zhong Y, Luo Y, Xu S, et al. Effects of extrusion treatment on physicochemical properties and in vitro digestion of pregelatinized high amylose maize flour. *J Cereal Sci.* (2016) 68:108–15. doi: 10.1016/j.jcs.2016.01.005

20. Zhang T, Li X, Chen L, Situ W. Digestibility and structural changes of waxy rice starch during the fermentation process for waxy rice vinasse. *Food Hydrocoll.* (2016) 57:38–45. doi: 10.1016/j.foodhyd.2016.01.004

21. Miao M, Jiang B, Zhang T. Effect of pullulanase debranching and recrystallization on structure and digestibility of waxy maize starch. *Carbohydr Polym.* (2009) 76:214–21. doi: 10.1016/j.carbpol.2008.10.007

22. Le Corre D, Bras J, Dufresne A. Starch nanoparticles: a review. *Biomacromolecules.* (2010) 11:1139–53. doi: 10.1021/bm901428y

23. Zurak D, Kljak K, Grbeša D. The composition of floury and vitreous endosperm affects starch digestibility kinetics of the whole maize kernel. *J Cereal Sci.* (2020) 95:103079. doi: 10.1016/j.jcs.2020.103079

24. Jiang H, Zhang Y, Hong Y, Bi Y, Gu Z, Cheng L, et al. Digestibility and changes to structural characteristics of green banana starch during invitro digestion. *Food Hydrocoll.* (2015) 49:192–9. doi: 10.1016/j.foodhyd.2015.03.023

25. Al-Rabadi GJ, Torley PJ, Williams BA, Bryden WL, Gidley MJ. Effect of extrusion temperature and pre-extrusion particle size on starch digestion kinetics in barley and sorghum grain extrudates. *Anim Feed Sci Technol.* (2011) 168:267–79. doi: 10.1016/j.anifeedsci.2011.04.097

26. Capriles VD, Coelho KD, Guerra-Matias AC, Arêas JAG. Effects of processing methods on amaranth starch digestibility and predicted glycemic index. *J Food Sci.* (2008) 73:H160–4. doi: 10.1111/j.1750-3841.2008.00869.x

27. Nadia J, Bronlund J, Singh RP, Singh H, Bornhorst GM. Structural breakdown of starch-based foods during gastric digestion and its link to glycemic response: In vivo and in vitro considerations. *Compr Rev Food Sci Food Saf.* (2021) 20:2660–98. doi: 10.1111/1541-4337.12749

28. González-Seligra P, Guz L, Ochoa-Yepes O, Goyanes S, Famá L. Influence of extrusion process conditions on starch film morphology. *Lwt.* (2017) 84:520–8. doi: 10.1016/j.lwt.2017.06.027

29. Román L, Martínez MM, Rosell CM, Gómez M. Changes in physicochemical properties and in vitro starch digestion of native and extruded maize flours subjected to branching enzyme and maltogenic α-amylase treatment. *Int J Biol Macromol.* (2017) 101:326–33. doi: 10.1016/j.ijbiomac.2017.03.109

30. Liu C, Zhang Y, Liu W, Wan J, Wang W, Wu L, et al. Preparation, physicochemical and texture properties of texturized rice produce by Improved Extrusion Cooking Technology. *J Cereal Sci.* (2011) 54:473–80. doi: 10.1016/j.jcs.2011.09.001

31. Liu Y, Chen J, Wu J, Luo S, Chen R, Liu C, et al. Modification of retrogradation property of rice starch by improved extrusion cooking technology. *Carbohydr Polym.* (2019) 213:192–8. doi: 10.1016/j.carbpol.2019.02.089

32. Willett JL, Millard MM, Jasberg BK. Extrusion of waxy maize starch: melt rheology and molecular weight degradation of amylopectin. *Polymer (Guildf).* (1997) 38:5983–9. doi: 10.1016/S0032-3861(97)00155-9

33. Liu Y, Chen J, Luo S, Li C, Ye J, Liu C, et al. Physicochemical and structural properties of pregelatinized starch prepared by improved extrusion cooking technology. *Carbohydr Polym.* (2017) 175:265–72. doi: 10.1016/j.carbpol.2017.07.084

34. Lee CJ, Moon TW. Structural characteristics of slowly digestible starch and resistant starch isolated from heat–moisture treated waxy potato starch. *Carbohydr Polym.* (2015) 125:200–5. doi: 10.1016/j.carbpol.2015.02.035

35. Zhu F, NMR. spectroscopy of starch systems. *Food Hydrocoll.* (2017) 63:611–24. doi: 10.1016/j.foodhyd.2016.10.015

36. Zhang Y, Zhang Y, Li B, Xu F, Zhu K, Tan L, et al. Retrogradation behavior of amylopectin extracted different jackfruit cultivars seeds in presence on the same amylose. *LWT - Food Sci Technol.* (2019) 114:108366. doi: 10.1016/j.lwt.2019.108366

37. Nakazawa Y, Wang Y-J. Acid hydrolysis of native and annealed starches and branch-structure of their Naegeli dextrins. *Carbohydr Res.* (2003) 338:2871–82. doi: 10.1016/j.carres.2003.09.005

38. Ren X, Chen J, Wang C, Molla MM, Diao X, Shen Q. In vitro starch digestibility, degree of gelatinization and estimated glycemic index of foxtail millet-derived products: effect of freezing and frozen storage. *J Cereal Sci.* (2016) 69:166–73. doi: 10.1016/j.jcs.2016.03.007

39. Qiao D, Xie F, Zhang B, Zou W, Zhao S, Niu M, et al. further understanding of the multi-scale supramolecular structure and digestion rate of waxy starch. *Food Hydrocoll.* (2017) 65:24–34. doi: 10.1016/j.foodhyd.2016.10.041

40. Sarawong C, Schoenlechner R, Sekiguchi K, Berghofer E, Ng PKW. Effect of extrusion cooking on the physicochemical properties, resistant starch, phenolic content and antioxidant capacities of green banana flour. *Food Chem.* (2014) 143:33–9. doi: 10.1016/j.foodchem.2013.07.081

41. Menegassi B, Pilosof AMR, Arêas JAG. Comparison of properties of native and extruded amaranth (Amaranthus cruentus L. - BRS Alegria) flour. *LWT Food Sci Technol.* (2011) 44:1915–21. doi: 10.1016/j.lwt.2011.04.008

42. Li B, Zhang Y, Zhang Y, Zhang Y, Xu F, Zhu K, Huang C. A novel underutilized starch resource— Lucuma nervosa ADC seed and fruit. *Food Hydrocoll.* (2021) 120:106934. doi: 10.1016/j.foodhyd.2021.106934

43. Noor F, Jiaur R, Sultan M, Sorifa A, Aminul Islam T, Maruf A. Physicochemical properties of flour and extraction of starch from jackfruit seed. *Int J Nutr Food Sci.* (2014) 3:347. doi: 10.11648/j.ijnfs.20140304.27

44. Ji Z, Yu L, Liu H, Bao X, Wang Y, Chen L. Effect of pressure with shear stress on gelatinization of starches with different amylose/amylopectin ratios. *Food Hydrocoll.* (2017) 72:331–7. doi: 10.1016/j.foodhyd.2017.06.015

frontiers | Frontiers in Nutrition

TYPE Original Research
PUBLISHED 24 August 2022
DOI 10.3389/fnut.2022.993828

OPEN ACCESS

EDITED BY
Yanjun Zhang,
Chinese Academy of Tropical Agricultural Sciences, China

REVIEWED BY
Chun Chen,
South China University of Technology, China
Haizhao Song,
Nanjing University of Finance and Economics, China

*CORRESPONDENCE
Mingwei Zhang
mwzhh@vip.tom.com
Fei Huang
hf1311@163.com

SPECIALTY SECTION
This article was submitted to Food Chemistry, a section of the journal Frontiers in Nutrition

RECEIVED 14 July 2022
ACCEPTED 03 August 2022
PUBLISHED 24 August 2022

CITATION
He C, Zhang R, Jia X, Dong L, Ma Q, Zhao D, Sun Z, Zhang M and Huang F (2022) Variation in characterization and probiotic activities of polysaccharides from litchi pulp fermented for different times. *Front. Nutr.* 9:993828. doi: 10.3389/fnut.2022.993828

Variation in characterization and probiotic activities of polysaccharides from litchi pulp fermented for different times

Chunmei He[1,2], Ruifen Zhang[2], Xuchao Jia[2], Lihong Dong[2], Qin Ma[2], Dong Zhao[2], Zhida Sun[1], Mingwei Zhang[1,2]* and Fei Huang[2]*

[1]College of Food Science and Technology, Huazhong Agricultural University, Wuhan, China, [2]Sericultural and Agri-Food Research Institute Guangdong Academy of Agricultural Sciences/Key Laboratory of Functional Foods, Ministry of Agriculture and Rural Affairs/Guangdong Key Laboratory of Agricultural Products Processing, Guangzhou, China

This study investigated the chemical structures and probiotic potential of different polysaccharides (LPs) extracted from the litchi pulp that fermented with *Lactobacillus fermentum* for different times (i.e., 0–72 h corresponding to LP-0 through LP-72, respectively). Fermentation times affected the yields, total sugar contents, uronic acid contents, molecular weights, and monosaccharide compositions of LPs. The LPs yields and uronic acid contents exhibited irregular trends in association with fermentation time, while total sugar contents decreased, and the molecular weights increased. Particularly, LP-6 contained the highest extraction yields (2.67%), lowest uronic acid contents, and smallest average Mw (104 kDa) ($p < 0.05$). Moreover, analysis of the monosaccharide composition in the fermented LPs indicated that the proportions of glucose decreased, while arabinose and galacturonic acid proportions increased relative to unfermented LP-0. Further, LP-6 demonstrated the highest growth for *Bifidobacterium* compared to LP-0, while the other fermentation time led to comparable or worse probiotic promoting activities. These results suggest that lactic acid bacteria fermentation alters the physicochemical properties of litchi polysaccharides, such that suitable fermentation time can enhance their probiotic activities.

KEYWORDS

litchi, fermentation, polysaccharide, chemical structure, probiotic activity

Introduction

Litchi (*Litchi chinensis Sonn.*) is a tropical to subtropical fruit that has become one of the most popular fruits because of its high nutritive value (1). Litchi is prone to spoilage and has a short shelf-life due to its rich nutrition content and maturation during high temperature and high humidity conditions. Processing is an important

way to prolong litchi shelf-life. Lactic acid bacteria fermentation is widely used in fruit processing, because it enhances fruit nutritional properties and improves flavors (2, 3), thereby representing a useful means of exploiting litchi nutritional content. For example, the total phenolic and total flavone contents in litchi juice dramatically increase after *Lactobacillus. casei* fermentation (4). The contents of total amino acids in litchi juice-soybean protein complexes decrease with lactic acid bacteria fermentation (5), while the species and contents of fatty acid groups increase (6). Additionally, *Lactobacillus plantarum* HU-C2W was used as a starter culture and enhanced the production of γ-aminobutyric acid in fermented litchi juice (7). Overall, investigations of lactic acid bacterial fermentation of litchi have primarily focused on changes in nutrient content, like those of polyphenols, flavonoids, fatty acids, and γ-aminobutyric acid. In contrast, few studies have evaluated the effects of lactic acid bacteria fermentation on the primary functional ingredients in litchi pulp. Previous studies have suggested that numerous health benefits of litchi pulp could be related to polysaccharides that exhibit immunostimulatory (8), antioxidant (9, 10), and antiproliferative effects (11). However, the effects of lactic acid bacterial fermentation on litchi pulp polysaccharides were unknown yet.

Previous studies showed that polysaccharides are indigestible food components and exhibit their bioactivities primarily depending on the regulation of intestinal flora and their metabolites (12). For example, *Lycium barbarum* polysaccharides significantly increase the abundances of some potential probiotic bacterial genera like *Akkermansia*, *Lactobacillus*, and *Prevotellaceae* that can promote immunostimulatory activity (13). In addition, the anti-diabetic effects of *Plantago asiatica* L. polysaccharides in type 2 diabetic rats may be associated with increased colon bacterial diversity and abundances, including those of *Lactobacillus fermentum* and *Prevotella loescheii* (14). Further, bitter gourd polysaccharides have been shown to improve intestinal flora disorders and increase the abundance of beneficial flora that can ameliorate rat obesity (3). Thus, polysaccharides exert health benefits by selectively promoting intestinal probiotic strains. Hence, an assessment of the probiotic activities of polysaccharides is essential for evaluating their potential health effects. Previous studies have reported that polysaccharides from pistachio hulls exhibit probiotic potential by promoting the proliferation of *L. plantarum* PTCC 1896 and *L. rhamnosus* GG (15). Similarly, yam polysaccharides have been shown to significantly promote *S. thermophilus* growth (16). Longan polysaccharides significantly improve *Leuconostoc mesenteroides* and *Lactobacillus casei* proliferation (17). In contrast, the potential probiotic activities of litchi polysaccharides remain unknown.

The present study aimed to investigate the influence of lactic acid bacterial fermentation on the physicochemical properties and probiotic activities of litchi pulp. To accurately identify changes in polysaccharide structures and prebiotic properties during fermentation, polysaccharides were prepared from different fermentation times (0, 6, 12, 24, 36, 48, 60, and 72 h), followed by the analysis of their chemical composition, monosaccharide composition, molecular weights (Mw), functional group characteristics, and their promotion of *Bifidobacteria* strain proliferation.

Materials and methods

Materials and chemicals

Plant materials and chemicals

Fresh litchi (cv. Hei-ye) fruits were provided by the Pomology Research Institute of Guangdong Academy of Agricultural Sciences (Guangzhou, China). Fresh litchi pulp was dried under hot air at 70°C for further analysis.

Standard dextran, rhamnose (Rha), arabinose (Ara), glucose (Glu), galactose (Gal), and mannose (Man) chemicals were purchased from Sigma (St. Louis, MO, United States). All other reagents were of analytical grade. Man-Rogosa-Sharpe (MRS) and sugar-free MRS were purchased from Guangdong Huankai Microbial Technology Co., Ltd. (Guangzhou, China). All other chemicals were purchased from Guangzhou Qiyun Biological Co., Ltd. (Guangzhou, China) and were of analytical grade.

Bacterial strains

Lactobacillus fermentum CICC 21828 was purchased from the China Center of Industrial Culture Collection (Beijing, China). *Bifidobacterium longum* ATCC 15707, *Bifidobacterium infantis* GDMCC 1.207 and *Bifidobacterium adolescentis* GDMCC 1.278 were purchased from the Guangdong Microbial Culture Collection Center (Guangzhou, China). Strains were stored in MRS broth containing 25% glycerol within liquid nitrogen until later use. Prior to use, bacterial strains were revived in MRS broth supplemented with 0.05% L-cysteine using previously described procedures (18).

Preparation of fermented litchi pulp

Dried litchi pulp pH was adjusted to 5.0 ± 0.2 with 2 M NaOH after homogenizing with water (1:7 w/v) for 5 min. Litchi juice was then sterilized at 121°C and 103.4 kPa for 20 min. Individual Erlenmeyer flask was used for 100 mL of sterilized litchi juice without any other nutrients. Each flask received 1 mL inoculum containing 6.0 log CFU/mL of activated *L. fermentum*. Fermentation was then initiated by incubation on a reciprocal shaker for 72 h at 37°C. Three duplicate samples were taken at 0,

6, 12, 24, 36, 48, 60, and 72 h to determine culture pH and extract polysaccharides. Enumeration of *L. fermentum* cell densities at each fermentation time point were also conducted using MRS agar.

Litchi polysaccharide extraction

Litchi polysaccharides were extracted as previously described (19), with slight modifications. Briefly, fermented litchi pulp was boiled for 10 min at 100°C to kill live *Lactobacillus*. Boiled juice was topped with 900 mL distilled water up to 1 L, followed by incubation at 90°C for 4 h before collecting filter liquor. The extraction process was repeated and the filtrates were collected, combined, and then vacuum concentrated at 65°C. To remove proteins, the extracted solutions were subjected to the Sevag method four times (20). Fourfold volumes of ethanol were added to the protein-removed solutions to achieve polysaccharide precipitation at 4°C for 24 h. The precipitates were collected by centrifugation at 4,000 × *g* for 10 min, washed with ethanol, and lyophilized to obtain the final litchi polysaccharides (LPs). The polysaccharides extracted from different time points during litchi pulp fermentation are referred as follows: LP-0, LP-6, LP-12, LP-24, LP-36, LP-48, LP-60, and LP-72, respectively.

Physicochemical properties of litchi polysaccharides

Chemical compositions

Total sugar contents were determined using the phenol-sulfuric acid method according to previously published methods (21) and with glucose as the standard. Briefly, 1 mL crude LP solution (0.25 mg/mL) was mixed with 500 μL 6% phenol and 2.5 mL concentrated H_2SO_4. After cooling in an ice bath for 30 min, the absorbance of the sample was measured using a UV–VIS spectrophotometer at 490 nm. Uronic acid contents were determined using a modified hydroxy diphenyl method and with galacturonic acid as the standards (11). Briefly, 0.25 mL of the crude LP solution (0.25 mg/mL) was added with 1.5 mL sulfuric/tetraborate and vortexed. The mixture was in a water bath at 100°C for 5 min. After cooling in an ice bath, 25 μL m-hydroxydiphenyl reagent was added. Then the absorbance of the sample was measured using a UV–VIS spectrophotometer at 524 nm. Lastly, protein concentrations were measured with the Bradford method using bovine serum albumin for standards (22). Briefly, 1 mL of the crude LP solution (10 mg/mL) was added with 5 mL of Bradford reagent and incubated at 37°C for 15 min in a water bath. Absorbance was read at 590 nm in a UV-VIS spectrophotometer.

Molecular weight analysis

To determine the molecular weights of the polysaccharides, the average molecular weights (Mw) were detected by high-performance gel permeation chromatography (HPGPC) using an Agilent technologies 1260 series instrument (Agilent Co., United States) equipped with a Shodex OH-pak SB-804 HQ column (8 mm × 300 mm). Chromatographic procedures and conditions were performed as previously described (23). Dextran standards with different molecular weights (6.7×10^5, 4.1×10^5, 2.7×10^5, 5×10^4, 2.5×10^4, 1.2×10^4, 5×10^3, and 1×10^3 Da) were used to calibrate the standard curve using the GPC software program (Agilent Technologies, Inc., United States, version 3.4).

Monosaccharide compositions

Litchi polysaccharides monosaccharide compositions were determined by HPLC with PMP precolumn derivatization (24). Briefly, polysaccharide samples (2.0 mg) were hydrolyzed with 0.2 mol/L trifluoroacetic acid at 120°C for 2 h. After hydrolysis, excess acid was removed by evaporation under a nitrogen atmosphere. Sodium hydroxide (0.1 mol/L) was added to dissolve the dried hydrolyzates. The mixtures were treated with 0.5 mol/L PMP in methanol and then incubated at 70°C for 30 min. After cooling to room temperature, the mixture was neutralized by adding 0.3 mol/L hydrochloric acid and then extracted with chloroform, followed by chloroform. The extractions were repeated three times. The aqueous phases were filtered through a 0.22 μm membrane and the resulting solutions were analyzed on an Agilent 1100 HPLC system (Agilent, United States) with a C18 column (4.6 mm × 250 mm, 5 μm) and a DAD detector. Elution was performed with a mixture of 0.1 M phosphate buffer solution (pH 7.0) and acetonitrile in a ratio of 82:18 (v/v), a flow rate of 1.0 mL/min, and a detection wavelength set as 250 nm.

Fourier transform infrared spectroscopy

A Fourier Transform Infrared (FT-IR) spectrophotometer (NEXUS 670, Nicolet, United States) was used to investigate the functional groups within LPs. Ground LPs were mixed with dry KBr and pressed into a mold to generate a tablet that was then subjected to the spectral region of 4000–400 cm^{-1} (25).

Probiotic activities

Three *Bifidobacterium* strains—*B. adolescentis*, *B. infantis*, and *B. longum* were used to investigate *in vitro* probiotic activities of the LPs isolated from the unfermented and fermented litchi pulps. Carbohydrate-free MRS broth supplemented with 0.05% (w/v) L-cysteine was used as the basal medium for the experiments and as the blank control, while fructooligosaccharide (FOS) was used for the positive control. All LPs and FOS were filter-sterilized and separately added to

the basal medium to obtain 1.0% (w/v) final concentrations. Activated *Bifidobacterium* strains were added to medium at final concentration of 1×10^6 CFU/mL and then incubated at 37°C for 48 h under anaerobic conditions (85% N_2, 10% CO_2 and 5% H_2). Bacterial growth was monitored by measuring culture optical density at 600 nm (OD_{600}) at 24 and 48 h, while culture pH was simultaneously measured using a pH meter (pH S-3C, Shanghai Precise Scientific Instrument Corp., China).

Statistical analyses

All experiments and analyses were performed in triplicate. Data analysis was performed using the SPSS statistical software program (version 19; SPSS, Inc., Chicago, IL, United States). Results are reported as means ± SD. Data were subjected to one-way ANOVA tests followed by Duncan's multiple range tests to identify statistical differences between values. Statistical significance was considered at $p < 0.05$.

Results and discussion

Litchi pulp fermentation

The effects of fermentation time on the growth of *L. fermentum* and litchi pulp pH were shown in Figure 1, where it can be seen that bacterial counts increased during fermentation (Figure 1A). Specifically, an initial population of 5.41 log fu/mL, slightly increased during the lag phase (0–2 h), and then rapidly increased to 8.49 log CFU/mL during the logarithmic phase (2–24 h). During the stationary phase, bacterial number slowly decreased until 60 h (8.28 log CFU/mL), then markedly decreased from 60 to 72 h (6.20 log CFU/mL) in the decay phase due to nutrient deficiencies.

The increased bacterial number indicated that *L. fermentum* used the nutrients within the litchi juice to grow. The consumption of sugars by lactic acid bacteria results in the accumulation of lactic acid and short-chain fatty acids (23). Consequently, the growth of probiotic microorganisms was also accompanied by decreased medium pH. Accordingly, the pH of litchi juice decreased throughout fermentation. Specifically, pH began at 5.16, slightly dropped over 2–4 h, then quickly fell to 3.95 at 12 h. And pH slowly continued to decline until reaching 3.81 at 60 h (Figure 1B).

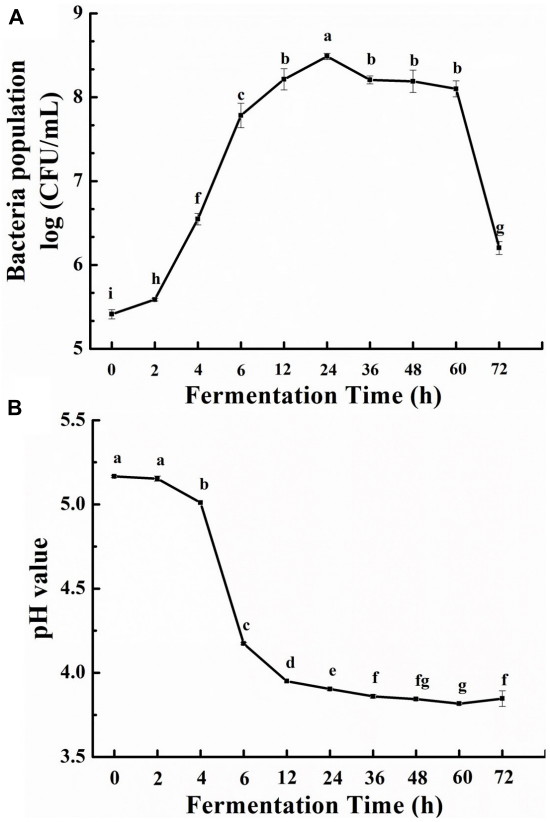

FIGURE 1
Growth effects of litchi pulp on *Lactobacillus fermentum* with different fermentation times **(A)**, and the pH of litchi pulp cultures **(B)**. Mean ± SD ($n = 3$). Different lowercase letters represent statistically significant differences among samples ($p < 0.05$).

Preliminary characterization of litchi polysaccharides

The yields and contents of total sugar, uronic acids, proteins, in addition to the molecular weights of isolated LPs were evaluated (Table 1). Compared with unfermented samples, polysaccharide yields first increased with fermentation at 6 h, then decreased with increasing fermentation time from 6 to 48 h, and then gradually increased in later fermentation times (48–72 h). LP-6 exhibited the highest yield among all samples ($p < 0.05$). The total sugar content of non-fermented litchi pulp polysaccharide was higher than those of fermented samples ($p < 0.05$). Similar decreases in carbohydrate contents have also been observed for polysaccharides from rice bran after *Grifola frondosa* fermentation (26). In addition, LP-72 exhibited the highest uronic acid content, while LP-6 exhibited the lowest ($p < 0.05$). The protein contents in fermented polysaccharides decreased with fermentation time ($p < 0.05$). Further, the protein contents in non-fermented polysaccharides were lower than in fermented samples (i.e., LP-6, LP-12, LP-24, LP-36, and LP-48) ($p < 0.05$).

The Mw of LPs were determined using GPC with RID. Overall, LPs Mw first decreased and then increased with fermentation time, while LP-6 exhibited the lowest Mw (Table 1). Similar results have also been observed for polysaccharide from longan pulp after fermentation for

TABLE 1 Physicochemical properties of polysaccharides derived from litchi pulp fermented with *Lactobacillus fermentum* for different times.

LPs	Extraction yield (%)	Total sugars (%)	Uronic acid (%)	Protein (%)	Mw (× 10^4 Da)
LP-0	1.73	65.27 ± 0.01^{a}	33.33 ± 0.93^{bc}	0.24 ± 0.01^{e}	13.60
LP-6	2.67	61.90 ± 0.00^{b}	20.87 ± 0.88^{e}	1.03 ± 0.02^{b}	10.40
LP-12	1.90	56.92 ± 0.01^{cd}	31.87 ± 0.86^{bc}	1.28 ± 0.01^{a}	13.80
LP-24	1.93	52.49 ± 0.01^{e}	24.84 ± 0.30^{d}	1.29 ± 0.01^{a}	14.50
LP-36	1.50	59.18 ± 0.01^{bc}	33.52 ± 0.04^{b}	0.61 ± 0.01^{c}	14.80
LP-48	1.66	53.21 ± 0.01^{e}	30.51 ± 0.05^{c}	0.40 ± 0.01^{d}	16.00
LP-60	2.08	54.66 ± 0.04^{de}	24.03 ± 0.10^{d}	0.01 ± 0.01^{f}	15.90
LP-72	2.34	55.45 ± 0.01^{de}	36.67 ± 0.66^{a}	0.02 ± 0.01^{f}	15.20

Different lowercase letters represent statistically significant differences among samples ($p < 0.05$).

TABLE 2 Monosaccharide compositions of polysaccharides derived from litchi pulp fermented with *Lactobacillus fermentum* for different times.

LPs	GalA (%)	Glu (%)	Ara (%)	Gal (%)	Man (%)	GlcA (%)	Xyl (%)	Rha (%)
LP-0	40.45 ± 5.01^{ab}	30.14 ± 3.83^{a}	18.72 ± 1.46^{ab}	5.35 ± 0.01^{ab}	2.59 ± 0.01^{c}	2.42 ± 0.21^{b}	0.17 ± 0.24^{a}	0.17 ± 0.24^{a}
LP-6	39.24 ± 0.25^{a}	33.41 ± 1.85^{a}	17.79 ± 1.77^{a}	5.04 ± 0.17^{a}	2.22 ± 0.08^{a}	1.95 ± 0.19^{a}	0.34 ± 0.06^{abc}	–
LP-12	48.04 ± 1.76^{c}	20.37 ± 0.50^{bc}	20.80 ± 0.67^{bc}	5.85 ± 0.03^{c}	2.18 ± 0.04^{a}	2.35 ± 0.04^{b}	0.25 ± 0.36^{ab}	0.15 ± 0.22^{a}
LP-24	38.79 ± 2.00^{a}	30.57 ± 2.05^{a}	19.74 ± 0.03^{abc}	5.49 ± 0.19^{b}	2.27 ± 0.08^{a}	2.37 ± 0.10^{b}	0.51 ± 0.09^{abc}	0.26 ± 0.00^{a}
LP-36	46.63 ± 4.48^{bc}	22.02 ± 2.85^{bc}	19.71 ± 1.47^{abc}	6.16 ± 0.13^{c}	2.42 ± 0.02^{b}	2.50 ± 0.17^{bc}	0.39 ± 0.05^{abc}	0.15 ± 0.21^{a}
LP-48	44.79 ± 0.12^{abc}	18.66 ± 0.56^{c}	23.53 ± 0.58^{de}	6.69 ± 0.12^{d}	2.50 ± 0.06^{bc}	2.86 ± 0.04^{cd}	0.67 ± 0.01^{bc}	0.30 ± 0.00^{a}
LP-60	38.82 ± 2.78^{a}	28.18 ± 1.53^{ab}	21.56 ± 0.64^{cd}	6.03 ± 0.12^{c}	2.17 ± 0.02^{a}	2.57 ± 0.20^{bc}	0.54 ± 0.09^{abc}	0.13 ± 0.18^{a}
LP-72	43.91 ± 1.90^{abc}	17.82 ± 0.50^{c}	24.29 ± 0.94^{e}	7.45 ± 0.27^{e}	2.48 ± 0.03^{bc}	3.14 ± 0.18^{d}	0.74 ± 0.21^{c}	0.17 ± 0.24^{a}

Different lowercase letters represent statistically significant differences among samples ($p < 0.05$).

different times (19). The prominent decrease in Mw of LP-6 could be related to the accumulation of carbohydrases secreted by bacteria during the lag and logarithmic phases (Figure 1A). Such activities would lead to the efficient hydrolysis of polysaccharides, thereby reducing overall Mw values and providing useable carbon sources for bacterial growth (27). However, the Mw of the fermented polysaccharides (except for LP-6) increased to various degrees compared to the LP-0 samples. The increased Mw likely arose from that the bacteria preferentially use the smaller Mw fractions over larger Mw fractions (28), thereby increasing the average Mw across fermentations over time.

Monosaccharide compositional analyses revealed that all LPs were heteropolysaccharides that comprised different ratios of galacturonic acid, glucose, arabinose, galactose, mannose, glucuronic acid, xylose, and/or rhamnose (Table 2). The monosaccharide compositions of the seven fermented polysaccharides were similar to those of unfermented polysaccharide, indicating that fermentation did not change the essential monosaccharide types identified within the litchi polysaccharides. However, the ratios of monosaccharide compositions considerably differed. The major monosaccharides in the LPs were galacturonic acid, glucose, and arabinose. Galacturonic acid was most abundant in all samples, with a minimum value of 38.79% in LP-24 and a maximum value of 48.55% in LP-12. The relative percentages of glucose

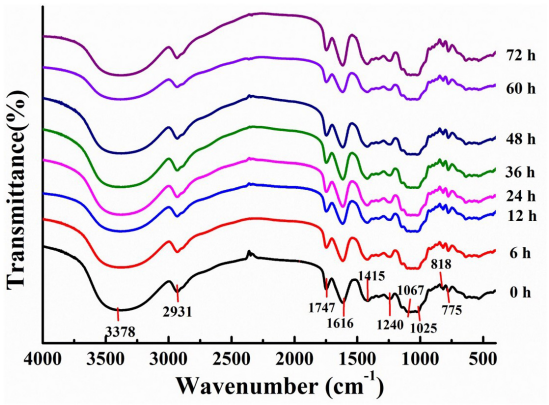

FIGURE 2
Fourier Transform Infrared (FT-IR) spectra for polysaccharides derived from litchi pulp fermented with *Lactobacillus fermentum* for different times.

in the other fermented LPs (except for LP-6) were lower than in the non-fermented LP-0 sample. Conversely, the percentage compositions of arabinose and galactose exhibited opposite trends. This was consistent with the other reported finding, as *Saccharomyces cerevisiae* and *Bacillus subtilis* fermentation decreased the molar ratio of glucose among wheat bran

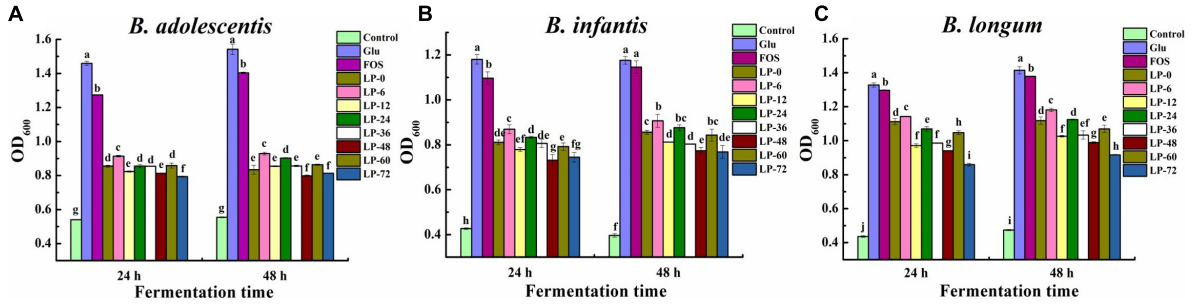

FIGURE 3
The growth of probiotic strains *Bifidobacterium adolescentis* **(A)**, *Bifidobacterium infanitis* **(B)**, and *Bifidobacterium longum* **(C)** cultivated on polysaccharides derived from litchi pulp fermented with *Lactobacillus fermentum* for different times. Mean ± SD (n = 3). Different letters indicate significant ($p < 0.05$) differences at the same incubation time.

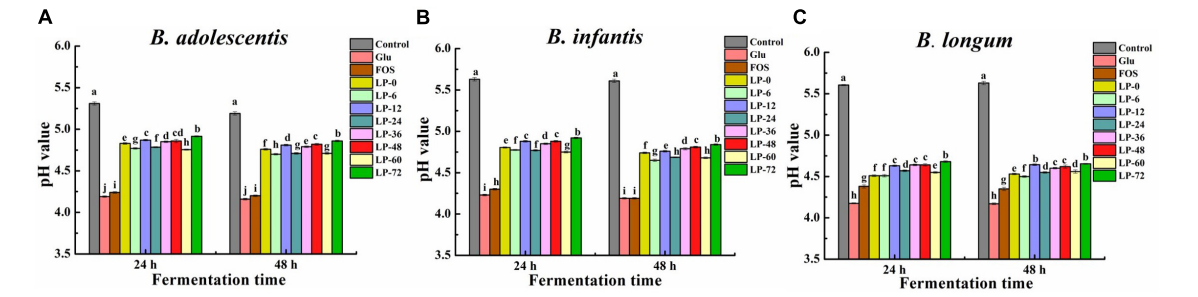

FIGURE 4
The pH of probiotic strains *Bifidobacterium adolescentis* **(A)**, *Bifidobacterium infanitis* **(B)**, and *Bifidobacterium longum* **(C)** cultivated on polysaccharides derived from litchi pulp fermented with *Lactobacillus fermentum* for different times. Mean ± SD (n = 3). Different letters indicate significant ($p < 0.05$) differences at the same incubation time.

polysaccharides, while increasing the molar ratio of arabinose and galactose (24).

Fourier Transform Infrared analysis of LPs was also conducted (**Figure 2**). All LPs fractions exhibited a strong broad peak at 3600–3200 cm^{-1} and a sharp weak band at 2930–2926 cm^{-1} in their FT-IR spectra, which arose from the O–H and C–H stretching vibrations, respectively (29). In addition, characteristic absorption peaks associated with uronic acid were observed at 1747 and 1616 cm^{-1} (30), while a characteristic absorption peak for galacturonic acid in pectic polysaccharides was observed at 1025 cm^{-1} (31). The observed absorption peaks near 1100–1000 cm^{-1} derived from characteristic C–O–C glycosidic bond vibrations and ring vibrations overlapping glycosidic bridges, indicating the presence of pyranose (32). Absorption signals near 890 cm^{-1} and 775 cm^{-1} were attributed to β– and α– type glycosidic linkages, respectively (33, 34). Together, these results provided important insights into potential LPs that represented acidic heteropolysaccharides with both α– and β– ring structures. The characteristic absorption peaks of LPs were similar, demonstrating that fermentation did not alter the primary functional group compositions of polysaccharides (35).

Litchi polysaccharides probiotic activity

Bacterial growth of three *Bifidobacterium* strains was evaluated when LPs, Glu, or FOS were used as carbon sources for 24 and 48 h incubation (**Figure 3**). In the case of *B. adolescentis*, all evaluated carbon sources supported significant growth of probiotic strain cultures when compared against the blank control (**Figure 3A**). This suggested LPs could be used by probiotic strains for growth similarly to FOS and Glu, and this was supported by previous findings (36). Bacterial growth dynamics were similar between 24 and 48 h and increased following the order of Glu >FOS >LPs at both fermentation time points ($p < 0.05$). Moreover, some fermented LPs (i.e., LP-6, LP-24, and LP-60) exhibited better probiotic activity at 48 h compared to unfermented polysaccharides (LP-0), with LP-6 exhibiting the highest microbial growth promotion.

Bifidobacterium infantis growth for both Glu and blank groups did not exhibit any obvious changes between different incubation times, while LPs and FOS cultures exhibited marginal increases at 48 h compared to 24 h (**Figure 3B**).

This result was consistent with a previous study (30) that the complex structures of LPs and FOS likely led to their slower metabolism rate and continuous probiotic growth at 48 h relative to Glu. Moreover, differences in bacterial growth on fermented litchi polysaccharides were exhibited compared to the unfermented control. LP-6 and LP-24 exhibited better probiotic activity compared to LP-0, while LP-6 activity was the highest at 48 h. The highest OD_{600} values of the LPs groups were generally observed at 48 h, with relative differences in the following order of LP-6 > LP-0 ≈ LP-24 ≈ LP-60 > LP-12 ≈ LP-36 > LP-48 ≈ LP-72.

The effects of LPs on the growth of *B. longum* strains were also evaluated (**Figure 3C**). All LPs, FOS and Glu supplements stimulated greater bacterial activity compared to the blank control. Bacterial growth increased in all test groups at 48 h relative to 24 h. The LP-6 exhibited the most bacterial growth among all LPs, while the LP-72 exhibited the worst growth ($p < 0.05$) at both 24 and 48 h. Further, only LP-6 exhibited the most bacterial growth among fermented LPs compared to unfermented LP-0, while the other fermented LPs exhibited comparable or worse growth of bacteria. The maximum OD_{600} values for LPs cultures at 48 h followed the order of LP-6 > LP-0 ≈LP-24 > LP-60 > LP-36 ≈ LP-12 > LP-48 > LP-72. Overall, these results indicated that the fermentation of litchi pulp with *L. fermentum* could influenced the probiotic effects of polysaccharides for the growth of *Bifidobacterium*.

The acidifying activities of probiotics, which were stimulated by LPs, FOS and Glu, were further investigated (**Figures 4A–C**). The pH of evaluated strains cultures decreased in the order of blank > LPs > Glu > FOS at 24 and 48 h. Among the experimental conditions for all three *Bifidobacteria*, the pH of LP-6 cultures was lower than in the LP-0 cultures but still higher than in the positive control FOS and Glu cultures. These results contrasted with the relative ordering of probiotic abundances when stimulated with polysaccharides, consistent with the results of a previous study (23). Minimum pH values reflected the acidifying activity of bacterial strains, in addition to the use of carbohydrates by the specified strain (37). Fermentation was not always promoted probiotic bacteria growth using litchi pulp polysaccharides compared with unfermented polysaccharides, contrasting with previous results for fermented longan pulp polysaccharides (19). Overall, these results indicated that a proper fermentation time by lactic acid bacteria for litchi pulp might facilitate the probiotic properties of its polysaccharides.

Structure-function relationship

Clarifying the relationships between the structures and probiotic properties of polysaccharides was important for understanding their mechanisms of action. Previous studies have indicated that the sugar contents of polysaccharides can affect their probiotic activity (36). In this study, obvious correlations were not apparent between the contents of total sugars and uronic acids in LPs with their probiotic effects. Similar results were also observed for polysaccharides from bamboo shoot residues that were prepared with four different drying methods (38). In addition, molecular weights also influenced the probiotic effects of carbohydrates. For example, some polysaccharides with lower molecular weights are potential probiotic influencing factors (39, 40). Different ratios of monosaccharides in various fractions of rapeseed polysaccharides have been shown to contribute to their differing probiotic effects (41). Further, polysaccharides that primarily comprise glucose, xylose, and galactose exert better growth-stimulating effects (42). In the present study, LP-6 exhibited the greatest stimulation of *Bifidobacteria* growth. This could be attributed to the LP-6 sample containing the lowest average molecular weight among all LPs. Furthermore, LP-6 primarily comprised glucose, galactose, and xylose, which were the most abundant components of all LPs. In contrast, LP-48 and LP-72 cultures exhibited lower bacterial growth associated with the lower proportions of the above three components and higher Mw values. These molecular structural features interactively influenced the probiotic activities of LPs. Previous studies have observed that fermentation can be an effective means to enhance probiotic activity (19, 43). This study further observed that an appropriate fermentation time was critical for increasing probiotic activities.

Conclusion

In this study, the impact of lactic acid bacteria fermentation on the physicochemical properties and probiotic activities of LPs was evaluated. The extraction yields, total sugar contents, uronic acid contents, molecular weights, and monosaccharide compositions of LPs varied as fermentation proceeded. Moreover, LP-6 exhibited the best probiotic activity by promoting the proliferation of *Bifidobacterium* strains. These results provide an experimental basis for the development of novel litchi polysaccharides and suggest that *Lactobacillus fermentum* fermentation can be used to generate prospective probiotic activity polysaccharides.

Data availability statement

The original contributions presented in this study are included in the article/supplementary material, further inquiries can be directed to the corresponding authors.

Author contributions

CH: experimental design, methodology, data curation, and writing-original draft. RZ: supervision and conceptualization. XJ, LD, QM, DZ, and ZS: supervision. MZ: conceptualization, supervision, writing-review and editing, and funding acquisition. FH: conceptualization, supervision, experimental design, writing-review and editing, and project administration. All authors listed have made a substantial, direct, and intellectual contribution to the work, and approved it for publication.

Funding

This study was supported by the National Natural Science Foundation of China (32072178 and 31801498), Guangdong special support program (2019BT02N112), Science and Technology Program of Guangzhou, China (202103000061), and the Special fund for scientific innovation strategy-construction of high level Academy of Agriculture Science (R2021PY-QY002).

Acknowledgments

We are grateful to all study participants for their enrolling in this study.

Conflict of interest

The authors declare that the research was conducted in the absence of any commercial or financial relationships that could be construed as a potential conflict of interest.

Publisher's note

References

1. Zhao L, Wang K, Wang K, Zhu J, Hu Z. Nutrient components, health benefits, and safety of litchi (*Litchi Chinensis Sonn.*): a review. *Compr Rev Food Sci Food Saf.* (2020) 19:2139–63. doi: 10.1111/1541-4337.12590

2. Zhang Z, Fan S, Huang D, Xiong T, Nie S, Xie M. Polysaccharides from Fermented *Asparagus Officinalis* with *Lactobacillus Plantarum* NCU116 alleviated liver injury via modulation of glutathione homeostasis, bile acid metabolism, and scfa production. *Food Funct.* (2020) 11:7681–95. doi: 10.1039/d0fo01435d

3. Wen JJ, Li MZ, Gao H, Hu JL, Nie QX, Chen HH, et al. Polysaccharides from fermented *Momordica Charantia* L. With *Lactobacillus Plantarum* NCU116 ameliorate metabolic disorders and gut microbiota change in obese rats. *Food Funct.* (2021) 12:2617–30. doi: 10.1039/d0fo02600j

4. Wen J, Ma L, Xu Y, Wu J, Yu Y, Peng J, et al. Effects of probiotic litchi juice on immunomodulatory function and gut microbiota in mice. *Food Res Int.* (2020) 137:109433. doi: 10.1016/j.foodres.2020.109433

5. Liu X, Liu Y, Chen M. Study on amino acid metabolism characteristics of litchi juice-soybean protein fermented by eight lactic acid bacteria. *Sci Technol Food Industry.* (2020) 41:106–13.

6. Xin L, Xue-Fang Z, Yun L, Zheng C, Jie-Ping W, Bo L. Dynamic of fatty acid group during fermentation of *Lactobacillus Rhamnosus* in the medium of lychee juice and soybean protein. *J Food Saf Q.* (2020) 11:3130–40.

7. Dongwei W, Yao W, Haibo L, Kai W, Lei Z, Zhuoyan H. Enhanced production of gamma-aminobutyric acid in litchi juice fermented by *Lactobacillus Plantarum* Hu-C2w. *Food Biosci.* (2021) 42:101155. doi: 10.1016/j.fbio.2021.101155

8. Jing Y, Huang L, Lv W, Tong H, Song L, Hu X, et al. Structural characterization of a novel polysaccharide from pulp tissues of litchi chinensis and its immunomodulatory activity. *J Agric Food Chem.* (2014) 62:902–11. doi: 10.1021/jf404752c

9. Gao W, Lin P, Zeng X-A, Brennan MA. Preparation, characterisation and antioxidant activities of litchi (*Litchi Chinensis Sonn.*) polysaccharides extracted by ultra-high pressure. *Int J Food Sci Technol.* (2017) 52:1739–50. doi: 10.1111/ijfs.13447

10. Hu XQ, Huang YY, Dong QF, Song LY, Yuan F, Yu RM. Structure characterization and antioxidant activity of a novel polysaccharide isolated from pulp tissues of *Litchi Chinensis*. *J Agric Food Chem.* (2011) 59:11548–52. doi: 10.1021/jf203179y

11. Huang F, Zhang R, Dong L, Guo J, Deng Y, Yi Y, et al. Antioxidant and antiproliferative activities of polysaccharide fractions from litchi pulp. *Food Funct.* (2015) 6:2598–606. doi: 10.1039/c5fo00249d

12. Huang F, Liu Y, Zhang R, Bai Y, Dong L, Liu L, et al. Structural characterization and in vitro gastrointestinal digestion and fermentation of litchi polysaccharide. *Int J Biol Macromol.* (2019) 140:965–72. doi: 10.1016/j.ijbiomac.2019.08.170

13. Zhu W, Zhou S, Liu J, McLean RJC, Chu W. Prebiotic, immuno-stimulating and gut microbiota-modulating effects of *Lycium Barbarum* Polysaccharide. *Biomed Pharmacother.* (2020) 121:109591. doi: 10.1016/j.biopha.2019.109591

14. Nie Q, Hu J, Gao H, Fan L, Chen H, Nie S. Polysaccharide from *Plantago Asiatica* L. Attenuates hyperglycemia, hyperlipidemia and affects colon microbiota in type 2 diabetic rats. *Food Hydrocolloids.* (2019) 86:34–42. doi: 10.1016/j.foodhyd.2017.12.026

15. Akbari-Alavijeh S, Soleimanian-Zad S, Sheikh-Zeinoddin M, Hashmi S. Pistachio hull water-soluble polysaccharides as a novel prebiotic agent. *Int J Biol Macromol.* (2018) 107(Pt A):808–16. doi: 10.1016/j.ijbiomac.2017.09.049

16. Ouyang J, Wang F, Li W, Li Q, Su X. Structure characterization of polysaccharide from Chinese Yam (*Dioscorea Opposite Thunb.*) and its growth-promoting effects on *Streptococcus Thermophilus*. *Foods.* (2021) 10:2698. doi: 10.3390/foods10112698

17. Huang F, Hong R, Zhang R, Yi Y, Dong L, Liu L, et al. Physicochemical and biological properties of longan pulp polysaccharides modified by *Lactobacillus Fermentum* fermentation. *Int J Biol Macromol.* (2019) 125:232–7. doi: 10.1016/j.ijbiomac.2018.12.061

18. Azmi AF, Mustafa S, Hashim DM, Manap YA. Prebiotic activity of polysaccharides extracted from *Gigantochloa Levis* (Buluh Beting) shoots. *Molecules.* (2012) 17:1635–51. doi: 10.3390/molecules17021635

19. Huang F, Hong R, Zhang R, Dong L, Bai Y, Liu L, et al. Dynamic variation in biochemical properties and prebiotic activities of polysaccharides from longan pulp during fermentation process. *Int J Biol Macromol.* (2019) 132:915–21. doi: 10.1016/j.ijbiomac.2019.04.032

20. Sevag MG, Lackman DB, Smolens J. Isolation of components of streptococcal nucleoproteins in serologically active form. *J Biol Chem.* (1938) 124:425–36.

21. DuBois M, Gilles KA, Hamilton JK, Rebers PA, Smith F. Colorimetric method for determination of sugars and related substances. *Anal Chem.* (2002) 28:350–6. doi: 10.1021/ac60111a017

22. Chen X, Zhang R, Li Y, Li X, You L, Kulikouskaya V, et al. Degradation of polysaccharides from sargassum fusiforme using Uv/H2o2 and its effects on structural characteristics. *Carbohydr Polym.* (2020) 230:115647. doi: 10.1016/j.carbpol.2019.115647

23. Zhang J, Chen H, Luo L, Zhou Z, Wang Y, Gao T, et al. Structures of fructan and galactan from *Polygonatum Cyrtonema* and their utilization by probiotic bacteria. *Carbohydr Polym.* (2021) 267:118219. doi: 10.1016/j.carbpol.2021.118219

24. Chen Q, Wang R, Wang Y, An X, Liu N, Song M, et al. Characterization and antioxidant activity of wheat bran polysaccharides modified by *Saccharomyces cerevisiae* and *Bacillus subtilis* fermentation. *J Cereal Sci.* (2021) 97:103157. doi: 10.1016/j.jcs.2020.103157

25. Wang T, Ye Z, Liu S, Yang Y, Dong J, Wang K, et al. Effects of crude *Sphallerocarpus Gracilis* polysaccharides as potential prebiotics on acidifying activity and growth of probiotics in fermented milk. *LWT.* (2021) 149:111882. doi: 10.1016/j.lwt.2021.111882

26. Liu Q, Cao X, Zhuang X, Han W, Guo W, Xiong J, et al. Rice bran polysaccharides and oligosaccharides modified by *Grifola Frondosa* fermentation: antioxidant activities and effects on the production of No. *Food Chem.* (2017) 223:49–53. doi: 10.1016/j.foodchem.2016.12.018

27. Jiang Y, Du J, Zhang L, Li W. Properties of pectin extracted from fermented and steeped hawthorn wine pomace: a comparison. *Carbohydr Polym.* (2018) 197:174–82. doi: 10.1016/j.carbpol.2018.06.001

28. Tang N, Wang X, Yang R, Liu Z, Liu Y, Tian J, et al. Extraction, isolation, structural characterization and prebiotic activity of cell wall polysaccharide from *Kluyveromyces Marxianus*. *Carbohydrate Polymers.* (2022) 289:119457. doi: 10.1016/j.carbpol.2022.119457

29. Yu C, Ahmadi S, Shen S, Wu D, Xiao H, Ding T, et al. Structure and fermentation characteristics of five polysaccharides sequentially extracted from sugar beet pulp by different methods. *Food Hydrocolloids.* (2022) 126:107462. doi: 10.1016/j.foodhyd.2021.107462

30. Song C, Huang F, Liu L, Zhou Q, Zhang D, Fang Q, et al. Characterization and prebiotic properties of pectin polysaccharide from *Clausena Lansium* (Lour.) skeels fruit. *Int J Biol Macromol.* (2022) 194:412–21. doi: 10.1016/j.ijbiomac.2021.11.083

31. Tan S, Luo Z, Cheng J. Effect of H2 O2-Vc degradation system on the structure and activity of polysaccharides from *Nymphaea Hybrid*. *Food Sci.* (2021) 42:48–53. doi: 10.7506/spkx1002-6630-20201202-036

32. Zhang W, Xiang Q, Zhao J, Mao G, Feng W, Chen Y, et al. Purification, structural elucidation and physicochemical properties of a polysaccharide from *Abelmoschus Esculentus* L (Okra) flowers. *Int J Biol Macromol.* (2020) 155:740–50. doi: 10.1016/j.ijbiomac.2020.03.235

33. Chen J, Zhang X, Huo D, Cao C, Li Y, Liang Y, et al. Preliminary characterization, antioxidant and alpha-glucosidase inhibitory activities of polysaccharides from *Mallotus Furetianus*. *Carbohydr Polym.* (2019) 215:307–15. doi: 10.1016/j.carbpol.2019.03.099

34. Bai Y, Huang F, Zhang R, Dong L, Jia X, Liu L, et al. Longan pulp polysaccharides relieve intestinal injury in vivo and in vitro by promoting tight junction expression. *Carbohydr Polym.* (2020) 229:115475. doi: 10.1016/j.carbpol.2019.115475

35. Wan YJ, Hong T, Shi HF, Yin JY, Koev T, Nie SP, et al. Probiotic fermentation modifies the structures of pectic polysaccharides from carrot pulp. *Carbohydr Polym.* (2021) 251:117116. doi: 10.1016/j.carbpol.2020.117116

36. Xing L, Miao Y, Li N, Jiang L, Chen JY. Molecular structure features and lactic acid fermentation behaviors of water- and alkali-soluble polysaccharides from *Dendrobium Officinale*. *J Food Sci Technol.* (2021) 58:532–40. doi: 10.1007/s13197-020-04564-6

37. Gullon P, Gonzalez-Munoz MJ, Parajo JC. Manufacture and prebiotic potential of oligosaccharides derived from industrial solid wastes. *Bioresour Technol.* (2011) 102:6112–9. doi: 10.1016/j.biortech.2011.02.059

38. Chen GJ, Hong QY, Ji N, Wu WN, Ma LZ. Influences of different drying methods on the structural characteristics and prebiotic activity of polysaccharides from bamboo shoot (*Chimonobambusa Quadrangularis*) residues. *Int J Biol Macromol.* (2020) 155:674–84. doi: 10.1016/j.ijbiomac.2020.03.223

39. Zhao Y, Bi J, Yi J, Wu X, Ma Y, Li R. Pectin and homogalacturonan with small molecular mass modulate microbial community and generate high scfas via in vitro gut fermentation. *Carbohydr Polym.* (2021) 269:118326. doi: 10.1016/j.carbpol.2021.118326

40. Feng R, Kou J, Chen S, Wang N, Wang W, Wang L, et al. Preparation optimization, characterization, and antioxidant and prebiotic activities of carboxymethylated polysaccharides from jujube. *J Food Q.* (2021) 2021:1–15. doi: 10.1155/2021/3268149

41. Wang X, Huang M, Yang F, Sun H, Zhou X, Guo Y, et al. Rapeseed polysaccharides as prebiotics on growth and acidifying activity of probiotics in vitro. *Carbohydr Polym.* (2015) 125:232–40. doi: 10.1016/j.carbpol.2015.02.040

42. Macfarlane GT, Steed H, Macfarlane S. Bacterial metabolism and health-related effects of galacto-oligosaccharides and other prebiotics. *J Appl Microbiol.* (2008) 104:305–44. doi: 10.1111/j.1365-2672.2007.03520.x

43. Lin S, Wen L, Yang B, Jiang G, Shi J, Chen F, et al. Improved growth of *Lactobacillus Bulgaricus* and *Streptococcus Thermophilus* as well as increased antioxidant activity by biotransforming litchi pericarp polysaccharide with aspergillus awamori. *Biomed Res Int.* (2013) 2013:413793. doi: 10.1155/2013/413793

frontiers | Frontiers in Nutrition

TYPE Original Research
PUBLISHED 02 September 2022
DOI 10.3389/fnut.2022.1003657

OPEN ACCESS

EDITED BY
Yanjun Zhang,
Chinese Academy of Tropical Agricultural Sciences, China

REVIEWED BY
Liu Guodong,
Yangzhou University, China
Ling Zhu,
Jiangnan University, China
Wang Zhenjiong,
Nanjing University of Finance and Economics, China

*CORRESPONDENCE
Yayuan Zhang
zyy810@yahoo.cn
Xiangrong You
youxiangrong@gxaas.net

SPECIALTY SECTION
This article was submitted to Food Chemistry, a section of the journal Frontiers in Nutrition

RECEIVED 26 July 2022
ACCEPTED 15 August 2022
PUBLISHED 02 September 2022

CITATION
Wei P, Fang F, Liu G, Zhang Y, Wei L, Zhou K, You X, Li M, Wang Y, Sun J and Deng S (2022) Effects of composition, thermal, and theological properties of rice raw material on rice noodle quality. *Front. Nutr.* 9:1003657. doi: 10.3389/fnut.2022.1003657

Effects of composition, thermal, and theological properties of rice raw material on rice noodle quality

Ping Wei[1,2], Fang Fang[3], Guoming Liu[1,2], Yayuan Zhang[1,2]*, Linyan Wei[1], Kui Zhou[1,2], Xiangrong You[1,2]*, Mingjuan Li[1,2], Ying Wang[1,2], Jian Sun[2] and Sili Deng[4]

[1]Agro-Food Science and Technology Research Institute, Guangxi Academy of Agricultural Sciences, Nanning, China, [2]Guangxi Key Laboratory of Fruits and Vegetables Storage-processing Technology, Nanning, China, [3]Whistler Center for Carbohydrate Research and Department of Food Science, Purdue University, West Lafayette, IN, United States, [4]Guangxi Institute of Botany, Guangxi Zhuang Autonomous Region and Chinese Academy of Sciences, Guilin, China

The study aims to evaluate the relationships between characteristics of regional rice raw material and resulting quality of rice noodles. Four of most commonly used rice cultivars in Guangxi for noodles production were investigated. The results showed that compositions of rice flour primarily affected gelatinization and retrogradation, which then influenced the textural and sensory properties of rice noodles. Amylose content had strong positive correlation with peak viscosity (PV) and trough viscosity (TV) of rice flour ($P < 0.01$). PV and TV had strong negative correlations with adhesive strength ($P < 0.01$) and positive correlations with chewiness ($P < 0.05$), hardness, peak load and deformation at peak of rice noodles ($P < 0.01$). Protein content had positive correlation with the Setback of rice flour ($P < 0.05$), which is known to have influences on retrogradation. In addition, solubility had positive correlations with cooking loss ($P < 0.01$) and broken rate ($P < 0.05$) of rice noodles and strong negative correlation with its springiness ($P < 0.01$). Swelling power had negative correlation with broken rate ($P < 0.05$). As sensory score of rice noodles was negatively correlated with broken rate ($P < 0.05$) and cooking loss ($P < 0.01$) and positively correlated with springiness ($P < 0.01$), solubility and swelling power of rice flours were presumed to be useful for predicting consumer acceptability of rice noodles.

KEYWORDS

rice, rice noodle, processing, cooking performance, sensory properties

Highlights

- Amylose content of rice is strongly correlated with the texture profile of rice noodle.
- Adhesive strength had a negative correlation with texture profile of rice noodles.
- Peak, trough, and final viscosities had positive correlations with texture of rice noodles.

- Rice with 24% amylose content could be a critical value used in different rice noodles processing.
- Sensory score correlated negatively with cooking qualities and positively with springiness.

Introduction

Rice noodles are very popular in southern China and some southeast Asian countries, such as Thailand and Sri Lanka. Rice noodles are commonly processed from indica rice, and classified into fresh, dried, and frozen products in various thicknesses and shapes (1, 2). Guangxi province is the top producer of rice noodles in China and has a large number of different types of rice noodles. Consumers have different requirements regarding taste and mouthfeel properties for different types of rice noodles. For example, snail noodles have relatively high hardness and springiness, while rolled noodles and Guilin rice noodles have soft texture.

Rice noodle quality is closely related to the physical and chemical properties of rice flour. Starch is the major component of rice. Just like other crop starch (3–5), the viscoelastic property of rice noodles depends primarily on the starch structure and properties (2, 6, 7). Zhou et al. (8) reported a highly significant correlation between amylose content and the sensory score of rice noodles, so amylose content was usually selected as the sensitive indexes to predict the quality of rice noodles. The amylose content suitable for processing the pressed fresh rice noodles were found to be in the range of 22.2–26.9 %. Xuan et al. (9) suggested that it is essential to use rice with an amylose content in the range of 20–25% for rice noodle production. Rice with amylose content of less 20% or more than 25% is not suitable for rice noodle production. It can be seen from the above that the recommended range of amylose content for rice noodle production by different researchers was different. The appropriate rice starch content should be selected according to the actual demand of rice noodle products. Rice protein (endosperm protein) is also an important component of rice. The protein content in rice varied greatly in different varieties growing in different environments. Martin et al. (10) suggested that the gelatinization characteristics of rice flour were influenced by the network structure formed by the protein binding with water and the formation of disulfide bond. Baxter et al. (11) concluded that rice protein indirectly affected the rice processing adaptability mainly by changing gelatinizing properties of starch, including its heat resistance, extrusion performance and retrogradation. Protein in rice could inhibit the water absorption and expansion of starch particles, resulting in higher gelatinization peak temperature of rice flour than that of starch alone. In addition, protein could strengthen the network structure of rice flour gel. Therefore, it is often considered that protein content can be used as an auxiliary index to choose the rice flour raw material for noodle production. The lipid content in rice starch is very low, but it is closely related to the gel properties of rice. Ibáñez et al. (12) reported that lipids had a greater effect on gelatinization and rheological properties compared to protein. Usually, the presence of lipids reduces the gelatinization heat enthalpy of starch and promotes the formation of gel system. The complex formed by lipids and starch prevents the amylose crystallization, reduces the dissolution of starch, maintains the stability of gel structure, and thereby inhibits the generation of aging and extends the shelf life of products. As lipid content in all kinds of rice varieties were usually very low, most previous reporter considered that it is no longer considered as an important quality index of raw rice used for rice noodles (line) production.

Different rice noodles are commonly produced from different sources of raw rice materials (mainly refer to the early polished indica rice), which is largely depends on the experiences of rice producer using regional rice varieties as raw materials. For example, dry rice noodles are usually made with Guichao varieties; some other rice varieties are combined with broken rice for snail rice noodles production; and rolled noodles are usually made from Zhengui varieties in Gxuangxi. It is very important to clarify the relationship between physical properties of rice varieties and the quality of regional rice noodles in China, which thereby could better guide the production of high-quality regional rice noodles. In the present study, four rice cultivars commonly use in rice noodle production in Guangxi were chosen to prepare rice flours. Their physicochemical composition, physicochemical characteristics, thermal properties, pasting properties, and rheological properties were investigated. Furthermore, the correlation between the physicochemical properties of rice starch and qualities (cooking qualities, texture properties and sensory quality) of rice noodles were analyzed. This study provides theoretical guidance regarding the selection of suitable rice raw materials for different rice noodle production, optimizing rice noodle processing technology, and improving rice noodle quality.

Materials and methods

Chemicals and reagents

Four early polished indica rice cultivars, including Zhengui (ZG), Shuanggui (SG), Guichao (GC), and Suimi (SM, belongs to GC variety) were selected and purchased from a local market in Nanning, China. Rice was ground by a high-speed grinder (WND-200, Zhejiang Lanxi Weinengda Electric Appliance Co., Ltd., Lanxi, China), passed through a 100-mesh sieve (CT410, FOSS Scino Co., Ltd., Suzhou, China), and then stored at 25°C in desiccator until further analysis. Amylose contents in rice standards were 0.40, 10.60, 16.20, and 26.50% w/w, respectively, which was provided by China National Rice Research Institute.

D-Glucose, α-amylase, and glucosidase were purchased from Sigma-Aldrich Ireland Ltd. (Dublin, Ireland). GOPOD was obtained from Megazyme (Bray, Ireland). Potassium hydroxide (cat. no.1310-58-3), sodium sulfite (cat. no.7757-83-7), sodium hydroxide (cat. no.1310-73-2) were from Sinopharm Chemical Reagent Co., Ltd. ethanoic acid (cat. no. 64-19-7), ethyl alcohol (cat. no. 64-17-5), acetic acid sodium salt (cat. no. 127-09-3), iodine (cat. no.7553-56-2), potassium iodide (cat. no.7681-11-0), ethanoic acid (cat. no.64-19-7) were from Shanghai anpu Experimental Technology Co., Ltd. All chemical reagents were of analytical grade.

Properties of rice flour

Compositions of rice flour

The moisture content, crude protein, and crude lipid contents in different rice flours were measured according to the method of Ministry of Health of the People's Republic of China (GB5009.3-2016, GB/T 5009.5-2016 and GB/T 5009.6-2016) respectively (13–15). The content of total starch in rice was determined using the method (AOAC, 996.11) provided by the Association of Official Agricultural Chemistry (16). The amylose contents were determined by measuring the absorbance at 700 nm via UV-Vis spectrophotometer (UV-2800, Unico Instrument Co., Ltd., Shanghai, China) following the method of Ministry of Health of the People's Republic of China (17). The adhesive strength of different rice flours was evaluated according to the method of Ministry of Health of the People's Republic of China (18). The chemical compositions of rice were determined in triplicate for each rice sample, and all results were reported on a dry weight basis.

Solubility and swelling power of rice flour

The solubility (S) and swelling power (SP) were determined following the method as described by Yi et al. (19) with minor modifications. Rice flour (1 g) in 100 mL deionized water was heated at 90 °C for 1 h with stirring. The sample was cooled to room temperature and centrifuged at 4,000 r/min for 15 min. The supernatant was dried in an oven at 105 °C until a constant weight was obtained. The S and SP were calculated using the following formulas:

$$S(\%) = \text{dry supernatant weight}/\text{dry sample weight} \times 100$$

$$SP = \text{wet sediment weight}/[\text{dry sample weight} \times (1 - S)]$$

Thermal properties of rice flour

Thermal properties of the rice flour were analyzed using a differential scanning calorimeter (DSC, TA Instruments, Q2000, USA). Rice flour and distilled water suspension (1:3) were sealed in aluminum pans and equilibrated at room temperature for 24 h before analysis. An empty aluminum pan was used as a reference. The gelatinization temperature and enthalpy were determined following the procedure of Wu et al. (20) with some modifications. The samples were heated at 10 °C/min over a temperature range of 30–105 °C. After that, the sealed pans were stored at 4°C for 7 d, followed by characterization of retrogradation with the same heating procedure. The onset temperature (To), peak temperature (Tp), conclusion temperature (Tc), enthalpies in gelatinization (ΔH_1) and retrogradation (ΔH_2) were recorded. The retrogradation degree (ΔH) was calculated as follows:

$$\Delta H/\% = \frac{\Delta H_2}{\Delta H_1} \times 100$$

Pasting properties of rice flour

The pasting properties of the rice flours were determined using a Rapid Visco Analyzer (RVA 4800, Perten Instruments Australia Pty Ltd., Sydney, Australia). The RVA parameters were previously described by Geng et al. (21). Rice flour (3.0 g, 14 g/100 g moisture basis) was weighted into an aluminum canister, and 25 g distilled water was added to attain a total sample weight of 28.0 g. The suspension was equilibrated at 50°C for 1 min, heated to 95°C at a rate of 12°C /min and maintained at 95°C for 2.5 min. It was then cooled to 50°C at the same rate and maintained at 50 °C for 2 min. The rotating speed of the paddle was kept at 160 rpm throughout the measurement. The parameters including Peak Viscosity (PV), Trough Viscosity (TV), Breakdown (BD), Final Viscosity (FV), and Setback (SB) values were obtained.

Rheological properties of rice flour

Rheologic properties of all samples were analyzed following the method as described by Meng (22) and carried out using a Discovery-1 rheometer (DHR-1, TA Instruments Ltd., New Castle, DE, USA). Rice flour suspensions (20%) were placed in the center of a Peltier plate attached to the rheometer. An aluminum parallel plate geometry (40 mm diameter) was used. The gap was set at 1,000 μm. Oscillation temperature ramp tests were performed at a strain of 2%, with a temperature ramp from 25 to 95°C to gelatinize the sample, followed by cooling down from 95 to 25°C for gel formation. The heating and cooling rates were both 5°C/min. Subsequently, frequency sweep tests were performed at 25°C in the range of 0.1–20 Hz at a strain of 2%. The 2% strain was in the linear viscoelastic region, according to the strain sweep results. Rheological parameters such as storage modulus (G') and loss modulus (G'') were obtained directly from rheometer data analysis software (Trios.Version 4.3.0.38388).

Rice noodles

Preparation of different rice noodles

Rice noodles were prepared using a One-step Modeling Rice Noodle Machine (MFD25C, Hunan Fenshifu Mechannical Technology Co., LTD, China). Before extrusion, rice was soaked in water at room temperature for 8 h. The soaked rice was poured into the extrusion pipe (preset temperature at 90°C) and extruded through a circular die with 0.20 cm round openings, and then and cut to the same length as they exited the extruder die. After extrusion, the rice noodles were placed in an incubator (YH0515T, Hunan Fenshifu Mechannical Technology Co., LTD, China) for 4 h at 75% humidity and 28°C to allow starch retrogradation to some extent. Finally, the rice noodles were taken out and dried at room temperature for 12 h to reduce the moisture content to below 14%. The dried noodles were kept in sealed plastic bags before analysis.

Cooking qualities of different rice noodles

The cooking time and broken rate of different rice noodles were determined by AACC standard methods (23). Five g of rice noodles with length of 15 cm for each strand were placed into 150 mL of boiling water and cooked. Cooking time was determined as the time required for the disappearance of white core as judged by gently squeezing the noodle between two glass slides. Broken rate was the ratio of the number of broken noodles to that of dried noodles. Noodles were drained, and the cooked water was collected in a beaker. The solid material content in the cooking water was determined by evaporating in a hot air oven at 105 °C overnight until a constant weight was reached. The cooking loss of noodles were determined according to Raungrusmee et al. (24) by the following equations:

$$\text{Cooking loss/ \%} = \frac{\text{remaining solid content after drying}}{\text{weight of fresh noodle}} \times 100$$

Sensory evaluation of rice noodles

The sensory properties of rice noodles were evaluated on a percentage point system (< 60 means poor, 61–80 means intermediate level, >80 means excellent) according to Wang et al. (25) with some modifications. The sensory panel was composed of 10 trained members who were 25–35 years old (five men and five women). All the cooked rice noodles were coded with random four-digit numbers. Meanwhile, water was provided for the panelist to gargle before testing different rice starch noodles. The samples were evaluated using a 100 point scale and the sensory characteristics include color (0–15 points), odor (0–10 points), tissue shape (0–15 points), firmness (0–20 points), smoothness (0–20 points) and elasticity (0–20 points), The value of each sensory characteristic was averaged and the total points were expressed as the sum of all sensory characteristics scores.

Textural properties of rice noodles

The textural profile of rice noodles was evaluated by texture profile analysis (TPA) and tensile properties using a texture analyzer (CT3, Brookfield, USA) according to a reported method (26). The rice noodles were cooked in boiling deionized water for the best cook time, followed by cooling to room temperature with deionized water, and drained off the water before measurement. For TPA, noodle samples were cut to 10 cm segments. There segments were placed in parallel with no space on the groove of the plate. The measurement parameters of TPA were: TA5 cylinder probe (diameter 12.5 mm and length 35 mm) at the test speed of 2.0 mm/s, 50% compression ratio, 5 g trigger force, 5 s interval between the compressions, and 200 pp/s data acquisition rate. TA-DGA model fixture was used for tensile properties testing. The samples were measured with a starting distance of 60 mm and target distance of 50 mm. The trigger force was set at 10 g with a tensile speed of 2 mm/s. Measurements were performed in six replicates.

Statistical analysis

The results are reported as mean and standard deviation of at least triplicate. The statistically analysis was performed by variance analysis (ANOVA) using SPSS 17.0 statistical software (SPSS Inc., Chicago, IL, USA). Significant differences between the means were determined by Duncan test ($P < 0.05$). Pearson's correlation coefficients among parameters were also calculated using SPSS 17.0 statistical software.

Results and discussion

Properties of rice flour

Compositions of rice flour

Total starch, amylose, crude protein and fat contents of different rice flours are shown in Table 1. the basic physical and chemical indexes of different rice varieties are different. Starch and protein are main rice compositions. The total starch and protein content in rice flour were 73.08–75.09 g/100 g (GC>SM>ZG>SG) and 7.31–8.04 g /100 g (GC>SM>SG>ZG), respectively. The amylose contents were in the range of 21.00–23.91 g/100 g following the order of GC>ZG>SG>SM. There were significant differences in amylose and protein content among different rice flours ($P < 0.05$).

TABLE 1 Physicochemical compositions of different rice flour.

Rice varieties	Moisture (%)	Total starch (%)	Amylose (%)	Protein (g/100 g)	Fat (g/100 g)
ZG	10.82 ± 0.57^{ab}	74.31 ± 0.07^{b}	22.44 ± 0.15^{c}	7.31 ± 0.00^{a}	0.82 ± 0.02^{a}
SG	10.11 ± 0.42^{a}	73.08 ± 0.08^{a}	21.96 ± 0.08^{b}	7.45 ± 0.00^{b}	1.03 ± 0.02^{b}
GC	10.98 ± 0.42^{bc}	75.09 ± 0.32^{c}	23.91 ± 0.12^{d}	8.04 ± 0.00^{d}	1.01 ± 0.01^{b}
SM	11.73 ± 0.16^{c}	74.46 ± 0.31^{a}	21.00 ± 0.10^{a}	7.74 ± 0.01^{c}	1.50 ± 0.01^{c}

ZG, zhengui; SG, shuanggui; GC, guichao; SM, suimi.
Means followed by different letters in the same column are significantly different at $P < 0.05$.

Solubility and swelling power of rice flour

The solubility (S) and swelling power (SP) are shown in Table 2. The lower S is associated with smaller cooking loss of rice noodles, and low SP of starch granules relates to relatively high anti-shear ability (27). Amylose content in ZG, SG and GC rice flours has no significant correlation with S, which was in agreement with previous reports. Li and Vasanthan suggested that samples with higher amylose content were less susceptible to swelling during gelatinization (28). Jiao et al. reported that starch-based material of pea starch forms a stronger gel due to a higher amylose content of pea starch, which is desirable in noodle processing (29). However, compare with ZG, SG, and GC, the solubility of SM rice flour increased significantly ($P < 0.05$) and the swelling power of SM rice flour decreased significantly ($P < 0.05$) with the amount of amylose decreased to 21.00%. The reason may be that S and SP were not only related to amylose content, but also related to the structure of amylopectin. Previous studies suggested that the value of SP depends on the magnitude of interaction between starch chains within the crystalline and amorphous domains (30). The SP of starch mainly reflects the insolubility of amylopectin, which is primarily caused by the formation of hydrogen bond between side chains of amylopectin (31). The expansion characteristic of amylopectin is also related to the length of the amylopectin chains (32). When rice amylose contents are close, contents of protein and fat, and damaged starch content that was caused during milling process may take a primary role in influencing the characteristics of rice gel (10–12). Tong et al. (2) found that physicochemical characteristics (the degree of starch damage, etc.) of rice flours prepared from wet-, dry- and semidry-milling methods were different. According, the resulting textural profile and cooking qualities of rice noodles prepared with these different milled rice flours were varied significantly.

Thermal properties of rice flour

The results of thermal properties are shown in Table 2. There were significant differences of thermal properties (T_P, T_C, and ΔH_1) in the four rice raw materials ($P < 0.05$). T_P, T_C and ΔH_1 of rice followed the order of SM>SG>GC>ZG. There were also significant differences of ΔH_2 between the four rice raw materials following the order of SM>GC>SG>ZG ($P < 0.05$). According to literature, gelatinization temperature is associated with internal arrangement of starch granules, and crystallinity degree affects gelatinization enthalpy (30). The structural changes in starch granules, including the interactions of amylose-lipid and amylose-amylose, could lead to changes in gelatinization properties (33). Therefore, a slight decline in T_p might be attributed to the arrangement of starch granules, the difference in crystallinity degree, and the interactions of amylose-amylose, amylose-lipid and amylose-protein in granules. The variation in chain-length distribution in amylopectin might also account for the evident increase of ΔH_1, because more energy was needed to dissociate longer linear chains (34, 35). These changes in gelatinization properties directly affected the cooking quality, as lower Tp meant shorter cooking time (36).

The results of retrogradation properties are also shown in Table 2. It is known that, retrogradation is an inevitable procedure during rice noodle processing (37). In this study, the retrogradation degree (ΔH) of different rice materials were significantly different among different varieties (31.61–52.19%). The ΔH values from high to low followed the order of GC (52.19%) >SM (48.62%) >SG (46.78%) >ZG (31.61%). Research showed that ΔH is highly correlated with amylose content and starch sources (35). In this study, GC had a higher ΔH than other three rice flours (Table 2), which may due to its higher amylose content (Table 1). However, it is interesting that when the amylose contents were close (ZG, SG, and SM), there was no correlation between the ΔH and the amylose. In this study, the amylose content in ZG rice was slightly higher than that in SG and SM, but its ΔH was the lowest, which may be affected by other factors such as protein or fat. The content of protein and fat in ZG rice is relatively low compared to other varieties. Our results were in agreement with Marcoa and Likitwattanasade et al. (38, 39), who found that ΔH increased with protein addition. Thus, when choosing raw materials for rice flour processing, the influence of amylose content should be considered first for the acute improvement of retrogradation degree. Meanwhile the influence of other ingredients such as proteins and fats content should be taken into account when amylose content were similar.

Pasting properties of rice flour

Pasting properties of starches can be used to estimate the applicability of rice noodle making (40). The pasting properties of different rice starch are presented in Table 2 and Figure 1. All

TABLE 2 Physicochemical properties of different rice flour.

Variety	Adhesive strength (mm)	Solubility (%)	Swelling power (g/g)	Thermal properties						Pasting properties				
				To (°C)	Tp (°C)	Tc(°C)	ΔH_1 (J/g)	ΔH_2 (J/g)	ΔH/%	PV (cP)	TV (cP)	FV (cP)	BD (cP)	SB (cP)
ZG	42.83 ± 0.76	4.53 ± 0.46^{a}	10.06 ± 0.99^{b}	64.43 ± 0.12^{a}	69.32 ± 0.17^{a}	78.39 ± 0.22^{a}	9.75 ± 0.10^{a}	3.08 ± 0.00^{a}	31.61 ± 0.31^{a}	250.00 ± 3.00^{c}	246.33 ± 2.08^{c}	401.33 ± 1.53^{b}	3.67 ± 1.15^{a}	155.00 ± 1.73^{a}
SG	46.10 ± 0.36	4.58 ± 0.87^{a}	10.47 ± 0.42^{b}	72.90 ± 0.36^{b}	77.76 ± 0.18^{c}	84.41 ± 0.23^{c}	11.86 ± 0.26^{c}	5.55 ± 0.10^{b}	46.78 ± 0.54^{b}	195.33 ± 1.53^{b}	193.33 ± 1.53^{b}	376.00 ± 4.36^{a}	2.00 ± 0.00^{a}	182.67 ± 3.06^{b}
GC	35.00 ± 0.20	4.48 ± 0.25^{a}	9.85 ± 0.37^{b}	73.07 ± 0.07^{b}	77.08 ± 0.08^{b}	83.68 ± 0.08^{b}	11.42 ± 0.02^{b}	5.96 ± 0.06^{c}	52.19 ± 0.43^{d}	365.25 ± 2.63^{d}	363.00 ± 2.94^{d}	604.00 ± 5.77^{d}	2.25 ± 0.50^{a}	241.00 ± 6.78^{d}
SM	49.50 ± 0.78	5.72 ± 0.12^{b}	8.66 ± 0.24^{a}	75.36 ± 0.27^{c}	79.86 ± 0.18^{d}	94.26 ± 0.18^{d}	13.40 ± 0.26^{d}	6.51 ± 0.09^{d}	48.62 ± 0.99^{c}	184.25 ± 0.50^{a}	181.50 ± 1.91^{a}	411.50 ± 6.45^{c}	2.75 ± 1.71^{a}	230.00 ± 5.94^{c}

ZG, zhengui; SG, shuanggui; GC, guichao; SM, suimi.
To, onset temperature; Tp, peak temperature; Tc, final temperature; ΔH_1, gelatinization enthalpy; ΔH_2, regenerative enthalpy; ΔH, The retrogradation degree.
PV, peak viscosity; TV, trough viscosity; FV, final viscosity; BD, breakdown; SB, setback.
Means followed by different letters in the same column are significantly different at $P < 0.05$.

samples exhibited a typical pasting property of native rice flour, which contained peak viscosity during heating and subsequent breakdown on holding at 95°C, followed by setback during cooling. The peak and trough viscosities of rice flour samples followed the same order of GC>ZG>SG>SM. Peak viscosity (PV) is the maximum viscosity obtained from gelatinized starch during heating in water, which indicates the water-binding capacity of the starch granules (19). High PV of rice batter enhances its adhesion properties (41). Through viscosity (TV) refers to the viscosity decreasing rapidly after reaching the peak and falling to the lowest viscosity at a high temperature. PV and TV had a positive correlation with amylose content ($P < 0.05$). Final viscosity (FV) is the viscosity of sample at the end of the test at 50°C. Pearson's correlation analysis showed that the FV of rice flours was not positive correlated with amylose content ($P > 0.05$). FV of GC was noticeably higher than SM and ZG followed by SG. the FV is not positive correlation with amylose content, as can be seen from Table 2. FV value of SM was larger than ZG and SG, the reason may be related to varieties, SM used in this study was the broken rice of GC varieties. The result of FV was contradictory to the previous study (20), Wu et al. reported that high FV was accompanied by high gel hardness. The breakdown (BD) indicates the propensity of starch granules for disintegration (42) and represents hot paste stability. BD was caused by structural disruption of gelatinized starches at high temperature and affected by amylose content and fine structure of amylopectin (19, 43). Among the four cultivars, BD had no significant difference and was not directly correlated with the amylose content. The setback (SB) determines the retrogradation tendency of the product and reflects short-term aging ability and cold paste stability of starch (19, 44). SB is affected by content and molecular size of amylopectin in a pure starch system (34). In a complex flour system, SB could be influenced by starch content, amylose: amylopectin ratio, structural characteristics of amylose, and other factors like protein and lipid contents.

Rheological properties of rice flour

Rice flours that were prepared from different rice cultivars had different rheological properties during a heat-cooling cycle in a temperature range of 25–95°C (Figure 2A). During heating, G' and G'' sharply increased at ∼70°C. When the temperature reached 80–85°C, G' and G'' reached the maximum values, which was caused by swelling and gelatinization of starch granules (45). With the continuous increases of temperature, G' and G'' began to decrease rapidly reaching the highest temperature, which was due to the deformation of swollen starch granules and breakdown of crystalline structure after treatment (36, 45). During cooling from 95 to 25°C, G' and G'' increased steadily. During this process, starch granules aggregated, and association formed between starch and other molecules (30, 46). G' and G'' values were higher for the rice flour samples with

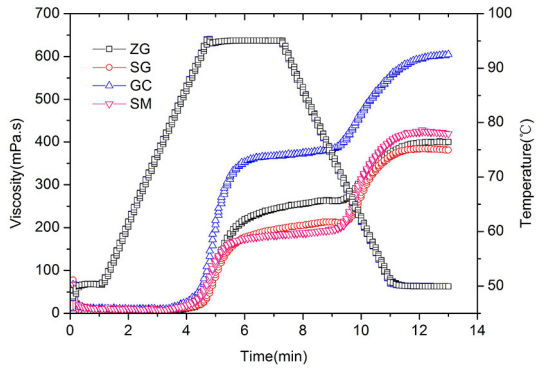

FIGURE 1
Pasting properties of rice flour. ZG, zhengui; SG, shuanggui; GC, guichao; SM, suimi.

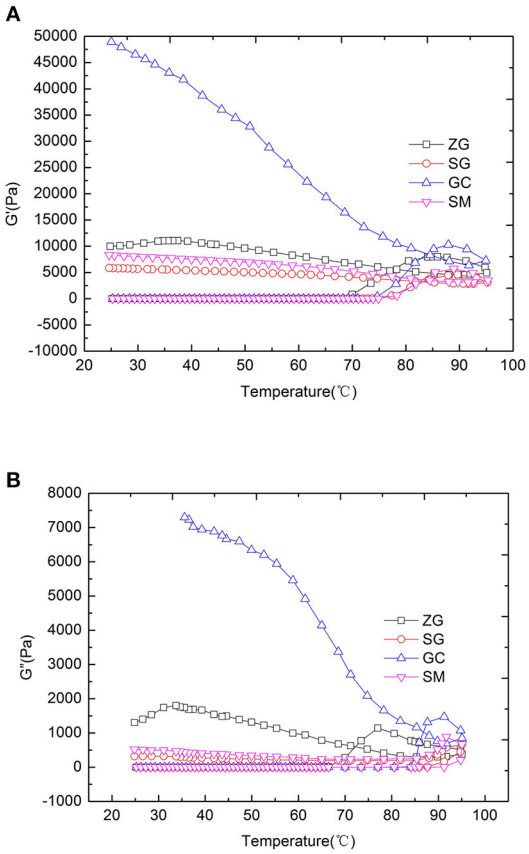

FIGURE 2
Rheological properties of different rice flours samples in the process of temperature ramp **(A)** for the G′ of samples, **(B)** for the G″ of samples. G′, storage modulus; G″, loss modulus; ZG, zhengui; SG, shuanggui; GC, guichao; SM, suimi.

higher amylose contents. As can be seen in Figures 2A, 3A, the G′ and G″ values of four kinds of rice were as follows: GC>ZG>SG>SM, which was in accordance with the results obtained by Charles et al. (47) who found that high contents of amylose contribute to gel firmness and stability. In addition, it is interesting to note the changes of G′ were not linear with the increases of amylose. Differences of amylose content between SG (21.96%) and SM (21.00%) resulted in small differences in G′, but the increases of amylose content to 23.91% (GC) seems to result in a large G′ value. The higher the amylose content of rice flour, the desirable the viscoelasticity of the gel system.

The gelatinized rice flour formed a strong gel (Figure 3). G′ had a notably higher value than G“ and had a weak dependence on frequency, suggesting a dominant elastic rheological behavior. G′ and G″ increased with increasing amylose content. Amylose has fewer branches than amylopectin, and it can retrogradation in a shorter time to form molecular aggregations and intermolecular double helices. Starch with a higher amylose content tends to form a stronger gel in a shorter time (47). Gels with higher G′ showed higher rigidity and strength (45, 48). Amylose content and starch type affect the viscoelasticity of gels (49). Extruded rice noodle is a kind of gel product, so the rheological analysis can be used as an auxiliary approach for selecting raw rice materials for noodle production.

Rice noodles qualities

Cooking qualities and sensory evaluation of rice noodles

Rehydration time, broken rate, and cooking loss of rice noodles are shown in Table 3. The rehydration time is associated with its cooking time, and the broken rate and cooking loss were two important indexes of the cooking qualities for rice noodles. ZG, SG, and GC had no significant difference in rehydration time (15–16 min, $P > 0.05$), which was significantly higher than SM (12 min). SM had approximately two times of broken rate higher than ZG, SG, and GC, while the latter three had no significant differences ($P > 0.05$). The cooking loss of rice noodles followed the order of GC<ZG<SG<SM. Overall, GC and ZG noodles had the best cooking quality with low broken rate and cooking loss, followed by SG. SM had the lowest cooking quality with highest broken rate and cooking loss. Previous research had reported that noodles with a higher amylose content generally had a shorter rehydration rate, higher gel strength, and smaller breaking rate and cooking loss (35, 37). In this paper, the similar phenomenon were observed. The morphology of rice noodles shown in Figure 4 was in agreement with the rice noodle quality analysis (Table 3). There were only slight differences of the rice noodles morphology among ZG, SG, and GC, as their starch granular structure was not destroyed during processing. The appearance of ZG, SG, and GC had negligible differences, but SM noodle had a darker color and more short segments, and the shape of rice noodles produced by

10.3389/fnut.2022.1003657

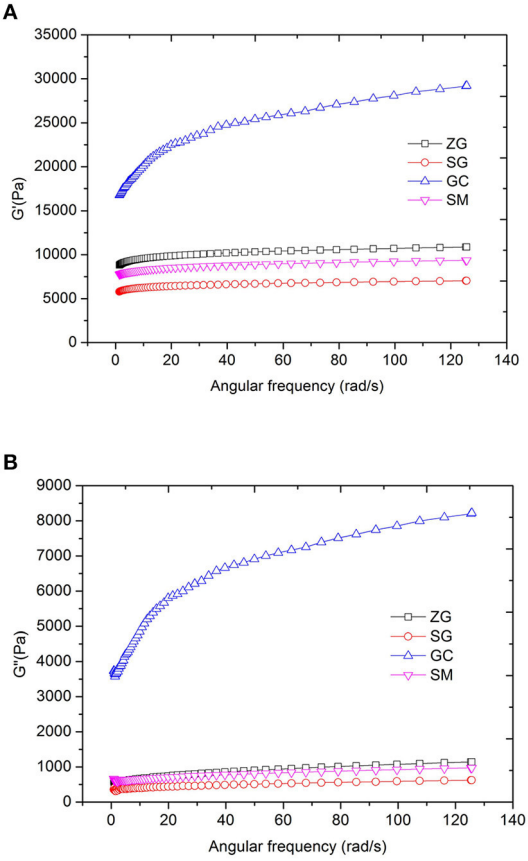

FIGURE 3
Rheological properties of different rice flours samples in the process of frequency sweep **(A)** for the G′ of samples, **(B)** for the G″ of samples). G′, storage modulus, G″, loss modulus, ZG, zhengui; SG, shuanggui; GC, guichao; SM, suimi.

SM was relatively poor. The reason may be the overall structure of the SM rice starch granules was damaged worse during the process of shucking and stripping.

The results of sensory evaluation are summarized in Table 3. There were no significant difference ($P > 0.05$) in odor of ZG, SG GC, and SM. While compared with noodles made from SM, there were significant increases in the color, tissue shape and smoothness points of noodles made by GC, ZG, and SG ($P < 0.05$). The firmness points were correlated with rice amylose content. As we can see in Table 3, firmness points significantly increased ($P < 0.05$) when amylose content of different rice increase from 21.00 to 23.91 % (GC>ZG>SG>SM). Elasticity points were also correlated with rice amylose content. Compared with noodles made from SM, there were significant increases elasticity points of noodles made by GC, ZG, and SG ($P < 0.05$). However, elasticity points of ZG and GC had no significantly differences ($P > 0.05$). The total score was calculated from the sum of color, odor, tissue shape, firmness, smoothness and

TABLE 3 Quality results of different rice noodles.

Variety	Rehydration time (min)	Cooking quality		TPA			Tensile properties		Sensory score						
		Broken rate (%)	Cooking loss (%)	Hardness (g)	Springiness (mm)	Chewiness (mJ)	Peak load (g)	Deformation at peak (mm)	Color	Odor	Tissue shape	Firmness	Smoothness	Elasticity	Total score
ZG	15.33 ± 0.58^{b}	10.33 ± 1.53^{a}	14.57 ± 0.31^{a}	1084.00 ± 175.74^{a}	1.53 ± 0.09^{c}	14.72 ± 2.49^{b}	30.20 ± 11.82^{a}	13.58 ± 4.32^{ab}	13.00 ± 1.58^{b}	9.00 ± 0.71^{a}	13.00 ± 1.41^{b}	16.00 ± 0.71^{c}	18.00 ± 1.00^{b}	17.00 ± 1.58^{c}	86.00 ± 2.45^{c}
SG	15.00 ± 1.00^{b}	10.33 ± 4.73^{a}	16.33 ± 0.42^{b}	1097.00 ± 190.50^{a}	1.36 ± 0.03^{b}	12.37 ± 2.41^{b}	26.00 ± 5.29^{a}	11.28 ± 4.09^{ab}	12.00 ± 1.58^{b}	9.00 ± 0.71^{a}	13.00 ± 1.58^{b}	14.00 ± 1.58^{b}	16.00 ± 1.58^{b}	14.00 ± 1.58^{b}	78.00 ± 3.32^{b}
GC	15.67 ± 0.58^{b}	9.00 ± 1.00^{a}	14.33 ± 0.42^{a}	1628.67 ± 64.04^{b}	1.55 ± 0.03^{c}	21.53 ± 3.21^{c}	56.00 ± 14.51^{b}	17.16 ± 4.38^{b}	11.00 ± 1.41^{b}	8.00 ± 0.71^{a}	13.00 ± 1.00^{b}	18.00 ± 0.71^{d}	17.00 ± 1.00^{b}	17.00 ± 0.71^{c}	84.00 ± 2.74^{c}
SM	12.00 ± 1.00^{a}	22.00 ± 2.65^{b}	25.50 ± 0.50^{c}	941.67 ± 214.72^{a}	0.95 ± 0.06^{a}	5.70 ± 1.32^{a}	19.60 ± 5.55^{a}	9.95 ± 4.13^{a}	8.00 ± 1.22^{a}	8.00 ± 0.71^{a}	10.00 ± 2.24^{a}	11.00 ± 0.71^{a}	13.00 ± 2.24^{a}	12.00 ± 1.58^{a}	62.00 ± 4.30^{a}

Means followed by different letters in a column are significantly different at $P < 0.05$.

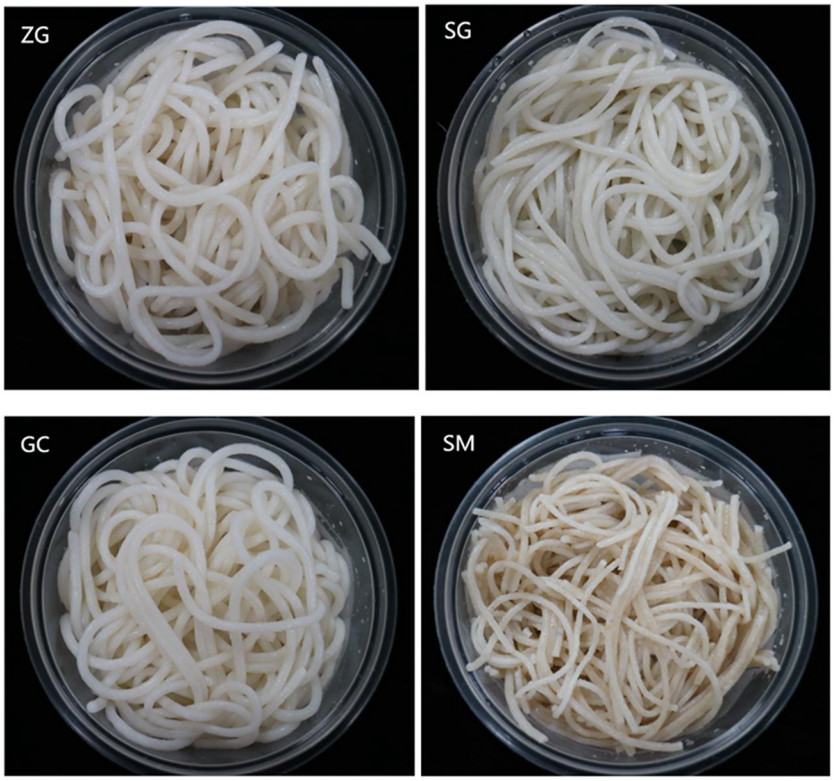

FIGURE 4
Morphology of rice noodles made from selected varieties of early polished indica rice. ZG, zhengui; SG, shuanggui; GC, guichao; SM, suimi.

elasticity scores. Total scores from high to low were: ZG, GC, SG, and SM. The total scores were not completely positive correlated with rice amylose content. As we can see, though the amylose content of GC rice (23.91%) was slightly higher than that of ZG rice (22.44%), its score (84.00) was not higher than that of ZG rice (86.00) ($P > 0.05$). Therefore, when the amylose content of different rice varieties were approximately, in addition to considering the main factor of starch, the influence of other factors such as protein also should be properly considered.

Texture properties of rice starch noodles

The texture of cooked noodles has substantial effects on the sensory properties and the resulting consumers' acceptance. In this study, noodle texture was analyzed using a compression test (texture profile analysis) and a tensile test (Table 3). In TPA, hardness is a measurement of force to compress the sample in the first bite with molar teeth. Springiness is the degree to which a sample returns to its original shape after partial compression with the molar teeth, and chewiness is the amount of work to chew the sample to get it ready to swallow. Chewiness is related to hardness, cohesion and elasticity, and it equals to product of hardness, cohesiveness and springiness. When the amylose content of GC rice was 23.91%, the hardness of the rice starch noodles was 1628.67 g and significantly higher ($P < 0.05$) than that of noodles made from ZG, SG, SM (with hardness of 1084.00, 1097.00, and 941.67 g, respectively), which is likely related to amylose content. The amylose content (23.91%) in GC rice flour had a higher amylose content than ZG, SG and SM, and GC starch formed a stronger gel strength than the other three (Table 1, Figures 2, 3). The hardness of ZG, SG and SM noodles had no significant differences ($P > 0.05$). In addition, the changes of springiness, chewiness, peak load and deformation at peak value of rice noodles were consistent with the changes of amylose content. There was no significant difference between GC and ZG in springiness, which was consistent with G′ (Table 3, Figures 2A, 3A). There was no significant difference of chewiness value between ZG and SG ($P >0$ .05). For the deformation at peak, there was no significant difference in the variation of other rice varieties in addition to SM, which indicated that although the amylose content of rice was dominant, the texture quality of rice flour also might be affected by other factors especially when the amylose content of different rice varieties are similar.

In summary, the texture profile of different rice noodles varied mainly depending on amylose content. Early indica rice of GC with higher amylose content (23.91%) was more suitable to produce rice noodles with higher elasticity, such as snail noodles.

TABLE 4 Correlations between physicochemical properties of rice starch and rice starch noodles qualities.

	Amylose	Protein	Adhesive strength	Solubility	Swelling power	ΔH	PV	TV	FV	BD	SB	Broken rate	Cooking lost	Hardness	Springiness	Chewiness	Peak load	Deformation at peak	Sensory score
Amylose	1																		
Protein	0.45	1																	
Adhesive strength	−0.99**	−0.51	1																
Solubility	−0.77	0.16	0.71	1															
Swelling power	0.49	−0.41	−0.4	−0.92*	1														
ΔH	0.13	0.83	−0.15	0.26	−0.29	1													
PV	0.96**	0.62	−0.98**	−0.57	0.23	0.22	1												
TV	0.96**	0.62	−0.98**	−0.57	0.23	0.23	1.00**	1											
FV	0.83	0.86	−0.87	−0.29	−0.04	0.52	0.93*	0.93*	1										
BD	−0.15	−0.51	0.12	0.06	−0.18	−0.86	−0.09	−0.1	−0.29	1									
SB	0.18	0.96*	−0.24	0.42	−0.59	0.89*	0.37	0.37	0.68	−0.54	1								
Broken rate	−0.79	0.12	0.73	1**	−0.91*	0.21	−0.60	−0.60	−0.33	0.11	0.37	1							
Cooking loss	−0.81	0.14	0.75	0.99*	−0.88	0.30	−0.63	−0.63	−0.34	−0.01	0.41	0.99**	1						
Hardness	0.95*	0.69	−0.96**	−0.59	0.30	0.43	0.96**	0.96**	0.94*	−0.37	0.46	−0.63	−0.62	1					
Springiness	0.85	−0.08	−0.81	−0.97**	0.80	−0.32	0.71	0.70	0.42	0.09	−0.40	−0.97**	−0.99**	0.66	1				
Chewiness	0.99**	0.35	−0.98**	−0.84	0.58	0.06	0.92*	0.92*	0.76	−0.14	0.07	−0.86	−0.87	0.92*	0.90*	1			
Peak load	0.97**	0.65	−0.98**	−0.61	0.30	0.33	0.99**	0.99**	0.94*	−0.25	0.41	−0.64	−0.65	0.99**	0.70	0.94*	1		
Deformation at peak	0.99**	0.49	−1.00**	−0.69	0.36	0.09	0.99**	0.99**	0.86	−0.04	0.22	−0.71	−0.74	0.94*	0.81	0.97**	0.97**	1	
Score	0.80	−0.17	−0.75	−0.96**	0.81	−0.41	0.64	0.64	0.33	0.17	−0.50	−0.95*	−0.99**	0.58	0.99**	0.86	0.63	0.76	1

*, **significant at $P<0.05$, $P<0.01$, respectively.

10.3389/fnut.2022.1003657

ZG and SG indica rice with moderate amylose content was more suitable for processing relatively soft taste of rice noodles such as rolled rice noodles and sliced rice noodles. In addition, although the textural properties of rice noodle made by SM was relatively poor, it can be mixed with some high amylose rice in food industry, which reduces production cost and increases quality of rice noodles.

Correlations between physicochemical properties of rice starch and qualities of rice noodles

Correlations between physicochemical properties of rice flour and the qualities of rice noodles were analyzed. Pearson's correlation coefficients are presented in Table 4. The physicochemical properties of rice flour had a significant influence on the qualities of rice noodles. Amylose content of the rice had a positive correlation with hardness of rice noodles ($P < 0.5$) and a strong positive correlation with peak and trough viscosities, chewiness, peak load and deformation at peak of rice starch noodles ($P < 0.01$). Adhesive strength had a strong negative correlation with hardness, chewiness, peak load and deformation at peak of rice starch noodles ($P < 0.01$). In addition, there were positive correlations between RVA paste viscosities and texture qualities of rice starch noodles ($P < 0.01$). PV and TV had positive correlations with chewiness ($P < 0.05$), and a strong positive correlation with hardness, peak load and deformation at peak of rice starch noodles ($P < 0.01$). FV also showed a positive correlation with hardness and peak load ($P < 0.05$). This was consistent with what was reported by Bhattacharya et al. (50). Who suggested the suitability and advantages of using pasting properties for selection of rice cultivars suitable for noodle preparation. The rice noodle properties in this study, including the cooking qualities, texture properties, and sensory evaluation score, were closely correlated with amylose content, adhesive strength, and pasting properties. Meanwhile, other influencing factors (e.g., protein) should also be considered.

Conclusions

The relationships between the characteristics of four rice raw materials, processing performance, and cooking and sensory properties of rice noodles were discussed in the present study. This study shows that amylose content, adhesive strength, and pasting properties had great influences on cooking qualities and sensory properties of rice noodles. Starch properties could be used for selection of suitable rice materials for noodle production and prediction of rice noodle quality. This study is useful for selecting rice for food industry in different regional markets for specific rice noodle product requirements. It provides information for formulating pre-extrusion material for rice noodle production by combining several dried rice flours, such as early indica rice, late indica rice and some plant starches with higher amylose than starch (e.g., corn starch). Further study could focus on optimizing rice noodle processing conditions and producing rice noodles with regional characteristics and high quality.

Data availability statement

The original contributions presented in the study are included in the article/supplementary material, further inquiries can be directed to the corresponding author/s.

Author contributions

PW: methodology, investigation, data curation, and writing—original draft. FF: investigation and writing—review and editing. GL: writing—review and editing. YZ: conceptualization, validation, and writing—review and editing. LW and KZ: software. XY: investigation, conceptualization, and supervision. YW: validation. ML: formal analysis. JS and SD: contributed helpful discussion and scientific advice during the preparation of manuscript. All authors contributed to the article and approved the submitted version.

Funding

This research was supported by Science and Technology Major Project of Guangxi (Grant Nos. Gui Ke AB21220045, AB21196067, and AA17202029), the Special Fund for Agro-Scientific Research in the Public Interest (Grant No. 201503001-6), Guangxi Science and Technology Pioneer Project (Grant No. 202115), Special Fund for Guangxi Bagui Scholars (Grant No. [2016]21), Foundation of Fundamental Research Project from Guangxi Academy of Agricultural Sciences (Grant Nos. JZ202019 and 2021JM103) and Dominant Discipline Team Project (Grant Nos. Gui Nong Ke 2015YT87 and 2018YM05).

Conflict of interest

The authors declare that the research was conducted in the absence of any commercial or financial relationships that could be construed as a potential conflict of interest.

Publisher's note

All claims expressed in this article are solely those of the authors and do not necessarily represent those of their affiliated

organizations, or those of the publisher, the editors and the reviewers. Any product that may be evaluated in this article, or claim that may be made by its manufacturer, is not guaranteed or endorsed by the publisher.

References

1. Fu BX. Asian noodles: history, classification, raw materials, and processing. *Food Res Int*. (2008) 41:888–902. doi: 10.1016/j.foodres.2007.11.007

2. Tong LT, Gao XX, Lin LZ, Liu YJ, Zhong K, Liu LY, et al. Effects of semidry flour milling on the quality attributes of rice flour and rice noodles in China. *J Cereal Sci*. (2015) 62:45–9. doi: 10.1016/j.jcs.2014.12.007

3. Zhang Y, Xu F, Wang Q, Zhang Y, Wu G, Tan L, et al. Effects of moisture content on digestible fragments and molecular structures of high amylose jackfruit starch prepared by improved extrusion cooking technology. *Food Hydrocolloid*. (2022) 133:108023. doi: 10.1016/j.foodhyd.2022.108023

4. Li B, Zhang Y, Xu F, Khan MR, Zhang Y, Huang C, et al. Supra molecular structure of Artocarpus heterophyllus Lam seed starch prepared by improved extrusion cooking technology and its relationship with in vitro digestibility. *Food Chem*. (2021) 336:127716. doi: 10.1016/j.foodchem.2020.127716

5. Zhang Y, Zuo H, Xu F, Zhu K, Tan L, Dong W, et al. The digestion mechanism of jackfruit seed starch using improved extrusion cooking technology. *Food Hydrocolloid*. (2021) 110:106154. doi: 10.1016/j.foodhyd.2020.106154

6. Sandhu KS, Kaur M, Mukesh. Studies on noodle quality of potato and rice starches and their blends in relation to their physicochemical, pasting and gel textural properties. *LWT-Food Sci Technol*. (2010) 43:1289–93. doi: 10.1016/j.lwt.2010.03.003

7. Kim Y, Kee JI, Lee S, Yoo SH. Quality improvement of rice noodle restructured with rice protein isolate and transglutaminase. *Food Chem*. (2014) 145:409–16. doi: 10.1016/j.foodchem.2013.08.078

8. Zhou X, Peng C, Zhang Y, Guo L, Xiong N. Quality analysis of early indica rice cultivars and their suitability for processing of pressed fresh noodle. *Food Sci*. (2018) 39:36–43 (in Chinese). doi: 10.7506/spkx1002-6630-201819007

9. Xuan Y, Yi Y, Liang H, Wei SQ, Chen NP, Jiang LG, et al. Amylose content and RVA profile characteristics of noodle rice under different conditions. *Agron J*. (2020) 112:117–29. doi: 10.1002/agj2.20079

10. Martin M, Fitzgerald MA. Proteins in rice grains influence cooking properties. *J Cereal Sci*. (2002) 36:285–94. doi: 10.1006/jcrs.2001.0465

11. Baxter G, Blanchard C, Zhao J. Effects of prolamin on the textural and pasting properties of rice flour and starch. *J Cereal Sci*. (2004) 40:205–11.doi: 10.1016/j.jcs.2004.07.004

12. Ibáñez AM, Wood DF, Yokoyama WH, Park IM, Tinoco MA, Hudson CA, et al. Viscoelastic properties of waxy and nonwaxy rice flours, their fat and protein-free starch, and the microstructure of their cooked kernels. *J Agri Food Chem*. (2007) 55:6761–71. doi: 10.1021/jf070416x

13. Ministry of Health of the People's Republic of China. GB/T 5009.3-2016. *Determination of Water in Foods*. Beijing: Standard Press of China (2016). (in Chinese).

14. Ministry of Health of the People's Republic of China. GB/T 5009.5-2016. *Determination of Protein in Foods*. Beijing: Standard Press of China (2016). (in Chinese).

15. Ministry of Health of the People's Republic of China. GB/T 5009.6-2016. *Determination of Lipid in Foods*. Beijing: Standard Press of China (2016). (in Chinese).

16. McCleary V, Gibson TS, Mugford DC. Measurement of total starch in cereal products by amyloglucosidase-α-amylase method: Collaborative study. *Journal-A O A C*. (1997) 80:571–9. doi: 10.1093/jaoac/80.3.571

17. Ministry of Health of the People's Republic of China. GB/T 15683-2008. *Rice-Determination of Amylose Content*. Beijing: Standard Press of China (2008). (in Chinese).

18. Ministry of Health of the People's Republic of China. GB/T 22294-2008. *Determination of Rice Adhesive Strength*. Beijing: Standard Press of China (2008). (in Chinese).

19. Yi C, Zhu H, Bao J, Quan K, Yang R. The texture of fresh rice noodles as affected by the physicochemical properties and starch fine structure of aged paddy. *LWT-Food Sci Technol*. (2020) 3:9610. doi: 10.1016/j.lwt.2020.109610

20. Wu FF, Meng YP, Yang N, Tao H, Xu XM. Effects of mung bean starch on quality of rice noodles made by direct dry flour extrusion. *LWT-Food Sci Technol*. (2015) 63:1199–205. doi: 10.1016/j.lwt.2015.04.063

21. Geng DH, Zhou SM, Wang LL, Zhou XR, Liu L, Lin ZX, et al. Effects of slight milling combined with cellulase enzymatic treatment on the textural and nutritional properties of brown rice noodles. *LWT-Food Sci Technol*. (2020) 128:109520. doi: 10.1016/j.lwt.2020.109520

22. Meng YP, Wu FF, Xu XM. Effects of canna edulis ker starch on physicochemical properties of rice flour and quality of rice noodles. *Food Sci*. (2015) 36:33–8.(In Chinese). doi: 10.7506/spkx1002-6630-201509007

23. Fu MX, Sun XY, Wu D, Meng LH, Feng X, Cheng WW, et al. Effect of partial substitution of buckwheat on cooking characteristics, nutritional composition, and in vitro starch digestibility of extruded gluten-free rice noodles. *LWT-Food Sci Technol*. (2020) 126:109332. doi: 10.1016/j.lwt.2020.109332

24. Raungrusmee S, Shrestha S, Sadi MB, Anal AK. Influence of resistant starch, xanthan gum, inulin and defatted rice bran on the physicochemical, functional and sensory properties of low glycemic gluten-free noodles. *LWT-Food Sci Technol*. (2020) 126:109279. doi: 10.1016/j.lwt.2020.109279

25. Wang L, Zhang C, Chen Z, Wang X, Wang K, Li Y, et al. Effect of annealing on the physico-chemical properties of rice starch and the quality of rice noodles. *J Cereal Sci*. (2018) 84:125–31. doi: 10.1016/j.jcs.2018.10.004

26. Wei P, Zhang YY, You XR, Sun J, Wang Y, Li MJ, et al. Properties of patota-india rice blend and its extruding quality. *J Chin Cereals Oils Assoc*. (2020) 35:42–9 (in Chinese). Available online at: http://kns.cnki.net/kcms/detail/11.2864.ts.20200331.1529.004.html

27. Sharma P, Singh V, Subramanian R. Pasting, swelling, and solubility characteristics of rice batter prepared from different wet grinding systems. *Starch/Starke*. (2013) 65:374–81. doi: 10.1002/star.201200126

28. Li JH, Vasanthan T. Hypochlorite oxidation of field pea starch and its suitability for noodle making using an extrusion cooker. *Food Res Int*. (2003) 36:381–6. doi: 10.1016/S0963-9969(02)00230-2

29. Jiao AQ, Yang YY, Li Y, Chen Y, Xu XM, Jin ZY. Structural properties of rice flour as affected by the addition of pea starch and its effects on textural properties of extruded rice noodles. *Int J Food Prop*. (2020) 23:809–19. doi: 10.1080/10942912.2020.1761830

30. Kaur M, Sandhu K S, Lim S T. Microstructure, physicochemical properties and in vitro digestibility of starches from different Indian lentil (*Lensculinaris*) cultivars. *Carbohyd Polym*. (2010) 79:349–55. doi: 10.1016/j.carbpol.2009.08.017

31. Tester R F, Morrison W R. Swelling and gelatinization of cereal starches. I. Effects of amylopectin, amylose and lipids. *Cereal Chem*. (1990) 67:551–7.

32. Sasaki T, Matsuki J. Effffect of wheat starch structure on swelling power. *Cereal Chem*. (1998) 75:525–9. doi: 10.1094/CCHEM.1998.75.4.525

33. Hoover R. The impact of heat-moisture treatment on molecular structures and properties of starches isolated from different botanical sources. *Crit Rev Food Sci*. (2010) 50:835–47.doi: 10.1080/10408390903001735

34. Klein B, Pinto VZ, Vanier NL, Zavareze EDR, Colussi R, do Evangelho JAD, et al. Effect of single and dual heat-moisture treatments on properties of rice, cassava, and pinhao starches. *Carbohyd Polym*. (2013) 98: 1578–84. doi: 10.1016/j.carbpol.2013.07.036

35. Qazi I M, Rakshit SK, Tran T. Effect of physico-chemical properties of tropical starches and hydrocolloids on rice gels texture and noodles water retention ability. *Starch-Starke*. (2011) 63:558–69.doi: 10.1002/star.201000140

36. Kaur L, Singh J, Singh N. Effect of glycerol monostearate on the physico-chemical, thermal, rheological and noodle making properties of corn and potato starches. *Food Hydrocolloid*. (2005) 19:839–49. doi: 10.1016/j.foodhyd.2004.10.036

37. Lii CY, Chang SM. Characterization of red bean (Phaseolus radiatus var. Aurea) starch and its noodle quality. *J Cereal Sci*. (1981) 46:78–81. doi: 10.1111/j.1365-2621.1981.tb14535.x

38. Marcoa C, Rosell CM. Effect of different protein isolates and transglutaminase on rice flour properties. *J Food Eng*. (2008) 84:132–9. doi: 10.1016/j.jfoodeng.2007.05.003

39. Likitwattanasade T, Hongsprabhas P. Effect of storage proteins on pasting properties and microstructure of Thai rice. *Food Res In*. (2010) 43:1402–9. doi: 10.1016/j.foodres.2010.04.011

40. Hormdok R, Noomhorm A. Hydrothermal treatments of rice starch for improvement of rice noodle quality. *LWT-Food Sci Technol*. (2007) 40:1723–31.doi: 10.1016/j.lwt.2006.12.017

41. Mukprasirt A, Herald TJ, Seib PA. Pasting characteristics of rice flour-based batter compared to wheat flour-based batter. *J Food Quality*. (2002) 25:139–54. doi: 10.1111/j.1745-4557.2002.tb01014.x

42. Mariotti M, Caccialanza G, Cappa C, Lucisano M. Rheological behavior of rice flour gels during formation: Influence of the amylose content and of the hydrothermal and mechanical history. *Food Hydrocolloid*. (2018) 84:257–66. doi: 10.1016/j.foodhyd.2018.06.006

43. Yuan ML, Lu ZH, Cheng YQ Li LT. Effect of spontaneous fermentation on the physical properties of corn starch and rheological characteristics of corn starch noodle. *J Food Eng*. (2008) 85:12–7. doi: 10.1016/j.jfoodeng.2007.06.019

44. Chung HJ, Liu Q, Lee L, Wei D. Relationship between the structure, physicochemical properties and in vitro digestibility of rice starches with different amylose contents. *Food Hydrocolloid*. (2011) 25:968–75. doi: 10.1016/j.foodhyd.2010.09.011

45. Li JY, Yeh AI. Relationships between thermal, rheological characteristics and swelling power for various starches. *J Food Eng*. (2001) 50:141–8. doi: 10.1016/S0260-8774(00)00236-3

46. Cham S, Suwannaporn P. Effect of hydrothermal treatment of rice flour on various rice noodles quality. *J Cereal Sci*. (2010) 51:284–91. doi: 10.1016/j.jcs.2010.01.002

47. Charles AL, Chang YH, Ko WC, Sriroth K, Huang TC. Influence of amylopectin structure and amylose content on the gelling properties of five cultivars of cassava starches. *J Agri Food Chem*. (2005) 53:2717–25. doi: 10.1021/jf048376

48. Suwannaporn P, Pitiphunpong S, Champangern S. Classification of rice amylose content by discriminant analysis of physicochemical properties. *Starch-Starke*. (2007) 59:171–7. doi: 10.1002/star.200600565

49. Singh H, Lin JH, Huang WH, Chang YH. Influence of amylopectin structure on rheological and retrogradation properties of waxy rice starches. *J Cereal Sci*. (2012) 56:367–73. doi: 10.1016/j.jcs.2012.04.007

50. Bhattacharya M, Zee SY, Corke H. Physicochemical properties related to quality of rice noodles. *Cereal Chem*. (1999) 76:861–7. doi: 10.1094/CCHEM.1999.76.6.861

frontiers | Frontiers in Nutrition

TYPE Review
PUBLISHED 13 September 2022
DOI 10.3389/fnut.2022.977548

OPEN ACCESS

EDITED BY
Bin Li,
Shenyang Agricultural University, China

REVIEWED BY
Yanglei Yi,
Northwest A&F University, China
Paripok Phitsuwan,
King Mongkut's University of Technology Thonburi, Thailand
Haisong Wang,
Dalian Polytechnic University, China

*CORRESPONDENCE
Shuangqi Tian
tianshuangqi@haut.edu.cn
Zhicheng Chen
chen_1958@163.com

SPECIALTY SECTION
This article was submitted to Food Chemistry, a section of the journal Frontiers in Nutrition

RECEIVED 24 June 2022
ACCEPTED 11 August 2022
PUBLISHED 13 September 2022

CITATION
Yan F, Tian S, Du K, Xue X, Gao P and Chen Z (2022) Preparation and nutritional properties of xylooligosaccharide from agricultural and forestry byproducts: A comprehensive review. *Front. Nutr.* 9:977548. doi: 10.3389/fnut.2022.977548

Preparation and nutritional properties of xylooligosaccharide from agricultural and forestry byproducts: A comprehensive review

Feng Yan, Shuangqi Tian*, Ke Du, Xing'ao Xue, Peng Gao and Zhicheng Chen*

College of Food Science and Technology, Henan University of Technology, Zhengzhou, China

Xylooligosaccharide (XOS) are functional oligosaccharides with prebiotic activities, which originate from lignocellulosic biomass and have attracted extensive attention from scholars in recent years. This paper summarizes the strategies used in the production of XOS, and introduces the raw materials, preparation methods, and purification technology of XOS. In addition, the biological characteristics and applications of XOS are also presented. The most commonly recommended XOS production strategy is the two-stage method of alkaline pre-treatment and enzymatic hydrolysis; and further purification by membrane filtration to achieve the high yield of XOS is required for prebiotic function. At the same time, new strategies and technologies such as the hydrothermal and steam explosion have been used as pre-treatment methods combined with enzymatic hydrolysis to prepare XOS. XOS have many critical physiological activities, especially in regulating blood glucose, reducing blood lipid, and improving the structure of host intestinal flora.

KEYWORDS

xylooligosaccharide (XOS), xylanase, nutritional properties, agricultural and forestry byproducts, application

Introduction

XOS are functional oligosaccharides, which are composed of 2–7 xylose molecules linked by β-1, 4-glycosidic bonds, and the relative molecular weight is generally about 200–300 kDa (1, 2). XOS have excellent physical and chemical properties, such as high heat and acid resistance (3). The sweetness of XOS is about 40%-50% of sucrose (4). The viscosity of XOS is lower than other oligosaccharides, which can reduce the water activity and improve the ability to hold water in water solution (5).

In addition to excellent physical and chemical properties, XOS are also the research hotspots of scholars from all walks of life as prebiotics (6). A large number of animal experiments have proved the beneficial effects of XOS in preventing caries, regulating blood glucose, reducing blood lipid, reducing cholesterol, preventing inflammatory, improving immunity, preventing oxidation, promoting calcium absorption, which are relating to the ability of regulating intestinal flora structure of XOS (7–16). In addition, XOS could effectively prevent obesity, cardiovascular disease, atherosclerosis, and intestinal diseases (17, 18). The International Association of probiotics and prebiotics (ISAPP) identified XOS as emergent prebiotic oligosaccharides in its latest update of its prebiotic definition (19).

Most XOS are prepared by degradation of agicultural biomass (20, 21). Typical raw materials for preparation of XOS include crop straws such as wheat and sugarcane, as well as processing byproducts such as corncob and rice husk (22). XOS can also be produced from the cotton stalk, corn straw, sugarcane bagasse, and other common agricultural wastes (23). There are three main methods of extracting XOS: autohydrolysis, acid hydrolysis, and enzymatic hydrolysis (24–26). At present, enzymatic hydrolysis preparation of XOS is the primary method (27).

XOS have great potential as food ingredients due to their price competitiveness, thermal stability and pH stability, sensory properties and multidimensional effects on human health and livestock compared with other prebiotics (28–30). Globally, XOS are mainly used in the feed industry (49.6%), followed by health and medical products (25.4%), food and beverage (23.2%), and other applications (1.8%) (31). In addition, the industry's interest in XOS is reflected in an increasing number of XOS patent applications (20). The global prebiotic ingredient market is estimated to be 4.07 billion in 2017, expected to reach $7.37 billion by 2023. The compound annual growth rate (CAGR) is 10.4% (32), and the Asia Pacific region, including China, India, and Japan, are expected to have the highest increase, exceeding 9.5% (33).

This article summarizes the research progress of preparation and purification methods of XOS in recent years and introduces the physiological activities and applications of XOS to provide the basis for the further development and application of XOS.

Preparation of XOS

Raw materials for XOS preparation

Figure 1 showed the schematic representation of the lignocellulosic biomass composition. Lignocellulose biomass are the non-starch part of renewable and abundant plant materials. Lignocellulose materials are mainly cellulose, hemicellulose, and lignin (35). The composition of lignocellulose varies, with an average of cellulose (30–50%), hemicellulose (20–40%), and lignin (15–25%) in the total dry matter (36). Cellulose is composed of a glucose molecular chain, which forms hydrogen bonds between different layers of polysaccharides and forms crystalline conformation. Xylan, the main component of hemicellulose, is the critical target of XOS production.

Figure 2 showed the structure of xylan. Xylan is the main component of hemicellulose (60–90%), a heteropolysaccharide with a degree of polymerization (DP) between 50 and 200, containing acetyl, 4-o-methyl-dglucouronosyl, and α-substituents of arabinofuranyl residues, related to the main chain of β-1,4-linked xylopyranose units (23, 37). Table 1 lists the composition of several common lignocellulose raw materials. The higher the xylan content of the raw materials, the lower the cost of XOS production. Among these lignocellulose biomass, the hemicelluose content of corncob, sugarcane bagasse, and wheat straw are relatively high, which are ideal raw materials for XOS industrial production.

Preparation of XOS

Acid hydrolysis

Xylan can be hydrolyzed into soluble XOS under acidic conditions. Generally, dilute hydrochloric acid and sulfuric acid are used to hydrolyze xylan with a high degree of polymerization to produce XOS. The purpose of acid treatment is to improve the hydrolysis degree of hemicellulose, to improve the yield of XOS. Hemicellulose is separated into oligosaccharides and monosaccharides with a wide range of DP through the breaking of glycosidic bonds of xylose (37, 47). However, acid hydrolysis leads to equipment corrosion, which limits its use. In addition, acid hydrolysis will produce excess xylose and other toxic reaction products at high temperatures, such as furfural and hydroxymethylfurfural (HMF), which are harmful to food applications (48, 49).

It was reported that the yield of XOS obtained by hydrolyzing poplar wood with 5% acetic acid at 170°C was 39.8% (50). Ying et al. elucidated that the increase of sulfuric acid dosage enhanced the lignin removal of poplar pretreated with hydrogen peroxide acetic acid (51). The maximum XOS yield was 68.5% when XOS were produced by hydrolyzing corncob with 5% propionic acid at 170°C for 50 min (52). It was reported that the product obtained by hydrolyzing brewer's grains with 1.85% sulfuric acid for 19.5 min contains 6.6 g/L *arabinoxylooligosaccharide* (AXOS) (53). The acetic acid pre-treatment of poplar could effectively produce XOS, with a yield of 55.8%, and acetylation degradation of lignin occurred after acetic acid pre-treatment (54).

Acid hydrolysis to obtain XOS has been widely used because it was a fast and easy technology (21). High XOS yield could be obtained by hydrolysis with sulfuric acid

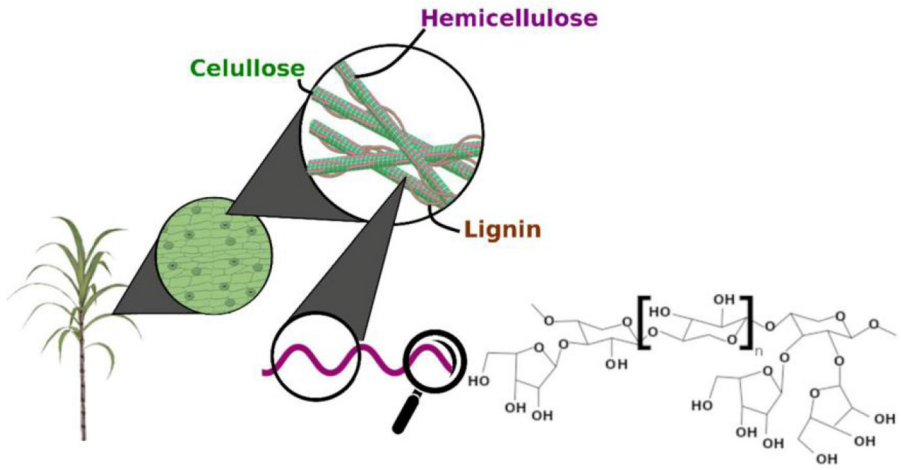

FIGURE 1
Schematic representation of the lignocellulosic biomass composition [Adopted from Capetti et al. (34)].

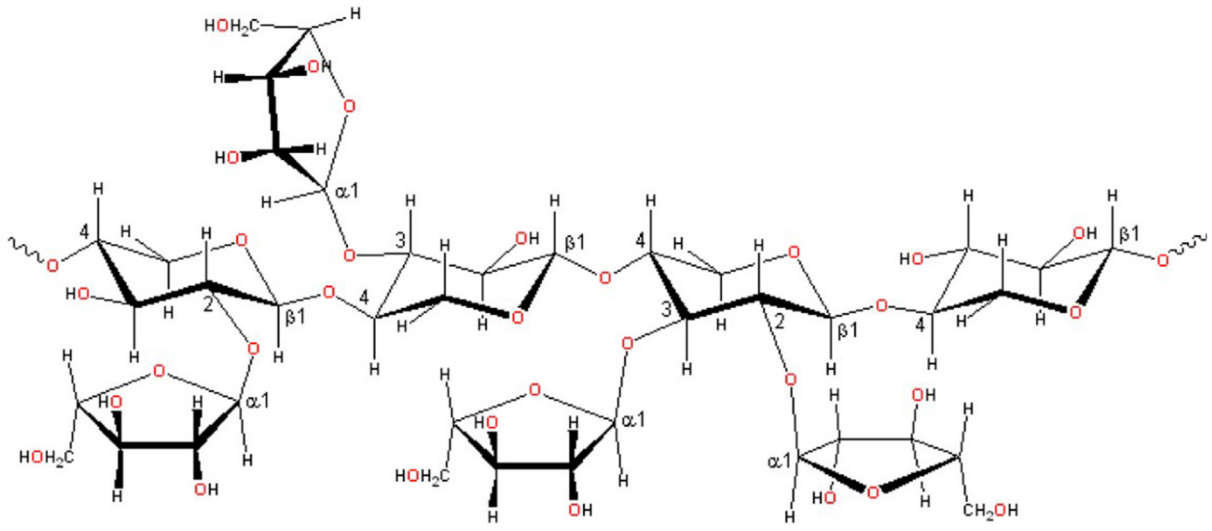

FIGURE 2
Xylan structure shows different intermolecular bonds [Adopted from Otieno et al. (7)].

of lignocellulose biomass. However, the yield of oligomers is lower than monomers, mainly due to the higher yield of xylose (6, 55). Even some methods change the acid conditions, improve the yield of XOS and optimize the existing preparation process; but the acid hydrolysis efficiency is still not high; there are still many impurities in the prepared products; and the content of XOS is still low.

Autohydrolysis

Agricultural plant biomass rich in xylan can also be directly hydrolyzed under high temperature and high pressure to produce XOS. Autohydrolysis is a non-chemical process, which refers to the deacetylation of D-xylan at high temperature in the presence of water (56). Autohydrolysis occurs under slightly acidic conditions due to the partial cleavage of acetyl groups in plant cell walls to form acetic acid (57). In the

TABLE 1 Cellulose, hemicellulose, lignin composition in raw lignocellulose biomass.

Biomass	Cellulose (%)	Hemicellulose (%)	Ligin (%)	References
Almond shell	34.3	20.2	28.8	(38)
Big blue stem	37	28	18	(36)
Birch wood	40	24	24	(39)
Beech wood	42.5	34.3	22.2	(40)
Corncob	30–42	31–38	18–22	(37)
Coconut husk	34.1	32.6	26.0	(41)
Chestnut husk	20.6	10.5	48.3	(42)
Corn stover	40	25	17	(36)
Hazelnut shell	18.7	28.9	46.7	(43)
Miscanthus	43	24	19	(36)
Olive pomace	13.8	18.9	31.2	(44)
Olive stones	15.3	20.3	42.1	(44)
Pineapple peel	20.9	31.9	10.4	(45)
Peanut shell	20.9	19.3	42.7	(46)

process of autohydrolysis, XOS are typical reaction intermediate, and their concentration depends on the balance between the decomposition of polymer hemicellulose into XOS and their further decomposition into monomer xylose. Therefore, under medium conditions, the yield of XOS will be higher. Treatment with increased severity resulted in decreased DP and increased decomposition of XOS into xylose. Hemicellulose is easily affected by water under high pressure and high temperature. Exposure of lignocellulosic biomass to water causes hemicellulose to penetrate the cellular structure, resulting in cellulose hydration and hemicellulose depolymerization. The action mode of hydrothermal treatment of lignocellulosic biomass was in the subcritical region of water (100–374°C) (58).

Autohydrolysis is heat treatment with steam or liquid water at high temperature or high pressure (55, 56). Under the autohydrolysis, the autoionization of water will produce ions, which leads to the depolymerization effect of hemicellulose (59). Acetic acid is usually added during autohydrolysis to increase the formation of hydrogen ions (23). The yield of XOS is the high under moderately severe operating conditions (60). It was reported that the maximum yield of XOS (55.3 wt%) was obtained by hydrothermal treatment of pecan shells at 160°C for 2 h. At the same time, high temperature (220°C) and short time (0.5 h) were helpful in hydrolyzing XOS with high DP, in which the yield of XOS (DP2-6) was 37.5 wt% (61). The autohydrolysis of almond shells (200°C, 5 min) resulted in low DP, and the concentration of XOS (xylobiose and xylotriose) was only 3.5% (38). Small-scale (150 tons of brewery waste grain per day) biological refineries could make profits by valuing the waste grain produced by large breweries and applying high-solid hydrothermal technology to produce high-value products xylitol and XOS (62). It was also elucidated that the recovery rate of high-purity polymeric hemicellulose with molecular weight (21–30 kDa) was 35–37% when high-purity hemicellulose (xylan) was partially extracted from wood waste by alkali mediated hydrothermal method; the separated hemicellulose could be chemically transformed into high-value commercial products, such as prebiotics (XOS) (63).

The main advantage of autohydrolysis method is that it has low or no requirements for corrosive compounds and is marked as an environmentally friendly process (36). In the past decades, hydrothermal treatment has been widely studied as the first step of biorefinery because of its environmentally friendly advantages and the selectivity of dissolving hemicellulose as oligosaccharides over other treatments (64, 65). Hydrothermal pre-treatment is considered an ecologically friendly and inexpensive alternative method to treat lignocellulose (66, 67). Autohydrolysis technology automatically ionizes water into hydrogen ions, allowing hemicellulose compounds to be released from lignocellulose, such as acetyl groups in acetic acid. This organic acid acts as a mild catalyst during the reaction, which is conducive to the subsequent dissolution of other hemicellulose-derived compounds (68, 69). Therefore, hydrothermal treatment is a technology to reduce the corrosion effect and cost of different solvents, and has high selectivity for hemicellulose.

Although the consumption of chemicals is low, due to the high pressure and temperature conditions, autohydrolysis process requires high energy consumption. The green characteristics of autohydrolysis will also depend on the energy used (70). It was reported that the most common temperature range to achieve high yield and minimum degradation of compounds was about 160–180°C (42, 71). The high temperature usually causes the release of many monomers (xylose) and impurities, such as furfural and HMF produced by sugar degradation, as well as the phenolic compounds produced by lignin (72, 73). The acidic hydrogen ion is formed due to the release of acetyl group in lignocellulosic biomass; acetyl group is the catalyst for hemicellulose depolymerization (71). The depolymerization of oligomers begins with the random breaking of the bond of xylose, producing oligomers short enough to be extracted from the biomass structure (74).

The main disadvantage of heat treatment is still to produce a large number of unwanted byproducts, such as other oligomers, monosaccharides, acetic acid, furfural, HMF, formic acid, levulinic acid, phenolic compounds, etc., (30, 75). It was observed that the degradation compounds released from the mixed biomass of hydrothermal treatment, had a significant inhibitory effect on the growth of *Lactobacillus brevis*. The dissolved lignin concentration of 1 g/L inhibited the growth of *Lactobacillus brevis*. After the adsorption purification step using Amberlite XAD 16N resin, the purified XOS showed the exact cell yield and product yield as commercial XOS (76). In general, a separation process is required to remove

unwanted compounds. The existence of the former compound in XOS mixture leads to serious purification difficulties, and then increases the production cost (56).

The release of degraded compounds depends on the composition of biomass and process conditions. Generally speaking, a separation process is required to remove unwanted compounds. The presence of the former compound in the XOS mixture leads to serious purification difficulties and consequent increased production costs (56). Another disadvantage of using autohydrolysis to produce XOS is that special equipment is required due to high temperature and high pressure (23, 24).

Enzymatic hydrolysis

Figure 3 showed the xylanase hydrolysis of lignocellulose. XOS can also be produced by enzymatic hydrolysis of xylan. Compared with acid hydrolysis and autohydrolysis, enzymatic degradation is an ideal XOS production method because it has specificity and the least byproducts. In addition, enzymatic hydrolysis does not require any special equipment. The current commercial process uses an enzyme process, which has mild operating conditions, and does not use toxic chemicals, so enzymatic hydrolysis is more in line with the viewpoint of biodegradation process. In addition, the use of xylanase is efficient and specific, allowing higher control of DP and reducing the production of unwanted xylose and other byproducts (77).

Enzymatic hydrolysis is usually used for the extraction of XOS due to the mild enzymatic hydrolysis conditions and high product quality (78). However, the isomerization of lignocellulosic materials will be seriously affected by the structure of composite lignin-hemicellulose. Therefore, it is essential to destroy the composite structure to expose more hemicellulose to improve the extraction efficiency. Physical and chemical pre-treatment technology have been used before enzymatic hydrolysis. In addition, the source of materials and xylanase have an impact on enzymatic hydrolysis.

Physical pre-treatment

Physical pre-treatment mainly includes the hydrothermal method, steam explosion method, ultrasonic method, and microwave method.

Steam explosion is instantaneous blasting under high temperature and high pressure. The hemicellulose recovery of corn cob after steam explosion at 196°C for 5 min was 22.8% (79). After a steam explosion at 204°C for 4 min and 180°C for 30 min, the yield of XOS in wheat straw was 8.9 and 13.9/100 g (72, 80). Steam explosion was also applied to the pre-treatment of rice husk, and the final output of XOS was 17.35 mg/mL xylan (81). In addition, after the steam explosion, 40% of xylan was degraded into XOS, and the degree of polymerization of steam explosion hydrolysates had good prebiotic properties (82).

The hydrothermal method processes materials in high-temperature or high-pressure hot water. It was reported that the xylan yield of wheat straw reached 56.2 g/kg after hydrothermal pre-treatment at 180°C for 40 min (39). After hydrothermal pre-treatment at 190°C, 1.8 MPa for 13 min, the extraction rate of xylan from corncob was 18% (6). The extraction rate of xylan was 23.82/100 g from dry corn straw subjected to non-isothermal hydrothermal pre-treatment (83). The extraction of XOS from corn fiber by hydrothermal pre-treatment at 160°C was also reported (84).

Ultrasonic and microwave had been applied to the pre-treatment of lignocellulose materials. Under 121°C ultrasonic pre-treatment, 39% of xylan in corncob was released, which was higher than the conventional extraction method (34%), and the extraction time shortened from 24 h to 43 min (85). After microwave pre-treatment at 185°C for 10 min, the recovery rate of xylan was higher than that of high-pressure steam pre-treatment, because microwave pre-treatment was easy to control the degree of reaction (86).

The results showed that physical pre-treatment was helpful to the release of xylan and XOS. The steam explosion can significantly improve the release of XOS, which has the advantages of simple operation, no pollution, low energy consumption, and a short production cycle. Therefore, the steam explosion is a promising pre-treatment method for XOS extraction in the future.

Chemical pre-treatment

Chemical pre-treatment mainly uses acid and alkali to extract xylan from lignocellulosic materials, and the yield of xylan varies according to the source of materials and extraction conditions. Table 2 lists the material sources, extraction conditions, and pre-treatment methods.

As shown in Table 2, the most commonly used chemical pre-treatment method was alkali extraction, which mainly used 5–24% sodium hydroxide and potassium hydroxide as extraction solvents. However, the yield of xylan was relatively low when alkali extraction is used alone. Auxiliary methods such as steam and ultrasound are needed to improve the yield of xylan. Xylan was extracted from corncob with sodium hydroxide and methanol solvent, and the extraction rate reached 11% (89). A similar xylan yield can be obtained when xylan is extracted from dry corncob with 10% sodium hydroxide at 75°C (89). The yields of XOS were 83 and 84.5%, respectively, when xylan were extracted from corncob and corn shells with 12% sodium hydroxide solution with the steam pre-treatment (6, 92). Ultrasonic assisted alkali extraction can significantly improve the yield of XOS in corncob, and the content of related XOS can reach 174.81 mg/g matrix (93).

Due to the low efficiency of acid extraction, acid extraction was rarely used and was usually assisted by physical methods. Xylan was extracted from corncob by acid electrolyte water (pH 2.0) combined with the steam explosion, and the extraction rate was 55% (87). After pretreated corncob with dilute acid and alkali to extract the lignin-saccharide complex, the yeild of XOS

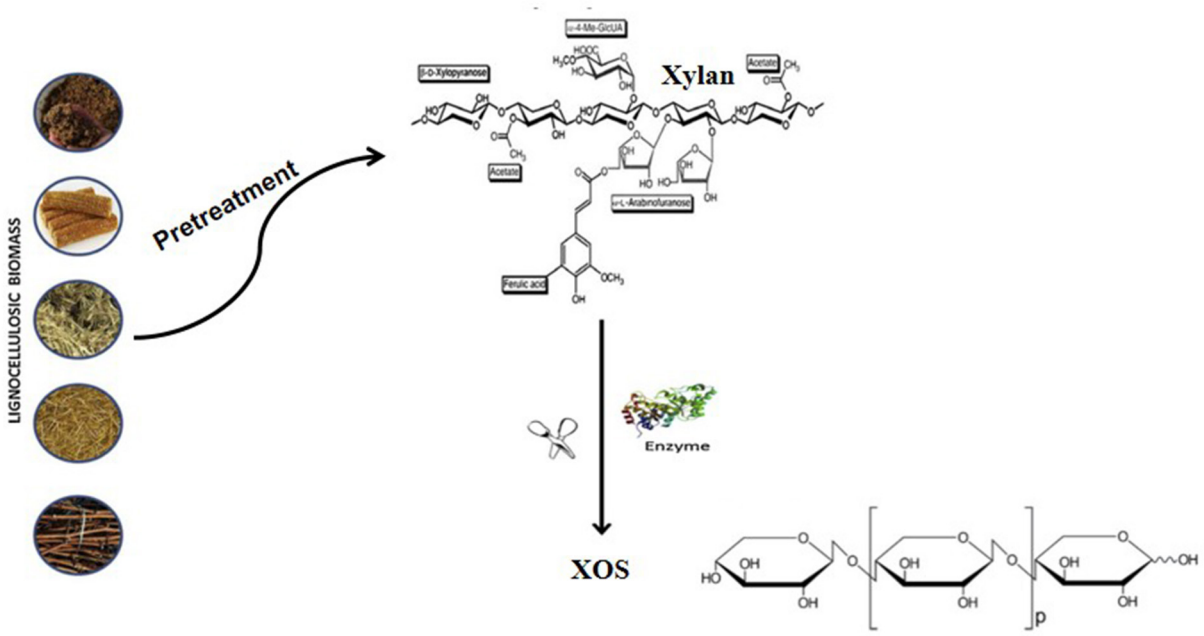

FIGURE 3
Schematic representation of XOS manufacture by enzymatic method.

was 5.80 ± 0.14 mg/mL from the complex by xylanase hydrolysis (94). According to reports, after being dissolved in 1.0 M H_2SO_4 for 12 h, XOS were extracted from corncob by high-pressure hydrolysis, and the maximum yield was 67.7% (95).

The alkali extraction method is greatly affected by temperature and the extraction rate increases with the increase of temperature. The alkali extraction method does not produce byproducts, which is better than the acid extraction method, but it have high requirements for equipment. Therefore, it is suggested to use physical processes (such as steam and ultrasonic) and chemical processes to improve the yield of xylan.

Xylanase hydrolysis

Xylanase systems include endo-xylanase and xylose releasing enzyme exo-xylanase, or β-xylosidase, and debranching enzyme (30, 96). For the production of XOS, only endo-xylanase are meaningful. Based on sequence conservation, these enzymes can be found in glycoside hydrolase families (GH) 5, 8, 10, 11, and 43. In addition, exo-xylanase or β-xylosidase preparations with low activities were needed to avoid xylose production (56). Xylanases have been isolated from many different fungi and bacteria, but most commercial xylanase hydrolysates are currently produced by transgenic xylanase strains (97, 98).

It was reported that the main product was xylobiose after the cauliflower stalk was hydrolyzed by natural endo-xylanase extracted from *Aspergillus niger* TCC9687. The cauliflower stalk XOS showed significantly high antioxidant and antibacterial activities and reduced the viability of human bone cancer MG-63 cells, both alone and in combination with (*Lactiplantibacillus plantarum*, *Bifidobacterium bifidum*, *Lactobacillus delbrueckiissp*. *Helveticus*); the antibacterial components of cauliflower stalkm XOS were dihydroxybenzoic acid and aspartic acid (99). Abdella et al. reported that after the xylanase produced by *Paecilomyces wallichii* was applied to beech xylan to produce different types of XOS; when the extract concentration was from 0.1 to 1.5 mg/mL, the antioxidant activity of XOS increased from 15.22 to 70.57% (100). XOS from oil palm empty fruit bunch hemicellulose produced by xylanase from *Thermomyces cyanobacterium* hydrolysis was composed of xylotriose and xylobiose. XOS was evaluated as the substrate of two probiotics (*Lactobacillus plantarum* WU-P19 makes better use of XOS than *Bifidobacterium* TISTR2129) found in the human gastrointestinal tract (101).

Table 3 lists the hydrolysis and yield of different raw materials with endo-xylanase from different sources. It can be seen from Table 3 that the yield of fungal xylanase is high. It is reported that bacteria such as bacillus and streptomyces could also produce xylanase (114). Recombinant xylanase could also obtain a relatively high yield, but large-scale natural production of recombinant enzyme required a highly complex purification process, which significantly increases the cost. Enzymatic hydrolysis of xylan could also be achieved *in situ* by microbial fermentation. In this process, bacteria were cultured to produce xylanase and secreted into the reaction medium, where the enzyme hydrolyzes xylan to produce XOS (115).

TABLE 2 Material sources, conditions, and xylan yield of commonly used chemical pre-treatment methods.

Material sources	Extraction method	Xylan yield	References
Corn cob	12% NaOH	83% of original xylan	(6)
	Acidic electrolyte water, pH 2.0	55%	(87)
	4% NaOH and methyl alcohol	11%	(88)
	10% NaOH, 75°C, 90 min	20%	(89)
Wheat straw	0.5 mol/L NaOH, 55°C, 2 h	49.3% of original xylan	(90)
Corn stalks	10% NaOH+1% $NaHBH_4$, 20°C, 10 h	54% of original hemicellulose	(91)
Corn husks	12% NaOH, 121°C, 0.2 MPa, steam 45 min	84.60 ± 2.19% of original xylan	(92)

Xylanase hydrolysis process is relatively soft and easy to purify. There is no apparent other production, and the color of XOS is relatively light. XOS prepared by enzymatic hydrolysis have good prebiotic potential and antioxidant performance. In addition, the use of xylanase has high efficiency and specificity, allowing higher control of DP and reducing the production of unwanted xylose and other byproducts. At present, xylanase hydrolysis is the primary method to produce XOS.

To sum up, the existing methods have optimized the preparation of XOS to a certain extent and improved product efficacy. In recent years, the industrial application of XOS has been greatly limited due to high content of impuritie XOS; and the product quality of XOS was not easy to control. Therefore, the refining, separation, and purification of XOS have also become the key to subsequent industrial application. At present, the development of XOS has not reached its peak. As a new generation of functional sugars, XOS have not been fully used. These production optimizations have promoted the application and development of XOS and laid the primary theoretical foundation for large-scale popularization and use in the future.

XOS purification

After XOS production, undesirable compounds and oligosaccharides were produced (116). The presence of unwanted compounds such as glucose and xylose will increase the calorific value of XOS and change their sweetness ability (56). On the other hand, the prebiotic effect of XOS also seems to depend on their purity level. It has been observed that high-purity XOS products have a more significant impact on biological function (57).

To remove unwanted components and obtain high-purity XOS, subsequent purification treatment is required (28). In particular, more components will effect the purity of product when the autohydrolysis method is adopted to treat lignocellulose (117).

The commonly used purification methods include adsorption separation, solvent extraction, membrane separation, and chromatographic separation.

Adsorption on the active solid surface is usually used in combination with the solvent elution step to separate oligomers from monomers and remove other unwanted pollutants. Commonly used adsorbents for purifying XOS include activated carbon, acid clay, bentonite, diatomite, aluminum hydroxide oxide, titanium, silica, and porous synthetic materials (1, 56, 118). Among them, activated carbon is the most commonly used evaluation method, whether in solution or fixed bed adsorption. Activated carbon treatment has proven to be a viable option for removing extract-derived, lignin-derived, and carbohydrate degrading compounds present in XOS mixtures (119). On the other hand, ion exchange resins are combined with different purification strategies to remove salts, heavy metal ions, charged organic compounds and pigments in XOS mixtures (56, 120).

Solvent extraction mainly removes the non-sugar components from the hydrolysate. The recovery and purification degree of the XOS mixture depend on the solvent used for extraction. Ethanol, acetone, and isopropanol are the most common options for refining crude XOS solutions (121–123). In XOS production, solvent extraction is usually used to recover hemicellulose derivatives from pre-treatment (55). In this case, vacuum evaporation is generally used in the first stage to remove volatile compounds and concentrate XOS solution (56). On the other hand, organic solvent precipitation allows the recovery of XOS or xylose while removing phenols and extracting derived compounds.

Chromatographic separation for XOS purification produces analytical grade high-purity components. Gel permeation chromatography (GPC) (124), water-soluble exclusion chromatography (SEC) (125), ion-exchange chromatography (IEC), and centrifugal partition chromatography (CPC) are some standard technologies for purifying XOS (126, 127), Ho et al. used GFC to purify XOS produced by autohydrolysis of agricultural residues. In this cases, GFC could effectively remove high DP oligosaccharides. More importantly, GFC could remove unwanted small molecules, such as monosaccharides, acetic acid, and degradation compounds (furfural, HMF, and phenol) (128).

Membrane separation is another powerful technique commonly used for oligomer purification. Ultrafiltration and nanofiltration based technology is the most promising processing strategy for manufacturing high-purity and

TABLE 3 Xylanase used for XOS production, operational conditions, and yield.

Xylanase	Biomass substrate	Xylanase ratio	Operational conditions	Hydrolysis yield	References
Wild-Type endo-xylanase	Paper mulberry pulp	125 U/g	53.8°C, 12 h	1.23 ± 0.09 g/L	(102)
Recombinant endo-xylanase	Paper mulberry pulp	125 U/g	53.8°C, 12 h	1.59 ± 0.07 g/L	(102)
Cellulase-Free xylanolytic enzyme from *Bacillus firmus* K-1	Corn cob	3 U/mL	50°C, pH4.8, 4 h	44.6% (intial xylan)	(103)
Endo-Xylanase from *Aspergillus niger* MTCC 9687	Lauliflower stalk	20 U/g	50°C, 5h, pH5.4	7.4 mg/mL	(104)
Crude fungal xylanases from A. flavus KUB2	Spent mushroom	20 U/g	50°C, 5h, pH5.4	1.37–1.48 mg/mL	(105)
GH10 from *Caldicellulosiruptor bescii* xylanase	Rice straw xylan Sugarcane bagasse	300 U/mL	50°C, pH 6.0, 72 h	2.93 mg/mL 1.12 mg/mL	(106)
GH11 from *Bacillus firmus* K-1 xylanase	Rice straw xylan Sugarcane bagasse	300 U/mL	50°C, pH6.0, 72 h	1.79 mg/mL 1.10 mg/mL	(106)
Two recombinant endo-xylanase from *Streptomyces thermos*-Riseus (StXyl10, StXyl11)	Red alga dulse	0.5 μg/mL Then 2.0 μg/mL	StXyl10 (50°C, 4 h) StXyl11(60°C, 36 h)	95.8% (intial xylan)	(107)
Crude xylanase produced with *Aureobasidium pullulans* NRRL Y−2311–1 from wheat bran	Autohydrolysis of hazelnut shells	240 U/g	50°C, pH 6.0, 24 h	22.5 g/L	(108)
Combinations of endo-β-(1,4)-D-xylanase enzyme with accessory enzymes (α-L-arabinofuranosidase, feruloy-esterase, and acetylxylan-esterase)	Barley straw	Endo-β-(1,4)-D-xylanase NS50030 7.2 U/mL; α-L-arabinofuranosidase 6.3 U/mL; feruloylesterase 0.05 U/mL, and acetylxylan esterase 5 U/mL	50°C, pH 4.8, 5 h	13.6 g XOS/100 g	(109)
Commercial xylanase	Rice husk arabinoxylan	50 U/g	50°C, pH 5.5 24 h	64.01%	(110)
Commercial xylanase	Rice straw arabinoxylan	100 U/g	50°C, pH 5.5, 24 h	59.52%	(110)
Crude xylanase from *Aureobasidium pullulans* CCT 1261	Beechwood xylan	260 U/g	40°C, pH 6.0 24 h	10.1 mg/mL	(111)
Aspergillus versicolor endo-xylanase	Xylan from sugarcane bagasse 0.17% substrate	65 UI/g	55°C, 24 h	67.43%	(112)
Aspergillus versicolorendoxylanase	Xylan from sugarcane leaf 0.17% substrate	65 UI/g	55°C, 24 h	69.71%	(112)
Xylanase complex fermentation by *Aspergillus niger*	Sugarcane extracted xylan	5 U/mL	55°C, pH 5.8, 1 h	3.1 g/L	(113)

concentrated oligosaccharides (55). The popularity of this technology can be attributed to its low energy consumption requirements, relatively easy amplification, and easy operation variables (13, 116, 129–131). Membrane technology is currently considered to be the most promising strategy for industrial production of high-purity XOS. In this case, the ultrafiltration separation of oligosaccharides from high molecular weight compounds has low energy consumption and is easy to operate and enlarge (128). However, its disadvantage is that its performance is poor when small molecules must be removed.

Meanwhile, purification strategies with different properties are often used in combination to improve the purification of XOS. It was reported that a combination of nanofiltration,

solvent extraction and dual ion exchange chromatography method could achieve 90.7% XOS purity (132).

Nutritional properties of XOS

Figure 4 showed the main nutritional properties of XOS. XOS have many important physiological activities, especially in regulating blood glucose, reducing blood lipids, improving antioxidant capacity, preventing cancer, preventing dental, and improving the structure of host intestinal flora.

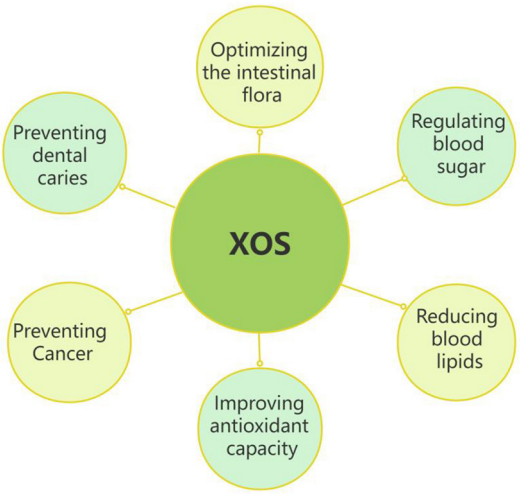

FIGURE 4
Nutritional properties of XOS.

Optimizing the intestinal flora

Figure 5 showed the role of XOS in regulating intestinal flora. XOS can change the composition of intestinal microorganisms, increase the number of probiotics and produce healthy fatty acids. It was found that XOS from giant awn could increase the number of *Bifidobacteria*, *Lactobacillus* and *Escherichia coli* without affecting the number of pathogenic bacteria such as *Clostridium perfringens* (134). XOS extracted from corn straw also had a significant effect on the proliferation of *Lactobacillus* and *Bacteroides* (80). The addition of XOS during fattening period would increase the concentration of acetic acid, linear fatty acids and short-chain fatty acids in pig intestinal contents, and change the composition and metabolic activity of intestinal flora (135). The intake of XOS could significantly increase the number of *Bifidobacteria* in human intestine (136). It was elucidated that *in vitro* fermentation of XOS from birch could significantly proliferated the number of *Bifidobacteria*, *Staphylococcus*, especially *Staphylococcus hominis*, which could produce *bacteriostasis* and inhibit corresponding pathogenic bacteria such as *Staphylococcus aureus* and *Helicobacter pylori* (137). Hald et al. elucidated that after ingestion of arabinoxylan, the number of *Bifidobacteria* in feces increased significantly, while the number of *Lactobacillus*, *Clostridium,* and *Akmann mucophilus* did not change significantly (138).

The reason that XOS selectively proliferate beneficial bacteria such as *Bifidobacteria* in the intestine is related to the production of vitamins and immune stimulation (139). The proliferation of *Bifidobacteria* in the intestine will also inhibit the growth and reproduction of pathogenic bacteria, produce some digestive enzymes and help the body rebuild the intestinal flora (140). The effect of XOS on intestinal health is also reflected in the large production of organic acids, such as short-chain fatty acids, acetic acid, propionic acid, and butyric acid, as well as other organic acids such as lactic acid, succinic acid, formic acid, isobutyric acid, valeric acid, caproic acid, and isohexanoic acid (99, 141). These organic acids play essential roles in preventing various intestinal diseases. The increase in acetic acid concentration was particularly significant after ingestion of Arabinoxylooligosaccharide (136). It was reported that the proliferation of *Bifidobacteria* caused by the intake of XOS is an essential reason for maintaining intestinal health and preventing intestinal diseases (30). The study found that after the intake of XOS, the number of *Enterobacteriaceae* and *Clostridium perfringens* decreased significantly, which effectively reduced the incidence of intestinal diseases caused by harmful bacteria (88, 142).

XOS can selectively proliferate beneficial bacteria for three reasons: (1) Providing energy materials for beneficial bacteria (143). (2) Proliferating beneficial bacteria form a microbial barrier to prevent pathogen colonization (144). (3) XOS are fermented and utilized by *Bifidobacteria* and other microorganisms in the intestine, and the organic acids produced reduce the pH of the intestine, and most pathogenic bacteria are suitable to grow in a neutral environment to inhibit the growth and reproduction of pathogenic microorganisms (145).

Regulating blood sugar

XOS have unique molecular structure of β-1, 4 glycosidic bonds so that the enzymes in the digestive tract in the body cannot decompose them and cannot be directly absorbed and utilized by the human body, so they do not affect the blood glucose concentration. XOS cannot be digested and absorbed by the animal gastrointestinal tract but can be fermented and utilized by beneficial bacteria such as *Bifidobacteria* in the intestine in the large intestine and produce a large number of organic acids such as short-chain fatty acids (146). It was found that type 2 diabetic patients had significantly lower blood sugar levels after 8 weeks of XOS intake (147). The intake of 5%

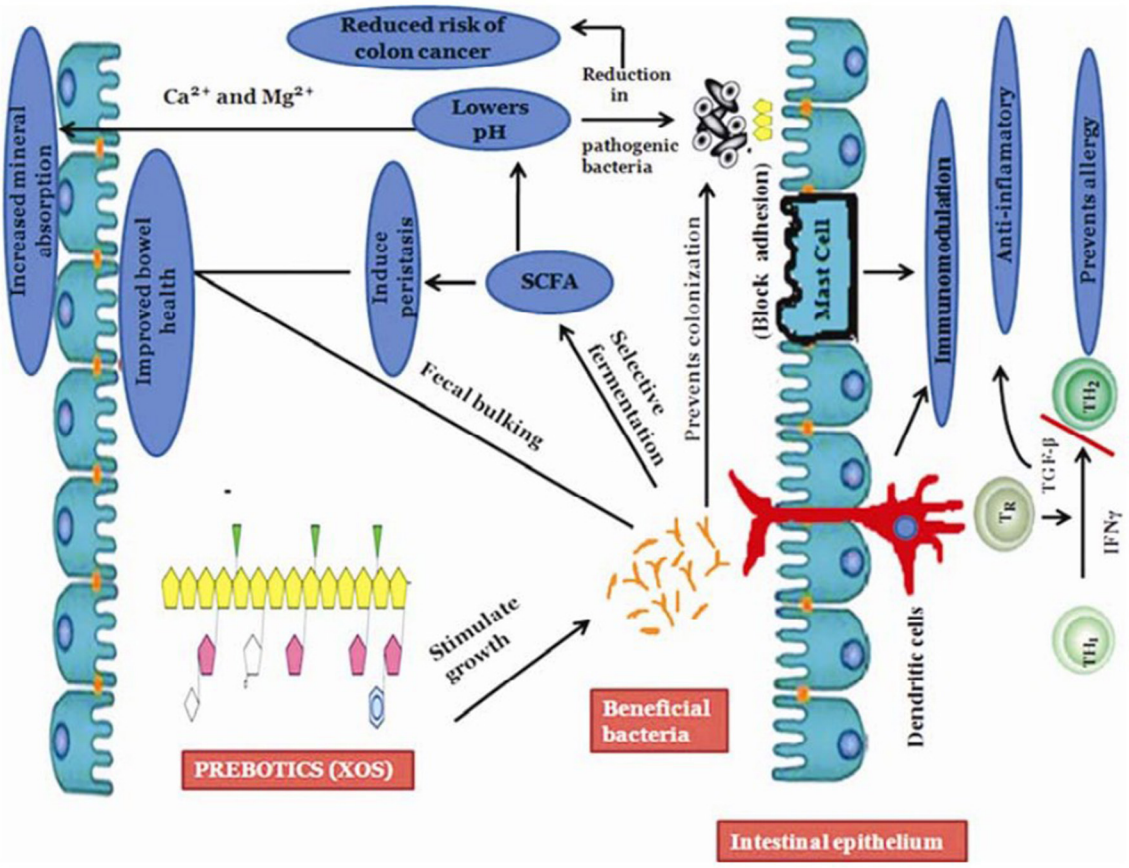

FIGURE 5
Illustration of benefits incurred by prebiotics on immune system: Stimulates growth of the beneficial bacterium in the large intestine that prevents colonization of harmful bacteria; increases production of short-chain fatty acids (SCFA) and helps in improving bowel health that reduces risks of colon cancer [Adopt from Slizewska et al. (133)].

XOS could significantly reduced the blood glucose of obese mice (146). XOS from cereals could effectively improve the blood glucose level of mammals (148).

It was reported that XOS regulated blood glucose and lipid metabolism in mammals depending on their fermentation process in the colon (148). Some researchers argued that XOS could improve glucose tolerance by reducing plasma glucose levels and enhancing insulin sensitivity (149). It was reported that after XOS were ingested by mammals, a large amount of propionic acid produced by the fermentation of beneficial bacteria in the intestine could stimulate the production of glucagon like peptide 1 (GLP-1), which stimulates the secretion of insulin, thereby increasing the synthesis of liver glycogen and reducing the level of plasma glucose (150).

To sum up, XOS play a regulatory role in blood glucose levels. For people with high glucose, diabetes, or impaired glucose tolerance, XOS intake has a positive effect on lowering blood sugar levels, which is consistent with most studies.

Reducing blood lipids

Many studies have shown that XOS could effectively reduce the lipid levels of obese people. For example, it was found that after 8 weeks of continuous intake of 4 g/d xylose, fat in patients with type 2 diabetes decreased significantly (147). XOS could reduce the levels of total cholesterol, low-density lipoprotein, triglyceride, and increase the level of high-density lipoprotein in obese mice with a high-fat diets (146). XOS could also reduce the fat level of broilers (151).

The intake of oligosaccharides will reduce the levels of total auxin and acylated auxin. In contrast, the reduction of acylated auxin will reduce food intake to improve obesity and control metabolism. It was found that the short-chain fatty acids produced by microbial fermentation of XOS in the intestine affect the metabolism of cholesterol, in which propionic acid was absorbed by the intestine and entered the blood through the portal vein to the liver to reduce the synthesis of cholesterol in the liver and improve the sensitivity of insulin to regulate the

body's lipid metabolism (152). In addition, some studies have explained the mechanism of XOS reducing blood lipid from the perspective of bile acid. It was found that the mechanism that XOS reduced the cholesterol level of patients with high cholesterol was the excessive excretion of bile acids (153).

Improving antioxidant capacity

XOS also have antioxidant activity (154). The antioxidant activities of XOS are mainly reflected in increasing the content of non-enzymatic antioxidant substances and improving the activity and level of antioxidant enzymes (147). It was found that XOS could significantly reduce the levels of oxidized glutathione (GSH) and malondialdehyde (MDA) in serum, heart and liver of high-fat diet mice, and normal mice (146). XOS intake could significantly increase the activity and level of antioxidant enzymes such as SOD (superoxide dismutase), CAT (catalase), and GSH PX (glutathione peroxidase) in the heart of mice with a high-fat diet (155). Abasubong et al. reported that 5% XOS (the mass fraction of 1.5%) could significantly improve the growth performance, antioxidant capacity, innate immunity, and hydrophilic bacilli resistance of *Sparus macrocephalus* (156). XOS could increase the contents of *Lactobacillus* and *Bifidobacterium* in mouse feces and reduce the contents of *Enterococcus*, *Enterobacter*, and *Clostridium*. The vitro antioxidant results showed that the conbination of XOS and *Lactobacillus plantarum* had free radical scavenging activity (154).

Preventing cancer

Short-chain fatty acids and other organic acids produced by XOS fermentation in the intestine have a specific role in preventing cancer, and their immune regulation in the body are essential means to prevent cancer (146, 157). Studies have shown that XOS could change the intestinal microbiota of mice and improve the intestinal barrier (158). It was demonstrated that XOS could reduce systemic inflammation, increase trabecular thickness, reduce osteoclasts and active erosive surfaces, and restore the rate of mineral deposition and bone formation in male *Wistar* rats (159). Yin et al. found that the inflammatory state and intestinal barrier of XOS-fed piglets improved significantly (160). Many reports have reported that the addition of oligosaccharides could reduce the expression of TNF-α (tumor necrosis factor) and NF-κβ (proinflammatory nuclear transcription factor protein) in the colon (161). It was also verified the anti-inflammatory activity of wheat arabinose oligosaccharides (162). XOS could also significantly increase the activation potential of T cells and B cells in tumor-bearing mice, as well as the immune ability in body fluids and cellular mediators, and play an anti-tumor role. It was also reported that the taking of XOS could minimize the risk of colon cancer, produce cytotoxic effects on leukemia cells, improve the immune system, and has a positive effect on type 2 diabetes (40, 163–165).

Beneficial bacteria can regulate immune factors and antibodies by using organic acids produced in the process of XOS to improve the immune function of the body (166). *Bifidobacterium* can increase the number of peripheral leukocytes so that the immune function is enhanced through the proliferation of *Bifidobacteria* (154). At the same time, XOS can increase the number of blood monocytes, serum alkaline phosphatase activity, and lysozyme activity. As an immune adjuvant, *Bifidobacterium* can recognize PP lymph nodes, activate intestinal lymph nodes, and induce lymphocyte outflow through lymphatic vessels; the immune system of the body is activated through lymphatic circulation (167). In addition, oligosaccharides directly bind to sugar receptors on the surface of immune cells to stimulate immune cell differentiation and increase activity; XOS can also be used as foreign antigens to effectively and permanently stimulate the immune system and promote the cell division and development of immune organs (153).

Other nutritional properties of XOS

At the same time, XOS can also prevent dental caries (168). XOS can not be decomposed by *Streptococcus mutans* and other bacteria in the mouth. The absorption rate of calcium was improved when XOS and calcium were ingested simultaneously (161). Kobayashi et al. found that the use of acidic XOS in mice with iron deficiency anemia significantly reduced the contents of ferritin in the liver and iron transporter in the small intestine, indicating that XOS could improve the body's iron absorption capacity and promote the body's absorption of minerals. XOS could promote the proliferation of beneficial bacteria in the intestine; and the enzymes (such as phytase) produced by the beneficial bacteria promoted the dissociation of mineral ions in the intestine and improved the intestinal absorption rate of the mineral (169).

Application of XOS

Figure 6 showed the different application of XOS. In the food industry, XOS are commonly used as gelling agents, viscosity regulators, foam stabilizers, and tablet adhesives (170). In addition, the use of XOS as fat substitute in dairy products improves the elasticity and hardness of low-fat cheese and improves the storage stability of the cheese (171, 172). Except in the food industry, XOS are also widely used in medicine, agriculture and feed and other field because of their good physical and chemical properties.

FIGURE 6
Application of XOS.

Application of XOS in food

Application of XOS in baked food

XOS are widely used in baked foods because of their excellent acid and thermal stability. The moisture retention and water retention of XOS can change the rheological properties of dough and control the best moisture effect to change the taste and appearance of baked food. It was reported that the partial substitution of 5% XOS for sucrose would not change the physical and chemical properties of biscuits but would triple the content of crude fiber and increase the content of dietary fiber by 35%; and the biscuits had the functions of storage stability and prebiotic function (173). The addition of XOS increased the baking characteristics of biscuits, which increased caramel flavor, darker color, and more brittle texture (174). The addition of XOS also increased the sweetness and overall taste intensity of biscuits, indicating that XOS play a role in flavor enhancement in baked products. XOS have proved to be a promising new substitute which can increase the dietary fiber content of cereal biscuits.

Application of XOS in beverages

With the addition of XOS to orange juice, pomegranate juice, and whey beverage, the overall sensory acceptance generally improved (170, 175). The strawberry whey beverage with XOS showed an inhibitory effect on the enzymes controlling hypertension and diabetes *in vitro*. With the addition of XOS, the viscosity of the beverage increased, which was attributed to the substantial network formed by hydrogen bonding between XOS and protein and the strong water holding capacity of XOS (176).

Application of XOS in fodder

XOS could promote the improvement of food-specific characteristics and have been incorporated into animal feed to improve health (20).

In poultry feed, XOS could effectively increase the number of *Lactobacillus* in the ruminant intestine and improve animal digestibility. It was elucidated that adding XOS to grain could improve the feed conversion rate by adjusting the nutrient digestibility and ileal morphology of laying hens, which might be due to the increase of bacterial richness and the change of microbial composition, especially the enrichment of *Lactobacillus* and short-chain fatty acid-producing bacteria and the decrease of *Bacteroides* abundance (177). The addition of XOS to the diet had a positive effect on the growth performance, nutrient digestibility, and SCFA ratio of broilers attacked by coccidia (178). Ribeiro et al. studied the effect of XOS on the performance of broilers and reported that the dietary supplementation of XOS increased the nutritional value of the wheat diet, and the improvement of animal performance was accompanied by the transfer of microbial population settled in the upper gastrointestinal tract (179).

In terms of livestock feed, the addition of 100 g/t XOS in a grain diet could increase the height of jejunal villus, the abundance of *Lactobacillus* and *Bifidobacterium,* as well as the concentration of acetic acid and short-chain fatty acids, and could significantly improve the intestinal ecosystem of Weaned Piglets (180). The addition of XOS had a positive impact on the growth performance, nutrient digestibility, and the proportion of short-chain fatty acids of pigs (181). The supplement of 100 g/t XOS in the growth completion stage of pigs would increase the relative abundance of *Lactobacillus* and short-chain fatty acids and biogenic amines (135). Yin et al. elucidated that the addition of XOS to the diet significantly enhanced the α-diversityof the intestinal microbiota of weaned piglets (157). The addition of XOS increased the villus height: crypt depth ratio in jejunum of weanling piglets. The addition of XOS alone (200 mg/kg) could improve the apparent digestibility of dry matter, nitrogen, and total energy on the 14th day, improve trypsin activity and reduce fecal NH_3 concentration. On day 14, taking XOS reduced the number of *E. coli* in feces and increased the number of *Lactobacilli* (182).

In terms of aquatic feed, XOS could promote the growth of aquatic animals, reduce the content of serum cholesterol and triglyceride, effectively control blood glucose level and enhance the immunity of aquatic animals. It was reported that after fed Caspian white fish with 3% XOS for 8 weeks, the antibacterial activity and total protein level of skin mucus was significantly improved. After taking XOS into the diet, the total number of intestinal heterotrophic bacteria and lactic acid bacteria increased significantly, which proved the beneficial effect of XOS on different skin mucosal immune parameters (183). Feeding juvenile triploid *O. mykiss* 5.0–10.0 g/kg XOS could increase the

number of *Lactobacillus* by promoting intestinal development, limiting intestinal injury and inflammation, and regulating the structure of the intestinal microbial community (182). The high-fat diet supplemented with 1–3% XOS promoted the growth of carp fed with high-fat diet; and XOS could improve the growth, digestive enzymes, antioxidants, and immune response of carp fed with a high-fat diet (184). The appropriate level of XOS supplement could improve the growth performance of grass carp, increase the number of *Lactobacillus* and *Bifidobacterium* and the concentration of short-chain fatty acids, improve the growth performance of grass carp and prevent intestinal cell apoptosis (185). It was reported that added 5% XOS to the diet could significantly improve the growth performance, antioxidant capacity, innate immunity, and hydrophilic bacilli resistance of *Megalobrama amblycephala* (156). Adding XOS to feed European bass (*Dicentrarchusla-brax*) could significantly increase body weight and protein efficiency ratio and feed conversion rate, improve growth, stimulate immunity, and enhance anti-infection ability (186).

Application of XOS in medical treatment

The unique physiological activities of XOS makes them widely used in medicine for the treatment and prevention of a variety of diseases. In medical care, XOS can be an option in preventing cardiovascular, tumor, and endocrine diseases. XOS can be used as anti-tumor stabilizers, immune stimulants, antioxidants, and drugs. XOS can also be widely added to health care products as functional factors to assist in treating of some human diseases. Through clinical verification, XOS can be combined with traditional Chinese medicine extracts or added to the formula of Western medicine to replace some auxiliary materials such as starch and dextrin, which can strengthen the efficacy of drugs. In addition, XOS can also directly develop health products and enhance the body's physique. According to clinical trials, XOS play an important role in treating diabetes, hypertension, hyperlipidemia, chronic hepatitis, irritable bowel syndrome, chronic gastroenteritis, osteoporosis, pruritus, and otitis (187). Sheu and other studies reported that 8 weeks of XOS as a dietary supplement could effectively improve blood glucose and lipid levels in type 2 diabetes (147). It was found that XOS was beneficial to the reversible change of intestinal microflora in diabetic patients, such as decreasing the growth of *Enterorhabdus*, *Howardella*, *SLackia,* and so on (48). At the same time, XOS could also reduce the OGTT-2h (2 h oral glucose tolerance test) of prediabetic patients. It was reported that ID-HWS1000 composed of *Lactobacillus* and *Bifidobacterium*, XOS, and dietary fiber directly improved the discomfort related to defecation, reduced the proportion of vertebrates, increased the proportion of *Bacteroides*, improved the perception of intestinal activity in patients with functional constipation, and produced positive changes (188). XOS supplementation could also improve intestinal function, calcium absorption and lipid metabolism, as well as reduce cardiovascular disease, and colon cancer (23).

Application of XOS in agriculture

XOS were also known as plant growth regulators (189). XOS could also be used as fertilizers to improve soil activity and promote crop growth. When XOS were used as soil conditioner, the number of soil microorganisms and enzyme activity increased significantly, and the soil ecosystem was improved (190). In XOS treatment, the content of *Brassinolide* (BRS) increased significantly. Some researchers pointed out that BRS could induce the accumulation of zeatin nucleoside in plants to enhance photoprotection by accumulating many cold shock proteins and effectively prevent the accumulation of cold induced proteins (191). Finally, the resistance of plants to low temperature increased (192). Chen et al. reported the effect of XOS on improving salt tolerance of Chinese cabbage (193). XOS had a force to increase root biomass (increased by 69.5%), and the absorption of auxin also increased significantly (194).

Other applications of XOS

It was reported that adding 3% XOS to a snakehead ball could increase the elasticity of the fishball by 1.32 times without changing the hardness (195). XOS were excellent food additives and could be used as sucrose substitutes in the hydrostatic preparation of high protein meat products. Maillard reaction of soybean protein isolate and XOS could prepare new antioxidant wall materials (196). Soy isolate protein and oligosaccharide conjugate based on Maillard reaction showed excellent potential in microencapsulation of probiotics. Neves and other studies reported that the spray drying blue coloring agent using XOS has shown great potential in many foods as functional ingredients, replacing artificial blue coloring agents and combining the prebiotic characteristics (197). XOS could induce stomatal closure through the production of reactive oxygen species (ROS) and nitric oxide (NO) mediated by salicylic acid signal (198). In addition, in the cosmetics industry, the antioxidant, moisturizing, stabilizer, and emulsifier capabilities of XOS, as well as their ability to restore the microflora, making XOS very attractive (20). Brazil International Flavor Association reported that probiotics and prebiotics were one of the most important active ingredients in the cosmetics market, which could promote the balance of skin microbiota, improve skin resistance, replenish water and alleviate irritation. It was

elucidated that XOS could avoid protein denaturation during frozen storage; shrimp soaked in XOS solution (3.0% w/v) had better water retention, stability of myofibrillar protein, and excellent texture characteristics (199). The mechanism of protein stability was described by the hydrogen bond between XOS and the polar residues of muscle protein and by limiting the fluidity of water to avoid the growth of ice crystals.

Conclusion

XOS are highly effective prebiotic nutritional oligosaccharudes, which can be produced by hydrolysis of hemicellulose, a rich component in agricultural residues rich in xylan. At present, the preparation of XOS mainly includes acid hydrolysis, autohydrolysis, and chemical enzyme synthesis. Although XOS can be produced by chemical hydrolysis; enzymatic hydrolysis has significant advantages because it usually does not produce byproducts, which is very important for the application of XOS. In the industrial environment, the need for biomass pre-treatment and the relatively low efficiency of subsequent enzymatic hydrolysis limit the yield of XOS. Therefore, the successful production of XOS requires strict and optimized conditions.

The existing methods optimize the preparation of XOS to a certain extent and improve the preparation efficiency. In recent years, the industrial application of xylan, a byproducts of agricultural products, has been greatly limited due to its high content of impurities, and the product quality is not easy to control. Therefore, the refining, separation, and purification of XOS have also become the key to their subsequent industrial application. At present, the development of XOS has not reached its peak, and as a new generation of functional sugars, XOS have not been fully used. These production optimizations have promoted the application and development of XOS and laid the primary theoretical foundation for large-scale popularization and use in the future.

The existing physiological activity studies of XOS are carried out in animals and can only speculate on the effect on human body according to the obtained data. The actual effects need further experimental verification. In the preparation process of XOS, the effects of different raw materials on the structure and physiological activity of XOS cannot be determined; further research is needed.

XOS have an auspicious future. With the continuous in-depth development and promotion of the health care industry, there are more and more customers' needs. The advantages of XOS are less addition, good stability, and high selectivity, which is in line with the general demand that capsules, tablets, and other dosage forms are easier to carry and take. These advantages are unmatched by other oligosaccharides. In addition, as relatively new feed additive, they also have excellent performance in bacteriostasis. XOS can further maintain the health and productivity of animals. With many countries have enacted laws, and more and more antibiotics are avoided outside the scope of feed additives, including the continuous improvement of various policies and the gradual diversification and innovation of industrial development, there will be a new opportunity for the sustainable development of the XOS industry.

Author contributions

FY: conceptualization, funding acquisition, and writing—original draft. ST: formal analysis, investigation, resources, and writing—review and editing. KD: investigation and resources. XX: investigation, methodology, and supervision. PG: investigation and methodology. ZC: investigation and supervision. All authors contributed to the article and approved the submitted version.

Funding

This research was supported by the Cultivation Programme for Young Backbone Teachers in Henan Province (2021GGJS059) and funded by Natural Science Innovation Fund Support Program from Henan University of Technology (2021ZKCJ12).

Conflict of interest

The authors declare that the research was conducted in the absence of any commercial or financial relationships that could be construed as a potential conflict of interest.

Publisher's note

References

1. Chapla D, Pandit P, Shah A. Production of xylooligosaccharides from corncob xylan by fungal xylanase and their utilization by probiotics. *Bioresour Technol.* (2012) 115:215–21. doi: 10.1016/j.biortech.2011.10.083

2. Yang H, Wang K, Song X, Xu F. Production of xylooligosaccharides by xylanase from *Pichia stipitis* based on xylan preparation from triploid *Populas tomentosa*. *Bioresour Technol.* (2011) 102:7171–6. doi: 10.1016/j.biortech.2011.03.110

3. Bouxin F, Marinkovic S, Bras JL, Estrine B. Direct conversion of xylan into alkyl pentosides. *Carbohydr Res.* (2010) 345:2469–73. doi: 10.1016/j.carres.2010.09.003

4. Samanta AK, Senani S, Kolte AP, Sridhar M, Sampath K, Jayapal TN, et al. Production and *in vitro* evaluation of xylooligosaccharides generated from corn cobs. *Food Bioprod Process.* (2012) 90:466–74. doi: 10.1016/j.fbp.2011.11.001

5. Peng P, Peng F, Bian J, Xu F, Sun R. Studies on the starch and hemicelluloses fractionated by graded ethanol precipitation from bamboo *Phyllostachys bambusoides* f. shouzhu Yi. *Food Chem.* (2011) 59:2680–8. doi: 10.1021/jf1045766

6. Samanta AK, Jayapal N, Kolte AP, Senani S, Sridhar M, Suresh KP, et al. Enzymatic production of xylooligosaccharides from alkali solubilized xylan of natural grass (Sehima nervosum). *Bioresour Technol.* (2012) 112:199–205. doi: 10.1016/j.biortech.2012.02.036

7. Otieno DO, Ahring BK. The potential for oligosaccharide production from the hemicellulose fraction of biomasses through pretreatment processes: xylooligosaccharides (XOS), arabinooligosaccharides (AOS), mannooligosaccharides (MOS). *Carbohydr Res.* (2012) 360:84–92. doi: 10.1016/j.carres.2012.07.017

8. Akpinar O, Erdogan K, Bakir U, Yilmaz L. Comparison of acid and enzymatic hydrolysis of tobacco stalk xylan for preparation of xylooligosaccharides. *LWT Food Sci Technol.* (2010) 43:119–25. doi: 10.1016/j.lwt.2009.06.025

9. Ahmed S, Riaz S, Jamil A. Molecular cloning of fungal xylanases: an overview. *Appl Microbiol Biotechnol.* (2009) 84:19–35. doi: 10.1007/s00253-009-2079-4

10. Kay H, Carola F. Novel xylan gels prepared from oat spelts. *Macromol Symp.* (2010) 294:141–50. doi: 10.1002/masy.200900169

11. Ochs M, Muzard M, Plantier-Royon ERB, Remond C. Enzymatic synthesis of alkyl b-D-xylosides and oligoxylosides from xylans and from hydrothermally pretreated wheat bran. *Green Chem.* (2011) 13:2380–8. doi: 10.1039/c1gc15719a

12. Brienzo M, Carvalho W, Milagres AMF. Xylooligosaccharides production from alkali-pretreated sugarcane bagasse using xylanases from *Thermoascus aurantiacus*. *Appl Biochem Biotechnol.* (2010) 162:1195–205. doi: 10.1007/s12010-009-8892-5

13. Nabarlatz D, Torras C, Garcia-Valls R, Montané D. Xylooligosaccharides production from alkali-pretreated sugarcane bagasse using xylanases from thermoascus aurantiacus. *Sep Purif Technol.* (2007) 53:235–43. doi: 10.1016/j.seppur.2006.07.006

14. Ahring O. A thermochemical pretreatment process to produce xylooligosaccharides (XOS), arabinooligosaccharides (AOS) and mannooligosaccharides (MOS) from lignocellulosic biomasses. *Bioresour Technol.* (2012) 112:285–92.

15. Lin YS, Tseng MJ, Lee WC. Production of xylooligosaccharides using immobilized endo-xylanase of *Bacillus halodurans*. *Process Biochem.* (2011) 46:2117–21. doi: 10.1016/j.procbio.2011.08.008

16. Dekker R, Barbosa AM, Giese EC. *Bioactive Oligosaccharides: Production, Biological Functions, and Potential Commercial Applications*. Nova Science Publishers, Incorporated (2010).

17. Nabarlatz D, Montané D, Kardošová A, Bekešová S, Hríbalová V, Ebringerová, A. Almond shell xylo-oligosaccharides exhibiting immunostimulatory. *Carbohydr Res.* (2007) 342:1122–8. doi: 10.1016/j.carres.2007.02.017

18. Zhou S, Liu X, Guo Y, Qiang W, Peng D, Cao L. Comparison of the immunological activities of arabinoxylans from wheat bran with alkali and xylanase-aided extraction. *Carbohydr Polym.* (2010) 81:784–9. doi: 10.1016/j.carbpol.2010.03.040

19. Swanson KS , Gibson GR, Hutkins RW. The International Scientific Association for Probiotics and Prebiotics (ISAPP) consensus statement on the definition and scope of synbiotics. *Nature Reviews Gastroenterol Hepatol.* (2020) 17: 1–15. doi: 10.1038/s41575-020-0344-2

20. Amorim C, Silvério SC, Prather KLJ, Rodrigues LR. From lignocellulosic residues to market: production and commercial potential of xylooligosaccharides. *Biotechnol Adv.* (2019) 37:107397. doi: 10.1016/j.biotechadv.2019.05.003

21. Akpinar O, Erdogan K, Bostanci S. Enzymatic production of xylooligosaccharide from selected agricultural wastes. *Food Bioprod Process.* (2009) 87:145–51. doi: 10.1016/j.fbp.2008.09.002

22. Wang J, Sun B, Cao Y, Wang C. *In vitro* fermentation of xylooligosaccharides from wheat bran insoluble dietary fiber by *Bifidobacteria*. *Carbohydr Polym.* (2010) 82:419–23. doi: 10.1016/j.carbpol.2010.04.082

23. Samanta AK, Jayapal N, Jayaram C, Roy S, Kolte AP, Senani S, et al. Xylooligosaccharides as prebiotics from agricultural byproducts: production and applications. *Bioact Carbohydr Diet.* (2015) 5:62–71. doi: 10.1016/j.bcdf.2014.12.003

24. Jayapal N, Samanta AK, Kolte AP, Kolte A, Senani S, Sridhar M, et al. Value addition to sugarcane bagasse: xylan extraction and its process optimization for xylooligosaccharides production. *Ind Crops Prod.* (2013) 42:14–24. doi: 10.1016/j.indcrop.2012.05.019

25. Terrasan C, Temer B, Duarte M, Carmona E. Production of xylanolytic enzymes by *Penicillium janczewskii*. *Bioresour Technol.* (2010) 101:4139–43. doi: 10.1016/j.biortech.2010.01.011

26. Miller PS, Blum PH. Extremophile inspired strategies for enzymatic biomass saccharification. *Environ Technol.* (2010) 31:1005–15. doi: 10.1080/09593330903536113

27. Almeida JRM, Runquist D, Nogué VS, Lidén G, Gorwa-Grauslund MF. Stress-related challenges in pentose fermentation to ethanol by the yeast *Saccharomyces cerevisiae*. *Biotechnol J.* (2011) 6:286–99. doi: 10.1002/biot.201000301

28. Australian Industry Development Corporation Inc. *PreticX-Optimize Your Flora*. Australian Industry Development Corporation Inc (2017). Availabler online at: http://storefronts.supplysideshow.com/~/media/Files/Storefronts/

29. Courtin CM, Swennen K, Verjans P, Delcour JA. Heat and pH stability of prebiotic arabinoxylooligosaccharides, xylooligosaccharides and fructooligosaccharides. *Food Chem.* (2009) 112:831–7. doi: 10.1016/j.foodchem.2008.06.039

30. Aachary AA, Prapulla SG. Xylooligosaccharides (XOS) as an emerging prebiotic: microbial synthesis, utilization, structural characterization, bioactive properties, and applications. *Rev Food Sci Food Saf.* (2011) 10:2–16. doi: 10.1111/j.1541-4337.2010.00135.x

31. Ahmad R. Better health with plant oligosaccharides: trends and future. In: *Proceeding of the 1st International Conference on Food and Agriculture* (2019).

32. Markets and Markets^{TM}. *Prebiotic Ingredients Market Worth 7.37 Billion USD by 2023*. Markets and Markets^{TM} (2018). Available online at: https://www.prnewswire.com/news-releases/prebiotic-ingredients-market-worth-737-billion-usd-by-2023-670471503

33. The Market Watch. *Prebiotics Market Annual Consumption Will Cross 1.4 Million Tonsby 2024*. The Market Watch (2018). Available online at: https://www.marketwatch.com/press-release/prebiotics-market-annual-consumption-will-cross-14-million-tons-by-2024-2018-09-10

34. Capetti CCDM, Vacilotto MM, Dabul ANG, Sepulchro AGV, Pellegrini VOA, Polikarpov I. Recent advances in the enzymatic production and applications of xylooligosaccharides. *J Microbiol Biotechnol.* (2021) 37:1–12. doi: 10.1007/s11274-021-03139-7

35. Perlack RD. *Biomass as Feedstock for a Bioenergy and Bioproducts Industry: The Technical Feasibility of a Billion-Ton Annual Supply*. Oak Ridge National Laboratory (2005). doi: 10.2172/885984

36. Otieno DO, Ahring BK. A thermochemical pretreatment process to produce xylooligosaccharides (XOS), arabinooligosaccharides (AOS) and mannooligosaccharides (MOS) from lignocellulosic biomasses. *Bioresour Technol.* (2012) 112:285–92. doi: 10.1016/j.biortech.2012.01.162

37. Poletto P, Pereira GN, Monteiro CRM, Pereira MAF, Oliveira DD. Xylooligosaccharides: transforming the lignocellulosic biomasses into valuable 5-carbon sugar prebiotics. *Process Biochem.* (2020) 91:352–63. doi: 10.1016/j.procbio.2020.01.005

38. Singh RD, Gracy C, Muir J, Arora A. Green and clean process to obtain low degree of polymerisation xylooligosaccharides from almond shell. *J Clean Prod.* (2019) 241:118237. doi: 10.1016/j.jclepro.2019.118237

39. Huang X, Ouyang X, Hendriks BMS, Gonzalez OMM, Zhu J, IKorányi T, et al. Selective production of mono-aromatics from lignocellulose over Pd/C

catalyst: the influence of acid co-catalysts. *Faraday Discuss.* (2017) 202:141–56. doi: 10.1039/C7FD00039A

40. Santibáñez L, Henríquez C, Corro-Tejeda R, Bernal S, Armijo B, Salazar O. Xylooligosaccharides from lignocellulosic biomass: a comprehensive review. *Carbohydr Polym.* (2021) 251:117118. doi: 10.1016/j.carbpol.2020.117118

41. Jnawali P, Kumar V, Tanwar B, Hirdyani H, Gupta P. Enzymatic production of xylooligosaccharides from brown coconut husk treated with sodium hydroxide. *Waste Biomass Valorization.* (2018) 9:1757–66. doi: 10.1007/s12649-017-9963-4

42. Gullón B, Eibes G, Dávila I, Moreira MT, Labidi J, Gullón P. Hydrothermal treatment of chestnut shells (*Castanea sativa*) to produce oligosaccharides and antioxidant compounds. *Carbohydr Polym.* (2018) 192:75–83. doi: 10.1016/j.carbpol.2018.03.051

43. Surek E, Buyukkileci AO. Production of xylooligosaccharides by autohydrolysis of hazelnut (*Corylus avellana* L.) shell. *Carbohydr Polym.* (2017) 174:565–71. doi: 10.1016/j.carbpol.2017.06.109

44. Miranda I, Simões R, Medeiros B, Nampoothiri KM, Sukumaran RK, Rajan D, et al. Valorization of lignocellulosic residues from the olive oil industry by pro-duction of lignin, glucose and functional sugars. *Bioresour Technol.* (2019) 292:121936. doi: 10.1016/j.biortech.2019.121936

45. Banerjee S, Patti AF, Ranganathan V, Arora A. Hemicellulose based biorefinery from pineapple peel waste : xylan extraction and its conversion into xylooligosaccharides. *Food Bioprod Process.* (2019) 117:38–50. doi: 10.1016/j.fbp.2019.06.012

46. Rico X, Gullón B, Alonso JL, Parajó JC, Yáñez R. Valorization of peanut shells :manufacture of bioactive oligosaccharides. *Carbohydr Polym.* (2018) 183:21–8. doi: 10.1016/j.carbpol.2017.11.009

47. Freitas CD, Carmona E, Brienzo M. Xylooligosaccharides production process from lignocellulosic biomass and bioactive effects. *Bioact Carbohydr Diet Fibre.* (2019) 18:100184. doi: 10.1016/j.bcdf.2019.100184

48. Yang J, Summanen PH, Henning SM, Mark H, Heiman L, Huang J, et al. Xylooligosaccharide supplementation alters gut bacteria in both healthy and prediabetic adults: a pilot study. *Front Physiol.* (2015) 6:216. doi: 10.3389/fphys.2015.00216

49. Biely P. Microbial xylanolytic systems. *Trends Biotechnol.* (1985) 3:286–90. doi: 10.1016/0167-7799(85)90004-6

50. Wen P, Zhang T, Wei L,Wang J, Zhang J. Effect of dilute acetic acid hydrolysis on xylooligosaccharide production and the inhibitory effect of cellulolytic enzyme lignin from poplar. *ACS Sustainable Chem Eng.* (2021) 9:11361–71. doi: 10.1021/acssuschemeng.1c02937

51. Ying W, Xu Y, Zhang J. Effect of sulfuric acid on production of xylooligosaccharides and monosaccharides from hydrogen peroxide-acetic acid-pretreated poplar. *Bioresour Technol.* (2021) 321:124472. doi: 10.1016/j.biortech.2020.124472

52. Liao H, Xu Y, Zhang J. Efficient production of xylooligosaccharides and fermentable sugars from corncob by propionic acid and enzymatic hydrolysis. *Bioresour Technol.* (2021) 342:125680. doi: 10.1016/j.biortech.2021.125680

53. Bedo S, Rozbach M, Nagy L, Fehér A, Fehér C. Optimised fractionation of brewer's spent grain for a biorefinery producing sugars, oligosaccharides, and bioethanol. *Processes.* (2021) 9:366. doi: 10.3390/pr9020366

54. Wang J, Xu Y, Meng X, Pu Y, Ragauskas A, Zhang J. Production of xylo-oligosaccharides from poplar by acetic acid pretreatment and its impact on inhibitory effect of poplar lignin. *Bioresour Technol.* (2021) 323:124593. doi: 10.1016/j.biortech.2020.124593

55. Qing Q, Li H, Kumar R, Wyman CE. Xylooligosaccharides production, quantification, and characterization in context of lignocellulosic biomass pretreatment, aqueous pretreatment. *Plant Biomass Biol Chem Conver Fuels Chem.* (2013) 19:391–415. doi: 10.1002/9780470975831.ch19

56. Vázquez MJ, Alonso JL, Dominguez H, Parajó JC. Xylooligosaccharides: manufacture and applications. *Trends Food Sci Technol.* (2000) 11:387–93. doi: 10.1016/S0924-2244(01)00031-0

57. Huang C, Wang X, Liang C, Jiang X, Yong Q. A sustainable process for procuring biologically active fractions of high-purity xylooligosaccharides and water-soluble lignin from moso bamboo prehydrolyzate. *Biotechnol Biofuels.* (2019) 12:1–13. doi: 10.1186/s13068-019-1527-3

58. Ruiz HA, Rodríguez-Jasso RM, Fernandes BD, Vicente AA, Teixeira JA. Hydrothermal processing, as an alternative for upgrading agriculture residues and marine biomass according to the biorefinery concept: a review. *Renew Sust Energ Rev.* (2013) 21:35–51. doi: 10.1016/j.rser.2012.11.069

59. Garrote G, Domi'nguez H, Parajó JC. Autohydrolysis of corncob: study of non-isothermal operation for xylooligosaccharide production. *J Food Eng.* (2002) 52:211–8. doi: 10.1016/S0260-8774(01)00108-X

60. Moure A, Gullón P, Domínguez H, Parajó JC. Advances in the manufacture, purification and applications of xylo-oligosaccharides as food additives and nutraceuticals. *Process Biochem.* (2006) 41:1913–23. doi: 10.1016/j.procbio.2006.05.011

61. Wang ZK, Huang C, Zhong JL, Wang Y, Tang L, Li B, et al. Valorization of Chinese hickory shell as novel sources for the efficient production of xylooligosaccharides. *Biotechnol Biofuels.* (2021) 14:1–13. doi: 10.1186/s13068-021-02076-9

62. Swart LJ, Metersen PA, Bedzo O, Bedzo OKK, Grgens JF. Techno?conomic analysis of the valorisation of brewers spent grains: production of xylitol and xylo, ligosaccharides. *J Chem. Technol Biotechnol.* (2021) 96:1632–44. doi: 10.1002/jctb.6683

63. Ghosh D, Tanner J, Lavoie JM, Gil G, Antonio AF. An integrated approach for hemicellulose extraction from forest residue. *BioResources.* (2021) 16:2524–47. doi: 10.15376/biores.16.2.2524-2547

64. Pablo G, Domínguez VD, Domínguez E, Gullón P, Gullón B, Garrote G, et al. Comparative study of biorefinery processes for the valorization of fast-growing paulownia wood. *Bioresour Technol.* (2020) 314:123722. doi: 10.1016/j.biortech.2020.123722

65. Romaní A, Tomaz PD, Garrote G, Teixeira JA, Domingues L. Combined alkali and hydrothermal pretreatments for oat straw valorization within a biorefinery concept. *Bioresour Technol.* (2016) 220:323–32. doi: 10.1016/j.biortech.2016.08.077

66. Pablo G, Gomes-Dias JS, Rocha CMR, Romaní A, Garrote G, Domingues L. Recent trends on seaweed fractionation for liquid biofuels production. *Bioresour Technol.* (2020) 299:122613. doi: 10.1016/j.biortech.2019.122613

67. Domínguez E, Nóvoa T, Pablo G, Garrote G. Sequential two-stage autohydrolysis biorefinery for the production of bioethanol from fast-growing paulownia biomass. *Energy Convers Manage.* (2020) 226:113517. doi: 10.1016/j.enconman.2020.113517

68. Fujimoto S, Inoue S, Yoshida M. High solid concentrations during the hydrothermal pretreatment of eucalyptus accelerate hemicellulose decomposition and subsequent enzymatic glucose production. *Bioresour Technol Rep.* (2018) 4:16–20. doi: 10.1016/j.biteb.2018.09.006

69. Vargas F, Domínguez E, Vila C, Rodríguez A, Garrote G. Biorefinery scheme for residual biomass using autohydrolysis and organosolv stages for oligomers and bioethanol production. *Energy Fuels.* (2016) 30:8236–45. doi: 10.1021/acs.energyfuels.6b00277

70. Naidu DS, Hlangothi SP, John MJ. Bio-based products from xylan: a review. *Carbohydr. Polym.* (2018) 179:28–41. doi: 10.1016/j.carbpol.2017.09.064

71. Gallina G, Cabeza Á, Grénman H, Biasi P, García-Serna J, Salmi T. Hemicellulose extraction by hot pressurized water pretreatment at 160 °C for 10 different woods: yield and molecular weight. *J Supercrit Fluids.* (2018) 133:716–25. doi: 10.1016/j.supflu.2017.10.001

72. Álvarez C, González A, Negro MJ, Ballesteros I, Oliva JM, Sáez F. Optimized use of hemicellulose within a biorefinery for processing high value-added xylooligosaccharides. *Ind Crops Prod.* (2017) 99:41–8. doi: 10.1016/j.indcrop.2017.01.034

73. Dávila I, Gordobil O, Labidi J, Gullón P. Assessment of suitability of vine shoots for hemicellulosic oligosaccharides production through aqueous processing. *Bioresour Technol.* (2016) 211:636–44. doi: 10.1016/j.biortech.2016.03.153

74. Cocero MJ, Cabeza A, Abad N, Adamovic T, Vaquerizo L, Martínez CM, et al. Understanding biomass fractionation in subcritical & supercritical water. *J Supercrit Fluids.* (2018) 133:550–65. doi: 10.1016/j.supflu.2017.08.012

75. Chen MH, Bowman MJ, Dien BS, Rausch KD, Tumbleson ME, Singh V. Autohydrolysis of miscanthus x giganteus for the production of xylooligosaccharides (XOS): kinetics, characterization and recovery. *Bioresour Technol.* (2014) 155:359–65. doi: 10.1016/j.biortech.2013.12.050

76. Hong C, Corbett D, Venditti R, Jameel H, Park S. Xylooligosaccharides as prebiotics from biomass autohydrolyzate. *LWT Food Sci Technol.* (2019) 111:703–10. doi: 10.1016/j.lwt.2019.05.098

77. Akpinar O, Ak O, Kavas A, Bakir U, Yilmaz L. Enzymatic production of xylooligosaccharides from cotton stalks. *Food Chem.* (2007) 55:5544–51. doi: 10.1021/jf063580d

78. Karlsson EN, Schmitz E, Linares-Pastén JA, Adlercreutz P. Endo-xylanases as tools for production of substituted xylooligosaccharides with prebiotic properties. *Appl Microbiol Biotechnol.* (2018) 102:9081–8. doi: 10.1007/s00253-018-9343-4

79. Teng C, Yan Q, Jiang Z, Fan G, Bo S. Production of xylooligosaccharides from the steam explosion liquor of corncobs coupled with enzymatic hydrolysis using a thermostable xylanase. *Bioresour Technol.* (2010) 101:7679–82. doi: 10.1016/j.biortech.2010.05.004

80. Álvarez C, González A, Alonso JL, Sáeza F, Negro MJ, Gullón B. Xylooligosaccharides from steam-exploded barley straw: structural features and assessment of bifidogenic properties. *Food Bioprod Process.* (2020) 124:131–42. doi: 10.1016/j.fbp.2020.08.014

81. Khat-udomkiri N, Sivamaruthi BS, Sirilun S, Narissara L, Sartjin P, Chaiyavat C. Optimization of alkaline pretreatment and enzymatic hydrolysis for the extraction of xylooligosaccharide from rice husk. *AMB Express.* (2018) 8:115. doi: 10.1186/s13568-018-0645-9

82. Carvalho AFA, Marcondes WF, Pedro DON, Pastore GM, Saddler JN, Arantes V. The potential of tailoring the conditions of steam explosion to produce xylo-oligosaccharides from sugarcane bagasse. *Bioresour Technol.* (2018) 250:221–9. doi: 10.1016/j.biortech.2017.11.041

83. Buruiana CT, Gómez B, Vizireanu C, Garrote G. Manufacture and evaluation of xylooligosaccharides from corn stover as emerging prebiotic candidates for human health. *LWT Food Sci Technol.* (2017) 77:449–59. doi: 10.1016/j.lwt.2016.11.083

84. Kim Y, Hendrickson R, Hosier N, Ladisch MR. Plug-flow reactor for continuous hydrolysis of glucans and xylans from pretreated corn fiber. *Energy Fuels*. (2005) 19:2189–200. doi: 10.1021/ef050106l

85. Yang W, Ajapur VK, Krishnamurthy K, Feng H, Yang R, Rababah TM. Expedited extraction of xylan from corncob by power ultrasound. *Int J Agric Biol Eng.* (2009) 2:76–83. Available online at: http://www.ijabe.org

86. Immerzeel P, Falck P, Galbe M, Adlercreutz P, Karlsson EN. Extraction of water-soluble xylan from wheat bran and utilization of enzymatically produced xylooligosaccharides by *Lactobacillus*, *Bifidobacterium* and *Weissella* spp. *LWT Food Sci Technol.* (2014) 56:321–7. doi: 10.1016/j.lwt.2013.12.013

87. Zhang H, Xu Y, Yu S. Co-production of functional xylooligosaccharides and fermentable sugars from corncob with effective acetic acid prehydrolysis. *Bioresour Technol.* (2017) 234:343–9. doi: 10.1016/j.biortech.2017.02.094

88. Oliveira EE, Silva AE, Júnior TN, Gomes MCS, Aguiar LM, Marcelino HR, et al. Xylan from corn cobs, a promising polymer for drug delivery: production and characterization. *Bioresour Technol.* (2010) 101:5402–6. doi: 10.1016/j.biortech.2010.01.137

89. Cai W, Chen Q, Xie L, Yang L, Zhang R. Extraction, sulfonation and anticoagulant activity of xylan from corncob. *Eur Food Res Technol.* (2015) 240:969–75. doi: 10.1007/s00217-014-2401-y

90. Ruzene DS, Silva DP, Vicente AA, Gonalves AR, Teixeira JA. An alternative application to the Portuguese agro-industrial residue: wheat straw. *Appl Biochem Biotechno.* (2007) 147:453–64. doi: 10.1007/978-1-60327-526-2_43

91. Egüés I, Sanchez C, Mondragon II, Labidi J. Effect of alkaline and autohydrolysis processes on the purity of obtained hemicelluloses from corn stalks. *Bioresour Technol.* (2012) 103:239–48. doi: 10.1016/j.biortech.2011.09.139

92. Samanta AK, Kolte AP, Elangovan AV, Dhali A, Roy S. Value addition of corn husks through enzymatic production of xylooligosaccharides. *Braz Arch Biol Technol.* (2016) 59. doi: 10.1590/1678-4324-2016160078

93. Kawee-ai A, Srisuwun A, Tantiwa N, Nontaman W, Boonchuay P, Kuntiy A, et al. Eco-friendly processing in enzymatic xylooligosaccharides production from corncob: influence of pretreatment with sonocatalytic–synergistic fenton reaction and its antioxidant potentials. *Ultrason Sonochem.* (2016) 31:184–92. doi: 10.1016/j.ultsonch.2015.12.018

94. Kumar R, Wyman CE. The impact of dilute sulfuric acid on the selectivity of xylooligomer depolymerization to monomers, the impact of dilute sulfuric acid on the selectivity of xylooligomer depolymerization to monomers. *Carbohydr Res.* (2008) 343:290–300. doi: 10.1016/j.carres.2007.10.022

95. Yang R, Xu S, Wang Z, Wang Y. Aqueous extraction of corncob xylan and production of xylooligosaccharides. *LWT Food Sci Technol.* (2005) 38:677–82. doi: 10.1016/j.lwt.2004.07.023

96. Mano M, Neri-Numa IA, Silva J, Paulino BN, Pessoa MG, Pastore GM. Oligosaccharide biotechnology: an approach of prebiotic revolution on the industry. *Appl Biochem Biotechnol.* (2018) 102:17–37. doi: 10.1007/s00253-017-8564-2

97. Yadav SK. Technological advances and applications of hydrolytic enzymes for valorization of lignocellulosic biomass. *Bioresour Technol.* (2017) 245:1727–39. doi: 10.1016/j.biortech.2017.05.066

98. Mussatto SI, Teixeira JA. *Lignocellulose as Raw Material in Fermentation Processes*. (2010). Available online at: http://hdl.handle.net/1822/16762

99. Li Z, Summanen PH, Komoriya TM. *In vitro* study of the prebiotic xylooligosaccharide (XOS) on the growth of *Bifidobacterium* spp and *Lactobacillus* spp. *Int J Food Sci Nutr.* (2015) 66:919–22. doi: 10.3109/09637486.2015.1064869

100. Abdella A, Ramadan S, Hamouda RA, Saddiq AA, Alhazmi NM, Al-Saman MA. Paecilomyces variotii xylanase production, purification and characterization with antioxidant xylo-oligosaccharides production. *Sci Rep.* (2021) 11:16468. doi: 10.1038/s41598-021-95965-w

101. Rathamat Z, Choorit W, Chisti Y, Prasertsan P. Two-step isolation of hemicellulose from oil palm empty fruit bunch fibers and its use in production of xylooligosaccharide prebiotic. *Ind Crops Prod.* (2021) 160:113124. doi: 10.1016/j.indcrop.2020.113124

102. Chaiyaso T, Boonchuay P, Takenaka S, Techapun C, Watanabe M. Efficient enzymatic process for mulberry paper production: an approach for xylooligosaccharide production coupled with minimizing bleaching agent doses. *Waste Biomass Valorization.* (2021) 12:5347–60. doi: 10.1007/s12649-021-01416-y

103. Su Y, Fang L, Wang P, Lai C, Huang C, Ling Z, et al. Efficient production of xylooligosaccharides rich in xylobiose and xylotriose from poplar by hydrothermal pretreatment coupled with post-enzymatic hydrolysis. *Bioresour Technol.* (2021) 342:125955. doi: 10.1016/j.biortech.2021.125955

104. Majumdar S, Bhattacharyya DK, Bhowal J. Evaluation of nutraceutical application of xylooligosaccharide enzymatically produced from cauliflower stalk for its value addition through a sustainable approach. *Food Funct.* (2021) 12:5501–23. doi: 10.1039/D0FO03120H

105. Seekram P, Thammasittirong A, Thammasittirong NR. Evaluation of spent mushroom substrate after cultivation of *Pleurotus ostreatus* as a new raw material for xylooligosaccharides production using crude xylanases from *Aspergillus flavus* KUB2. *3 Biotech.* (2021) 11:1–9. doi: 10.1007/s13205-021-02725-8

106. Gufe C, Ngenyoung A, Rattanarojpong T, Khunra P. Investigation into the effects of CbXyn10C and Xyn11A on xylooligosaccharide profiles produced from sugarcane bagasse and rice straw and their impact on probiotic growth. *Bioresour Technol.* (2022) 344:126319. doi: 10.1016/j.biortech.2021.126319

107. Fujii Y, Kobayashi M, Miyabe Y, Kishimura H, Hatanaka T, Kumagai Y. Preparation of β(1→ 3)/β(1→ 4)-xylooligosaccharides from red alga dulse by two xylanases from *Streptomyces thermogriseus*. *Bioresour Biopro.* (2021) 8:1–10. doi: 10.1186/s40643-021-00390-6

108. Surek E, Buyukkileci AO, Yegin S. Processing of hazelnut (*Corylus avellana* L.) shell autohydrolysis liquor for production of low molecular weight xylooligosaccharides by *Aureobasidium pullulans* NRRL Y−2311–1 xylanase. *Ind Crops Prod.* (2021) 161:113212. doi: 10.1016/j.indcrop.2020.113212

109. Cristina L, Alberto G, Ignacio B, Negro MJ. Production of xylooligosaccharides, bioethanol, and lignin from structural components of barley straw pretreated with a steam explosion. *Bioresour Technol.* (2021) 342:125953. doi: 10.1016/j.biortech.2021.125953

110. Jaichakan P, Nakphaichit M, Rungchang S, Weerawatanakorn M, Phongthai S, Klangpetch W. Two-stage processing for xylooligosaccharide recovery from rice by-products and evaluation of products: promotion of lactic acid-producing bacterial growth and food application in a high-pressure process. *Food Res Int.* (2021) 147:110529. doi: 10.1016/j.foodres.2021.110529

111. Gautério GV, Hübner T, Ribeiro TDR, Ziotti APM, Kalil SJ. Xylooligosaccharide production with low xylose release using crude xylanase fromaureobasidium pullulans: effect of the enzymatic hydrolysis parameters. *Appl Biochem Biotechnol.* (2021) 194:862–81. doi: 10.1007/s12010-021-03658-x

112. Forsan CF, Freitas CD, Masarin F, Brienzo M. Xylooligosaccharide production from sugarcane bagasse and leaf using aspergillus versicolor endoxylanase and diluted acid. *Biomass Convers Biorefin.* (2021) 1–16. doi: 10.1007/s13399-021-01403-2

113. Valladares-Diestra KK, Vandenberghe L, Soccol CR. A biorefinery approach for enzymatic complex production for the synthesis of xylooligosaccharides from sugarcane bagasse. *Bioresour Technol.* (2021) 333:125174. doi: 10.1016/j.biortech.2021.125174

114. Álvarez-Cervantes J. Mycosphere essay 10: properties and characteristics of microbial xylanases. *Mycosphere.* (2016) 7:1600–19. doi: 10.5943/mycosphere/si/3b/12

115. Azzouz Z, Bettache A, Boucherba N, Eugenio LD. Optimization of β-1,4-endoxylanase production by an *Aspergillus niger*. Strain growing on wheat straw and application in xylooligosaccharides production. *Molecules.* (2020) 26:2527. doi: 10.3390/molecules26092527

116. Gullón P, Moura P, Esteves MP, Girio FM, Domínguez H, Parajó JC. Assessment on the fermentability of xylooligosaccharides from rice husks by probiotic bacteria. *J Agric Food Chem.* (2008) 56:7482–7. doi: 10.1021/jf800715b

117. Illanes A, Guerrero C, Vera C, Wilson L, Conejeros R, Scott F. *Lactose-Derived Prebiotics: A Process Perspective*. Academic Press (2016).

118. Zhu Y, Kim TH, Lee YY, Chen R, Elander RT. Enzymatic production of xylooligosaccharides from corn stover and corn cobs treated with aqueous ammonia. *Appl Biochem Biotechnol.* (2006) 130:586–98. doi: 10.1385/ABAB:130:1:586

119. Montané D, Nabarlatz D, Martorell A, Torné-Fernández V, Fierro V. Removal of lignin and associated impurities from xylo-oligosaccharides by activated carbon adsorption. *Ind Eng Chem Res.* (2006) 45:2294–302. doi: 10.1021/ie051051d

120. Chen MH, Bowman MJ, Cotta MA, Dien BS, Iten LB, Whitehead TR, et al. Miscanthus× giganteus xylooligosaccharides: purification and fermentation. *Carbohydr Polym.* (2016) 140:96–103. doi: 10.1016/j.carbpol.2015.12.052

121. Gullón P, Gullón B, Moure A, Alonso JL, Parajó JC. Manufacture of prebiotics from biomass sources. In: *Prebiotics and Probiotics Science and Technology*. (2009). p. 535–89. doi: 10.1007/978-0-387-79058-9_14

122. Vegas R, Alonso JL, Domínguez H, Paraj,ó JC. Manufacture and refining of oligosaccharides from industrial solid wastes. *Ind Eng Chem Res.* (2005) 44:614–20. doi: 10.1021/ie049289+

123. Swennen K, Courtin CM, Bruggen BV, Vandecasteele C, Delcour JA. Ultrafiltration and ethanol precipitation for isolation of arabinoxylooligosaccharides with different structures. *Carbohydr Polym.* (2005) 62:283–92. doi: 10.1016/j.carbpol.2005.08.001

124. Sun HJ, Yoshida S, Park NH, Kusakabe I. Preparation of (1→ 4)-β-D-xylooligosaccharides from an acid hydrolysate of cotton-seed xylan: suitability of cotton-seed xylan as a starting material for the preparation of (1→ 4)-β-D-xylooligosaccharides. *Carbohydr Res.* (2002) 337:657–61. doi: 10.1016/S0008-6215(02)00031-9

125. Jacobs A, Palm M, Zacchi G, Dahlman O. Isolation and characterization of water-soluble hemicelluloses from flax shive. *Carbohydr Res.* (2003) 338:1869–76. doi: 10.1016/S0008-6215(03)00308-2

126. Marchal L, Legrand J, Foucault A. Centrifugal partition chromatography: a survey of its history, and our recent advances in the field. *Chem Rec.* (2003) 3:133–43. doi: 10.1002/tcr.10057

127. Lau CS, Bunnell KA, Clausen EC, Thoma GJ, Lay JO, Gidden J, et al. Separation and purification of xylose oligomers using centrifugal partition chromatography. *Ind Microbiol Biotechnol.* (2011) 38:363–70. doi: 10.1007/s10295-010-0799-1

128. Ho AL, Carvalheiro F, Duarte LC, Roseiro LB, Charalampopoulos D, Rastall RA. Production and purification of xylooligosaccharides from oil palm empty fruit bunch fibre by a non-isothermal process. *Bioresour Technol.* (2014) 152:526–9. doi: 10.1016/j.biortech.2013.10.114

129. Pinelo M, Jonsson G, Meyer AS. Membrane technology for purification of enzymatically produced oligosaccharides: molecular and operational features affecting performance. *Sep Purif Technol.* (2009) 70:1–11. doi: 10.1016/j.seppur.2009.08.010

130. Cano À, Palet C. Xylooligosaccharide recovery from agricultural biomass waste treatment with enzymatic polymeric membranes and characterization of products with MALDI-TOF-MS. *J Memb Sci.* (2007) 291:96–105. doi: 10.1016/j.memsci.2006.12.048

131. Yuan QP, Zhang H, Qian ZM, Yang XJ. Pilot-plant production of xylo-oligosaccharides from corncob by steaming, enzymatic hydrolysis and nanofiltration. *J Chem Technol Biotechnol.* (2004) 79:1073–9. doi: 10.1002/jctb.1071

132. Vegas R, Luque S, Alvarez JR, Alonso JL, Domínguez H, Parajó JC. Membrane-Assisted processing of xylooligosaccharide-containing liquors. *J Agric Food Chem.* (2006) 54:5430–6. doi: 10.1021/jf060525w

133. Slizewska K, Kapuśniak J, Barczyńska R, Jochym K. Riesistant dextrins as prebiotic. In: *Carbohydrates–Comprehensive Studies on Glycobiology and Glycotechnology*. (2012). p. 261. doi: 10.5772/51573

134. Chen MH, Swanson KS, Fahey GCJ, Dien BS, Beloshapka AN, Bauer LL, et al. *In vitro* fermentation of xylooligosaccharides produced from Miscanthus× giganteus by human fecal microbiota. *J Agric Food Chem.* (2016) 64:262–7. doi: 10.1021/acs.jafc.5b04618

135. Pan J, Yin J, Zhan K, Xie P, Ding H, Huang X, et al. Dietary xylo-oligosaccharide supplementation alters gut microbial composition and activity in pigs according to age and dose. *Amb Express.* (2019) 9:1–10. doi: 10.1186/s13568-019-0858-6

136. Maki KC, Gibson GR, Dickmann RS, Kendall CWCC, Chen YO, Costabile A, et al. Digestive and physiologic effects of a wheat bran extract, arabino-xylan-oligosaccharide in breakfast cereal. *Nutrition.* (2012) 28:1115–21. doi: 10.1016/j.nut.2012.02.010

137. Nieto-Domínguez M, Eugenio LI, York-Durán MJ, Rodríguez-Colinas B, Plou FJ, Chenoll E, et al. Prebiotic effect of xylooligosaccharides produced from birchwood xylan by a novel fungal GH11 xylanase. *Food Chem.* (2017) 232:105–13. doi: 10.1016/j.foodchem.2017.03.149

138. Hald S, Schioldan AG, Moore ME, Dige A, Lærke HN, Agnholt J, et al. Effects of arabinoxylan and resistant starch on intestinal microbiota and short-chain fatty acids in subjects with metabolic syndrome: a randomised crossover study. *PLoS ONE.* (2016) 11:e0159223. doi: 10.1371/journal.pone.0159223

139. Roberfroid M, Gibson GR, Hoyles L, Mccartney AL, Meheust A. Prebiotic effects: metabolic and health benefits. *Br J Nutr.* (2010) 104:1–63. doi: 10.1017/S0007114510003363

140. Grootaert C, Abbeele PV, Marzorati M, Broekaert WF, Courtin CM, Delcour JA, et al. Comparison of prebiotic effects of arabinoxylan oligosaccharides and inulin in a simulator of the human intestinal microbial ecosystem. *FEMS Microbiol Ecol.* (2009) 69:231–42. doi: 10.1111/j.1574-6941.2009.00712.x

141. Geraylou Z, Souffreau C, Rurangwa E, Meester LD, Courtin CM, Delcour JA, et al. Effects of dietary arabinoxylan-oligosaccharides (AXOS) and endogenous probiotics on the growth performance, non-specific immunity and gut microbiota of juvenile *Siberian sturgeon* (*Acipenserábaerii*). *Fish Shellfish Immunol.* (2013) 35:766–75. doi: 10.1016/j.fsi.2013.06.014

142. Cheng L, Zhang X, Hong Y, Li Z, Li C, Gu Z. Characterisation of physicochemical and functional properties of soluble dietary fibre from potato pulp obtained by enzyme-assisted extraction. *Int J Biol Macromol.* (2017) 101:1004–11. doi: 10.1016/j.ijbiomac.2017.03.156

143. Soleimani A, Taghizadeh M, Bahmani F, Badroj N, Asemi Z. Metabolic response to omega-3 fatty acid supplementation in patients with diabetic nephropathy: a randomized, double-blind, placebo-controlled trial. *Clin Nutr.* (2017) 36:79–84. doi: 10.1016/j.clnu.2015.11.003

144. Haenen D, Silva CS, Zhang J, Koopmans SJ, Bosch G, Vervoort J, et al. Resistant starch induces catabolic but suppresses immune and cell division pathways and changes the microbiome in the proximal colon of male pigs. *Nutrition.* (2013) 143:1889–98. doi: 10.3945/jn.113.182154

145. Gibson GR, Scott KP, Rastall RA, Tuohy KM, Hotchkiss A, Dubert-Ferrandon A, et al. Dietary prebiotics: current status and new definition. *Food Sci Technol Bull Funct Foods.* (2010) 7:1–19. doi: 10.1616/1476-2137.15880

146. Wang J, Cao Y, Wang C, Sun B. Wheat bran xylooligosaccharides improve blood lipid metabolism and antioxidant status in rats fed a high-fat diet. *Carbohydr Polym.* (2011) 86:1192–7. doi: 10.1016/j.carbpol.2011.06.014

147. Sheu WHH, Lee IT, Chen W, Chan YC. Effects of xylooligosaccharides in type 2 diabetes mellitus. *J Nutr Sci Vitaminol.* (2008) 54:396–401. doi: 10.3177/jnsv.54.396

148. Broekaert WF, Courtin CM, Verbeke K, Tom V, Verstraete W, Delcour JA. Prebiotic and other health-related effects of cereal-derived arabinoxylans, arabinoxylan-oligosaccharides, and xylooligosaccharides. *Crit Rev Food Sci Nutr.* (2011) 51:178–94. doi: 10.1080/10408390903044768

149. Strader AD, Woods SC. Gastrointestinal hormones and food intake. *Gastroenterology.* (2005) 128:175–91. doi: 10.1053/j.gastro.2004.10.043

150. Delzenne NM, Cani PD, Neyrinck AMJ. Modulation of glucagon-like peptide 1 and energy metabolism by inulin and oligofructose: experimental data. *Nutrition.* (2007) 137:2547–51. doi: 10.1093/jn/137.11.2547S

151. Frost GS, Brynes AE, Dhillo WS, Bloom SR, Mcburney MI. The effects of fiber enrichment of pasta and fat content on gastric emptying, GLP-1, glucose, and insulin responses to a meal. *Eur J Clin Nutr.* (2003) 57:293–8. doi: 10.1038/sj.ejcn.1601520

152. Ooi LG, Liong MT. Cholesterol-lowering effects of probiotics and prebiotics: a review of *in vivo* and *in vitro* findings. *Int J Mol Sci.* (2010) 11:2499–522. doi: 10.3390/ijms11062499

153. Gunness P, Williams BA, Gerrits WJJ, Bird AR, Kravchuk O, Gidley MJ. Circulating triglycerides and bile acids are reduced by a soluble wheat arabinoxylan via modulation of bile concentration and lipid digestion rates in a pig model. *Nutr Food Res.* (2016) 60:642–51. doi: 10.1002/mnfr.201500686

154. Gobinath D, Madhu AN, Prashant G, Srinivasan K, Prapulla SG. Beneficial effect of xylo-oligosaccharides and fructo-oligosaccharides in streptozotocin-induced diabetic rats. *Br J Nutr.* (2010) 104:40–7. doi: 10.1017/S0007114510000243

155. Veenashri BR, Muralikrishna G. *In vitro* antioxidant activity of xylooligosaccharides derived from cereal and millet bran-A comparative study. *Food Chem.* (2011) 126:1475–81. doi: 10.1016/j.foodchem.2010.11.163

156. Abasubong KP, Liu WB, Zhang DD, Yuan XY, Xia SL, Xu C, et al. Fishmeal replacement by rice protein concentrate with xylooligosaccharides supplement benefits the growth performance, antioxidant capability and immune responses against aeromonas hydrophila in blunt snout bream (Megalobrama amblycephala). *Fish Shellfish Immunol.* (2018) 78:177–86. doi: 10.1016/j.fsi.2018.04.044

157. Hromádková Z, Paulsen BS, Polovka M, Košťálová Z, Ebringerová A. Structural features of two heteroxylan polysaccharide fractions from wheat bran with anti-complementary and antioxidant activities. *Carbohydr Polym.* (2013) 93:22–30. doi: 10.1016/j.carbpol.2012.05.021

158. Hansen CHF, Larsen CS, Petersson HO, Zachariassen LF, Vegge A, Lauridsen C, et al. Targeting gut microbiota and barrier function with prebiotics to alleviate autoimmune manifestations in NOD mice. *Diabetologia.* (2019) 62:1689–700. doi: 10.1007/s00125-019-4910-5

159. Eaimworawuthikul S, Tunapong W, Chunchai T, Suntornsaratoon P, Charoenphandhu N, Thiennimitr P, et al. Altered gut microbiota ameliorates bone pathology in the mandible of obese–insulin-resistant rats. *Eur J Nutr.* (2020) 59:1453–62. doi: 10.1007/s00394-019-02002-8

160. Yin J, Li F, Kong XC, Wen Q, Guo L, Zhang W, et al. Dietary xylo-oligosaccharide improves intestinal functions in weaned piglets. *Food Funct.* (2019) 10:2701–9. doi: 10.1039/C8FO02485E

161. Rodríguez-Cabezas ME, Galvez J, Lorente MD, Concha A, Camuesco D, Azzouz S, et al. Dietary fiber down-regulates colonic tumor necrosis factor α and nitric oxide production in trinitrobenzenesulfonic acid-induced colitic rats. *J Nutr.* (2002) 132:3263–71. doi: 10.1093/jn/132.11.3263

162. Mendis M, Simsek S. Arabinoxylans and human health. *Food Hydrocolloids.* (2014) 42:239–43. doi: 10.1016/j.foodhyd.2013.07.022

163. López-Almela I, Romaní-Pérez M, Bullich-Vilarrubias C, Benítez-Páez A, Pulgar EMGD, Francés R, et al. Bacteroides uniformis combined with fiber amplifies metabolic and immune benefits in obese mice. *Gut Microbes.* (2021) 13:1–20. doi: 10.1080/19490976.2020.1865706

164. Palaniappan A, Antony U, Emmambux MN. Current status of xylooligosaccharides: production, characterization, health benefits and food application. *Trends Food Sci Technol.* (2021) 111:506–19. doi: 10.1016/j.tifs.2021.02.047

165. Remón J, Li T, Chuck CJ, Matharu AS, Clark JH. Toward renewable-based, food-applicable prebiotics from biomass: a one-step, additive-free, microwave-assisted hydrothermal process for the production of high purity xylo-oligosaccharides from beech wood hemicellulose. *ACS Sustainable Chem Eng.* (2019) 7:16160–72. doi: 10.1021/acssuschemeng.9b03096

166. Annison G, Topping DL. Nutritional role of resistant starch: chemical structure vs physiological function. *Ann Rev Nutr.* (1994) 14:297–320. doi: 10.1146/annurev.nu.14.070194.001501

167. Lavin JH, Read NW. The effect on hunger and satiety of slowing the absorption of glucose: relationship with gastric emptying and postprandial blood glucose and insulin responses. *Appetite.* (1995) 25:89–96. doi: 10.1006/appe.1995.0043

168. Antov MG, Dordević TR. Environmental-friendly technologies for the production of antioxidant xylooligosaccharides from wheat chaff. *Food Chem.* (2017) 235:175–80. doi: 10.1016/j.foodchem.2017.05.058

169. Kobayashi Y, Ohbuchi T, Fukuda T, Etsuko W, Risa Y, Mai H, et al. Acidic xylooligosaccharide preserves hepatic iron storage level in adult female rats fed a low-iron diet. *J Nutr Sci Vitaminol.* (2011) 57:292–7. doi: 10.3177/jnsv.57.292

170. Hesam F, Tarzi BG, Honarvar M, Jahadi M. Valorization of sugarcane bagasse to high value-added xylooligosaccharides and evaluation of their prebiotic function in a synbiotic pomegranate juice. *Biomass Convers Biorefin.* (2020) 1–13. doi: 10.1007/s13399-020-01095-0

171. Ferrão LL, Ferreira MVS, Cavalcanti RNA, Carvalho FA, Pimentel TC, Silva HLA, et al. The xylooligosaccharide addition and sodium reduction in requeijão cremoso processed cheese. *Food Res Int.* (2018) 107:137–47. doi: 10.1016/j.foodres.2018.02.018

172. Leddomado LS, Silva R, Guimarães JT, Carvalho AFA, Pimentel TC, Silva HLA, et al. Technological benefits of using inulin and xylooligosaccharide in dulce de leche. *Food Hydrocolloids.* (2021) 110:106158. doi: 10.1016/j.foodhyd.2020.106158

173. Ayyappan P, Abirami A, Anbuvahini N, Kumaran PST, Naresh M, Malathi D, et al. Physicochemical properties of cookies enriched with xylooligosaccharides. *Food Sci Technol Int.* (2016) 22:420–8. doi: 10.1177/1082013215617567

174. Juhász R, Penksza P, Sipos L. Effect of xylo-oligosaccharides (XOS) addition on technological and sensory attributes of cookies. *Food Sci Nutr.* (2020) 8:5452–60. doi: 10.1002/fsn3.1802

175. Silva EK, Arruda HS, Pastore GM, Meireles MAA, Saldana MD. Xylooligosaccharides chemical stability after high-intensity ultrasound processing of prebiotic orange juice. *Ultrason Sonochem.* (2020) 63:104942. doi: 10.1016/j.ultsonch.2019.104942

176. Souza FP, Balthazar CF, Guimarães JT, Pimentel TC, Esmerino EA, Freitas MQ, et al. The addition of xyloligoosaccharide in strawberry-flavored whey beverage. *LWT Food Sci Technol.* (2019) 109:118–22. doi: 10.1016/j.lwt.2019.03.093

177. Zhou J, Wu S, Qi G, Fu Y, Wang W, Zhang H, et al. Dietary supplemental xylooligosaccharide modulates nutrient digestibility, intestinal morphology, and gut microbiota in laying hens. *Anim Nutr.* (2021) 7:152–62. doi: 10.1016/j.aninu.2020.05.010

178. Craig AD, Khattak F, Hastie P, Bedford MR, Olukosi OA. Dietary supplemental xylooligosaccharide modulates nutrient digestibility, intestinal morphology, and gut microbiota in laying hens. *PLoS ONE.* (2021) 7:152–62.

179. Ribeiro T, Cardoso V, Ferreira LMA, Lordelo MMS, Coelho E, Moreira ASP, et al. Xylo-oligosaccharides display a prebiotic activity when used to supplement wheat or corn-based diets for broilers. *Fontes Poult Sci.* (2018) 97:4330–41. doi: 10.3382/ps/pey336

180. Su J, Zhang W, Ma C, Xie P, Blachier F, Kong X. Dietary supplementation with xylo-oligosaccharides modifies the intestinal epithelial morphology, barrier function and the fecal microbiota composition and activity in weaned piglets. *Front Vet Sci.* (2021) 8:680208. doi: 10.3389/fvets.2021.680208

181. Liu JB, Cao SC, Liu J, Xie YN, Zhang HF. Asian-Australas. Effect of probiotics and xylo-oligosaccharide supplementation on nutrient digestibility, intestinal health and noxious gas emission in weanling pigs. *J Anim Sci.* (2018) 31:1660. doi: 10.5713/ajas.17.0908

182. Wang C, Xu Z, Lu S, Jiang H, Li J, Wang L, et al. Effects of dietary xylooligosaccharide on growth, digestive enzymes activity, intestinal morphology, and the expression of inflammatory cytokines and tight junctions genes in triploid oncorhynchus mykiss fed a low fishmeal diet. *Aquacult Rep.* (2022) 22:100941. doi: 10.1016/j.aqrep.2021.100941

183. Hoseinifar SH, Sharifian M, Vesaghi MJ, Khalili M, Esteban MÁ. The effects of dietary xylooligosaccharide on mucosal parameters, intestinal microbiota and morphology and growth performance of Caspian white fish (*Rutilus frisii kutum*) fry. *Fish Shellfish Immunol.* (2014) 39:231–6. doi: 10.1016/j.fsi.2014.05.009

184. Abasubong KP, Li XF, Adjoumani JJY, Jiang GZ, Desouky HE, Liu WB. Effects of dietary xylooligosaccharide prebiotic supplementation on growth, antioxidant and intestinal immune-related genes expression in common carp cyprinus carpio fed a high-fat diet. *Anim Nutr.* (2022) 106:403–18. doi: 10.1111/jpn.13669

185. Sun C, Liu Y, Feng L, Jiang W, Wu P, Jiang J, et al. Xylooligosaccharide supplementation improved growth performance and prevented intestinal apoptosis in grass carp. *Aquaculture.* (2021) 535:736360. doi: 10.1016/j.aquaculture.2021.736360

186. Abdelmalek BE, Driss D, Kallel F, Guargouri M, Missaoui H, Chaabouni SE, et al. Effect of xylan oligosaccharides generated from corncobs on food acceptability, growth performance, haematology and immunological parameters of *Dicentrarchus labrax* fingerlings. *Fish Physiol Biochem.* (2015) 41:1587–96. doi: 10.1007/s10695-015-0110-5

187. Mhetras N, Mapre V, Gokhale D. Xylooligosaccharides (XOS) as emerging prebiotics: its production from lignocellulosic material. *Adv Microbiol.* (2019) 9:14–20. doi: 10.4236/aim.2019.91002

188. Kim MC, Lee S, Park JK, Park J, Lee D, Park J, et al. Effects of ID-HWS1000 on the perception of bowel activity and microbiome in subjects with functional constipation: a randomized, double-blind placebo-controlled study. *J Med Food.* (2021) 24:883–93. doi: 10.1089/jmf.2020.4746

189. Belorkar SA, Gupta AK. Oligosaccharides: a boon from nature's desk. *Amb Express.* (2016) 6:1–11. doi: 10.1186/s13568-016-0253-5

190. Katapodis P, Kavarnou A, Kintzios S, Pistola E, Kekos D, Macris BJ, et al. Production of acidic xylo-oligosaccharides by a family 10 endoxylanase from *Thermoascus aurantiacus* and use as plant growth regulators. *Biotechnol Lett.* (2002) 24:1413–6. doi: 10.1023/A:1019898414801

191. Fang P, Yan M, Chi C, Wang M, Zhou Y, Zhou J, et al. Brassinosteroids act as a positive regulator of photoprotection in response to chilling stress. *Plant Physiol.* (2019) 180:2061–76. doi: 10.1104/pp.19.00088

192. Ahammed GJ, Li X, Liu A, Chen S. Brassinosteroids in plant tolerance to abiotic stress. *J Plant Growth Regul.* (2020) 39:1451–4. doi: 10.1007/s00344-020-10098-0

193. Chen W, Chen G, Hussain S, Zhu B, Wu L. Role of xylo-oligosaccharides in protection against salinity-induced adversities in Chinese cabbage. *Sci Pollut Res.* (2016) 23:1254–64. doi: 10.1007/s11356-015-5361-2

194. He J, Han W, Wang J, Qian Y, Saito M, Bai W, et al. Functions of oligosaccharides in improving tomato seeding growth and chilling resistance. *J Plant Growth Regul.* (2021) 41:535–45. doi: 10.1007/s00344-021-10319-0

195. Liu H, Li Y, Tang B, Peng Y, Wu X, Che L, et al. Effects of xylooligosaccharide on angiotensin I-converting enzyme inhibitory activity of fish actomyosin and quality of snakehead balls with or without high hydrostatic pressure treatment. *LWT Food Sci Technol.* (2021) 140:110803. doi: 10.1016/j.lwt.2020.110803

196. Zhong SR, Li MF, Zhang ZH, Zong MH, Wu XL, Lou WY. Novel antioxidative wall materials for lactobacillus casei microencapsulation via the maillard reaction between the soy protein isolate and prebiotic oligosaccharides. *J Agric Food Chem.* (2021) 69:13744–53. doi: 10.1021/acs.jafc.1c02907

197. Neves MIL, Strieder MM, Prata AS, Silva EK, Meireles MAA. Xylooligosaccharides as an innovative carrier matrix of spray-dried natural blue colorant. *Food Hydrocolloids.* (2021) 121:107017. doi: 10.1016/j.foodhyd.2021.107017

198. Zhang C, Song Z, Jin P, Zhou X, Zhang H. Xylooligosaccharides induce stomatal closure via salicylic acid signaling-regulated reactive oxygen species and nitric oxide production in *Arabidopsis*. *Physiol Plant.* (2021) 172:1908–18. doi: 10.1111/ppl.13403

199. Zhang B, Hao GJ, Cao HJ, Tang H, Zhang YY, Deng SG. The cryoprotectant effect of xylooligosaccharides on denaturation of peeled shrimp (*Litopenaeus vannamei*) protein during frozen storage. *Food Hydrocolloids.* (2017) 77:228–37. doi: 10.1016/j.foodhyd.2017.09.038

frontiers | Frontiers in Nutrition

TYPE Original Research
PUBLISHED 15 September 2022
DOI 10.3389/fnut.2022.1013020

OPEN ACCESS

EDITED BY
Jianhua Xie,
Nanchang University, China

REVIEWED BY
Haixing Li,
Nanchang University, China
Jianhua Liu,
Zhejiang University of Technology, China

*CORRESPONDENCE
Dandan Gao
gaodan0322@163.com

SPECIALTY SECTION
This article was submitted to Food Chemistry, a section of the journal Frontiers in Nutrition

RECEIVED 06 August 2022
ACCEPTED 29 August 2022
PUBLISHED 15 September 2022

CITATION
Yang X, Liu H, Yang J, Ma Z, Guo P, Chen H and Gao D (2022) Purification, structural characterization and immunological activity of *Sibiraea laexigata (L.) Maxim* polysaccharide. *Front. Nutr.* 9:1013020. doi: 10.3389/fnut.2022.1013020

Purification, structural characterization and immunological activity of *Sibiraea laexigata (L.) Maxim* polysaccharide

Xuhua Yang[1], Honghai Liu[2], Jutian Yang[1,3], Zhongren Ma[1], Penghui Guo[1,3], Hong Chen[1] and Dandan Gao[1,3]*

[1]China-Malaysia National Joint Laboratory, College of Life Sciences and Engineering, Northwest Minzu University, Lanzhou, China, [2]Technology Research and Development Center, Gansu Tobacco Industry Co., Ltd., Lanzhou, China, [3]Taizishan Ecosystem Observatory of Carbon Neutralization, Northwest Minzu University, Lanzhou, China

Sibiraea laexigata (L.) Maxim (SLM) has been used as an herbal tea for treating stomach discomfort and indigestion for a long time in china. Polysaccharides have been identified as one of the major bioactive compounds in the SLM. In the present paper, ultrasonic-assisted enzymatic extraction (UAEE) method was employed in polysaccharides extraction derived from SLM using polyethylene glycol (PEG) as extraction solvent, two SLM polysaccharides (SLMPs) fractions (SLMPs-1-1 and SLMPs-2-1) were purified by DEAE Cellulose-52 and Sephadex G-100 chromatography in sequence. Then, the preliminarily structure of the two factions were characterized by chemical composition analysis, molecular weight measurement, UVS, HPLC-PMP, FT-IR, nuclear magnetic resonance (NMR) spectra analysis and SEM. The results showed that SLMPs-1-1 and SLMPs-2-1 with different molecular weights of 1.03 and 1.02 kDa, mainly composed of glucose (46.76 and 46.79%), respectively. The results of structural characterization from FT-IR, ^{1}H NMR, and SEM revealed that SLMPs-1-1 and SLMPs-2-1 contained the typical pyranoid polysaccharide with α-glycosidic bond and β-glycosidic bond. Furthermore, it was found that SLMPs-1-1 could increase the levels of tumor necrosis factor-α (TNF-α) and interleukin-2 (IL-2), and alleviated the immune organs tissue damage of cyclophosphamide (Cy)-treated mice. RT-qPCR and Western-Blot analysis showed that SLMPs-1-1 could significantly up-regulated the levels of NF-κB, TLR4, which revealed that SLMPs-1-1 could participate in immunosuppressive protection of Cy-treated mice. These findings suggested that the potential of SLMPs-1-1 as an alternative immunostimulator could be used in food and pharmaceutical industries.

KEYWORDS

***Sibiraea laexigata (L.) Maxim*, polysaccharides, purification, structural characterization, immunological activity**

Introduction

Polysaccharides, a kind of natural macromolecular polymers, have been reported to have various biological activities, including antioxidant (1), anti-tumor (2) and enhancing immune activity (3), etc. In recent years, many natural plant polysaccharides have emerged as one of the hot topics and are widely perceived as ideal candidates for immunomodulatory agents in functional food (4) and practical medical fields due to their relatively low side effects and toxicity (5). For example, a polysaccharide derived from Astragalus has been developed as an immune enhancer using for adjuvant treatment of cancer in China (6).

Sibiraea laexigata (L.) Maxim (SLM), which belongs to the *Rosaceae* family *(Genus Xianbei)*, mainly distributed in the shrub of 3,000–4,000 m in the western part of China. The aerial part of *SLM* is called "Liucha," which has been used as a herbal tea and is typically utilized for the treatment of stomach discomfort and indigestion by Tibetans in Tibetan folk medicine of China for a long time (7). It has been found that the significant effective ingredients of SLM include polysaccharides (8), triterpenoids (9), flavonoids (10), and monoterpenes (11). However, previous studies about SLM mainly focused on extensive phytochemical investigations and the extraction of crude SLMPs, lacking a detailed study of the structures characterization and their immunomodulatory effects *in vivo* (12).

In present work, SLMPs was extracted by PEG-UAEE method and purified by DEAE Cellulose-52 and Sephadex G-100 chromatography in sequence. Then, the preliminary structure characterization of SLMPs-1-1 and SLMPs-2-1 were measured by chemical composition analysis, molecular weight measurement, UVS, PMP-HPLC, FT-IR, nuclear magnetic resonance (NMR) spectra analysis, and SEM. Furthermore, the immunoregulatory of SLMPs-1-1 and underlying mechanisms were thoroughly investigated by modulating CTX-induced immunocompromised mice *via* TLR4 and NF-kB receptor signaling pathways.

Materials and methods

Materials and reagents

SLM leaves were obtained from Hezuo City (102°54′E, 34°58′N, Gansu Province, China), dried and ground in a BJ-400 high disintegrator (Yongkang Boou Instrument Co., Ltd., Shanghai, China), sieved (80 mesh), and stored at 4°C until use. 1-phenyl-3-methyl-5-pyrazolone (PMP), monosaccharide standard products and TFA were purchased from Sigma-Aldrich Chemical Co., Ltd. (Louis, United States). DEAE Cellulose-52, Sephadex G-100, Cytokine (IL-2 and TNF-α) ELISA kits and Total ribonucleic acid (RNA) Purification Kits were purchased from Solarbio Biological Reagent Co., Ltd. (Beijing, China). Injectable cyclophosphamide (Cy) and Injectable levamisole (LH) were purchased from Shanghai Sangon Biotech Co., Ltd. (Shanghai, China). All other reagents used in experiments were all analytically pure.

Extraction and purification of *Sibiraea laexigata (L.) Maxim* polysaccharides

The PEG-UAEE method was employed in crude polysaccharides extraction from SLM leaves (13). Briefly, 3.0 g pretreated SLM sample powder was immersed in a 45 mL aqueous PEG complex enzyme solution (E/S ratio of 21 U/g), the mixture was treated by a SB-500DTYultrasonic extraction equipment (Ningbo Xinzhi Biotechnology Co., Ltd., China) under an ultrasonic power of 400 W, ultrasonic times of 2.0 h, and ultrasonic temperature at 80°C. Then, the resultant extracts were centrifuged (Heraeus Multifuge X1R, Thermo Co., United States) at 5,000 r/min for 15 min, the supernatants were collected and concentrated to one-third of the initial volume using a RE52CS-1 vacuum distillation (Shanghai Yarong Biochemical Instrument Co., Ltd., China). The concentrated solution was sufficiently mixed with 3 times volumes of anhydrous ethanol and stored at 4°C for 24 h. The precipitate was dried by a LGJ-100F vacuum freezing dryer (Thermo Co., United States) at –80°C for 36 h to obtain the crude SLMPs (14). Sevage reagent was used to eliminate the proteins, and activated carbon was used to remove the pigment from the crude SLMPs (15). The yield of polysaccharides was calculated as:

$$Y(\%) = \frac{W_1}{W_0} \times 100\% \quad (1)$$

Y is the yield of SLMPs (%, w/w), W_1 is the weight of the crude SLMPs (g), and W_0 is the weight of SLM leaves (g).

The crude SLMPs was re-dissolved in distilled water (20 mg/mL), then loaded onto a column of DEAE Cellulose-52 (50 cm × 2.6 cm) and successively eluted by the deionized water and NaCl solutions of different concentrations (0, 0.3, 0.6, 0.9, and 1.0 mol/L) at a flow rate of 1.0 mL/min (16). The absorbance of each tube was measured at 490 nm to analyze polysaccharide content of SLMPs according to the phenol–sulphuric acid method, then the eluents were dialyzed overnight at 4°C to remove salt, lyophilized, yielding two polysaccharide fractions (SLMPs-1 and SLMPs-2). These two purification fractions were further loaded on a Sephadex G-100 column (50 × 2.6 cm) eluting with deionized water (3 mL/min, 10 mL/tube) to afford SLMPs-1-1 and SLMPs-2-1, respectively.

Structural characterization of *Sibiraea laexigata (L.) Maxim* polysaccharides-1-1 and *Sibiraea laexigata (L.) Maxim* polysaccharides-2-1

Chemical composition analysis

Phenol-sulfuric acid method was used to determine the total sugar content of SLMPs-1-1 and SLMPs-2-1 and glucose was used as a standard (17). The protein content of SLMPs-1-1 and SLMPs-2-1 were quantified by Bradford methods using bovine serum albumin (BSA) as a standard (18). The uronic acid content of SLMPs-1-1 and SLMPs-2-1 were estimated according to vitriol-carbazole method using D-glucuronic acid as the standard (19).

Molecular weight distribution

The molecular weights (Mw) of SLMPs-1-1 and SLMPs-2-1 were determined using a Waters 1260 Infinity HPLC system (Waters Co., United States) with 2410 differential refractive index detector and Ultrahydroge1TM-inear (300 × 7.8 mm, 8 μm, Agilent Co., United States) column. Dextrans (MWs: 1, 5, 10, 21, 40, and 84 kDa) were used as standards for calibration. The column temperature was maintained at 40°C, with 0.1 mol/L $NaNO_2$ solution as the mobile phase and a flow rate of 1.0 mL/min (20). The regression equation of the standard curve was $\log_{Mw} = -0.6493x + 6.1564$ ($R^2 = 0.9987$); where Mw is the molecular weight; x is the retention time (min).

Monosaccharide composition analysis

The monosaccharide compositions of the purified SLMPs-1-1 and SLMPs-2-1 were determined according to Chen et al. with slight modification (21). 10.00 mg of freeze-dried SLMPs-1-1 and SLMPs-2-1 were treated with TFA (2 mol/L, 5 mL) at 110°C for 5 h. After cooling, the pH of the mixture was adjusted to 7.0 with NaOH (3 mol/L) and centrifuged to obtain supernatant. Then, 0.2 mL supernatant, 0.2 mL PMP methanol solution (0.5 mol/L), and 0.2 mL NaOH solution (0.3 mol/L) and were mixed and reacted at 70°C for 1 h. Finally, the reaction solution was neutralized by adding 1 mL trichloromethane and 0.1 mL HCl solution (0.5 mol/L), extracted with chloroform, repeated 3 times, centrifuged and collected the supernatant, which was filtered through 0.22 μm membrane and used for monosaccharide composition analysis by HPLC.

The determination process of monosaccharide composition was carried out with an Agilent 1260 HPLC system (ARC, Agilent Co., United States) equipped with a C_{18} column (4.6 × 250 mm, 5 μm, Agilent Co., United States) and a DAD detector. The mobile phase was a mixture of phosphate buffer (0.02 mol/L, pH 6.8) and acetonitrile in a ratio of 81: 19 (v/v) at flow rate 1.0 mL/min with column temperature of 28°C, and monitored at 250 nm. The monosaccharide standards, including Rha, Glu, Gal, Fru, and Ara were analyzed by HPLC in the same way as above.

FT-IR spectrometric analysis

The purified SLMPs-1-1 or SLMPs-2-1 were mixed with spectroscopic-grade KBr powder (Sigma Aldrich Co., United States), ground, and then pressed into 1 mm pellets for spectral measurement in the frequency range of 4000–400 cm^{-1} using a Nicolet 6700 FT-IR spectrometer (Thermo Co., United States) (22).

Nuclear magnetic resonance analysis

The NMR sample was prepared by mixing the 20 mg freeze-dried SLMPs-1-1 or SLMPs-2-1 with 0.5 mL of deuterated water (D_2O), and NMR spectra of different fractions were obtained using a Bruker AVANCE III HD 400 spectrometer (Bruker Co., Germany) equipped with 5 mm double-tuned BBO probe and operating at 300 MHz for ^1H. Each experiment was carried out at 80°C using a single-pulse experiment, an acquisition time of 1.66 s, a recycle delay of 5 s, and a spectral width of 10 kHz. The spectra were referenced at 0.0 ppm (23).

Scanning electron micrograph analysis

The morphological features of purified SLMPs-1-1 and SLMPs-2-1 were analyzed by a Zesis EVO18 field emission scanning electron microscope under 20.00 kV (Bruker Co., Germany). To render the power conductive, SLMPs-1-1 or SLMPs-2-1 was fixed on the sample stage with conductive adhesive for gold spraying and the appearance morphology was observed under different multiples (24).

Congo red staining assay

The Congo red staining assay was carried out to analyze the triple-helix arrangements of SLMPs-1-1 and SLMPs-2-1 according to the method reported by Huang et al. (25). Briefly, 1.5 mL Congo red solution (0.2 mmol/L), 1.0 mL sample solution of polysaccharides (2 mg/mL), and 3 mL NaOH solution with different concentrations (0, 0.2, 0.4, 0.6, 0.8, and 1.0 mol/L) were mixed thoroughly and reacted at 28°C for 1 h. Furthermore, the full-wavelength scan of the reaction solution in different concentrations of NaOH solution was performed by a UV-visible spectrophotometer (UV-1800, Shimadzu, Japan) at a wavelength of 200–800 nm, respectively, and the maximum absorption wavelength of the sample reaction was recorded.

Immune activity analysis

Animals treatment and experimental design

A total of 60 Female Balb/c mice (specific-pathogen free grade,18–24 g, 5 weeks) were purchased from the Laboratory Animal Center of Lanzhou University and kept in room temperature at 24 ± 2°C and relative humidity of 60 ± 5% under an automatic 12 h light/12 h dark cycle. Six groups (10 mice in

each group) were used in experiments: group 1 (normal saline control, PS): animals were treated with saline (1–30 d); group 2 (cyclophosphamide, CTX): animals were administrated with cyclophosphamide (1–10 d) (80 mg kg^{-1}·bw) and saline (11–30 d); group 3 (levamisole hydrochloride, LH): animals were administrated with cyclophosphamide (1–10 d) and levamisole hydrochloride (11–30 d); group 4 (High-SLMPs-1-1 doses, SLMPs-H): animals were administrated with cyclophosphamide (1–10 d) and SLMPs (11–30 d, 800 mg kg^{-1}·bw); group 5 (Mid-SLMPs-1-1 doses, SLMPs-M): animals were administrated with cyclophosphamide (1–10 d) and SLMPs (11–30 d, 400 mg kg^{-1}·bw); group 6 (Low-SLMPs-1-1 doses, SLMPs-L): animals were administrated with cyclophosphamide (1–10 d) and SLMPs (11–30 d, 400 mg kg^{-1}·bw); At the end of the treatment, mice were sacrificed within 24 h, and their spleen and thymus were dissected under sterile conditions (26).

Determination the cytokine content in serum

The whole blood samples of mice in each group was obtained by taking eyeball under sterile conditions and the serum was separated by centrifugation (8,000 rpm, 5 min) at 4°C for 10 min. The levels of IgG, IFN-γ, IL-4, and TNF-α in mice serum were determined using a ELISA kits (Solarbio Biological Reagent Co., Ltd., Beijing, China) by the manufacturer's instructions. The color intensity was read using absorbance (A_{450}) by a tunable microplate reader (Fisher FC, Thermo Co., United States), and the concentration of different cytokine were calculated according to a standard curve (27).

Histological observations of spleen and thymus

The spleen and thymus tissues were fixed in 10% PFA for at 37°C for 24 h, washed by flowing water for 24 h, dehydrated in a graded series of ethanol, soaked in xylene for 5 min, embedded in paraffin, and sectioned at 5 μm using a Leica RM2255 a microtome (Leica Biosystems Inc., Germany). Then the paraffin sections were stained with hematoxylin and eosin (HE) method, and observed under an Olympus Simon-01 microscope (Olympus Optical Co., Japan) (28).

Ribonucleic acid isolation, cDNA synthesis and RT-qPCR

RT-qPCR analysis was employed in detection of the mRNA expression of TLR4 and NF-κB in mice spleens extracted from each group (29). The total RNA of mice spleens in each group was extracted using a Trizol reagent Kit (TransGen Biotech Co., China). The concentration and purity of RNA were determined by ultraviolet spectrophotometry at 260 and 280 nm, aliquoted and stored at –80°C for future use. RNA was reverse-transcribed to cDNA using a PrimeScript^{TM} RT reagent kit with cDNA Eraser (Takara Biotechnology Co., Ltd., Dalian, China) according to the manufacturer's introduction. RT-qPCR was performed to quantify mRNA expression by a CFX96 Real-time PCR System (Bio-Rad, Hercules, United States) with SYBR Green Real-time Master Mix (Toyobo, Japan). The PCR program was: 95°C, 10 min; 95°C, 15 s; 60°C, 30 s, 40 cycles; melting curve analysis 65→95°C to detect the fluorescence signal every 0.5°C –cycle, and the reaction system was 2.0 μL cDNA, 1.5 μL 2.5 μM primers, 7.5 μL 2 × RT-qPCR Mix, 4 μL ddH_2O, a total of 15 μL. The used primers are presented in **Table 1**.

Protein sample preparation and western blot

A protein extraction Kit (Solarbio, China) was used to isolated the total protein of the spleen tissue in each group mice, and a BCA protein quantitative Kit (Solarbio, China) was used to measure protein concentration. Then the protein (20 μg) was separated by 10% SDS-PAGE gel, transferred onto a 0.2 μm polyvinylidene difluoride (PVDF) membrane through a trans-blot Turbo transfer system (Bio-Rad, Hercules, United States) for 10 min at 25 V. The membrane was blocked in 0.02 mol/L PBS buffer (containing 5% skim milk powder (w/v) and 0.05% Tween-20, pH 7.5) at room temperature for 1 h, then incubated in a primary antibody solution at 4°C for 24 h. Thereafter, the membrane washed by TBST, incubated with secondary antibody at room temperature for 1 h. The protein bands were observed by using the ECL Western Blotting Analysis System (Bio-Rad, Hercules, United States) on an Image Quant LAS 4000 mini imager (GE, Life Science, United States) (30).

Statistical analysis

All the experimental data were analyzed by SPSS statistical software version 19.0 (SPSS, Chicago, United States). The significant differences of each groups were determined by using a one-way analysis of variance (ANOVA) and Duncan's test, taking $P < 0.01$ as extremely significant difference, and $P < 0.05$ as significant difference. Each experiment was performed in triplicate, and the data are demonstrated as mean ± standard deviation (SD).

Results and discussion

Extraction, isolation and purification of crude *Sibiraea laexigata (L.) Maxim* polysaccharides

The crude SLMPs were extracted by PEG-UAEE method, alcohol precipitation, deproteinization, and freeze-drying with a yield of 10.95 ± 0.13%, which was calculated using the weight of the dried SLM leaves. Since PEG can provide more -OH groups, it can enhance the solubility of polysaccharides in water and thus increase the yield of polysaccharides (1).

As shown in **Figure 1**, the crude SLMPs was firstly separated into two fractions (SLMPs-1 and SLMPs-2) purified by a DEAE

TABLE 1 The primer sequence for RT-qPCR.

Gene	Product (bp)	Primer pair	Primer sequence (5′–3′)
GAPDH	133	Forward	CCTCGTCCCGTAGACAAAATG
		Reverse	TGAGGTCAATGAAGGGGTCGT
NF-κB	212	Forward	CGAGTCTCCATGCAGCTACG
		Reverse	TTTCGGGTAGGCACAGCAATA
TLR4	151	Forward	GGAACAAACAGCCTGAGACACTT
		Reverse	CAAGGGATAAGAACGCTGAGAA

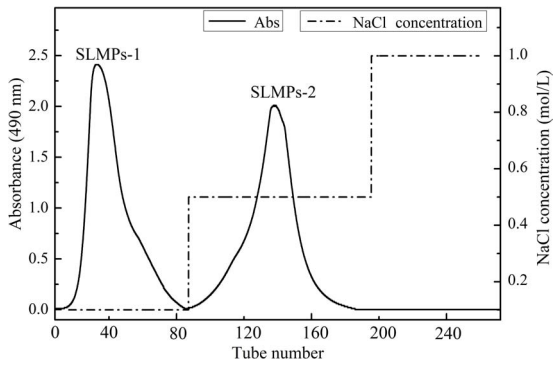

FIGURE 1
Elution profile of SLMPs by anion exchange chromatography on a DEAE-52 cellulose column.

cellulose-52 anion exchange chromatographic column on with gradient elution of 0–1.0 mol/L NaCl; These two fractions were collected, dialyzed, concentrated, freeze-dried, and loaded onto Sephadex G-100 gel filtration chromatographic column for further purification, respectively. As shown in Figure 2, each fraction generated only one single elution peak, representing SLMPs-1-1 and SLMPs-2-1, with yields of 61.4 and 54.9%, respectively. There is also a difference in the order of the collection tubes of SLMPs-1-1 and SLMPs-2-1, indicating that these two fractions are not only relatively pure single polymers, but also have different molecular weights.

Characterization of the *Sibiraea laexigata (L.) Maxim* polysaccharides

Physicochemical property

As shown in Table 2, the total sugar contents of SLMPs-1-1 and SLMPs-2-1 were 82.08 and 81.64%, respectively, the two purified components had no significant difference. Table 2 also showed that the two fractions still contain a small amount of glycosyl-bound protein (0.18–0.21%), indicating that the protein was primarily removed by the Sevage method many times. However, after being separated and purified by DEAE cellulose-52 anion exchange chromatographic column and Sephadex G-100 gel filtration chromatographic column, the protein content of SLMPs-1-1 and SLMPs-2-1 were significantly reduced by 0.30 ± 0.94% and 0.33 ± 0.93% compared with SLMPs, indicating that the purified polysaccharide was relatively pure, and the process of purification were effective in removing the protein. Besides, the sulfate content in SLMPs-1-1 was significantly higher than that in SLMPs-2-1, and the two fractions were both acidic polysaccharides because they contained higher uronic acid content (22.4 and 20.3%, respectively). Many studies have shown that the polysaccharide can show good bioactive functions when sulfate content is higher, so SLMPs-1-1 will be preferred for further animal experiments (31).

Ultraviolet spectral analysis

As shown in Figure 3, at a concentration of 1 mg/mL, SLMPs-1-1 and SLMPs-2-1 had no prominent absorption peaks appeared at the wavelengths of 260 and 280 nm in the UV spectral and negative responses to the Bradford test, which indicates absence of nucleic acid and protein in SLMPs-1-1 and SLMPs-2-1.

Molecular weight determination

HPGPC has been widely used in determination of polysaccharide molecular weight from different plants due to its advantage of rapid, great accuracy, good reproducibility, and high resolution (32). As shown in Table 2, both SLMPs-1-1 and SLMPs-2-1 are homogeneous polysaccharide, because they were gave a single symmetrical peak in Sephadex G-100 gel filtration chromatographic profile (Figure 2). The molecular weight of SLMPs-1-1 and SLMPs-2-1 were determined to be 1.29×10^3 Da and 1.27×10^3 Da on HPGPC in reference to standard glucans, respectively. Compared with the similar studies, the molecular weight of SLMPs was lower than other published polysaccharides (33). In addition, polydispersity values (Mw/Mn) could reflect the width of molecular mass distribution, thus the higher the polydispersity value represents the wider the distribution of polysaccharides. The value of Mw/Mn was close to 1, indicating that the two fractions had a relatively low polydispersity index and a homogeneity molecular weight distribution.

Monosaccharide composition analysis

The monosaccharide composition of SLMPs-1-1 and SLMPs-2-1 were determined by HPLC-PMP (Figure 4). The results suggested that SLMPs-1-1 and SLMPs-2-1 had different monosaccharide compositions and content, although they were separated from the same native fraction SLMPs. SLMPs-1-1 and SLMPs-2-1 contained the same types of monosaccharides components (Ara, Glu, Gal, and Rha) and peak times. It may be since, during purification, the higher concentration of NaCl solution preferentially acts on the hydrogen bonds on the glycosidic bonds near fructose and arabinose, which

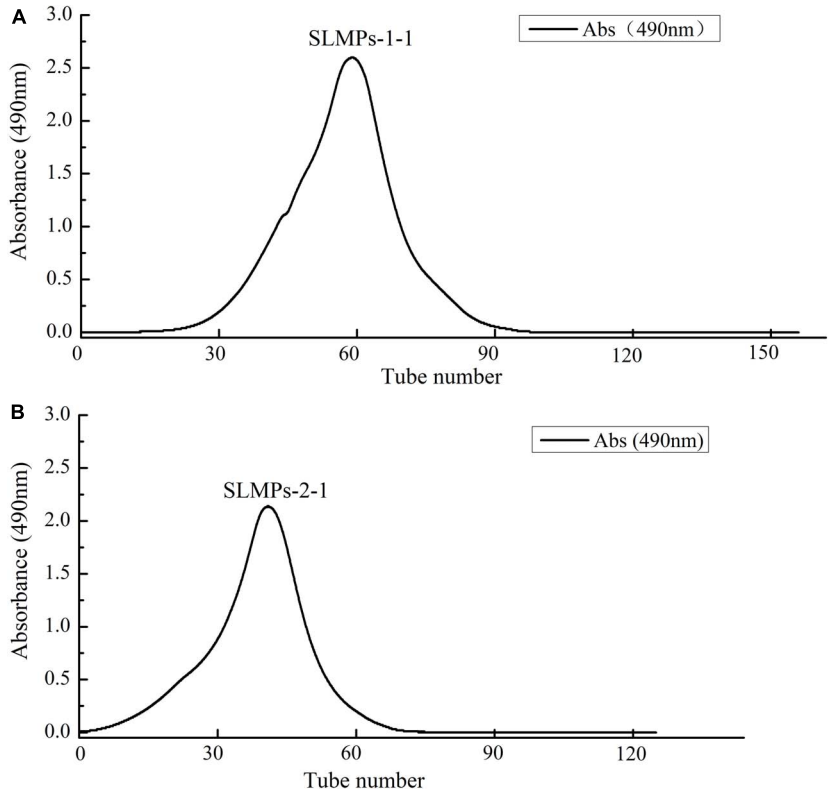

FIGURE 2
Elution curve of SLMPs-1-1 **(A)** and SLMPs-2-1 **(B)** on Sephadex G-100 column to obtain SLMPs-1 and SLMPs-2.

TABLE 2 Chemical composition and relative molecular weight analysis of SLMPs-1-1 and SLMPs-2-1 ($\bar{x} \pm s$, $n = 3$).

Sample	Yield (%)	Total sugar content (%)	Protein content (%)	Sulfate content (%)	Uronic acid content (%)	Mw/Mn
SLMPs	10.95 ± 0.13	87.82 ± 0.17	0.52 ± 0.05	8.62 ± 0.12	21.8 ± 0.24	/
SLMPs-1-1	6.37 ± 0.15	82.08 ± 0.21	0.21 ± 0.11	6.51 ± 0.08	22.4 ± 0.17	1.03
SLMPs-2-1	4.58 ± 0.21	81.64 ± 0.18	0.18 ± 0.12	5.73 ± 0.09	20.3 ± 0.14	1.02

reduces the degree of polysaccharide polymerization. SLMPs-1-1 was composed of Glu, Ara, Fru, Rha and Gal in the ratio (molar) of 46.79%: 13.96%: 13.04%: 8.69%:3.07%, and the monosaccharide composition of SLMPs-2-1 was Ara, Gal, Glu, and Rha, in molar ratio of 31.98%: 34.14%: 21.06%: 12.68%, indicating that the purification method might affect the structure and physicochemical properties of polysaccharides (34). Several studies have revealed that the biological activities of polysaccharides derived from different herbs primarily depend on these structural features, including inmonosaccharide composition and molecular weight (33).

FT-IR spectrum

FT-IR spectra of SLMPs-1-1 and SLMPs-2-1 are compared in **Figure 5**. The robust ant broad absorption band at 3366.11 cm^{-1}, which was attributed to the stretching vibration of O-H in the constituent sugar residues, and the strong absorbance band at around 2879.75 cm^{-1} was represented the stretching vibration of C-H in the sugar ring. These two absorbance peaks are characteristic of sugars, which proves that SLMPs-1-1 and SLMPs-2-1 were polysaccharide (35). The absorbance band at 1732.76 cm^{-1} was related to the bending vibration of bond water. Moreover, the absorption peak at 1436.25 and 1611.16 cm^{-1} were attributed to the carboxylic groups (COO-) and stretching vibrations of ester carbonyl groups (C = O), respectively, which indicated that purified SLMPs-1-1 and SLMPs-2-1 were acidic polysaccharides with uronic acid units, the locations of these peaks were similar to the investigations of *Atratylodes macrocephala* polysaccharides by FT-IR (36). This is consistent with the analytical results of monosaccharide compositions of SLMPs-1-1 and SLMPs-2-1. In addition, the absorbance band at 1,060 cm^{-1} was caused by C-O-C stretching and angular vibration in the sugar ring, the results suggested that the monosaccharide of purified

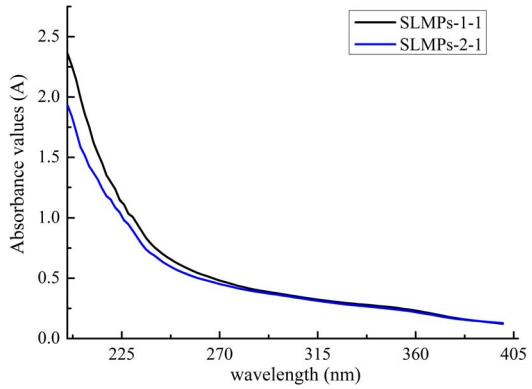

FIGURE 3
UV spectra of SLMPs-1-1 and SLMPs-2-1.

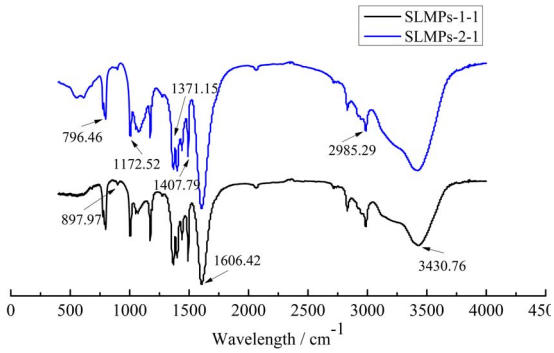

FIGURE 5
Infrared spectra of SLMPs-1-1 and SLMPs-2-1.

SLMPs-1-1 and SLMPs-2-1 had pyranose rings. Moreover, the characteristic absorbance at 840.82 cm^{-1} suggested the presence of α-pyranose in SLMPs-1-1 and SLMPs-2-1, while the characteristic absorbance at 947.92 cm^{-1} related to the presence of a β-anomeric configuration in SLMPs-1-1 and SLMPs-2-1. It can be inferred that SLMPs-1-1 and SLMPs-2-1 were α- and β-type polysaccharides according to the more critical peak value of FT-IR spectra (37).

Nuclear magnetic resonance spectroscopic analysis

The structure identification and analysis of polysaccharides mostly use ^{1}H NMR as the primary method to study the types of glycosidic bonds. The range of δ4.5–5.5 in the ^{1}H NMR spectrum is the region where the proton signal mainly exists in the glycosidic bond of the polysaccharide, so there are several proton signals in this region in the ^{1}H NMR spectrum, indicating that the sugar has several

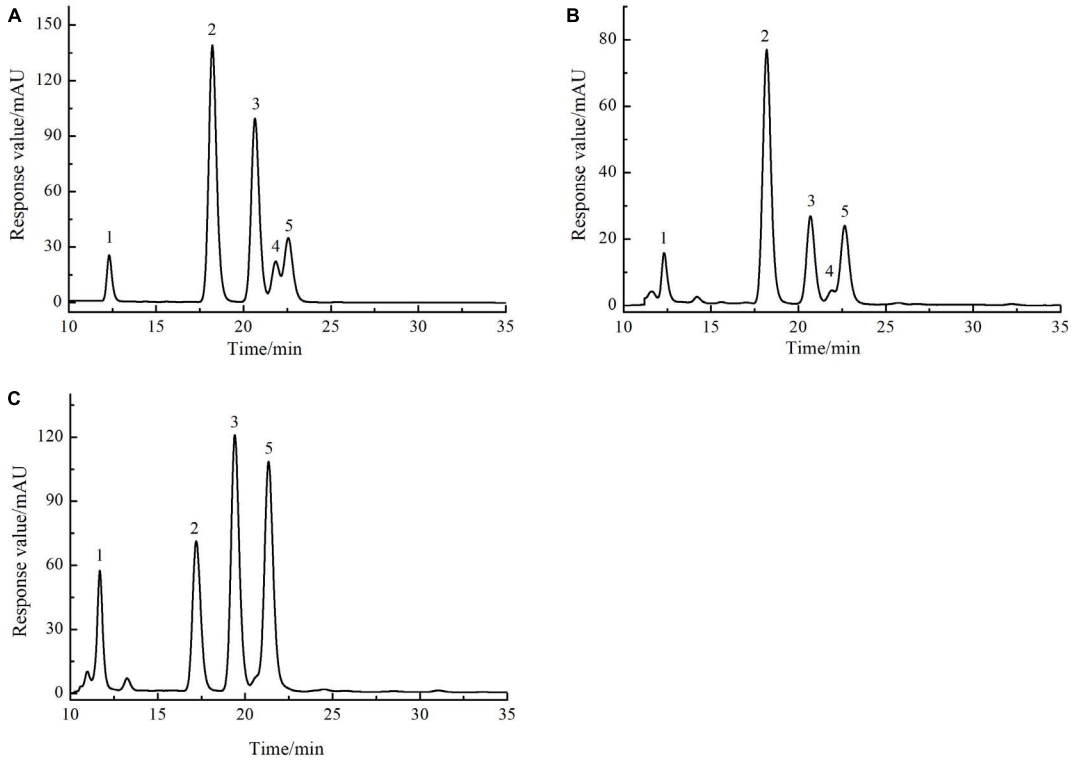

FIGURE 4
The HPLC chromatogram of monosaccharides of reference substances solution **(A)**, SLMPs-1-1 **(B)**, and SLMPs-2-1 **(C)**.

monosaccharide species. While other hydrogen signals are mainly concentrated in the narrow region of δ3.3–4.3, and the signal peaks overlap seriously. Among them, δ5.0 is the critical value of the proton signal to distinguish the configuration of pyranose. When the proton shift of the first carbon is more significant than 5.0, it is an α-glycoside, and when it is less than 5.0, it is a β-glycoside. The one-dimensional ^{1}H NMR spectra of SLMPs-1-1 and SLMPs-2-1 can be seen in **Figure 6**. It can be seen from the figure that SLMPs-1-1 have 4 proton signal peaks, and in SLMPs-2-1, only two signal peaks were detected in the range of δ4.5∼5.5, this may be due to the overlap and interference between proton signals, leading to the lack of monosaccharide composition analysis (38), Furthermore, anomeric hydrogen appears in the range of δ4.2–4.4 and δ5.0–5.8 signal, indicating that there are both α-glycosidic bonds and β-glycosidic bonds in SLMPs-1-1 and SLMPs-2-1, which was consistent with the result from FT-IR analysis.

Microstructure analysis

The microscopic scanning electron micrographs (SEM) structure of purified SLMPs-1-1 and SLMPs-2-1 (**Figure 7**) revealed that the single particle had irregular shapes, rough surface with different dimensions, which are typical characteristics of amorphous powders. The irregular-shaped particle also accompanied by fold structure with holes which is similar to the *Macroalgae* polysaccharides prepared by hot water extraction (39). It can be proved that SLMPs-1-1 and SLMPs-2-1 have a prominent amorphous structure and relatively complete structural morphology.

Conformational analysis

The triple-helix arrangements of SLMPs-1-1 and SLMPs-2-1 were measured by Congo red test, and the results were displayed in **Figure 8**. It was apparently observed that the maximum absorbance wavelength of each sample in different concentration of NaOH (0.1–0.8 mol/L) had a certain degree of redshift compared with Congo red solution. The degree of

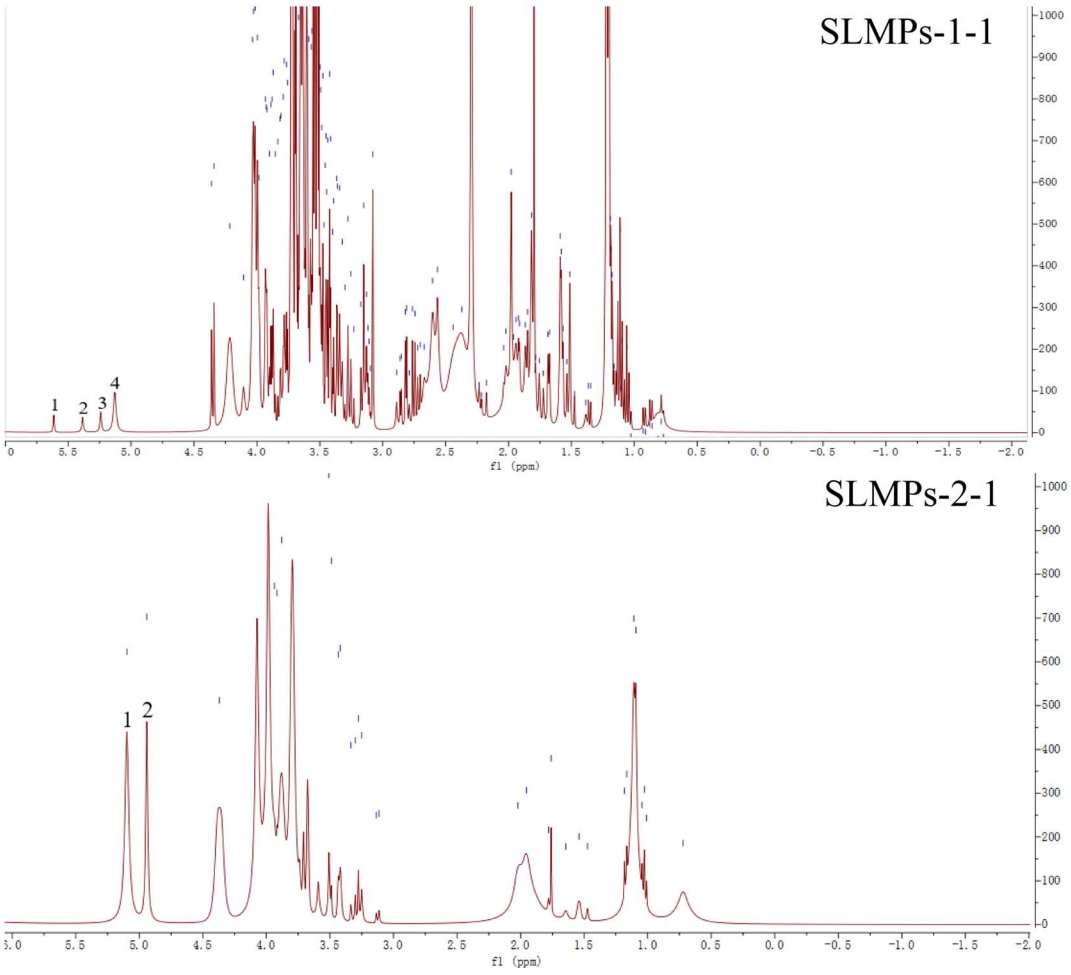

FIGURE 6
^{1}H nuclear magnetic resonance (NMR) spectra of SLMPs-1-1 and SLMPs-2-1.

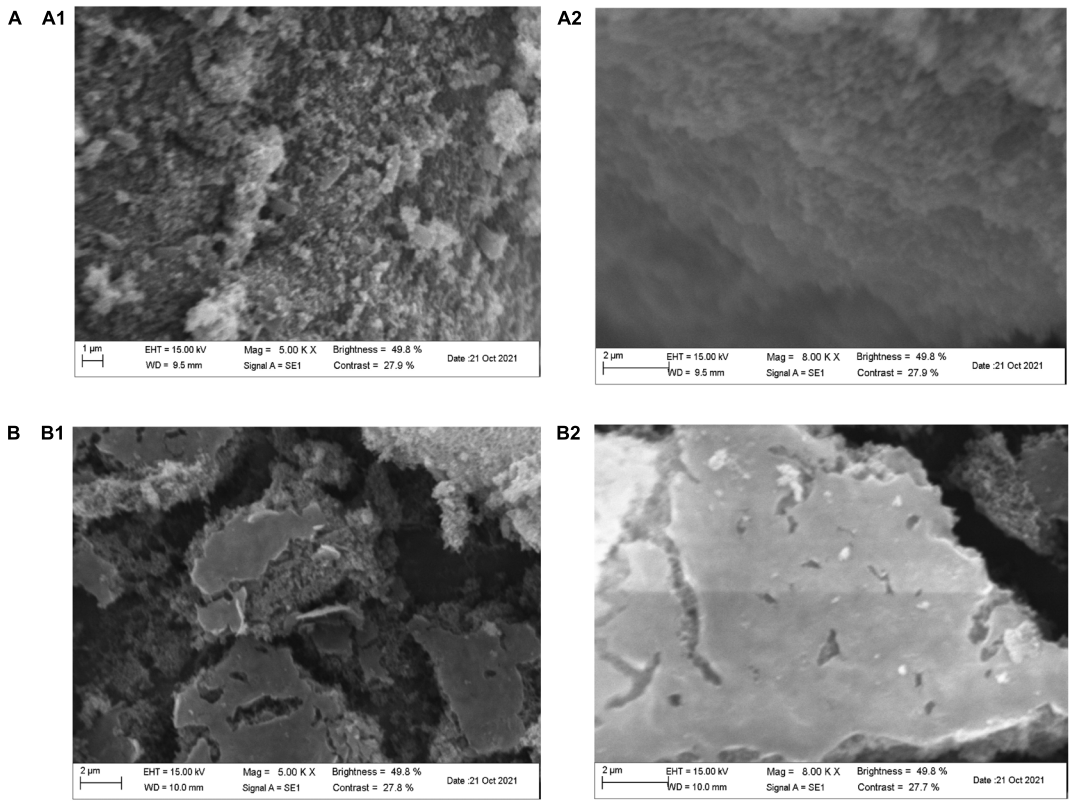

FIGURE 7
Scanning electron microscopy of SLMPs-1-1 and SLMPs-2-1. [**(A)** 5.00 KX; **(B)** 8.00 KX].

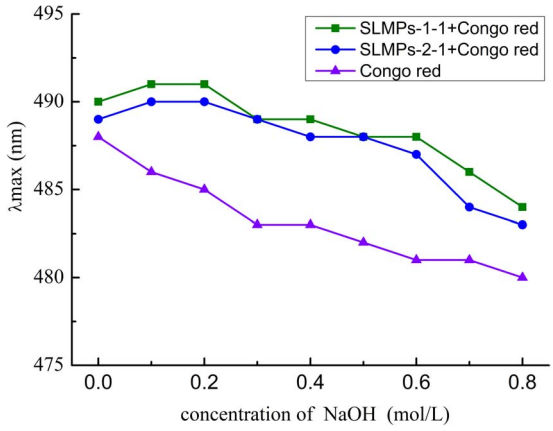

FIGURE 8
Conformation transition analysis of SLMPs-1-1 and SLMPs-2-1 at different concentration of NaOH.

redshift of SLMPs-1-1 was more dramatic than SLMPs-2-1, indicating that SLMPs-1-1 has a tighter triple-helical structure (40). With an increase in the concentration of NaOH, the degree of redshift of SLMPs-1-1, SLMPs-2-1 become smaller. This was because a high concentration of NaOH could destroy the hydrogen bond of the polysaccharide and induce the degradation of polysaccharides This indicated that SLMPs-1-1 and SLMPs-2-1 could form a regular ordered triple-helix structure in the neutral or weakly alkaline range (41).

Effect of SLMPs-1-1 on serum IgG, IL-4, TNF-α, and IFN-γ levels

Immune globulin (Ig) and cytokines are mainly present in plasma, tissues and body fluids, playing an essential roles in immune response and regulation (42). As shown in **Table 3**, the serum levels of IgG, IL-4, TNF-α and IFN-γ in the mice treated with different SLMPs-1-1 concentrations were evaluated relative to CTX mice and PS group, respectively. It was found that IgG, IL-4, TNF-α and IFN-γ level in the CTX group was significantly lower than these in the PS group ($P < 0.01$), indicating that the CTX-treated mouse immunocompromised model was successfully established. IgG, IL-4, TNF-α, and IFN-γ level of each SLMPs-1-1 dose groups were significantly increased compared with the CTX group ($P < 0.01$), and the levels of IgG, IL-4, TNF-α, and IFN-γ in the mid-doses of SLMPs-1-1 was the highest in three different dose of SLMPs-1-1 groups ($P < 0.05$). Moreover, after 20 days of SLMPs-1-1 feeding,

compared with the CTX group, the level of IgG, IL-4, TNF-α, and IFN-γ in the mid-dose of SLMPs-1-1 group was increased by 4.4, 8.13, 11.2, and 10.95%, respectively. This phenomenon indicated that SLMPs-1-1 could enhance immune regulatory through upregulating regulatory cytokines secretions (43).

Histological observations of spleen and thymus

As shown in Figure 9, the histopathology of the thymus and spleen were observed with an optical microscope. The histopathology of the spleen and thymus from PS group mice had clear medullar structure, visible the medulla inside and regular shape of the thymus cortex. Compared with that in the PS group, the boundary between the medulla and cortex was not clear, and the lymphatic sheath around the arteries was severely damaged in the CTX group, indicating that the model in this experiment was successful (44). Compared with the CTX group, the border between the red pulp and the white pulp were evident in the mid-dose group of SLMPs-1-1, and the boundary between the cortex and medulla was not evident in the high- and low-dose of SLMPs-1-1 groups, but slightly better than that in the CTX group. Similarly, in the LH group and mid-dose group

TABLE 3 Comparison of plasma levels of IL-4, TNF-α, IFN-γ, and IgG in each group of mice.

Group	IL-4 (ng/mL)	TNF-α (ng/mL)	IFN-γ (pg/mL)	IgG (ng/mL)	*P*			
					IL-4	TNF-α	IFN-γ	IgG
PS	3.070 ± 0.09	2.722 ± 0.04	243.485 ± 2.22	3.812 ± 0.04				
CTX	2.831 ± 0.03	1.213 ± 0.05	165.983 ± 1.24	2.827 ± 0.05	0.000①	0.000①	0.000①	0.000①
LH	2.865 ± 0.03	2.570 ± 0.04	251.416 ± 0.84	3.576 ± 0.02	0.000②	0.000②	0.000②	0.000②
SLMPs-L	2.487 ± 0.04	2.115 ± 0.03	215.640 ± 0.69	3.267 ± 0.03	0.000③	0.000③	0.000③	0.000③
SLMPs-M	2.648 ± 0.02	2.307 ± 0.04	237.624 ± 1.31	3.412 ± 0.04	0.000④ 0.004⑥	0.000④ 0.002⑥	0.000④ 0.000⑥	0.000④ 0.024⑥
SLMPs-H	2.393 ± 0.03	1.704 ± 0.13	214.753 ± 1.27	3.174 ± 0.10	0.000⑤ 0.007⑦ 0.018⑧	0.000⑤ 0.003⑦ 0.000⑧	0.000⑤ 0.008⑦ 0.000⑧	0.000⑤ 0.004⑦ 0.000⑧

① Compare CTX group with PS group; ② Compare LH group with CTX group; ③ Compare SLMPs-L group with CTX group; ④ Compare SLMPs-M group with CTX group; SLMPs-L group comparison; ⑦ SLMPs-H group compared with SLMPs-L group; ⑧ SLMPs-H group compared with SLMPs-M group.

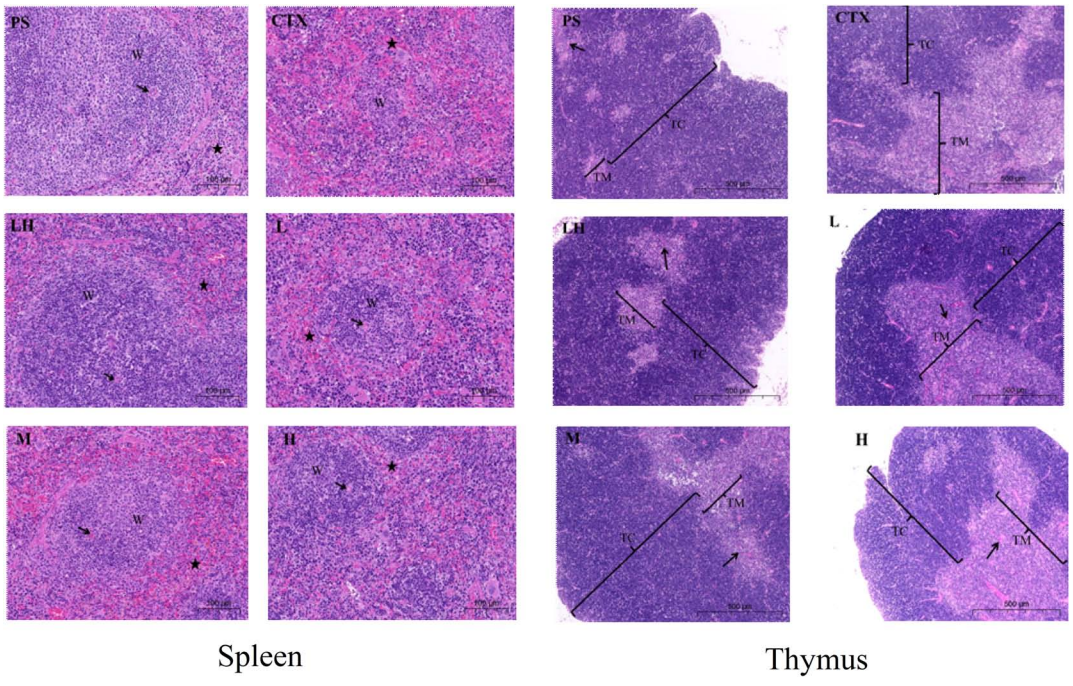

FIGURE 9
Effect of SLMPs-1-1 on spleen and thymus histomorphology in mice. → Represents periarterial lymphatic sheath, W represents white pulp, ⋆ represents red pulp.

of SLMPs-1-1, the increase in the area of white pulp was more prominent, and the white pulp and red pulp were close to the PS group. The results indicated that SLMPs-1-1 could prevent damage to the spleen and thymus cells in CTX-induced mice (45).

Effects of SLMPs-1-1 on TLR4 and NF-κB mRNA expression in spleen

The relative gene expression levels of TLR4 and NF-κB in the spleen of CTX-induced immune deficiency model mice were detected by the RT-qPCR, aiming to demonstrate that SLMPs-1-1 can improve the immune suppression effect of mice by regulating the expression level of immune regulatory factors in the spleen.

TLR4 is a membrane protein expressed on immune cells and epithelial cells (46), and its mainly distributed in macrophages, renal tubular epithelial cells, and other parts, which can be activated without the need for foreign pathogens to invade Innate immune inflammatory response (47). It mainly uses the MyD88-dependent pathway as a classic signal transduction pathway, and mediates the production of NF-κB to stimulate downstream inflammatory effects (48). Changes in the expression level of TLR4 mRNA detected by RT-qPCR in the spleen of different groups mice are shown in **Figure 10A**, a melting curve analysis has been used to verify the presence of a single gene-specific peak and the absence of primer dimer (49). The results showed the ratio of TLR4 mRNA in the CTX group and LH group was 0.44 and 0.96, and the mRNA expression level of TLR4 in SLMPs-1-1 first increased and then decreased with the increase of dose. The LH group and SLMPs-1-1 dose groups were significantly up-regulated ($P < 0.01$) compared with the CTX group, and there were significant differences between SLMPs-1-1 dose groups ($P < 0.05$), but the mid-dose group of SLMPs-1-1 had no significant up-regulation effect ($P > 0.05$). In conclusion, the effect of SLMPs-1-1 on the expression level of TLR4 mRNA in the spleen tissue of CTX-induced immunocompromised model mice was obvious, and the dose-response relationship was in the range of 200–400 mg/kg.

NF-κB is an essential to signal transduction, cell activation, and transcriptional activator in the TLR4 immune regulatory network's downstream signaling pathway, which regulates cytokines levels, immune receptors, and anti-apoptotic proteins; therefore, NF-κB induces inflammatory immune responses (50). In addition, the dissolution curves of each hand have no signs of non-specific dissolution peaks or miscellaneous peaks, which confirmed the high specificity of the primers and indicated the amplified products have sure accuracy and can be used for experiments analyze (51). The mRNA expression levels of NF-κB in different dose groups were significantly decreased ($P < 0.05$, $P < 0.01$) compared to the PS group (**Figure 10B**). It was

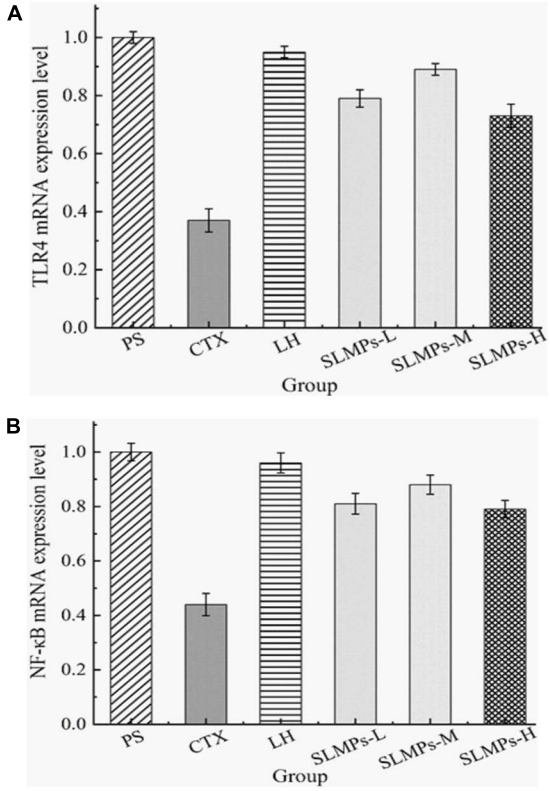

FIGURE 10
Effect of SLMPs-1-1 on the regulation of TLR4 and NF-κB gene expression in mouse tissues. **(A)** TLR4 gene expression in mouse tissues, **(B)** NF-κB gene expression in mouse tissues.

apparently observed that the mRNA expression levels of NF-κB in the LH group and each dose group were significantly increased ($P < 0.01$) compared with the CTX group. Among them, the mRNA expression level of NF-κB in the mid-dose group of SLMPs-1-1 was the highest ($P < 0.01$). This indicated that the dose of SLMPs-1-1 should be fully considered if the SLMPs-1-1 was used as an alternative immunostimulator in food and pharmaceutical industries.

Effects of SLMPs-1-1 on related proteins expression in spleen

The protein expression levels of TLR4, and NF-κB in mice spleen were determined by western blotting (**Figure 11**). It was found that the proteins expression levels of NF-κB and TLR4 in the CTX group were significantly lower than those in the other groups ($P < 0.05$), and the proteins expression levels in the LH group and the mid-dose group of SLMPs-1-1 were higher than those in the CTX group ($P < 0.05$). The proteins expression levels of TLR4 and NF-κB were higher in the low- and high-dose group of SLMPs-1-1 group compared

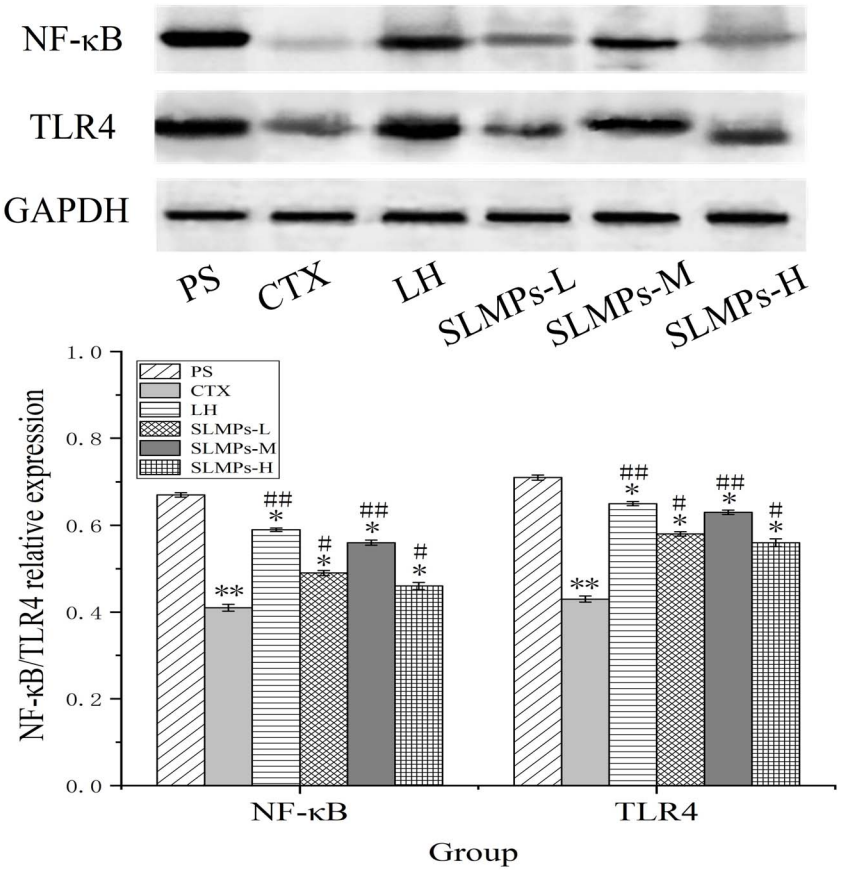

FIGURE 11
Effects of SLMPs-1-1 on the proteins expression of NF-κB and TLR4 in spleen [compared with PS group (*$P < 0.05$; **$P < 0.01$); compared with CTX group ($^{\#}P < 0.05$; $^{\#\#}P < 0.01$)].

with the CTX group but were still significantly lower than those in the mid-dose group of SLMPs-1-1 ($P < 0.05$), and the dose of SLMPs-1-1 showed a dose-response relationship in the range of 200–400 mg/kg. This indicated that SLMPs-1-1 effectively improved the expression of NF-κB and TLR4 in the spleen tissue of CTX-induced immunocompromised mice, consequently playing a protective role during immune regulation.

Conclusion

In this study, two SLMPs fractions (SLMPs-1-1 and SLMPs-2-1), with average molecular weight of 1.29×10^3 and 1.27×10^3 Da, respectively, were isolated and purified. The main components of the two polysaccharides were Glu and Gal (46.79 and 34.14%). The two polysaccharides fractions exhibited absorption peaks of characteristic α-glycosidic and β-glycosidic bonds pyranoid polysaccharides. The results showed that SLMPs-1-1 could accelerated recovery of spleen and thymus indexes, and up-regulate the levels of IgG, IL-4, TNF-α, and IFN-γ in the serum of the Cy-treated mice. SLMPs-1-1 also could improve the adaptive immune function by increasing the mRNA and protein expression of TLR4 and NF-κB. These results suggest that SLMPs-1-1 can be used as an immunostimulator to stimulate both the innate and adaptive immune responses for application in immunological diseases and functional foods.

Data availability statement

The raw data supporting the conclusions of this article will be made available by the authors, without undue reservation.

Ethics statement

The animal study was reviewed and approved by the Laboratory Animal Ethics of Northwest Minzu University.

Author contributions

DG and ZM designed the whole experiment. XY and HC prepared SLMPs. JY, HL, and PG determined the structure of SLMPs. XY and DG wrote the manuscript. All authors discussed the results and contributed to the article.

Funding

This work was supported by the National Natural Science Foundation of China (31960461), the Fundamental Research Funds for the Central Universities of Northwest Minzu University (31920220024, 31920210001, and BELTY201901), the Young Doctor Fund of Gansu Province (2021QB-147), the Education and Teaching Reform Project of the Northwest Minzu University (2021XJYBJG-55), and the Science and Technology Project of Gansu Province (21JR1RA218).

Conflict of interest

Author HL was employed by the Gansu Tobacco Industry Co., Ltd.

The remaining authors declare that the research was conducted in the absence of any commercial or financial relationships that could be construed as a potential conflict of interest.

Publisher's note

References

1. Gao DD, Chen H, Liu HH, Yang XH, Guo PH, Cao X, et al. Structure characterization and antioxidant activity analysis of polysaccharides from *Lanzhou Lily*. *Front. Nutr.* (2022) 9:976607. doi: 10.3389/fnut.2022.976607

2. Guo L, Tan DC, Hui FY, Gu F, Xiao KM, Hua Y. Optimization of the cellulase-ultrasonic synergistic extraction conditions of polysaccharides from *Lenzites betulina*. *Chem Biodivers.* (2019) 16:e1900369. doi: 10.1002/cbdv.201900369

3. Zhu H, Liu C, Hou J, Long H, Wang B, Guo D, et al. *Gastrodia elata Blume* polysaccharides: a review of their acquisition, analysis, modification, and pharmacological activities. *Molecules.* (2019) 24:2436. doi: 10.3390/molecules24132436

4. Yu Y, Zhu H, Shen M, Yu Q, Chen Y, Xie J. Sulfation modification enhances the intestinal regulation of *Cyclocarya paliurus* polysaccharides in cyclophosphamide-treated mice *via* restoring intestinal mucosal barrier function and modulating gut microbiota. *Food Funct.* (2021) 12:12278–90. doi: 10.1039/D1FO03042F

5. Xie JH, Wang ZJ, Shen MY, Nie SP, Gong B, Li HS, et al. Sulfated modification, characterization and antioxidant activities of polysaccharide from *Cyclocarya paliurus*. *Food Hydrocolloid.* (2016) 53:7–15. doi: 10.1016/j.foodhyd.2015.02.018

6. Zhu M, Huang R, Wen P, Song Y, He B, Tan J, et al. Structural characterization and immunological activity of pectin polysaccharide from *kiwano (Cucumis metuliferus)* peels. *Carbohydr Polym.* (2021) 254:117371. doi: 10.1016/j.carbpol.2020.117371

7. Liu H, Zhang T, Jiang P, Zhu W, Yu S, Liu Y, et al. Hypolipidemic constituents from the aerial portion of *Sibiraea angustata*. *Bioorg Med Chem Lett.* (2020) 30:127161. doi: 10.1016/j.bmcl.2020.127161

8. Chen R, Li H, Li S, Jin C, Lu J. Extraction optimization, preliminary characterization and immunological activity of polysaccharides from figs. *Int J Biol Macromol.* (2015) 72:185–94. doi: 10.1016/j.ijbiomac.2014.08.021

9. Wang Y, Han S, Li R, Cui B, Ma X, Qi X, et al. Structural characterization and immunological activity of polysaccharides from the tuber of *Bletilla striata*. *Int J Biol Macromol.* (2019) 122:628–35. doi: 10.1016/j.ijbiomac.2018.10.201

10. Chen J, Tian S, Shu X, Du H, Li N, Wang J. Extraction, characterization and immunological activity of polysaccharides from *Rhizoma gastrodiae*. *Int J Mol Sci.* (2016) 17:1011. doi: 10.3390/ijms17071011

11. Li B, Chen X, Wang Z, Liu H, Liu B, Yu S, et al. Two new monoterpenes and one dicaffeic acid ester from *Sibiraea angustata* with hypolipidemic activities in HepG2 cells in Vitro. *Phytochem Lett.* (2015) 13:319–23. doi: 10.1016/j.phytol.2015.07.009

12. Luo B, Dong LM, Xu QL, Zhang Q, Liu WB, Wei XY, et al. Characterization and immunological activity of polysaccharides from *Ixeris polycephala*. *Int J Biol Macromol.* (2018) 113:804–12. doi: 10.1016/j.ijbiomac.2018.02.165

13. Zhang L, Wang M. PEG-based ultrasound-assisted extraction of polysaccharides from superfine ground *Auricularia auricular*. *J Food Process Preserv.* (2017) 42:e13445. doi: 10.1111/jfpp.13445

14. Deng W, Wu J, Da Y, Ma Z. Effect of temperature treatment on fruit quality and immunoregulation of *Satsuma (Citrus unshiu Marc.)* during storage. *Food Sci Nutr.* (2020) 8:5443–51. doi: 10.1002/fsn3.1771

15. Liu N, Dong Z, Zhu X, Xu H, Zhao Z. Characterization and protective effect of *Polygonatum sibiricum* polysaccharide against cyclophosphamide-induced immunosuppression in Balb/c mice. *Int J Biol Macromol.* (2018) 107(Pt. A):796–802. doi: 10.1016/j.ijbiomac.2017.09.051

16. Wu YT, Huo YF, Xu L, Xu YY, Wang XL, Zhou T. Purification, characterization and antioxidant activity of polysaccharides from *Porphyra haitanensis*. *Int J Biol Macromol.* (2020) 165(Pt. B):2116–25. doi: 10.1016/j.ijbiomac.2020.10.053

17. Duan S, Huang Q, Shen X, Hu J, Yi X, Li Z, et al. Deproteinization of four macroporous resins for rapeseed meal polysaccharides. *Food Sci Nutr.* (2020) 8:322–31. doi: 10.1002/fsn3.1309

18. Shi H, Wang Y, Cheng Z, Ye T, Chan Z. Analysis of natural variation in bermudagrass *(Cynodon dactylon)* reveals physiological responses underlying drought tolerance. *PLoS One.* (2012) 7:e53422. doi: 10.1371/journal.pone.0053422

19. Gao H, Zhang W, Wang B, Hui A, Du B, Wang T, et al. Purification, characterization and anti-fatigue activity of polysaccharide fractions from okra (*Abelmoschus esculentus (L.) Moench*). *Food Funct.* (2018) 9:1088–101. doi: 10.1039/c7fo01821e

20. Yuan Q, Xie Y, Wang W, Yan Y, Ye H, Jabbar S, et al. Extraction optimization, characterization and antioxidant activity *in vitro* of polysaccharides from mulberry (*Morus alba L.*) leaves. *Carbohydr Polym.* (2015) 128:52–62. doi: 10.1016/j.carbpol.2015.04.028

21. Chen G, Kan J. Ultrasound-assisted extraction, characterization, and antioxidant activity *in vitro* and *in vivo* of polysaccharides from Chestnut rose *(Rosa roxburghii tratt)* fruit. *J Food Sci Technol.* (2018) 55:1083–92. doi: 10.1007/s13197-017-3023-8

22. Hammami N, Gara AB, Bargougui K, Ayedi H, Abdalleh FB, Belghith K. Improved *in vitro* antioxidant and antimicrobial capacities of polysaccharides isolated from *Salicornia arabica*. *Int J Biol Macromol.* (2018) 120(Pt. B):2123–30. doi: 10.1016/j.ijbiomac.2018.09.052

23. Wang YF, Hou GH, Li JL, Surhio MM, Ye M. Structure characterization, modification through carboxymethylation and sulfation, and *in vitro* antioxidant and hypoglycemic activities of a polysaccharide from *Lachnum sp*. *Process Biochem.* (2018) 72:177–87. doi: 10.1016/j.procbio.2018.06.002

24. Chen X, Ji H, Zhang C, Liu A. Optimization of extraction process from *Taraxacum officinale* polysaccharide and its purification, structural characterization, antioxidant and anti-tumor activity. *J Food Meas Charact.* (2019) 14:194–206. doi: 10.1007/s11694-019-00281-7

25. Huang Q, He W, Khudoyberdiev I, Ye CL. Characterization of polysaccharides from *Tetrastigma hemsleyanum* Diels et Gilg Roots and their effects on antioxidant activity and H_2O_2-induced oxidative damage in RAW 264.7 cells. *BMC Chem.* (2021) 15:9. doi: 10.1186/s13065-021-00738-1

26. Jena GB, Nemmani KV, Kaul CL, Ramarao P. Protective effect of a polyherbal formulation (Immu-21) against cyclophosphamide-induced mutagenicity in mice. *Phytother Res.* (2003) 17:306–10. doi: 10.1002/ptr.1125

27. Xu C, Wang Y, Sun R, Qiao X, Shang X, Niu W. Modulatory effects of vasoactive intestinal peptide on intestinal mucosal immunity and microbial community of weaned piglets challenged by an enterotoxigenic *Escherichia coli* (K88). *PLoS One.* (2014) 9:e104183. doi: 10.1371/journal.pone.0104183

28. Huang Z, Jin S, Lv Z. Dietary genistein supplementation alters mRNA expression profile and alternative splicing signature in the thymus of chicks with lipopolysaccharide challenge. *Poult Sci.* (2022) 101:101561. doi: 10.1016/j.psj.2021.101561

29. Zhong D, Zhang M, Yu J, Luo ZP. Local tensile stress in the development of posttraumatic osteoarthritis. *Biomed Res Int.* (2018) 2018:4210353. doi: 10.1155/2018/4210353

30. Liao X, Xie H, Li S, Ye H, Li S, Ren K, et al. 2′, 5′-oligoadenylate synthetase 2 (OAS2) inhibits zika virus replication through activation of type iota IFN signaling pathway. *Viruses.* (2020) 12:418. doi: 10.3390/v12040418

31. Drira M, Elleuch J, Ben Hlima H, Hentati F, Gardarin C, Rihouey C, et al. Optimization of exopolysaccharides production by porphyridium sordidum and their potential to induce defense responses in arabidopsis thaliana against *Fusarium Oxysporum*. *Biomolecules.* (2021) 11:282. doi: 10.3390/biom11020282

32. Zhang L, Zhang W, Wang Q, Wang D, Dong D, Mu H, et al. Purification, antioxidant and immunological activities of polysaccharides from *Actinidia Chinensis* roots. *Int J Biol Macromol.* (2015) 72:975–83. doi: 10.1016/j.ijbiomac.2014.09.056

33. Ji Y, Wang R, Peng Y, Peng C, Li X. Purification, preliminary characterization, and immunological activity of polysaccharides from Crude Drugs of sijunzi formula. *Evid Based Complement Alternat Med.* (2017) 2017:2170258. doi: 10.1155/2017/2170258

34. Li B, Zhang N, Wang DX, Jiao L, Tan Y, Wang J, et al. Structural analysis and antioxidant activities of neutral polysaccharide isolated from Epimedium koreanum Nakai. *Carbohydr Polym.* (2018) 196:246–53. doi: 10.1016/j.carbpol.2018.05.037

35. Tian Y, Zeng H, Xu Z, Zheng B, Lin Y, Gan C, et al. Ultrasonic-assisted extraction and antioxidant activity of polysaccharides recovered from white button mushroom (*Agaricus bisporus*). *Carbohyd Polym.* (2012) 88:522–9. doi: 10.1016/j.carbpol.2011.12.042

36. Pu JB, Xia BH, Hu YJ, Zhang HJ, Chen J, Zhou J, et al. Multi-optimization of ultrasonic-assisted enzymatic extraction of *Atratylodes macrocephala* polysaccharides and antioxidants using response surface methodology and desirability function approach. *Molecules.* (2015) 20:22220–35. doi: 10.3390/molecules201219837

37. Ma DL, Du HR, Wen ZS, Wang L, Li J, Zheng YG. "Optimization of ultrasonic-assisted extraction of polysaccharides from trichosanthin and antioxidant activities *in vitro*," in *Proceedings of the 2018 9th International Conference on Information Technology in Medicine and Education (ITME)*. (Piscataway, NJ: IEEE) (2018). p. 894–9.

38. Zhang W, Hu Y, Zhao J, Zhang Y, Guo D, Gao C, et al. Immunoregulation and antioxidant activities of a novel acidic polysaccharide from Radix Paeoniae Alba. *Glycoconj J.* (2020) 37:361–71. doi: 10.1007/s10719-020-09916-0

39. Malafronte L, Yilmaz-Turan S, Krona A, Martinez-Sanz M, Vilaplana F, Lopez-Sanchez P. Macroalgae suspensions prepared by physical treatments: effect of polysaccharide composition and microstructure on the rheological properties. *Food Hydrocolloid.* (2021) 120:106989. 106989.10.1016/j.foodhyd.2021.106989 doi: ARTN

40. Yuan E, Nie S, Liu L, Ren J. Study on the interaction of *Hericium erinaceus* mycelium polysaccharides and its degradation products with food additive silica nanoparticles. *Food Chem X.* (2021) 12:100172. doi: 10.1016/j.fochx.2021.100172

41. Liu P, Xue J, Tong S, Dong W, Wu P. Structure characterization and hypoglycaemic activities of two polysaccharides from *Inonotus obliquus*. *Molecules.* (2018) 23:1948. doi: 10.3390/molecules23081948

42. Xiong L, Ouyang KH, Chen H, Yang ZW, Hu WB, Wang N, et al. Immunomodulatory effect of *Cyclocarya paliurus* polysaccharide in cyclophosphamide induced immunocompromised mice. *Bioact Carbohydr Dietary Fibre.* (2020) 24:100224. doi: 10.1016/j.bcdf.2020.100224

43. Qi Q, Dong Z, Sun Y, Li S, Zhao Z. Protective effect of bergenin against cyclophosphamide-induced immunosuppression by immunomodulatory effect and antioxidation in balb/c mice. *Molecules.* (2018) 23:2668. doi: 10.3390/molecules23102668

44. Hwang YP, Lee GH, Pham TH, Kim MY, Kim CY, Lee SY, et al. Immune-enhancing effect of submerged culture of *Ceriporia lacerata* mycelia on cyclophosphamide-induced immunosuppressed mice and the underlying mechanisms in macrophages. *Int J Mol Sci.* (2022) 23:592. doi: 10.3390/ijms23020597

45. Parveen A, Zahiruddin S, Agarwal N, Akhtar Siddiqui M, Husain Ansari S, Ahmad S. Modulating effects of the synergistic combination of extracts of herbal drugs on cyclophosphamide-induced immunosuppressed mice. *Saudi J Biol Sci.* (2021) 28:6178–90. doi: 10.1016/j.sjbs.2021.06.076

46. Wang W, Wang J. Toll-like receptor 4 (TLR4)/cyclooxygenase-2 (COX-2) regulates prostate cancer cell proliferation, migration, and invasion by NF-kappaB activation. *Med Sci Monit.* (2018) 24:5588–97. doi: 10.12659/MSM.906857

47. Hegde A, Denburg MR, Glenn DA. Acute kidney injury and pediatric bone health. *Front Pediatr.* (2020) 8:635628. doi: 10.3389/fped.2020.635628

48. Yang JJ, Wang SJ, Gao X, Wang B, Dong YT, Bai Y, et al. Toll-like receptor 4 (TLR-4) pathway promotes pulmonary inflammation in chronic intermittent hypoxia-induced obstructive sleep apnea. *Med Sci Monit.* (2018) 24:7152–61. doi: 10.12659/MSM.910632

49. Li Y, Zhao Y, Xu X, Zhang R, Zhang J, Zhang X, et al. Overexpression of Toll-like receptor 4 contributes to the internalization and elimination of *Escherichia coli* in sheep by enhancing caveolae-dependent endocytosis. *J Anim Sci Biotechnol.* (2021) 12:63. doi: 10.1186/s40104-021-00585-z

50. Xu X, Zhang J, Chen L, Sun Y, Qing D, Xin X, et al. *Alhagi pseudalhagi* extract exerts protective effects against intestinal inflammation in ulcerative colitis by affecting TLR4-dependent NF-kappaB signaling pathways. *Front Pharmacol.* (2021) 12:764602. doi: 10.3389/fphar.2021.764602

51. Jiang Q, Lyu XM, Yuan Y, Wang L. Plasma miR-21 expression: an indicator for the severity of Type 2 diabetes with diabetic retinopathy. *Biosci Rep.* (2017) 37:BSR20160589. doi: 10.1042/BSR20160589

frontiers | Frontiers in Nutrition

TYPE Review
PUBLISHED 15 September 2022
DOI 10.3389/fnut.2022.1004966

OPEN ACCESS

EDITED BY
Yanjun Zhang,
Chinese Academy of Tropical Agricultural Sciences, China

REVIEWED BY
Jinhu Tian,
Zhejiang University, China
Zhili Ji,
Wuhan Polytechnic University, China
Xiaoyan Tan,
Nanjing Tech University, China

*CORRESPONDENCE
Chengdeng Chi
c_cd@fjnu.edu.cn
Meiying Wang
mwang15@uoguelph.ca

SPECIALTY SECTION
This article was submitted to Food Chemistry, a section of the journal Frontiers in Nutrition

RECEIVED 27 July 2022
ACCEPTED 23 August 2022
PUBLISHED 15 September 2022

CITATION
Chi C, Shi M, Zhao Y, Chen B, He Y and Wang M (2022) Dietary compounds slow starch enzymatic digestion: A review. *Front. Nutr.* 9:1004966. doi: 10.3389/fnut.2022.1004966

Dietary compounds slow starch enzymatic digestion: A review

Chengdeng Chi[1]*, Miaomiao Shi[2], Yingting Zhao[3,4], Bilian Chen[1], Yongjin He[1] and Meiying Wang[5]*

[1]College of Life Sciences, Fujian Normal University, Fuzhou, China, [2]College of Food and Biological Engineering, Zhengzhou University of Light Industry, Zhengzhou, China, [3]Center for Nutrition and Food Sciences, The University of Queensland, Queensland Alliance for Agriculture and Food Innovation, Brisbane, QLD, Australia, [4]College of Food Science, Fujian Agriculture and Forestry University, Fuzhou, China, [5]School of Engineering, University of Guelph, Guelph, ON, Canada

Dietary compounds significantly affected starch enzymatic digestion. However, effects of dietary compounds on starch digestion and their underlying mechanisms have been not systematically discussed yet. This review summarized the effects of dietary compounds including cell walls, proteins, lipids, non-starchy polysaccharides, and polyphenols on starch enzymatic digestion. Cell walls, proteins, and non-starchy polysaccharides restricted starch disruption during hydrothermal treatment and the retained ordered structures limited enzymatic binding. Moreover, they encapsulated starch granules and formed physical barriers for enzyme accessibility. Proteins, non-starchy polysaccharides along with lipids and polyphenols interacted with starch and formed ordered assemblies. Furthermore, non-starchy polysaccharides and polyphenols showed robust abilities to reduce activities of α-amylase and α-glucosidase. Accordingly, it can be concluded that dietary compounds lowered starch digestion mainly by three modes: (i) prevented ordered structures from disruption and formed ordered assemblies chaperoned with these dietary compounds; (ii) formed physical barriers and prevented enzymes from accessing/binding to starch; (iii) reduced enzymes activities. Dietary compounds showed great potentials in lowering starch enzymatic digestion, thereby modulating postprandial glucose response to food and preventing or treating type II diabetes disease.

KEYWORDS

starch digestion, dietary compounds, starch structure, enzyme activity, nutrition

Introduction

Starch which is a polysaccharide composed of linear chains (amylose) or branched chains (amylopectin) is a major source of energy in the human diet. Starch digestion is accomplished by two type of enzymes in human gastrointestinal tract (GIT): (i) salivary and pancreatic α-amylases and (ii) intestinal brush border glucoamylases, maltase-glucoamylase, and sucrase-isomaltase (1). Amylase digests amylose into maltose subunits (disaccharide) and amylopectin into branched chains (i.e., dextrins). Both maltose and dextrins are digested by enzymes located in intestinal brush border, which in turn

produced glucose. The glucose released from starch is subsequently absorbed in the intestine and hydrolyzed to produce adenosine triphosphate or stored in animals as the polysaccharide glycogen. Accordingly, starch-based diets are commonly the main foods that provide the necessary energy. However, rapid digestion of starch contributes to postprandial hyperglycaemia, which in turn possibly results in an impaired insulin secretion and the incidence of chronic diseases such as obesity and type II diabetes (2, 3). Slowing starch enzymatic digestion in the GIT is of great interest in preventing the incidence of chronic diseases.

Enzymatic reactions consist of three steps: diffusion of enzymes to the solid surfaces, absorption/binding, and catalysis (1). Regarding to starch enzymatic digestion, there are two factors influencing the extent and rate of starch digestion: (i) barriers that slow down or prevent digestive enzymes from accessing/binding to starch and (ii) starch structural features that limit enzyme action after initial binding (4). Starch structuration on fine structure, helical structure, crystalline structure, lamellar structure, short-range ordered structure, and nanoscale aggregate structure significantly slowed enzymes binding with starch and reduced enzymes catalyzation toward starch (5–13). It has been summarized that slowly digestible starch (SDS) was the fraction with high α-1,6 linkages, short branch chains [degree of polymerization (DP) < 13], long chains with DP 25–36, or imperfect helical and crystalline structures, while the resistant starch (RS) was the fraction rich in high amylose content, double helix-promoting chains with DP *ca.* 12–24 and DP $\geq$ 37, along with some chains with DP 25–36, perfectly-packed double helices and crystalline structures, V-type crystals, or densely-packed crystalline lamellae and more ordered reassembled aggregate structures (8). According to previous studies (14–19), starch digestion was affected not only by its intrinsic structures but also by the interactions between starch and dietary non-starchy compounds and between digestive enzymes and non-starchy foods. At present, many reviews have indicated dietary compounds such as polyphenols, lipids, and non-starchy polysaccharides significantly affected starch digestion (15–20). However, the effects of dietary compounds such as cell walls, protein, lipids, non-starchy polysaccharides, and polyphenols on starch digestion and their underlying mechanisms have been not systematically summarized yet.

Therefore, this review provided a survey of the latest developments on dietary strategies for slowing starch enzymatic digestion, with a particular focus on the mechanisms underlying the modulation of starch digestion. Future perspectives regarding the dietary strategies for the control of starch digestion will be proposed. This review can provide better insights into the modulation of starch enzymatic digestion through complexation with dietary compounds.

Cell walls slow starch digestion

The basic architecture of plant cell wall is shown in Figure 1. Plant cell walls are cellulose-based assemblies containing cellulose and non-cellulosic polysaccharides (e.g., pectin, xyloglucans, heteroxylans, and β-glucans), lignin and some proteins (20, 21). Cellulose fibrils assembled and served as scaffold filling with amorphous non-starchy polysaccharides (20). While the filling non-starchy polysaccharides prevented aggregation and collapse of the cellulose/hemicellulose network, the interactions of the non-starchy polysaccharides significantly contributed to the density and porosity of cell walls and in turn determined the permeability of hydrolases through the cell walls (22, 23).

Effects of cell walls on starch gelatinization and enzyme-starch interaction are shown in Figure 1 (21). Cell walls entrapped starch granules, thereby limiting the enzymatic digestion through the physical barriers (24). In addition, non-starchy polysaccharides-rich cell walls of starchy foods retained their intact structures during food processing, and in turn significantly slowed starch enzymatic digestion (25, 26). Non-starchy polysaccharides were not digested in the GIT due to the lack of corresponding enzymes. Therefore, the cell walls of processed foods provided physical barriers for enzymes diffusion to starch and hydrolyzation of starch molecules. Li et al. suggested that the integrity of cell walls of pulse significantly affected starch digestion (27). Food processing yielded disorganization of cell walls, which in turn increased cell wall permeability and facilitated enzyme diffusion through the cell walls along with increased starch enzymatic digestion (27–31). Treatments with a higher temperature or a longer time promoted starch swelling, weakening the physical barriers, and increasing the degree of process-induced cell wall permeability, which in turn increased starch enzymatic digestion (29, 31). Although decreasing cell intactness has been shown to increase the rate but not the extent of starch digestion (26), most of studies indicated that the increase in cell permeability slowed the rate and reduced the extent of starch digestion *in vitro* (24, 25, 28–30, 32–34).

Li et al. indicated that enzymatic digestion of starch granules entrapped within cell walls in pulses depended on both the intactness of cell walls as well as the ordered structures of pulses after food processing (27). Cell walls not only limited enzymes diffusion onto starch molecules, but also delayed starch gelatinization, retarded starch granules swelling and leaching of starch molecules. Accordingly, ordered structures (e.g., helical structures, crystalline structures, granular form) of starch granules within cell walls retained as shown in Figure 1

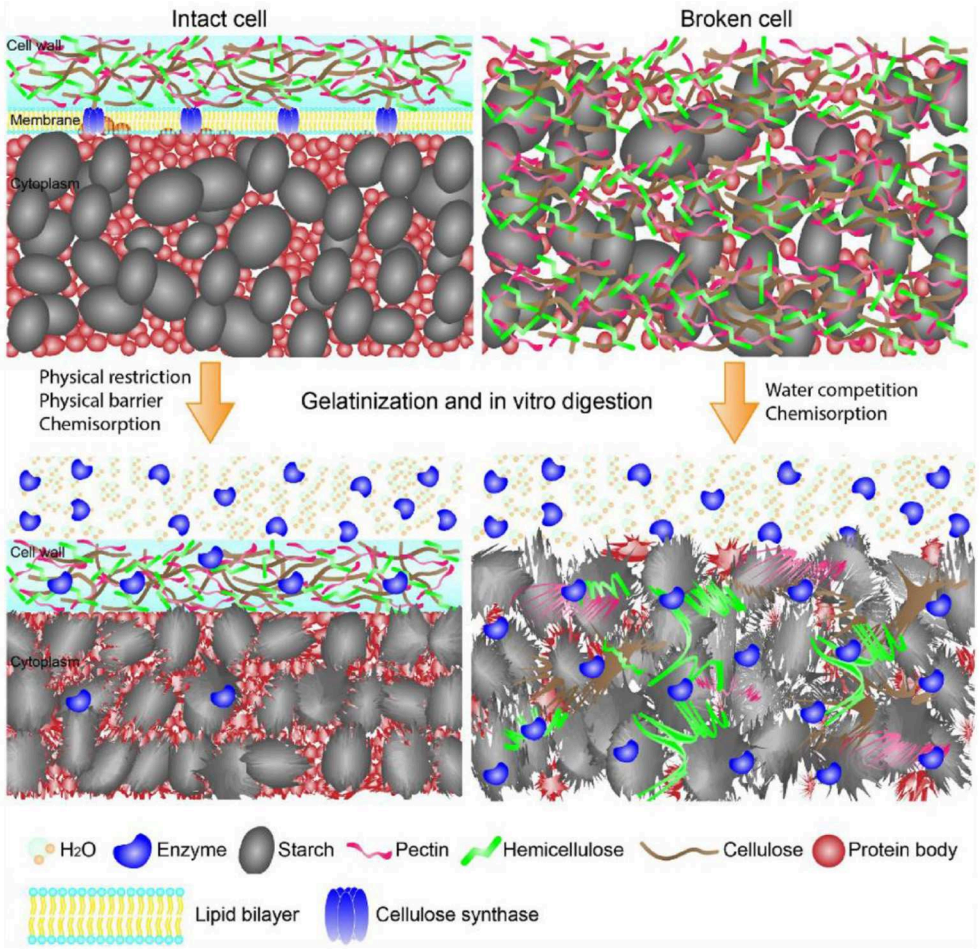

FIGURE 1
Schematic showing the structures of starch-containing intact and broken cells during gelatinization and *in vitro* digestion. The intact cell walls limited enzymes and water diffusion onto starch, while the intact cell walls yielded starch complete gelatinization and enzymes diffusion onto starch surface. The graph is collected from Li et al. (21).

(21, 27–29, 32, 34, 35). The retained starch ordered structures significantly slowed starch enzymatic digestion (7, 8). Thus, the cell walls slowed starch digestion through retarding the disruption of starch ordered structures during food hydrothermal processing.

In addition to the roles of cell walls on starch ordered structures, cell walls also bound with enzymes and affected hydrolyzation activities of the enzymes (25, 34). The non-catalytic binding of amylase on cell walls limited enzymes diffusion onto starch molecules, which reduced the amylolysis of starch within intact cells (25, 34). Starchy foods like pulses contained α-amylase inhibitors such as tannins, lectins and other proteinaceous inhibitors (36). Li et al. reported that both soluble and insoluble components from pulse cells showed a significant inhibition (*ca.* 3–15%) on enzymes activities, thereby slowing the enzymatic digestion of starch within pulse cells (34).

Proteins slow starch digestion

Protein is one of the most important compounds in foods systems. It has been summarized that proteins could non-covalently interact with starch through hydrogen bonding, hydrophobic interactions, electrostatic forces, ionic interactions, and van der Waals force (17). Endogenous rice protein interacted with rice starch significantly lowered starch digestion extent through reducing swelling of starch granules and suppressing the accessibility of enzymes to starch granules (37). Potato protein isolate interacted with starch and in turn restricted starch disorganization and reduced starch digestion extent (38). Denatured plant proteins interacted with starch through hydrogen bonds and electrostatic interactions and restricted starch hydration and enzymatic cleavage (39). Whey protein interacted with starch to form starch-protein assemblies, which significantly increased starch short-range

ordered structure while lowering starch digestion extent (40). Enzymatically hydrolyzed (the combination of pepsin and pancreatin) rice protein interacted with rice starch to promote the formation of V-type crystals and lowered starch digestion extent (41). In addition to the role of proteins on structures of pure starch and starch-protein assemblies, some proteins bound with enzymes and lowered enzymes activities and finally reduced the digestion rate and extent of starch (41–43). Water soluble barley proteins bound with α-amylase, which reduced α-amylase activity and slowed starch digestion rate and lowered starch digestion extent (42). Rice proteins hydrolyzed by pepsin and pancreatin bound with α-amylase, and in turn, inhibited α-amylase activity [the IC_{50} value (the half maximal inhibitory concentration) was in the range of 1.75–2.15 mg/mL] and lowered starch digestion extent (41). The activity of α-amylase was decreased greatly from 0.42 to 0.07 units by native gluten pepsin-hydrolyzed gluten (43).

Although the effects of protein structures on starch digestion in foods systems has not been resolved yet, it can be preliminarily concluded that dietary protein has a strong ability to mitigate starch enzymatic digestion. Dietary proteins affected starch enzymatic digestion *via* different pathways: (i) proteins acted as physical barriers and restricted the interaction of enzymes with starch molecules (37); (ii) proteins interacted with starch and restricted starch swelling and disorganization during hydrothermal treatment, which increased ordered structures and blocked the binding sites of starch molecules for digestive enzymes (39, 41); (iii) proteins or their hydrolysates interacted with starch to form ordered structures which were slowly digestible or not digestible (40, 41); (iv) proteins bound with α-amylase and lowered α-amylase activities and starch digestion extent (41, 42).

Lipids slow starch digestion

Lipids are the important hydrophobic dietary compounds in foods. In starch-containing foods systems, lipids tended to interact with starch through hydrophobic interaction and formed starch-lipid inclusion complexes or starch-lipid-protein complexes (18). According to Dhital et al. (4), the access of enzymes to the glucosidic bonds in the substrate is a key factor affecting starch enzymatic digestion. The interaction between lipids and starch significantly changed the torsion angles of the glucosidic bonds, forming the starch helical structure and in turn affecting the binding activity of the amylolytic enzymes (18). The intact structures of starch-lipids inclusion complexes did not favor the formation of enzyme-substrate complexes (44). Accordingly, starch-lipids inclusion complex was classified into type-5 RS (45). Promoting the formation of starch-lipids inclusion complexes significantly lowered starch digestion extent.

Starch structures, lipid type and structures, and the preparation conditions significantly affected the formation of starch-lipid inclusion complexes. Amylose is much easier to interact with lipids compared with amylopectin. Starches with higher amylose content formed more starch-lipids complexes compared with less amylose-containing starches (46, 47). Debranching using pullulanase or isoamylase increased amylose content, which favored the formation of starch-lipid complexes and reduced starch digestion extent in a higher magnitude (48). A suitable polymerization of amylose is required for the formation of starch-lipid complexes (44, 49, 50). Increasing the chain length of amylose favored the formation of starch-lipid inclusion complexes (49), while a very long amylose hampered the formation of starch-lipid inclusion complexes (50).

Increasing lipids concentration favored the interaction of lipids with starch, thereby lowering starch digestion in a higher magnitude (51). However, lipids might self-assemble at a high concentration and reduce the content of starch-lipid inclusion complexes formed during the reaction (52). Free fatty acids formed starch-lipid inclusion complexes as a function of concentration (51, 53). Monoglycerides and phosphatidylcholine could also interact with starch and formed starch-lipids inclusion complexes (54, 55). Since monoglycerides had higher solubility in water compared with fatty acids, they were more likely to interact with starch and formed more starch-lipid inclusion complexes (56). However, diglycerides (e.g., dipalmitate glycerol) and triglycerides (e.g., tripalmitate glycerol) could not form inclusion complexes with starch because of their steric hindrance and low solubility in water (56). By reducing the carbon chain length of free fatty acids, the complexation index of fatty acids increased and the content of starch-lipid inclusion complexes significantly increased (57). The degree of unsaturation also affected the formation of starch-lipid inclusion complexes and starch digestibility. Fatty acids with a lower unsaturation could formed more inclusion complexes with starch, thereby greatly decreasing starch digestion extent (58, 59).

Proteins in food systems affected the formation of starch-lipid inclusion complexes. β-lactoglobulin favored lipids (e.g., fatty acids and monoglyceride) dissolution in water and promoted lipid-starch entanglement (58, 60–62). Notably, β-lactoglobulin promoted fatty acids which had a shorter length and lower unsaturation interaction with starch and formed starch-fatty acids-β-lactoglobulin complexes, while β-lactoglobulin in the binary system of starch, β-lactoglobulin, and monoglyceride rather promoted the formation of starch-monoglyceride complexes (61). Fatty acids contained carboxyl groups and might behave negatively in food systems, allowing fatty acids to interact with starch through hydrophobic interactions and with proteins through electrostatic interactions (63–65). However, monoglyceride is neutrally charged and cannot electrostatically bridge the formation of the starch-monoglyceride-β-lactoglobulin (61). In addition to the lipid

types, protein types also affected the formation of starch-lipids inclusion complexes (66). Whey protein isolate and A-type gelatin promoted linoleic acid interaction with starch because of their emulsifiability. A-type gelatin showed a weaker ability to promote the formation of starch-linoleic acid inclusion complexes, which was attributed to the fact that A-type gelatin which had an isoelectric point higher than 7.0 might compete with starch for linoleic acid and reduce the accessibility of linoleic acid to starch hydrophobic cavity (66).

During the preparation of starch-lipid inclusion complexes, the temperature, complexation time and modes, pH, NaCl, and cooling rate significantly affected the formation of the complexes (67–71). A higher temperature and a longer time of the complexation, better-defined structures of the inclusion complexes had (67, 68, 71, 72). Regarding the complexation of swelled normal corn starch granules with lauric acid, the modes of adding lauric acid to the starch slurry [adding the lauric acid to the heated starch suspension (method I) or adding the lauric acid to the starch suspension and then heating (method II)] affected the content of starch-lauric acid inclusion complexes formed during the reaction (73). The method I was more beneficial to the formation of starch-lauric acid inclusion complexes than that of method II, because the lauric acid interacted with starch granules on surface, thereby inhibiting the migration of lauric acid into interior starch granules to form the complexes (73). A system with a higher pH promoted the formation of starch-lauric acid inclusion complexes and starch-lauric acid-β-lactoglobulin complexes, which was attributed to the greater solubility of lauric acid and higher leaching of amylose in the system (69). The presence of NaCl promoted the formation of starch-fatty acid inclusion complexes due to the improved solubility of fatty acids in NaCl-containing aqueous medium (70). The cooling rate of starch paste affected starch mobility during the cooling, which significantly affected structures of starch-lipid inclusion complexes (74, 75). At a higher cooling rate, amylose reorganized faster and more lipids could be entrapped into amylose hydrophobic cavity to form starch-lipid inclusion complexes (71).

Non-starchy polysaccharides slow starch digestion

Non-starchy polysaccharides affected starch gelatinization, the viscosity of starch paste, starch reorganization, and enzymes activities, which affected starch digestion by different modes. Polysaccharides such as chitosan, guar gum, and xanthan interacted with starch granules and lowered starch swelling and amylose leaching during hydrothermal treatment (76–80). Pectin, κ-carrageenan, guar gum, arabic gum, pullulan, *Cordyceps* polysaccharides, *Mesona chinensis* polysaccharides, agar, xanthan gum and konjac glucomannan restricted starch disruption during the hydrothermal treatment and interacted with starch to form ordered structures, and in turn, lowered starch digestion extent (77, 78, 81, 82). Xanthan gum, guar gum, pectin, and konjac-glucomannan might interact starch and form physical barriers around starch molecules, reducing enzymes accessibility to starch molecules and lowering starch digestion extent (83, 84).

Due to the interaction between starch and non-starchy polysaccharides, the viscosity of starch suspension which complexed with xanthan gum, guar gum, konjac glucomannan, pectin, and chitosan significantly increased (85, 86). The increased viscosity of starch suspension in turn retarded enzymes diffusion onto starch surface, leading to a significant reduction in starch digestion extent (85, 86). Other soluble fibers including locust bean gum, fenugreek gum, fenugreek gum, and soy soluble polysaccharide also limited enzymes diffusion toward starch molecules and retarded glucose liberated from the starch-polysaccharide systems (86). It seems that starch digestion rate and extent could be controlled through modulating the viscosity of the starchy food systems.

The interaction between starch and non-starchy polysaccharides also significantly affected properties of matrix structures formed by starch and non-starchy polysaccharides (82, 87–89). Agar, xanthan gum and konjac glucomannan in starch pastes significantly promoted the formation of gel-like matrix structures, and in turn, lowered starch digestion rate and extent (87). The interaction between starch and non-starch polysaccharides and the increased gel rigidity of the matrix were the key factors affecting starch enzymatic digestion (87). *Mesona chinensis* polysaccharides also interacted with starch and significantly promoted the formation of a more ordered structure of blended systems of starch and *Mesona chinensis* polysaccharides, which remarkably lowered starch digestion rate and extent (82, 88, 89). Comparing with xanthan, guar, locust bean gum, and agar, starch-*Mesona chinensis* polysaccharides complexes had better-defined gel structures and the *Mesona chinensis* polysaccharides were found to be the most effective polysaccharides in reducing wheat starch digestion (88).

Starch digestion was controlled not only by starch ordered structures and food viscosity, but also by the activities of enzymes. Pectin bound with pancreatic amylase to reduce amylase activity, resulting in slower starch enzymatic digestion (90). Polysaccharides from oat (*Avena sativa L.*), *Camellia oleifera* Abel. fruit hull, oolong tea, shaddock (*Citrus aradise*), *Coriolus versicolor* LH1, mulberry fruit, pumpkin (*Cucurbita moschata*) fruit, fermented puerh tea, green tea flower, corn silk, *Acacia tortilis gum* exudate, Chinese traditional medicine Huidouba, *Mallotus furetianus*, hemp (*Cannabis sativa L.*), *Fagopyrum tartaricum*, blackberry fruit, *Rosa roxburghii* Tratt fruit, *Annona squamosa*, wax apple, *Chaenomeles speciosa* seeds, and *Momordica charantia*, significantly reduced the activities of α-glucosidase or α-amylase, which showed great potentials in slowing starch enzymatic digestion (19, 91–99). The

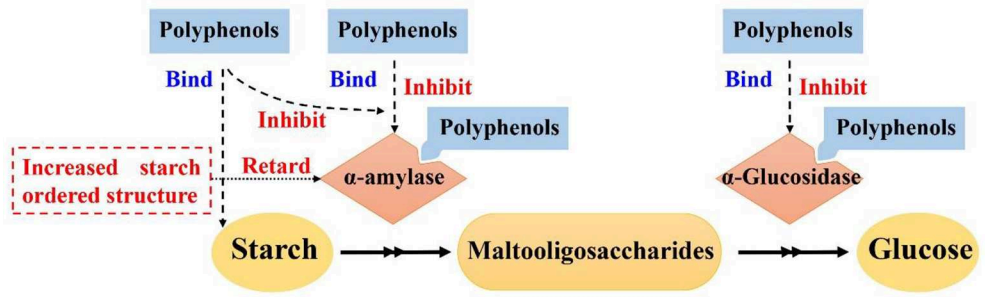

FIGURE 2
Mechanism scheme for effects of polyphenols on starch digestion. Figure was adapted from Sun and Miao (16).

structure-function of polysaccharides toward enzymes activity has been not revealed yet.

Accordingly, non-starchy polysaccharides lowered starch digestion rate and extent by four different ways: (i) interacted with starch granules and restricted starch disruption during food processing (77–80); (ii) increased systems viscosity and in turned restricted enzymes diffusion onto starch molecules (85, 86); (iii) formed matrix structure with starch and increased rigidity and ordered structures of starch-non-starchy polysaccharide complexes (82, 88, 89); (iv) interacted with α-glucosidase or α-amylase and reduced enzymes activities (91).

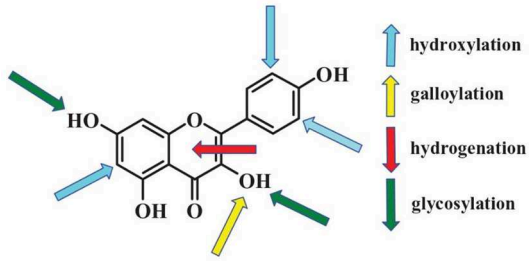

FIGURE 3
Flavonoids key sites that affecting activities of α-glucosidase. The *up arrows* and *down arrows* represent increasing and reducing the inhibition activity, respectively. Figure was collected from Xiao et al. (102).

Polyphenols slow starch digestion

Effects of polyphenols on starch digestion are schematically shown in Figure 2. α-amylase and α-glucosidase are two key enzymes for starch digestion. Accordingly, starch digestion could be significantly lowered through reducing activities of α-amylase and α-glucosidase. Tea polyphenols, flavonoids, phenolic acids, and tannins significantly reduced activities of α-amylase and α-glucosidase, which showed great potentials in mitigating starch digestion as summarized in previous reviews (16, 100–102). Polyphenols with different structures showed great differences in inhibition of activities of α-amylase and α-glucosidase. Effects of flavonoids structures on the inhibitory activity of α-glucosidase is schematically shown in Figure 3. The hydroxylation and galloylation of flavonoids improved the inhibitory activity, while the glycosylation of hyroxyl group and hydrogenation of the C2=C3 double bond on flavonoids, and the mono-glycosylation of chalcones reduced the inhibition (102). Cooperating polyphenols into starchy foods systems can remarkably slowed starch enzymatic digestion.

Polyphenols could interact with starch and form ordered starch structures, and in turn, lowering starch digestion as shown in Figure 2. It has been reported that polyphenols could interact with starch and promote the formation of starch ordered structures (103–110). Tea polyphenols, sorghum phenolic compounds, gallic acid could non-covalently interact with starch to form ordered structures for lowering starch digestion extent (103, 105, 106, 111–114). V-type crystals are the structures that are highly resistant to enzymatic digestion (8). Tannins, proanthocyanidins, and longan seed polyphenols interacted with starch and formed V-type crystals, which significantly lowered starch digestion rate and extent (105, 107–109, 111). Proanthocyanidins with a higher degree of polymerization had stronger abilities to interact with starch and form more V-type crystals (107, 114). Controlling the molecular weight of proanthocyanidins would be a promising pathway to control the formation of V-type crystals and thus starch enzymatic digestion (114). Hydrophilic polyphenols were hardly to form V-type with starch using conventional complexation method (e.g., high speed shearing) (115). However, high pressure homogenization could promote starch interaction with gallic acid and green tea polyphenols, thereby forming V-type crystals and short-range ordered structures for lowering starch enzymatic digestion (105, 112). In addition to V-type crystals, gallic acid might form "hamburger-like" structure of starch-polyphenol-starch

complexes, which increased ordered structure of starch gel and lowered starch digestion extent (103).

Other dietary compounds

In addition to the compounds discussed above, other dietary compounds such as NaCl and phytosterols also affected starch digestibility (70, 116, 117). NaCl would promote the formation of starch-lipid inclusion complexes, which would slow starch enzymatic digestion in a higher magnitude (70). Generally, retrograded starch showed a low digestibility due to its ordered structures (118). Co-crystallization with NaCl to produce single-helix amylopectin was regarded as a promising strategy to retard starch retrogradation (116), suggesting NaCl potentially increased digestibility of retrograded starch. Phytosterols, which showed robust abilities in lowering enzymes activities (117), indicating phytosterols could slow starch digestion significantly *via* inhibiting enzymes activities.

Concluding remarks and future directions

This review summarized effects of dietary compounds including cell walls, proteins, lipids, non-starchy polysaccharides, and polyphenols on starch enzymatic digestion and their underlying mechanisms were discussed. Dietary compounds lowered starch digestion through three pathways: (i) retained starch ordered structures or formed ordered assemblies chaperoned with these dietary compounds; (ii) formed physical barriers and prevented enzymes from accessing/binding to starch; (iii) reduced enzymes activities. Cell walls, proteins, and non-starchy polysaccharides restricted starch disruption during hydrothermal treatment and the retained ordered structures limited enzymatic binding. In addition, they encapsulated starch granules and formed physical barriers for enzymes accessing. Proteins, non-starchy polysaccharides along with lipids and polyphenols interacted with starch and formed ordered assemblies. Non-starchy polysaccharides and polyphenols showed robust ability to reduce activities of α-amylase and α-glucosidase. Comparing with cell walls, protein, and non-starchy polysaccharides, lipids and polyphenols had stronger ability to slow starch digestion.

Food systems are relative complex with cell walls, proteins, lipids, non-starchy polysaccharides, polyphenols, vitamin, minerals, sugar, salts, etc. Dietary compounds might interact with each other and affect starch digestion in complicated pathways. How the complex dietary compounds affected starch digestion in real foods systems must be further investigated. Currently, effects of dietary compounds on starch digestion were interrogated *in vitro*. Dietary compounds would be digested and absorbed in the gastrointestinal tract and in turn affected starch digestibility. Starch *in vitro* digestibility may quite different to *in vivo* digestibility. Accordingly, *in vivo* glycemic response is the most important property of starchy foods. Further studies are needed to investigate the roles of dietary compounds on starch *in vivo* glycemic response. In addition, different groups of people such as children, athletes, middle- and old-aged human have different requirements for starch digestion rate and extent. Targeted structuring food structures and starch digestion behaviors *via* complexation with dietary compounds remains of interest.

Author contributions

CC: conceptualization, literature analysis, reviewing, and editing. MS: reviewing and editing. YZ: supervision, writing, reviewing, and editing. BC: investigation, writing, and editing. YH: investigation and reviewing. MW: supervision, reviewing, and editing. All authors contributed to the article and approved the submitted version.

Funding

The research was financially supported from project of the Scientific Research Innovation Program Xiyuanjiang River Scholarship of College of Life Sciences, Fujian Normal University (22FSSK004).

Conflict of interest

The authors declare that the research was conducted in the absence of any commercial or financial relationships that could be construed as a potential conflict of interest.

Publisher's note

References

1. Zhang B, Li H, Wang S, Junejo SA, Huang Q. *In vitro Starch Digestion: Mechanisms and Kinetic Models. Starch Structure, Functionality and Application in Foods*. Singapore: Springer (2020) 151–67.

2. Bindels LB, Walter J, Ramer-Tait AE. Resistant starches for the management of metabolic diseases. *Curr Opin Clin Nutr Metab Care.* (2015) 18:559. doi: 10.1097/MCO.0000000000000223

3. Zhang G, Hamaker BR. Slowly digestible starch: concept, mechanism, and proposed extended glycemic index. *Crit Rev Food Sci Nutr.* (2009) 49:852–67. doi: 10.1080/10408390903372466

4. Dhital S, Warren FJ, Butterworth PJ, Ellis PR, Gidley MJ. Mechanisms of starch digestion by α-amylase—Structural basis for kinetic properties. *Crit Rev Food Sci Nutr.* (2015) 57:875–92. doi: 10.1080/10408398.2014.922043

5. Wang H, Xu K, Liu X, Zhang Y, Xie X, Zhang H. Understanding the structural, pasting and digestion properties of starch isolated from frozen wheat dough. *Food Hydrocoll.* (2021) 111:106168. doi: 10.1016/j.foodhyd.2020.106168

6. Wang H, Ding J, Xiao N, Liu X, Zhang Y, Zhang H. Insights into the hierarchical structure and digestibility of starch in heat-moisture treated adlay seeds. *Food Chem.* (2020) 318:126489. doi: 10.1016/j.foodchem.2020.126489

7. Chi C, Li X, Zhang Y, Chen L, Li L, Miao S. Progress in tailoring starch intrinsic structures to improve its nutritional value. *Food Hydrocoll.* (2020) 113:106447. doi: 10.1016/j.foodhyd.2020.106447

8. Chi C, Li X, Huang S, Chen L, Zhang Y, Li L, et al. Basic principles in starch multi-scale structuration to mitigate digestibility: a review. *Trends Food Sci Technol.* (2021) 109:154–68. doi: 10.1016/j.tifs.2021.01.024

9. Tian J, Ogawa Y, Shi J, Chen S, Zhang H, Liu D, et al. The microstructure of starchy food modulates its digestibility. *Crit Rev Food Sci Nutr.* (2018) 59:3117–28. doi: 10.1080/10408398.2018.1484341

10. Zhang B, Dhital S, Gidley MJ. Densely packed matrices as rate determining features in starch hydrolysis. *Trends Food Sci Technol.* (2015) 43:18–31. doi: 10.1016/j.tifs.2015.01.004

11. Li B, Zhang Y, Xu F, Khan MR, Zhang Y, Huang C, et al. Supramolecular structure of *Artocarpus heterophyllus* Lam seed starch prepared by improved extrusion cooking technology and its relationship with *in vitro* digestibility. *Food Chem.* (2021) 336:127716. doi: 10.1016/j.foodchem.2020.127716

12. Zhang Y, Xu F, Wang Q, Zhang Y, Wu G, Tan L, et al. Effects of moisture content on digestible fragments and molecular structures of high amylose jackfruit starch prepared by improved extrusion cooking technology. *Food Hydrocoll.* (2022) 133:108023. doi: 10.1016/j.foodhyd.2022.108023

13. Zhang Y, Zuo H, Xu F, Zhu K, Tan L, Dong W, et al. The digestion mechanism of jackfruit seed starch using improved extrusion cooking technology. *Food Hydrocoll.* (2021) 110:106154. doi: 10.1016/j.foodhyd.2020.106154

14. Toutounji MR, Farahnaky A, Santhakumar AB, Oli P, Butardo VM, Blanchard CL. Intrinsic and extrinsic factors affecting rice starch digestibility. *Trends Food Sci Technol.* (2019) 88:10–22. doi: 10.1016/j.tifs.2019.02.012

15. Sun L, Warren FJ, Gidley MJ. Natural products for glycaemic control: polyphenols as inhibitors of alpha-amylase. *Trends Food Sci Technol.* (2019) 91:262–73. doi: 10.1016/j.tifs.2019.07.009

16. Sun L, Miao M. Dietary polyphenols modulate starch digestion and glycaemic level: a review. *Crit Rev Food Sci Nutr.* (2020) 60:541–55. doi: 10.1080/10408398.2018.1544883

17. Zhang B, Qiao D, Zhao S, Lin Q, Wang J, Xie F. Starch-based food matrices containing protein: recent understanding of morphology, structure, and properties. *Trends Food Sci Technol.* (2021) 114:212–31. doi: 10.1016/j.tifs.2021.05.033

18. Wang S, Chao C, Cai J, Niu B, Copeland L, Wang S. Starch–lipid and starch–lipid–protein complexes: a comprehensive review. *Compreh Rev Food Sci Food Safety.* (2020) 19:1056–79. doi: 10.1111/1541-4337.12550

19. Wu J, Shi S, Wang H, Wang S. Mechanisms underlying the effect of polysaccharides in the treatment of type 2 diabetes: a review. *Carbohydr Polym.* (2016) 144:474–94. doi: 10.1016/j.carbpol.2016.02.040

20. Li H, Chen S, Bui A, Xu B, Dhital S. Natural 'capsule' in food plants: cell wall porosity controls starch digestion and fermentation. *Food Hydrocoll.* (2021) 117:106657. doi: 10.1016/j.foodhyd.2021.106657

21. Li C, Hu Y, Zhang B. Plant cellular architecture and chemical composition as important regulator of starch functionality in whole foods. *Food Hydrocoll.* (2021) 117:106744. doi: 10.1016/j.foodhyd.2021.106744

22. Fleischer A, O'Neill MA, Ehwald R. The pore size of non-graminaceous plant cell walls is rapidly decreased by borate ester cross-linking of the pectic polysaccharide rhamnogalacturonan II. *Plant Physiol.* (1999) 121:829–38. doi: 10.1104/pp.121.3.829

23. Hiroya F, Kyoko M. Synthesis of borate cross-linked rhamnogalacturonan II. *Front Plant Sci.* (2015) 6:223. doi: 10.3389/fpls.2015.00223

24. Dhital S, Bhattarai RR, Gorham J, Gidley MJ. Intactness of cell wall structure controls the *in vitro* digestion of starch in legumes. *Food Funct.* (2016) 7:1367–79. doi: 10.1039/C5FO01104C

25. Bhattarai RR, Dhital S, Mense A, Gidley M, Shi Y. Intact cellular structure in cereal endosperm limits starch digestion *in vitro*. *Food Hydrocoll.* (2018) 81:139–48. doi: 10.1016/j.foodhyd.2018.02.027

26. Rovalino-Cordova AM, Fogliano V, Capuano E. A closer look to cell structural barriers affecting starch digestibility in beans. *Carbohydr Polym.* (2018) 181:994–1002. doi: 10.1016/j.carbpol.2017.11.050

27. Li P, Zhang B, Dhital S. Starch digestion in intact pulse cells depends on the processing induced permeability of cell walls. *Carbohydr Polym.* (2019) 225:115204. doi: 10.1016/j.carbpol.2019.115204

28. Ding L, Xie Z, Fu X, Wang Z, Huang Q, Zhang B. Structural and *in vitro* starch digestion properties of potato parenchyma cells: effects of gelatinization degree. *Food Hydrocoll.* (2021) 113:106464. doi: 10.1016/j.foodhyd.2020.106464

29. Ding L, Huang Q, Li H, Wang Z, Fu X, Zhang B. Controlled gelatinization of potato parenchyma cells under excess water condition: structural and *in vitro* digestion properties of starch. *Food Funct.* (2019) 10:5312–22. doi: 10.1039/C9FO00928K

30. Xiong W, Zhang B, Huang Q, Li C, Pletsch EA, Fu X. Variation in the rate and extent of starch digestion is not determined by the starch structural features of cooked whole pulses. *Food Hydrocoll.* (2018) 83:340–7. doi: 10.1016/j.foodhyd.2018.05.022

31. Pallares Pallares A, Alvarez Miranda B, Truong NQA, Kyomugasho C, Chigwedere CM, Hendrickx M, et al. Process-induced cell wall permeability modulates the *in vitro* starch digestion kinetics of common bean cotyledon cells. *Food Funct.* (2018) 9:6544–54. doi: 10.1039/C8FO01619D

32. Do DT, Singh J, Oey I, Singh H. Modulating effect of cotyledon cell microstructure on *in vitro* digestion of starch in legumes. *Food Hydrocoll.* (2019) 96:112–22. doi: 10.1016/j.foodhyd.2019.04.063

33. Tian J, Chen S, Zhang H, Fang H, Sun Y, Liu D, et al. Existing cell wall fragments modify the thermal properties and hydrolysis of potato starch. *Food Hydrocoll.* (2018) 85:229–32. doi: 10.1016/j.foodhyd.2018.07.033

34. Li P, Dhital S, Fu X, Huang Q, Liu R, Zhang B, et al. Starch digestion in intact pulse cotyledon cells depends on the extent of thermal treatment. *Food Chem.* (2020) 315:126268. doi: 10.1016/j.foodchem.2020.126268

35. Chen Z, Huang Q, Xia Q, Zha B, Sun J, Xu B, et al. Intact endosperm cells in buckwheat flour limit starch gelatinization and digestibility *in vitro*. *Food Chemietry.* (2020) 330:127318. doi: 10.1016/j.foodchem.2020.127318

36. Sathe SK. Dry beans of a review. Part 3. *Crit Rev Food Sci Nutr.* (1984) 21:137–95. doi: 10.1080/10408398409527399

37. Ye J, Hu X, Luo S, McClements DJ, Liang L, Liu C. Effect of endogenous proteins and lipids on starch digestibility in rice flour. *Food Res Int.* (2018) 106:404–9. doi: 10.1016/j.foodres.2018.01.008

38. Lu ZH, Donner E, Yada RY, Liu Q. Physicochemical properties and *in vitro* starch digestibility of potato starch/protein blends. *Carbohydr Polym.* (2016) 154:214–22. doi: 10.1016/j.carbpol.2016.08.055

39. López-Barón N, Gu Y, Vasanthan T, Hoover R. Plant proteins mitigate in vitro wheat starch digestibility. *Food Hydrocoll.* (2017) 69:19–27. doi: 10.1016/j.foodhyd.2017.01.015

40. Yang C, Zhong F, Douglas Goff H, Li Y. Study on starch-protein interactions and their effects on physicochemical and digestible properties of the blends. *Food Chem.* (2019) 280:51–8. doi: 10.1016/j.foodchem.2018.12.028

41. Chi C, Li X, Zhang Y, Chen L, Li L. Understanding the mechanism of starch digestion mitigation by rice protein and its enzymatic hydrolysates. *Food Hydrocoll.* (2018) 84:473–80. doi: 10.1016/j.foodhyd.2018.06.040

42. Yu W, Zou W, Dhital S, Wu P, Gidley MJ, Fox GP, et al. The adsorption of α-amylase on barley proteins affects the *in vitro* digestion of starch in barley flour. *Food Chem.* (2018) 241:493–501. doi: 10.1016/j.foodchem.2017.09.021

43. Xu H, Zhou J, Yu J, Wang S, Wang S. Mechanisms underlying the effect of gluten and its hydrolysates on *in vitro* enzymatic digestibility of wheat starch. *Food Hydrocoll.* (2021) 113:106507. doi: 10.1016/j.foodhyd.2020.106507

44. Putseys JA, Lamberts L, Delcour JA. Amylose-inclusion complexes: formation, identity and physico-chemical properties. *J Cereal Sci.* (2010) 51:238–47. doi: 10.1016/j.jcs.2010.01.011

45. Gutiérrez TJ, Tovar J. Update of the concept of type 5 resistant starch (RS5): self-assembled starch V-type complexes. *Trends Food Sci Technol.* (2021) 109:711–24. doi: 10.1016/j.tifs.2021.01.078

46. Liu P, Kang X, Cui B, Gao W, Wu Z, Yu B. Effects of amylose content and enzymatic debranching on the properties of maize starch-glycerol monolaurate complexes. *Carbohydr Polym.* (2019) 222:115000. doi: 10.1016/j.carbpol.2019.115000

47. Cai J, Chao C, Niu B, Copeland L, Yu J, Wang S, et al. New insight into the interactions among starch, lipid and protein in model systems with different starches. *Food Hydrocoll.* (2021) 112:106323. doi: 10.1016/j.foodhyd.2020.106323

48. Zhang B, Huang Q, Luo F, Fu X. Structural characterizations and digestibility of debranched high-amylose maize starch complexed with lauric acid. *Food Hydrocoll.* (2012) 28:174–81. doi: 10.1016/j.foodhyd.2011.12.020

49. Gelders G, Duyck J, Goesaert H, Delcour J. Enzyme and acid resistance of amylose-lipid complexes differing in amylose chain length, lipid and complexation temperature. *Carbohydr Polym.* (2005) 60:379–89. doi: 10.1016/j.carbpol.2005.02.008

50. Gelders GG, Vanderstukken TC, Goesaert H, Delcour JA. Amylose–lipid complexation: a new fractionation method. *Carbohydr Polym.* (2004) 56:447–58. doi: 10.1016/j.carbpol.2004.03.012

51. Liu K, Chi C, Huang X, Li X, Chen L. Synergistic effect of hydrothermal treatment and lauric acid complexation under different pressure on starch assembly and digestion behaviors. *Food Chem.* (2019) 278:560–7. doi: 10.1016/j.foodchem.2018.11.097

52. Tang MC, Copeland L. Analysis of complexes between lipids and wheat starch. *Carbohydr Polym.* (2007) 67:80–5. doi: 10.1016/j.carbpol.2006.04.016

53. Chi C, Li X, Feng T, Zeng X, Chen L, Li L. Improvement in nutritional attributes of rice starch with dodecyl gallate complexation: a molecular dynamic simulation and *in vitro* study. *J Agric Food Chem.* (2018) 66:9282–90. doi: 10.1021/acs.jafc.8b02121

54. Cheng W, Luo Z, Li L, Fu X. Preparation and characterization of debranched-starch/phosphatidylcholine inclusion complexes. *J Agric Food Chem.* (2015) 63:634–41. doi: 10.1021/jf504133c

55. Chen B, Zeng S, Zeng H, Guo Z, Zhang Y, Zheng B. Properties of lotus seed starch–glycerin monostearin complexes formed by high pressure homogenization. *Food Chem.* (2017) 226:119–27. doi: 10.1016/j.foodchem.2017.01.018

56. Chao C, Yu J, Wang S, Copeland L, Wang S. Mechanisms underlying the formation of complexes between maize starch and lipids. *J Agric Food Chem.* (2018) 66:272–8. doi: 10.1021/acs.jafc.7b05025

57. Chen B, Guo Z, Miao S, Zeng S, Jia X, Zhang Y, et al. Preparation and characterization of lotus seed starch-fatty acid complexes formed by microfluidization. *J Food Eng.* (2018) 237:52–9. doi: 10.1016/j.jfoodeng.2018.05.020

58. Zheng M, Chao C, Yu J, Copeland L, Wang S, Wang S. Effects of chain length and degree of unsaturation of fatty acids on structure and *in vitro* digestibility of starch-protein-fatty acid complexes. *J Agric Food Chem.* (2018) 66:1872–80. doi: 10.1021/acs.jafc.7b04779

59. Sun S, Jin Y, Hong Y, Gu Z, Cheng L, Li Z, et al. Effects of fatty acids with various chain lengths and degrees of unsaturation on the structure, physicochemical properties and digestibility of maize starch-fatty acid complexes. *Food Hydrocoll.* (2021) 110:106224. doi: 10.1016/j.foodhyd.2020.106224

60. Wang S, Zheng M, Yu J, Wang S, Copeland L. Insights into the formation and structures of starch-protein-lipid complexes. *J Agric Food Chem.* (2017) 65:1960–6. doi: 10.1021/acs.jafc.6b05772

61. Chao C, Cai J, Yu J, Copeland L, Wang S, Wang S. Toward a better understanding of starch-monoglyceride-protein interactions. *J Agric Food Chem.* (2018) 66:13253–9. doi: 10.1021/acs.jafc.8b04742

62. Cai J, Chao C, Niu B, Yu J, Copeland L, Wang S, et al. Effects of debranching on the formation of maize starch-lauric acid-beta-lactoglobulin complexes. *J Agric Food Chem.* (2021) 69:9086–93. doi: 10.1021/acs.jafc.0c07230

63. Zhang G, Maladen M, Campanella OH, Hamaker BR. Free fatty acids electronically bridge the self-assembly of a three-component nanocomplex consisting of amylose, protein, and free fatty acids. *J Agric Food Chem.* (2010) 58:9164–70. doi: 10.1021/jf1010319

64. Liu J, Fei L, Maladen M, Hamaker BR, Zhang G. Iodine binding property of a ternary complex consisting of starch, protein, and free fatty acids. *Carbohydr Polym.* (2009) 75:351–5. doi: 10.1016/j.carbpol.2008.08.015

65. Bhopatkar D, Feng T, Chen F, Zhang G, Carignano M, Park SH, et al. Self-assembled nanoparticle of common food constituents that carries a sparingly soluble small molecule. *J Agric Food Chem.* (2015) 63:4312–9. doi: 10.1021/acs.jafc.5b00037

66. Lin L, Yang H, Chi C, Ma X. Effect of protein types on structure and digestibility of starch-protein-lipids complexes. *LWT Food Sci Technol.* (2020) 134:110175. doi: 10.1016/j.lwt.2020.110175

67. Reddy CK, Choi SM, Lee D-J, Lim S.-T. Complex formation between starch and stearic acid: effect of enzymatic debranching for starch. *Food Chem.* (2018) 244:136–42. doi: 10.1016/j.foodchem.2017.10.040

68. Reddy CK, Lee D-J, Lim S-T, Park EY. Enzymatic debranching of starches from different botanical sources for complex formation with stearic acid. *Food Hydrocoll.* (2019) 89:856–63. doi: 10.1016/j.foodhyd.2018.11.059

69. Niu B, Chao C, Cai J, Yan Y, Copeland L, Yu J, et al. Effect of pH on formation of starch complexes with lauric acid and β-lactoglobulin. *LWT Food Sci Technol.* (2020) 132:109915. doi: 10.1016/j.lwt.2020.109915

70. Niu B, Chao C, Cai J, Yan Y, Copeland L, Wang S, et al. The effect of NaCl on the formation of starch-lipid complexes. *Food Chem.* (2019) 299:125133. doi: 10.1016/j.foodchem.2019.125133

71. Niu B, Chao C, Cai J, Yu J, Wang S, Wang S. Effects of cooling rate and complexing temperature on the formation of starch-lauric acid-beta-lactoglobulin complexes. *Carbohydr Polym.* (2021) 253:117301. doi: 10.1016/j.carbpol.2020.117301

72. Marinopoulou A, Papastergiadis E, Raphaelides SN. An investigation into the structure, morphology and thermal properties of amylomaize starch-fatty acid complexes prepared at different temperatures. *Food Res Int.* (2016) 90:111–20. doi: 10.1016/j.foodres.2016.10.035

73. Chang F, He X, Huang Q. Effect of lauric acid on the V-amylose complex distribution and properties of swelled normal cornstarch granules. *J Cereal Sci.* (2013) 58:89–95. doi: 10.1016/j.jcs.2013.03.016

74. Fanta GF, Kenar JA, Felker FC. Nanoparticle formation from amylose-fatty acid inclusion complexes prepared by steam jet cooking. *Ind Crops Prod.* (2015) 74:36–44. doi: 10.1016/j.indcrop.2015.04.046

75. Bhosale RG, Ziegler GR. Preparation of spherulites from amylose–palmitic acid complexes. *Carbohydr Polym.* (2010) 80:53–64. doi: 10.1016/j.carbpol.2009.10.069

76. Zheng M, Su H, You Q, Zeng S, Zheng B, Zhang Y, et al. An insight into the retrogradation behaviors and molecular structures of lotus seed starch-hydrocolloid blends. *Food Chem.* (2019) 295:548–55. doi: 10.1016/j.foodchem.2019.05.166

77. He H, Chi C, Xie F, Li X, Liang Y, Chen L. Improving the *in vitro* digestibility of rice starch by thermomechanically assisted complexation with guar gum. *Food Hydrocoll.* (2020) 102:105637. doi: 10.1016/j.foodhyd.2019.105637

78. He H, Bian H, Xie F, Chen L. Different effects of pectin and κ-carrageenan on the multiscale structures and *in vitro* digestibility of extruded rice starch. *Food Hydrocoll.* (2021) 111:106216. doi: 10.1016/j.foodhyd.2020.106216

79. Zheng M, Su H, Luo M, Shen J, Zeng S, Zheng B, et al. Effect of hydrocolloids on the retrogradation of lotus seed starch undergoing an autoclaving-cooling treatment. *J Food Sci.* (2019) 84:466–474. doi: 10.1111/1750-3841.14480

80. Zheng M, You Q, Lin Y, Lan F, Luo M, Zeng H, et al. Effect of guar gum on the physicochemical properties and *in vitro* digestibility of lotus seed starch. *Food Chem.* (2019) 272:286–91. doi: 10.1016/j.foodchem.2018.08.029

81. Chen L, Zhang H, McClements DJ, Zhang Z, Zhang R, Jin Z, et al. Effect of dietary fibers on the structure and digestibility of fried potato starch: a comparison of pullulan and pectin. *Carbohydr Polym.* (2019) 215:47–57. doi: 10.1016/j.carbpol.2019.03.046

82. Xiao Y, Liu S, Shen M, Jiang L, Ren Y, Luo Y, et al. Effect of different Mesona chinensis polysaccharides on pasting, gelation, structural properties and *in vitro* digestibility of tapioca starch-Mesona chinensis polysaccharides gels. *Food Hydrocoll.* (2020) 99:105327. doi: 10.1016/j.foodhyd.2019.105327

83. Zhang B, Bai B, Pan Y, Li X, Cheng J, Chen H. Effects of pectin with different molecular weight on gelatinization behavior, textural properties, retrogradation and *in vitro* digestibility of corn starch. *Food Chem.* (2018) 264:58–63. doi: 10.1016/j.foodchem.2018.05.011

84. Sasaki T, Sotome I, Okadome H. *In vitro* starch digestibility and in vivo glucose response of gelatinized potato starch in the presence of non-starch polysaccharides. *Starch.* (2015) 67:415–23. doi: 10.1002/star.201400214

85. Sasaki T, Kohyama K. Influence of non-starch polysaccharides on the *in vitro* digestibility and viscosity of starch suspensions. *Food Chem.* (2012) 133:1420–6. doi: 10.1016/j.foodchem.2012.02.029

86. Sasaki T. Influence of anionic, neutral, and cationic polysaccharides on the *in vitro* digestibility of raw and gelatinized potato starch. *J Sci Food Agric.* (2020) 100:2435–42. doi: 10.1002/jsfa.10259

87. Sasaki T, Kohyama K. Effect of non-starch polysaccharides on the *in vitro* digestibility and rheological properties of rice starch gel. *Food Chem.* (2011) 127:541–6. doi: 10.1016/j.foodchem.2011.01.038

88. Yuris A, Goh KKT, Hardacre AK, Matia-Merino L. The effect of gel structure on the *in vitro* digestibility of wheat starch-Mesona chinensis polysaccharide gels. *Food Funct.* (2019) 10:250–8. doi: 10.1039/C8FO01501E

89. Luo Y, Shen M, Li E, Xiao Y, Wen H, Ren Y, et al. Effect of *Mesona chinensis* polysaccharide on pasting, rheological and structural properties of corn starches varying in amylose contents. *Carbohydr Polym.* (2020) 230:115713. doi: 10.1016/j.carbpol.2019.115713

90. Bai Y, Atluri S, Zhang Z, Gidley MJ, Li E, Gilbert RG. Structural reasons for inhibitory effects of pectin on α-amylase enzyme activity and in-vitro digestibility of starch. *Food Hydrocoll.* (2021) 114:106581. doi: 10.1016/j.foodhyd.2020.106581

91. Chen J, Li L, Zhou X, Li B, Zhang X, Hui R. Structural characterization and α-glucosidase inhibitory activity of polysaccharides extracted from Chinese traditional medicine Huidouba. *Int J Biol Macromol.* (2018) 117:815–9. doi: 10.1016/j.ijbiomac.2018.05.192

92. Chen J, Zhang X, Huo D, Cao C, Li Y, Liang Y, et al. Preliminary characterization, antioxidant and α-glucosidase inhibitory activities of polysaccharides from *Mallotus furetianus*. *Carbohydr Polym.* (2019) 215:307–15. doi: 10.1016/j.carbpol.2019.03.099

93. Wang X-T, Zhu Z-Y, Zhao L, Sun H-Q, Meng M, Zhang J-Y, et al. Structural characterization and inhibition on α-d-glucosidase activity of non-starch polysaccharides from *Fagopyrum tartaricum*. *Carbohydr Polym.* (2016) 153:679–85. doi: 10.1016/j.carbpol.2016.08.024

94. Dou Z, Chen C, Fu X. The effect of ultrasound irradiation on the physicochemical properties and α-glucosidase inhibitory effect of blackberry fruit polysaccharide. *Food Hydrocoll.* (2019) 96:568–76. doi: 10.1016/j.foodhyd.2019.06.002

95. Wang L, Chen C, Zhang B, Huang Q, Fu X, Li C. Structural characterization of a novel acidic polysaccharide from *Rosa roxburghii* Tratt fruit and its α-glucosidase inhibitory activity. *Food Funct.* (2018) 9:3974–85. doi: 10.1039/C8FO00561C

96. Ren Y, Zhu Z, Sun H, Chen L. Structural characterization and inhibition on α-glucosidase activity of acidic polysaccharide from *Annona squamosa*. *Carbohydr Polym.* (2017) 174:1–12. doi: 10.1016/j.carbpol.2017.05.092

97. Wang B-H, Cao J-J, Zhang B, Chen H-Q. Structural characterization, physicochemical properties and α-glucosidase inhibitory activity of polysaccharide from the fruits of wax apple. *Carbohydr Polym.* (2019) 211:227–36. doi: 10.1016/j.carbpol.2019.02.006

98. Deng Y, Huang L, Zhang C, Xie P, Cheng J, Wang X, et al. Novel polysaccharide from *Chaenomeles speciosa* seeds: structural characterization, α-amylase and α-glucosidase inhibitory activity evaluation. *Int J Biol Macromol.* (2020) 153:755–66. doi: 10.1016/j.ijbiomac.2020.03.057

99. Tan H-F, Gan C-Y. Polysaccharide with antioxidant, α-amylase inhibitory and ACE inhibitory activities from *Momordica charantia*. *Int J Biol Macromol.* (2016) 85:487–96. doi: 10.1016/j.ijbiomac.2016.01.023

100. Zhu J, Chen C, Zhang B, Huang Q. The inhibitory effects of flavonoids on alpha-amylase and alpha-glucosidase. *Crit Rev Food Sci Nutr.* (2020) 60:695–708. doi: 10.1080/10408398.2018.1548428

101. Sun L, Wang Y, Miao M. Inhibition of α-amylase by polyphenolic compounds: substrate digestion, binding interactions and nutritional intervention. *Trends Food Sci Technol.* (2020) 104:190–207. doi: 10.1016/j.tifs.2020.08.003

102. Xiao J, Kai G, Yamamoto K, Chen X. Advance in dietary polyphenols as alpha-glucosidases inhibitors: a review on structure-activity relationship aspect. *Crit Rev Food Sci Nutr.* (2013) 53:818–36. doi: 10.1080/10408398.2011.561379

103. Chi C, Li X, Zhang Y, Chen L, Xie F, Li L, et al. Modulating the *in vitro* digestibility and predicted glycemic index of rice starch gels by complexation with gallic acid. *Food Hydrocoll.* (2019) 89:821–8. doi: 10.1016/j.foodhyd.2018.11.016

104. Zhu F. Interactions between starch and phenolic compound. *Trends Food Sci Technol.* (2015) 43:129–43. doi: 10.1016/j.tifs.2015.02.003

105. Liu Y, Chen L, Xu H, Liang Y, Zheng B. Understanding the digestibility of rice starch-gallic acid complexes formed by high pressure homogenization. *Int J Biol Macromol.* (2019) 134:856–63. doi: 10.1016/j.ijbiomac.2019.05.083

106. Amoako DB, Awika JM. Resistant starch formation through intrahelical V-complexes between polymeric proanthocyanidins and amylose. *Food Chem.* (2019) 285:326–33. doi: 10.1016/j.foodchem.2019.01.173

107. Xu J, Dai T, Chen J, He X, Shuai X, Liu C, et al. Effects of three types of polymeric proanthocyanidins on physicochemical and *in vitro* digestive properties of potato starch. *Foods.* (2021) 10:1394. doi: 10.3390/foods10061394

108. Xu J, Li X, Chen J, Dai T, Liu C, Li T. Effect of polymeric proanthocyanidin on the physicochemical and *in vitro* digestive properties of different starches. *LWT Food Sci Technol.* (2021) 148:111713. doi: 10.1016/j.lwt.2021.111713

109. He T, Wang K, Zhao L, Chen Y, Zhou W, Liu F, et al. Interaction with longan seed polyphenols affects the structure and digestion properties of maize starch. *Carbohydr Polym.* (2021) 256:117537. doi: 10.1016/j.carbpol.2020.117537

110. Xu T, Li X, Ji S, Zhong Y, Simal-Gandara J, Capanoglu E, et al. Starch modification with phenolics: methods, physicochemical property alteration, and mechanisms of glycaemic control. *Trends Food Sci Technol.* (2021) 111:12–26. doi: 10.1016/j.tifs.2021.02.023

111. Amoako DB, Awika JM. Polymeric tannins significantly alter properties and *in vitro* digestibility of partially gelatinized intact starch granule. *Food Chem.* (2016) 208:10–7. doi: 10.1016/j.foodchem.2016.03.096

112. Zhao B, Wang B, Zheng B, Chen L, Guo Z. Effects and mechanism of high-pressure homogenization on the characterization and digestion behavior of lotus seed starch–green tea polyphenol complexes. *J Funct Foods.* (2019) 57:173–81. doi: 10.1016/j.jff.2019.04.016

113. Barros F, Awika JM, Rooney LW. Interaction of tannins and other sorghum phenolic compounds with starch and effects on *in vitro* starch digestibility. *J Agric Food Chem.* (2012) 60:11609–17. doi: 10.1021/jf3034539

114. Barros F, Awika J, Rooney LW. Effect of molecular weight profile of sorghum proanthocyanidins on resistant starch formation. *J Sci Food Agric.* (2014) 94:1212–7. doi: 10.1002/jsfa.6400

115. Chi C, Li X, Zhang Y, Chen L, Li L, Wang Z. Digestibility and supramolecular structural changes of maize starch by non-covalent interactions with gallic acid. *Food Funct.* (2017) 8:720–30. doi: 10.1039/C6FO01468B

116. He Z, Wang D, Lian X, Guo J, Zhu W. The anti-retrogradation properties of maize amylopectin treated by being co-crystallized with NaCl. *Int J Biol Macromol.* (2022) 219:508–18. doi: 10.1016/j.ijbiomac.2022.08.011

117. Li X, Bai Y, Jin Z, Svensson B. Food-derived non-phenolic α-amylase and α-glucosidase inhibitors for controlling starch digestion rate and guiding diabetes-friendly recipes. *LWT Food Sci Technol.* (2022) 153:112455. doi: 10.1016/j.lwt.2021.112455

118. Wang S, Li C, Copeland L, Niu Q, Wang S. Starch retrogradation: a comprehensive review. *Compreh Rev Food Sci Food Safety.* (2015) 14:568–85. doi: 10.1111/1541-4337.12143

frontiers | Frontiers in Nutrition

TYPE Original Research
PUBLISHED 03 November 2022
DOI 10.3389/fnut.2022.1035619

OPEN ACCESS

EDITED BY
Yanjun Zhang,
Chinese Academy of Tropical Agricultural Sciences, China

REVIEWED BY
Fuqiang Zhao,
Chongqing University, China
Qiuting Zhang,
Nanjing Normal University, China
Yan Zhou,
Guizhou Medical University, China

*CORRESPONDENCE
Kexue Zhu
zhukexue163@163.com
Lehe Tan
tlh3687@163.com

†These authors have contributed equally to this work and share first authorship

SPECIALTY SECTION
This article was submitted to Food Chemistry, a section of the journal Frontiers in Nutrition

RECEIVED 03 September 2022
ACCEPTED 07 October 2022
PUBLISHED 03 November 2022

CITATION
Zeng S, Cao J, Chen Y, Li C, Wu G, Zhu K, Chen X, Xu F, Liu Q and Tan L (2022) Polysaccharides from *Artocarpus heterophyllus* Lam. (jackfruit) pulp improves intestinal barrier functions of high fat diet-induced obese rats. *Front. Nutr.* 9:1035619. doi: 10.3389/fnut.2022.1035619

Polysaccharides from *Artocarpus heterophyllus* Lam. (jackfruit) pulp improves intestinal barrier functions of high fat diet-induced obese rats

Shunjiang Zeng[1,2†], Jun Cao[2†], Yuzi Chen[1,3], Chuan Li[2], Gang Wu[1], Kexue Zhu[1,4*], Xiaoai Chen[1,4], Fei Xu[1,4], Qibing Liu[5] and Lehe Tan[1*]

[1]Spice and Beverage Research Institute, Chinese Academy of Tropical Agricultural Sciences, Wanning, China, [2]College of Food Science and Engineering, Hainan University, Haikou, China, [3]College of Food Science and Technology, Huazhong Agricultural University, Wuhan, China, [4]Key Laboratory of Processing Suitability and Quality Control of the Special Tropical Crops of Hainan Province, Wanning, China, [5]Department of Pharmacology, School of Basic Medicine and Life Science, Hainan Medical University, Haikou, China

Polysaccharides show protective effects on intestinal barrier function due to their effectiveness in mitigating oxidative damage, inflammation and probiotic effects. Little has been known about the effects of polysaccharides from *Artocarpus heterophyllus* Lam. pulp (jackfruit, JFP-Ps) on intestinal barrier function. This study aimed to investigate the effects of JFP-Ps on intestinal barrier function in high fat diet-induced obese rats. H&E staining and biochemical analysis were performed to measure the pathological and inflammatory state of the intestine as well as oxidative damage. Expression of the genes and proteins associated with intestinal health and inflammation were analyzed by RT-qPCR and western blots. Results showed that JFP-Ps promoted bowel movements and modified intestinal physiochemical environment by lowering fecal pH and increasing fecal water content. JFP-Ps also alleviated oxidative damage of the colon, relieved intestinal colonic inflammation, and regulated blood glucose transport in the small intestine. In addition, JFP-Ps modified intestinal physiological status through repairing intestinal mucosal damage and increasing the thickness of the mucus layer. Furthermore, JFP-Ps downregulated the inflammatory genes (TNF-α, IL-6) and up-regulated the free fatty acid receptors (GPR41 and GPR43) and tight junction protein (occludin). These results revealed that JFP-Ps showed a protective effect on intestinal function through enhancing the biological, mucosal, immune and mechanical barrier functions of the intestine, and activating SCFAs-GPR41/GPR43 related signaling pathways. JFP-Ps may be used as a promising phytochemical to improve human intestinal health.

KEYWORDS

***Artocarpus heterophyllus* Lam. polysaccharide, intestinal function, inflammation, protective effect, obese rats**

Introduction

The intestine is the largest digestive and immune organ which closely linked to the body health, participates in the digestion and absorption of nutrients. The intestine also provides a favorable anaerobic environment for microbial colonization, plays an important role in defending the host from pathogens, and regulating the host's immune system (1–4). The contents of short-chain fatty acids (SCFAs) and colonic water, and colonic pH value are basic indicators for intestinal health, which is closely linked to the body health (5). Changes in dietary composition can affect the development of gastrointestinal disease and the integrity of the gut by altering the growth and metabolism of the intestinal flora (6). Wang et al. (7) found that walnut green husk polysaccharides alleviated obesity, chronic inflammatory responses, non-alcoholic fatty liver disease and colonic tissue damage *via* regulating gut microbiota and SCFAs content.

Polysaccharides have been reported to improve gut health *via* enhancing intestinal barrier function and restoring intestinal homeostasis, and regulate intestinal function *via* mitigating oxidative damage and inflammation, and probiotic function (8, 9). Polysaccharides from *Cyclocarya paliurus* leaves, *Dendrobium officinale,* fruiting body of *Hericium erinaceus* and polysaccharide-rich sage weed extracts were found to maintain intestinal health through lowering fecal pH value, increasing fecal water content and SCFAs concentration (5, 6, 10, 11). Gao et al. (12) reported that polysaccharide fractions from okra improved intestinal function *via* increasing the contents of SCFAs and caecum moisture, thickness of mucosa and muscular layer. *Dendrobium huoshanense* polysaccharide improved intestinal mucosal barrier function by modifying intestinal mucosal structures, regulating the production of cytokines and promoting the expression of the tight junction proteins (8).

Polysaccharides from *Artocarpus heterophyllus* Lam (jackfruit) pulp (JFP-Ps) has been demonstrated to possess immunomodulatory effects (13). In the past few years, our team has investigated the isolation, purification, *in vitro* digestive properties, antioxidant activity and *in vivo* prebiotic effects of JFP-Ps (14–16). However, to our knowledge, little has been known about the protective effects of JFP-Ps on intestinal health. Therefore, the present study aimed to investigate the protective effects of JFP-Ps on intestinal function of obese rats induced by a high-fat diet.

Abbreviations: JFP-Ps, polysaccharides from *Artocarpus heterophyllus* Lam. (jackfruit) pulp; SOD, superoxide dismutase; GSH-Px, glutathione peroxidase; CAT, catalase; MDA, malondialdehyde; MPO, myeloperoxidase; TNF-α, tumor necrosis factor-α; IL-1β, interleukin-1β; IL-6, interleukin-6; IL-10, interleukin-10; SGLT1, sodium-glucose cotransporter 1; GPR43, G protein-coupled receptor 43; GPR41, G protein-coupled receptor 41; SCFAs, short-chain fatty acids.

Materials and methods

Materials and reagents

Jackfruit fruits were collected from Xinglong Tropical Botanical Garden (Wanning, Hainan, China). JFP-Ps was extracted from the *Artocarpus heterophyllus* Lam pulp using hot water extraction and ethanol precipitation as previously described by Zhu et al. (14). JFP-Ps was mainly composed of Rha, Ara, Gal, Glc, Xyl, and GalA, with an average molecular weight of approximately 1,668 kDa.

The normal-chow diet (D12450H, 10% calories from fat) and high-fat diet (D12451, 45% calories from fat) were obtained from Jiangsu Synergy Pharmaceutical and Biological Engineering Co., Ltd., (Jiangsu, China). Assay kits for the activity of superoxide dismutase (SOD), glutathione peroxidase (GSH-Px) and catalase (CAT) and the content of malondialdehyde (MDA) were obtained from Suzhou Grace Biotechnology Co., Ltd., (Jiangsu, China). ELISA kits for myeloperoxidase (MPO), tumor necrosis factor-α (TNF-α), interleukin-1β (IL-1β), interleukin-6 (IL-6), interleukin-10 (IL-10) and sodium-glucose cotransporter 1 (SGLT1) were purchased from Shanghai Enzyme-linked Biotechnology Co., Ltd., (Shanghai, China). The qPCR primers for TNF-α, IL-6, G protein-coupled receptor 43 (GPR43), G protein-coupled receptor 41 (GPR41) and β-actin were purchased from Sangon Biotech (Shanghai) Co., Ltd., (Shanghai, China). TriQuick reagent and bicinchoninic acid (BCA) assay kits were purchased from Beijing Solarbio Science & Technology Co., Ltd., (Beijing, China). SuperReal Premix Plus assay kits were purchased from Tiangen Biotech (Beijing) Co., Ltd., (Beijing, China). Rabbit-derived polyclonal antibodies against occludin (27260-1-AP) and secondary antibody (SA00001-2) were purchased from Proteintech Group, Inc., (Wuhan Sanying, Hubei, China). BeyoRT^{TM} III first-strand synthesized kit, BeyoECL Plus reagent, poly (vinylidene fluoride) (PVDF) membrane, rabbit-derived monoclonal antibodies against β-actin (AF5003) and paraformaldehyde were purchased from Beyotime Biotechnology (Shanghai, China).

Animal experiments

Sprague-Dawley rats (SPF-grade, male), with body weights (BW) ranging from 180 to 200 g, were purchased from Hunan Silaikejingda Experimental Animal Co., Ltd., (Changsha, China) with the experimental animal production license SCXK (Xiang) 2019-0004. All rats were housed in an animal facility under controlled interior temperature (23 ± 2°C), relative humidity (55 ± 15%), noise (≤60 dB) and lighting cycle (12:12 h light-dark). After 1-week acclimation, the rats were divided into two groups: normal control (NC) group (n = 8) fed with normal-chow diet, obesity group (n = 45) fed with high fat diet

(HFD). After 12 weeks, the average body weight (BW) of the obesity group was significantly higher than that in the normal group ($p < 0.01$). The animals in obesity group were further randomly divided into five groups: HFD group, inulin group, low-, medium- and high- dose JFP-Ps groups (JFP-Ps-L, JFP-Ps-M, JFP-Ps-H), and continually fed with the high fat diet. During the diet intervention, the NC group and HFD group were treated daily with an equivalent volume of distilled water by oral gavage. The inulin group was treated daily with inulin (1.5 g/kg BW) by oral gavage (17, 18). The JFP-Ps-L group, JFP-Ps-M group and JFP-Ps-H group were treated daily with 50, 100, and 200 mg/kg JFP-Ps by oral gavage, respectively. The diet intervention was lasted for 6 weeks. The recipes of the diets are listed in S1 and S2. All animal experimental procedures were approved by the Animal Ethics Committee of Hainan University and Hainan Medical University with experimental animal use permit SYXK (Qiong) 2017-0013.

Sample collection

All the rats were fasted for 12 h and anesthetized with chloral hydrate by intraperitoneal injection, and then dissected. Fecal samples were collected, immersed immediately in liquid nitrogen, and stored at −80°C for water content and pH value analysis. The length of the colon was measured and the intestinal tissue was rinsed with pre-cooled saline, blotted on filter paper, and divided into three portions for further analysis.

Water content and pH value of feces

A portion of fecal sample was heated in an air-oven at 105 ± 2°C to a constant weight. The water content of the feces was calculated from the mass of the feces before and after drying. The other part of fecal sample was diluted with distilled water at a ratio of 1:10 (w/v) and the pH value was determined using a SevenCompact^{TM} S220 pH meter (Mettler Toledo, Switzerland).

Antioxidant activities analysis

One hundred milligram colon tissue were mixed with pre-cooled saline (4°C, 0.9%, w/w) at a ratio of 1:10 (w/v), homogenized over ice for 3 min, and centrifuged (12,000 × g, 15 min, 4°C) to gather supernatants. The activities of SOD, GSH-Px and CAT and the content of MDA were determined using the biochemical kits following the manufacturer's protocols.

Enzyme-linked immunoassay

One hundred milligram of colon tissue were homogenized with 1.0 mL pre-cooled saline (4°C, 0.9%, w/w) over ice for 5 min. Then tissue homogenate was centrifuged (12,000 × g, 20 min, 4°C) to collect supernatants. The activity of MPO and the concentrations of TNF-α, IL-1β, IL-6, and IL-10 in the colon were measured by ELISA assay kits following the manufacturer's instructions. The activity of SGLT1 in the small intestine was analyzed following the manufacturer's instructions.

Histological examination

The small intestine tissue was fixed in 4% paraformaldehyde overnight, dehydrated with graded alcohol, imbedded in a paraffin wax, and whittled down to 4 μm thickness. Then the sections were mounted onto clean glass slides, soaked in graded xylene and alcohol, stained with hematoxylin and eosin. Lastly, slides were sealed with neutral balsam for inspection under a binocular microscope.

RT-qPCR analysis

The mRNA levels of TNF-α, IL-6, GPR43, and GPR41 were determined by RT-qPCR. Total RNA was extracted from the small intestine tissue with the TriQuick reagent according to the manufacturer's protocol. The purity and concentration of total RNA was determined by Thermo Scientific^{TM} NanoDrop^{TM} 2000C spectrophotometer. cDNA was generated by reverse transcription of RNA using BeyoRT^{TM} III first-strand synthesized kit. RT-qPCR analysis of the target genes was performed on the Bio-Rad®CFX96 Real Time PCR System using a SuperReal PreMix Color (SYBR Green). The relative expression levels of the genes were calculated according to the $2^{-\Delta\Delta\ Ct}$ method and normalized to the housekeeping gene, β-actin. Primer information is listed in **Table 1**.

Western blot analysis

Fifty milligram of small intestine tissue were homogenized with 0.5 mL pre-cooled RIPA buffer, 5 μL PMSF lysis buffer and 5 μL protease inhibitor cocktail over ice for 5 min, and centrifuged (12,000 × g, 10 min, 4°C) to collect supernatants. The protein concentrations were quantified by BCA Protein Assay Kit. Denatured protein samples were fractionated on a 10% SDS-PAGE and transferred onto 0.45 μm PVDF membranes. After the membranes were blocked with 5% skimmed milk at room temperature for 60 min, the membranes were incubated overnight with primary antibodies (1:1,300) at 4°C, and then HRP-conjugated secondary antibody (1:1,000) following the manufacturer's instructions. Protein bands were developed using an ultrasensitive ECL chemiluminescence kit and visualized using a Tanon 5200 Multi chemiluminescent imaging system, and lastly quantified using Image J software.

10.3389/fnut.2022.1035619

TABLE 1 The primer sequences for amplification in RT-qPCR.

Target gene	Primer	Sequence (5′–3′)	Product size (bp)
β-actin	Forward	TGTCACCAACTGGGACGATA	165
	Reverse	GGGGTGTTGAAGGTCTCAAA	
TNF-α	Forward	AAAGGACACCATGAGCACGGAAAG	136
	Reverse	CGCCACGAGCAGGAATGAGAAG	
IL-6	Forward	ACTTCCAGCCAGTTGCCTTCTTG	110
	Reverse	TGGTCTGTTGTGGGTGGTATCCTC	
GPR43	Forward	TGCACCATCGTCATCATCGTTCAG	137
	Reverse	ACCAGGCACAGCTCCAGTCG	
GPR41	Forward	TCTGCTCCTCTTCCTGCCATTCC	150
	Reverse	CGTTCTATGCTCACCGTCATCAGG	

Statistical analysis

Results are expressed as means ± standard error of the mean (SEM). Data were analyzed by one-way analysis of variance (ANOVA), followed by Duncan's multiple comparison tests with SPSS Statistics 26 software (IBM, USA). $p < 0.05$ indicated a statistically significant difference.

Results

Effects of JFP-Ps on water content and pH value of feces

The water content of feces was significantly lower in the HFD group (56.75 ± 2.64%) than that in the NC group (64.68 ± 1.28%) (Figure 1A). JFP-Ps and inulin treatments increased water content as compared with HFD treatment. Moreover, the water content in the JFP-Ps-H group (67.05 ± 1.34%) was close to that in the inulin group (67.47 ± 2.02%), which was slightly higher than that in the normal group. As shown in Figure 1B, the pH value of feces in the HFD group was significantly higher than the NC group ($p < 0.05$). After feeding with JFP-Ps and inulin, the pH values of feces were significantly decreased in obese rats compared with the HFD treatment. The results indicated that JFP-Ps significantly increased fecal water content and decreased fecal pH value in obese rats.

Effects of JFP-Ps on colon length and intestinal micromorphology

As shown in Figures 2A,B, the colon of the HFD group was significantly shorter than the NC group ($p < 0.05$). JFP-Ps and inulin significantly inhibited the decrease of colon length compared with the HFD group ($p < 0.01$).

Morphological changes in jejunal tissue between the groups were visualized by H&E staining. As shown in Figure 2C, the jejunum in the NC group showed clear tissue structure, with finger-shaped villi closely and evenly arranged, a large number of cup-shaped cells within the columnar epithelium,

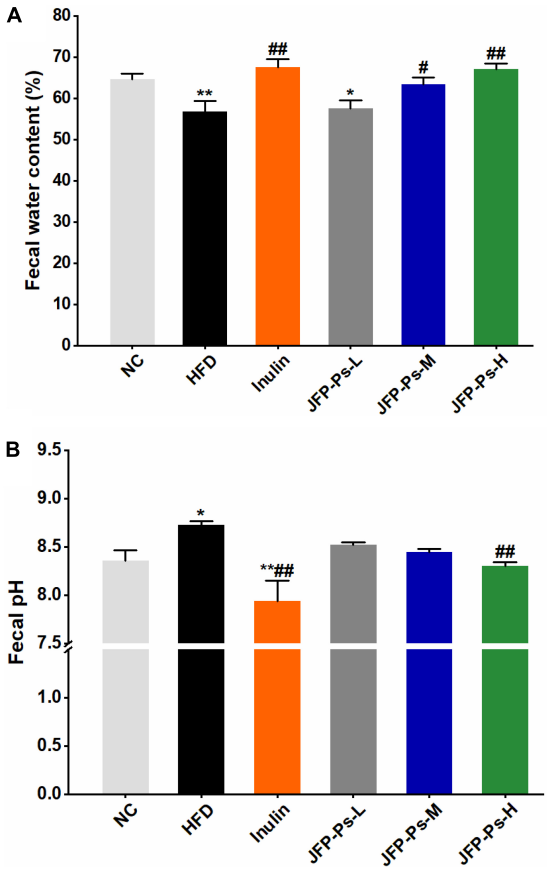

FIGURE 1
Effect of JFP-Ps on fecal water content **(A)** and fecal pH value **(B)** in obese rats. Data are expressed as mean ± SEM ($n = 6$ for each group) and analyzed using one-way ANOVA. *$p < 0.05$, **$p < 0.01$ compared to the NC group; $^{\#}p < 0.05$, $^{\#\#}p < 0.01$ compared with the HFD group.

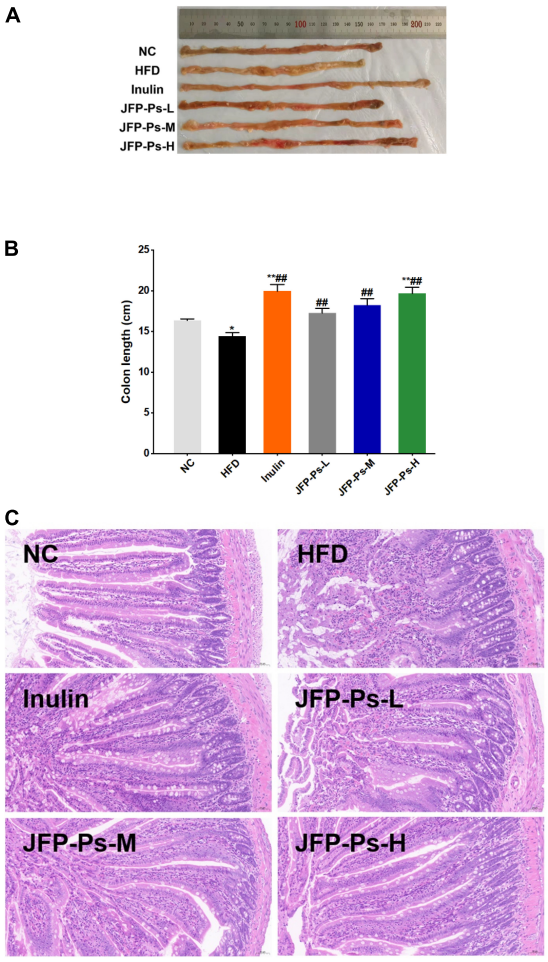

FIGURE 2
Effect of JFP-Ps on colon length and intestinal micromorphology in obese rats. **(A)** Representatives of colonic tissue in each group, **(B)** colon length, **(C)** jejunal micromorphology (original magnification 20X). Data are expressed as mean ± SEM (n = 6 for each group) and analyzed using one-way ANOVA. *$p < 0.05$, **$p < 0.01$ compared to the NC group; $^{\#\#}p < 0.01$ compared with the HFD group.

and a clear demarcation between the submucosa and the muscular layer. In the HFD group, the mucosal layer of jejunum was disorganized; the shape of the villi was not clear; and the tips of the villi were mixed and accompanied by severe inflammatory infiltration, with cup-shaped cells visible only at the base of the villi. Comparison to the HFD group, the jejunum of the JFP-Ps-L group and JFP-Ps-M group showed clearer structure, with the villi gradually becoming clearer in shape and more uniformly arranged, with less mixing of the villi apices and less inflammatory infiltration, and a gradual increase in the distribution of cupped cells within the columnar epithelium. The morphology and structure of the jejunal tissue in the JFP-Ps-H group was similar to that in the NC group, but the length and number of villi increased. Moreover, villi were more closely arranged; the volume of the intestinal lumen decreased; more cup-shaped cells were distributed within the columnar epithelium and the thickness of the mucosal layer increased. The results showed that JFP-Ps restored intestinal mucosal damage induced by a high-fat diet in obese rats, increased the thickness of the mucus layer and protected the barrier function of the intestinal mucosa, which in turn had a positive effect on intestinal health.

Effects of JFP-Ps on antioxidant activities in colon

As shown in Table 2, in comparison to the NC group, the activities of SOD, GSH-Px, and CAT in the HFD group were decreased and the content of MDA in the HFD group was increased ($p < 0.01$). Compared with HFD group, JFP-Ps treatment increased the activities of SOD, GSH-Px and CAT, and the activities of GSH-Px increased significantly ($p < 0.01$). Moreover, JFP-Ps decreased the content of MDA significantly ($p < 0.01$). The results indicated that JFP-Ps may alleviate oxidative damage in the colon of obese rats and improve integrity of the intestinal epithelium by enhancing the activities of antioxidant enzymes in the colon.

Effects of JFP-Ps on inflammation-related indicators in colon

As shown in Table 3, the MPO activity in the HFD group was significantly increased ($p < 0.05$), and the contents of pro-inflammatory cytokines (TNF-α, IL-1β, and IL-6) increased, and the content of anti-inflammatory cytokine (IL-10) decreased, compared to that in the NC group. However, compared with HFD group, the MPO activity in the JFP-Ps group was significantly decreased ($p < 0.01$), the contents of pro-inflammatory cytokines were decreased in a dose-dependent manner, and the level of the anti-inflammatory cytokine was increased. The results indicated that JFP-Ps may decrease the inflammation in the colon of obese rats induced by high-fat diet.

Effects of JFP-Ps on glucose transport in the small intestine

As shown in Figure 3, SGLT1 activity in the small intestine of rats from the HFD group was decreased compared with the NC group. The JFP-Ps intervention reduced SGLT1 activity in HFD group. The results showed that JFP-Ps may inhibit glucose transport in the small intestine by reducing SGLT1 activity in the intestinal epithelium of obese rats.

TABLE 2 Effect of JFP-Ps on antioxidant activities in the colon of obese rats.

Group	SOD (U/mL)	GSH-Px (nmol/mL)	CAT (μ mol/mL)	MDA (nmol/mL)
NC	39.64 ± 2.57	97.35 ± 3.91	117.16 ± 18.75	2.47 ± 0.17
HFD	22.72 ± 2.28	54.92 ± 2.38**	77.48 ± 2.72	3.85 ± 0.10**
Inulin	33.40 ± 1.59	109.12 ± 3.54##	104.28 ± 17.24	2.44 ± 0.14##
JFP-Ps-L	25.08 ± 9.18	96.73 ± 1.63##	98.42 ± 15.27	2.94 ± 0.45#
JFP-Ps-M	30.24 ± 8.80	108.34 ± 4.32##	113.46 ± 32.90	2.06 ± 0.18##
JFP-Ps-H	34.68 ± 3.05	105.87 ± 5.33##	115.53 ± 12.86	1.80 ± 0.06##

Data are presented as mean ± SEM ($n = 6$). **$p < 0.01$ compared to the NC group; #$p < 0.05$, ##$p < 0.01$ compared with the HFD group.

TABLE 3 Effect of JFP-Ps on inflammation-related factors in the colon of obese rats.

Group	MPO (U/L)	TNF-α (ng/L)	IL-1β (ng/L)	IL-6 (pg/mL)	IL-10 (ng/L)
NC	50.74 ± 0.71	82.25 ± 6.29	5.55 ± 0.12	29.68 ± 0.70	6.70 ± 1.53
HFD	58.10 ± 3.44*	89.87 ± 12.44	6.30 ± 0.54	36.98 ± 5.73	4.21 ± 0.33
Inulin	47.71 ± 2.11#	81.89 ± 1.56	4.91 ± 0.30#	32.12 ± 2.75	6.34 ± 0.30
JFP-Ps-L	46.67 ± 2.61##	83.32 ± 8.35	5.67 ± 0.12	32.39 ± 5.24	5.67 ± 0.60
JFP-Ps-M	46.63 ± 2.68##	73.92 ± 4.03	5.59 ± 0.41	27.88 ± 2.90	5.79 ± 0.95
JFP-Ps-H	45.70 ± 1.32##	72.37 ± 0.95	5.24 ± 0.37	26.44 ± 1.85	5.86 ± 0.26

Data are presented as mean ± SEM ($n = 6$). *$p < 0.05$ compared to the NC group; #$p < 0.05$, ##$p < 0.01$ compared with the HFD group.

Effects of JFP-Ps on the expression of gut barrier function-related genes in small intestine

The levels of TNF-α and IL-6 mRNA expression were significantly increased in the small intestine of the HFD group, and the gene expression levels of GPR41 and GPR43 were slightly down-regulated (Figures 4A–D). Interestingly, treatment with JFP-Ps decreased the expression of TNF-α and IL-6, while increased the gene expression of GPR43 and GPR41 in a dose-dependent manner. These results showed that JFP-Ps may inhibit inflammation and enhance immune function in the small intestine of obese rats.

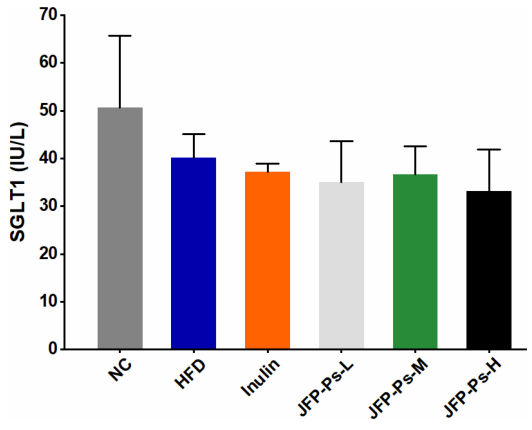

FIGURE 3
Effect of JFP-Ps on SGLT1 activity in small intestinal tissues. Data are expressed as mean ± SEM ($n = 6$ for each group) and analyzed using one-way ANOVA. No significant difference was observed.

Effects of JFP-Ps on the protein expression level of occludin in small intestine

Western blot analysis showed that protein expression level of occludin in the HFD group was significantly lower than the NC group ($p < 0.01$) (Figures 4E,F). JFP-Ps significantly increased the protein expression of occludin in a concentration-dependent manner ($p < 0.01$). The result showed that JFP-Ps may enhance mechanical barrier function in the small intestine.

Discussion

Intestine is the largest digestive and immune organ in the body, provides a favorable and anaerobic environment for microbial colonization and performs an important role in nutrient absorption, detoxification and immune regulation (2, 3). Intestinal dysfunction is closely associated with obesity and other related metabolic diseases (19, 20). Natural polysaccharides could prevent and treat intestinal diseases caused by various factors *via* restoring intestinal barrier function (21). The results of this study indicated that JFP-Ps possessed a protective effect on the intestine *via* improving intestinal barrier function and alleviating intestinal inflammation.

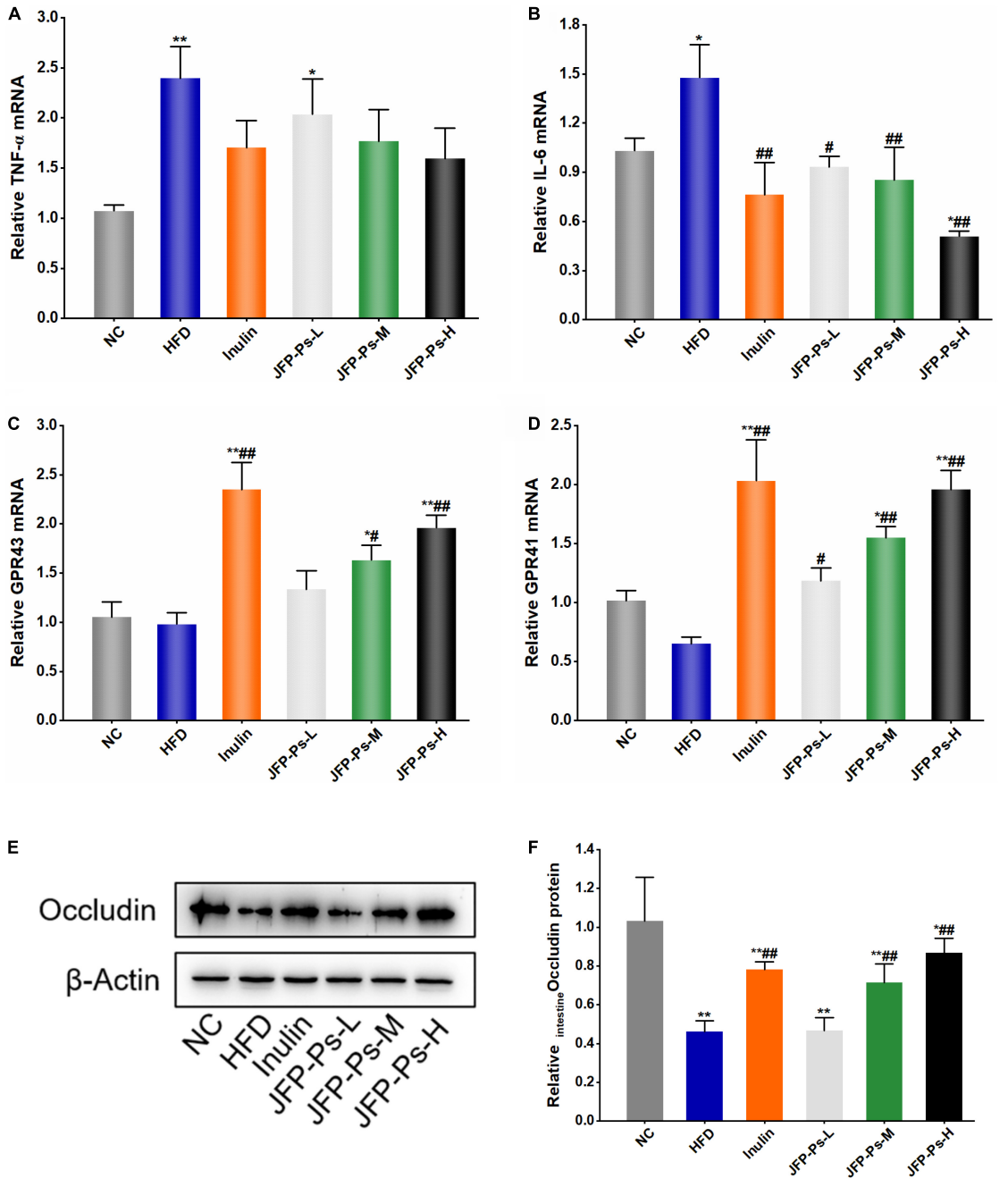

FIGURE 4
Effect of JFP-Ps on the expression of inflammatory genes, free fatty acid receptor genes and tight junction protein in the small intestine of obese rats. **(A)** TNF-α, **(B)** IL-6, **(C)** GPR43, **(D)** GPR41, **(E)** protein expression of occludin, **(F)** relative band intensities of occludin. Data are expressed as mean ± SEM (n = 6 for each group) and analyzed using one-way ANOVA. $^{*}p < 0.05$, $^{**}p < 0.01$ compared to the NC group; $^{\#}p < 0.05$, $^{\#\#}p < 0.01$ compared with the HFD group.

The higher water content in the feces is accompanied by an increase in the volume and looseness of the feces, which facilitates the body's bowel movements (22). A high water content in feces also indicates a high moisture environment in the intestine, which may help the exchange and transport of substances and the intestinal mucus layer in dissolving mucins, immune factors, electrolytes, etc., thus maintaining the integrity of the intestinal mucosal layer and the balance of osmotic pressure and protecting the intestinal barrier (23–25). In addition, water in the intestinal lumen enters the enterocytes in the villi by osmosis, causing the cells to swell and the tissue to thicken, leading to spontaneous bending of adjacent

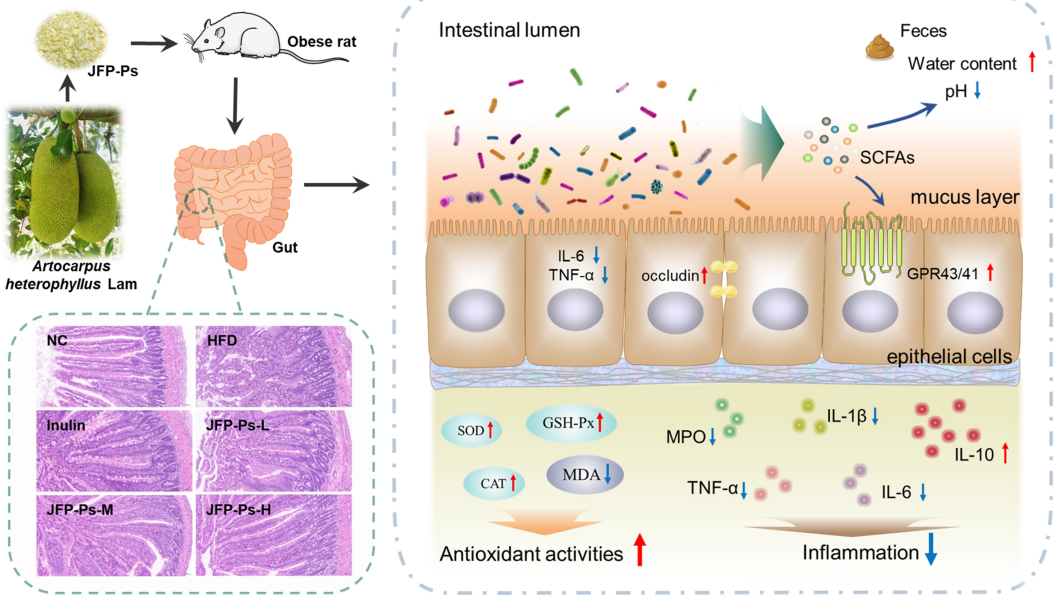

FIGURE 5
The beneficial effects of JFP-Ps on intestinal barrier function in high fat diet-induced obese rats.

tissue, promoting the formation of crypt foci in the intestine, and reducing the lumen volume (26). Do et al. (27) reported that polysaccharide fraction from greens of *Raphanus sativus* increased water content in the feces of obese mice induced by high-fat diet. JFP-Ps increased the water-holding capacity of feces and promoted the body's bowel movements, implying that the intake of JFP-Ps may contribute to the integrity of the intestinal mucosal layer, formation of the crypt, and protection of the intestinal barrier.

The pH value of the intestinal contents is an important parameter in measuring intestinal health (28). An increased intestinal pH value is associated with a decrease in the abundance of probiotic bacteria (such as *Lactobacillus* and *Bifidobacterium*) and an increase in the abundance of pathogenic bacteria. Oligosaccharides were fermented by intestinal microorganisms to produce SCFAs, lowering intestinal pH value and promoting the growth of probiotic bacteria (29). In the study, JFP-Ps was found to decrease intestinal pH value, suggesting that JFP-Ps may be fermented by intestinal microorganisms to produce SCFAs, creating an acidic intestinal environment, inhibiting the growth of harmful bacteria, promoting the growth of probiotic bacteria and the balance of intestinal flora, thereby enhancing the biological barrier function of the intestine in the obese rats. The results were consistent with our previous study (16).

The colon acts as an important site for absorbing water and salt from food residues and provides a habitat for intestinal flora. Dietary fibers are fermented in the colon, and the timing and effect of fermentation is influenced by the growth state of the colon (30). The colon length may be shortened due to intestinal diseases. However, the butyric acid produced by intestinal probiotics (e.g., *Lactobacillus*, *Bifidobacterium*, etc.) from the fermentation of dietary polysaccharides provides 60–70% energy for the colon cells, promoting the regeneration and growth of colon epithelial cells, which in turn increases colon length (30, 31). Polysaccharide fraction from greens of *Raphanus sativus* was reported to increase colon length and restore intestinal barrier function in high-fat diet induced obese mice (27). In the study, JFP-Ps increased colon length in a dose-dependent manner, restored intestinal mucosal damage and increased the thickness of the mucus layer in obese rats induced by a high-fat diet, suggesting that JFP-Ps may enhance intestinal barrier function and reduce the risk of intestinal diseases.

The antioxidant enzymes SOD, GSH-Px and CAT constitute the body's enzymatic antioxidant system, play an important role in protecting the body from oxidative damage, and are regarded as the first line of defense against oxidative damage (32). MDA is a product of lipid peroxidation in tissues and organs, and its level reflects the degree of tissue damage. A high-fat diet causes oxidative damage in the body and promotes the development of obesity. Wang et al. (7) reported that walnut green husk polysaccharides could prevent colonic oxidative stress and inflammation damage caused by high-fat diets. Our previous study has found that JFP-Ps exhibited a strong free radical scavenging activity (14). Consistent with these reports, JFP-Ps increased the activities of SOD, GSH-Px and CAT and decreased the content of MDA, suggesting that JFP-Ps may maintain the integrity of intestinal epithelium by increasing

the activities of antioxidant enzymes in the colon of obese rats induced by a high-fat diet.

Weakening of the intestinal mucosal barrier allows a large number of foreign antigens to enter the intestinal wall, inducing an inflammatory response in the gut and accumulation of inflammatory cells and inflammatory cytokines, and triggering an immune response and damage (33). MPO is a hemoglobin enriched in neutrophils, and MPO activity was used to reflect neutrophil aggregation and tissue inflammation. TNF-α, IL-1β and IL-6 are typical pro-inflammatory cytokines that promote the inflammatory cascade; IL-10 is an anti-inflammatory cytokine that inhibits the inflammatory response. Liu et al. (34) reported that *Rheum tanguticum* polysaccharide significantly reduced MPO activity in the colonic mucosa of rats with colitis. A polysaccharide purified from *Arctium lappa* inhibited the increase of pro-inflammatory factors in the colon of mice with colitis (35). *Angelica sinensis* polysaccharide increased IL-10 level in the colon of rats with immune colonic injury (36). Consistent with these reports, JFP-Ps decreased the contents of TNF-α, IL-1β and IL-6, and increased the content of IL-10, suggesting that JFP-Ps may alleviate colonic inflammation in high-fat diet-induced obesity rats.

SGLT1 is a key transporter mainly expressed in small intestinal tissues, which involved in glucose absorption in the intestinal lumen, and closely associated with metabolic diseases, such as obesity and diabetes (37). In obese patients with type 2 diabetes, the overexpression of SGLT1 caused an abnormal increase in blood glucose in the body (38). Inhibition of SGLT1 expression can reduce glucose absorption in small intestine, the escaped glucose transferred into the large intestine and fermented to produce SCFAs, which in turn reduces the occurrence of obesity and type 2 diabetes (37, 39). Consistent with the previous study, JFP-Ps reduced SGLT1 activity in the intestinal epithelial cells of obese rats, suggesting that JFP-Ps may alleviate the development of obesity.

The expression levels of TNF-α and IL-6 in small intestinal tissues may reflect the inflammatory status of small intestinal tissues in obese rats. Han et al. (40) found that polysaccharide from *Gracilaria Lemaneiformise* reduced intestinal inflammation and prevented colitis in mice by decreasing the levels of pro-inflammatory factors in the mouse colon. GPR41 and GPR43 is a group of free fatty acid receptors that are activated by SCFAs. Intestinal microbes can ferment indigestible dietary fiber to produce SCFAs, which in turn activate GPR41 and GPR43, and mediate immune function in the small intestine (41–43). Consistent with these reports, our results showed that JFP-Ps down-regulated the expression of pro-inflammatory genes (TNF-α, IL-6), up-regulated the expression of GPR41 and GPR43. These results suggested that JFP-Ps could alleviate inflammation and enhance immune barrier function of the small intestine in obese rats *via* inhibiting the expression of pro-inflammatory genes and activating SCFA- and GPR41/GPR43-related signaling pathways in the small intestine of obesity rats.

Occludin is a tight junction protein and is believed to be directly involved in the barrier and fence functions of tight junctions (44). Occludin has been identified as an important component of the intestinal mechanical barrier and regulates macromolecule flux across the intestinal epithelial tight junction barrier (45). Sang et al. (46) reported that polysaccharide from sporoderm-broken spore of *Ganoderma lucidum* up-regulated the expression of occludin protein in the ileum of mice fed with high-fat diet. In line with this report, JFP-Ps increased the protein expression of occludin in a concentration-dependent manner, suggesting that JFP-Ps may enhance mechanical barrier function in the small intestine of obese rats.

Conclusion

In conclusion, JFP-Ps exhibited a protective effect on intestinal function and was beneficial to intestinal health. As shown in **Figure 5**, JFP-Ps promoted bowel movements and modified intestinal physiochemical environment by lowering fecal pH value and increasing fecal water content. Meanwhile, JFP-Ps was found to increase the length of the colon, alleviate oxidative damage of the colon, relieve intestinal colonic inflammation, and inhibit glucose transport in the small intestine. In addition, JFP-Ps repaired intestinal mucosal damage, and increased the thickness of the mucus layer. The potential mechanism of JFP-Ps improved intestinal barrier functions involved in inhibiting the expression of the inflammatory genes (TNF-α, IL-6), promoting the expression of the tight junction protein (occludin), and activating SCFA-GPR41/GPR43 related signaling pathways. Our findings would provide theoretical support for the development of JFP-Ps as a promising phytochemical to improve human health.

Data availability statement

The data presented in this study are included in the article/**Supplementary material**, further inquiries can be directed to the corresponding authors.

Ethics statement

This animal study was approved by the Animal Ethics Committee of Hainan Medical University.

Author contributions

SZ, JC, KZ, QL, and LT designed the experiments. SZ and YC conducted the experiments. CL, GW, XC, and FX analyzed the data. SZ, JC, KZ, and LT wrote and revised the manuscript and gave the final approval. All authors contributed to the article and approved the submitted version.

Funding

This work was financially supported by the National Natural Science Foundation of China (No. 31901649) and the Central Public-interest Scientific Institution Basal Research Fund for Chinese Academy of Tropical Agricultural Sciences (No. 1630142022009).

Acknowledgments

We are grateful to Wuhan Servicebio Technology Co., Ltd., and Shanghai Majorbio Bio-Pharm Technology Co., Ltd., (Shanghai, China) for their outstanding technical assistance they provided.

Conflict of interest

The authors declare that the research was conducted in the absence of any commercial or financial relationships that could be construed as a potential conflict of interest.

The handling editor declared a shared parent affiliation with the several authors KZ and LT at the time of review.

Publisher's note

Supplementary material

The Supplementary Material for this article can be found online at: https://www.frontiersin.org/articles/10.3389/fnut.2022.1035619/full#supplementary-material

References

1. Sekirov, I, Russell SL, Antunes LCM, Finlay BB. Gut microbiota in health and disease. *Physiol Rev.* (2009) 90:859–904. doi: 10.1152/physrev.00045.2009

2. Liska DJ. The detoxification enzyme systems. *Altern Med Rev.* (1998) 3:187–98.

3. Zhou CB, Zhou YL, Fang JY. Gut microbiota in cancer immune response and immunotherapy. *Trends Cancer.* (2021) 7:647–60. doi: 10.1016/j.trecan.2021.01.010

4. Wu YB, Wan JW, Choe U, Pham Q, Schoene NW, He Q, et al. Interactions between food and gut microbiota: impact on human health. *Annu Rev Food Sci Technol.* (2019) 10:389–408. doi: 10.1146/annurev-food-032818-121303

5. Zhang GY, Nie SP, Huang XJ, Hu JL, Cui SW, Xie MY, et al. Study on dendrobium officinale o-acetyl-glucomannan (dendronan). 7. improving effects on colonic health of mice. *J Agr Food Chem.* (2016) 64:2485–91. doi: 10.1021/acs.jafc.5b03117

6. Huang YL, Chau CF. Improvement in intestinal function of hamsters as influenced by consumption of polysaccharide-rich sage weed extracts. *Food Chem.* (2012) 133:1618–23. doi: 10.1016/j.foodchem.2012.02.062

7. Wang GL, Yang XY, Wang J, Zhong DY, Zhang RG, Zhang YN, et al. Walnut green husk polysaccharides prevent obesity, chronic inflammatory responses, nonalcoholic fatty liver disease and colonic tissue damage in high-fat diet fed rats. *Int J Biol Macromol.* (2021) 182:879–98. doi: 10.1016/j.ijbiomac.2021.04.047

8. Xie SZ, Liu B, Ye HY, Li QM, Pan LH, Zha XQ, et al. Dendrobium huoshanense polysaccharide regionally regulates intestinal mucosal barrier function and intestinal microbiota in mice. *Carbohyd Polym.* (2019) 206:149–62. doi: 10.1016/j.carbpol.2018.11.002

9. Huo JY, Wu ZY, Sun WZ, Wang ZH, Wu JH, Huang MQ, et al. Protective effects of natural polysaccharides on intestinal barrier injury: a review. *J Agr Food Chem.* (2022) 70:711–35. doi: 10.1021/acs.jafc.1c05966

10. Min FF, Wan YJ, Nie SP, Xie MY. Study on colon health benefit of polysaccharide from *Cyclocarya paliurus* leaves in vivo. *J Funct Foods.* (2014) 11:203–9. doi: 10.1016/j.jff.2014.10.005

11. Wang XY, Yin JY, Nie SP, Xie MY. Isolation, purification and physicochemical properties of polysaccharide from fruiting body of *Hericium erinaceus* and its effect on colonic health of mice. *Int J Biol Macromol.* (2018) 107:1310–9. doi: 10.1016/j.ijbiomac.2017.09.112

12. Gao H, Zhang WC, Wu ZY, Wang HY, Hui AL, Meng L, et al. Preparation, characterization and improvement in intestinal function of polysaccharide fractions from okra. *J Funct Foods.* (2018) 50:147–57. doi: 10.1016/j.jff.2018.09.035

13. Tan YF, Li HF, Lai WY, Zhang JQ. Crude dietary polysaccharide fraction isolated from jackfruit enhances immune system activity in mice. *J Med Food.* (2013) 16:663–8. doi: 10.1089/jmf.2012.2565

14. Zhu KX, Zhang YJ, Nie SP, Xu F, He SZ, Gong D, et al. Physicochemical properties and in vitro antioxidant activities of polysaccharide from *Artocarpus heterophyllus* lam. pulp. *Carbohyd Polym.* (2017) 155:354–61. doi: 10.1016/j.carbpol.2016.08.074

15. Zhu KX, Yao SW, Zhang YJ, Liu QB, Xu F, Wu G, et al. Effects of in vitro saliva, gastric and intestinal digestion on the chemical properties, antioxidant activity of polysaccharide from *Artocarpus heterophyllus* lam. (Jackfruit) pulp. *Food Hydrocolloid.* (2019) 87:952–9. doi: 10.1016/j.foodhyd.2018.09.014

16. Zhu KX, Fan HF, Zeng SJ, Nie SP, Zhang YJ, Tan LH, et al. Polysaccharide from *Artocarpus heterophyllus* lam. (jackfruit) pulp modulates gut microbiota composition and improves short-chain fatty acids production. *Food Chem.* (2021) 364:130434. doi: 10.1016/j.foodchem.2021.130434

17. Thøgersen R, Castro-Mejía JL, Kræmer Sundekilde U, Hansen LH, Gray N, Kuhnle G, et al. Inulin and milk mineral fortification of a pork sausage exhibits distinct effects on the microbiome and biochemical activity in the gut of healthy rats. *Food Chem.* (2020) 331:127291. doi: 10.1016/j.foodchem.2020.127291

18. Massot-Cladera M, Azagra-Boronat I, Franch À, Castell M, Rodríguez-Lagunas MJ, Pérez-Cano FJ. Gut health-promoting benefits of a dietary supplement of vitamins with inulin and acacia fibers in rats. *Nutrients.* (2020) 12:2196. doi: 10.3390/nu12082196

19. Winer DA, Winer S, Dranse HJ, Lam TKT. Immunologic impact of the intestine in metabolic disease. *J Clin Invest.* (2017) 127:33–42. doi: 10.1172/JCI88879

20. Khan S, Luck H, Winer S, Winer DA. Emerging concepts in intestinal immune control of obesity-related metabolic disease. *Nat Commun.* (2021) 12:2598. doi: 10.1038/s41467-021-22727-7

21. Ma S, Xu JX, Lai T, Xu WN, Zhang J, Zhang HC, et al. Inhibitory effect of fermented flammulina velutipes polysaccharides on mice intestinal inflammation. *Front Nutr.* (2022) 9:934073. doi: 10.3389/fnut.2022.934073

22. Roberfroid M. Dietary fiber, inulin, and oligofructose: a review comparing their physiological effects. *Crit Rev Food Sci Nutr.* (1993) 33:103–48. doi: 10.1080/10408399309527616

23. Okazaki Y, Katayama T. Dietary phytic acid modulates characteristics of the colonic luminal environment and reduces serum levels of proinflammatory cytokines in rats fed a high-fat diet. *Nutr Res.* (2014) 34:1085–91. doi: 10.1016/j.nutres.2014.09.012

24. Da Silva JK, Cazarin CBB, Bogusz Junior S, Augusto F, Maróstica Junior MR. Passion fruit (*Passiflora edulis*) peel increases colonic production of short-chain fatty acids in wistar rats. *LWT Food Sci Technol.* (2014) 59:1252–7. doi: 10.1016/j.lwt.2014.05.030

25. Hughes MR. Regulation of salt gland, gut and kidney interactions. Comparative biochemistry and physiology. *Comput Biochem Physiol Mol Integr Physiol.* (2003) 136:507–24. doi: 10.1016/j.cbpb.2003.09.005

26. Yang QT, Xue SL, Chan CJ, Rempfler M, Vischi D, Maurer-Gutierrez F, et al. Cell fate coordinates mechano-osmotic forces in intestinal crypt formation. *Nat Cell Biol.* (2021) 23:733–44. doi: 10.1038/s41556-021-00700-2

27. Do MH, Lee HB, Oh MJ, Jhun H, Choi SY, Park HY. Polysaccharide fraction from greens of *Raphanus sativus* alleviates high fat diet-induced obesity. *Food Chem.* (2021) 343:128395. doi: 10.1016/j.foodchem.2020.128395

28. Chung YC, Hsu CK, Ko CY, Chan YC. Dietary intake of xylooligosaccharides improves the intestinal microbiota, fecal moisture, and pH value in the elderly. *Nutr Res.* (2007) 27:756–61. doi: 10.1016/j.nutres.2007.09.014

29. Mehta S, Huey SL, McDonald D, Knight R, Finkelstein JL. Nutritional interventions and the gut microbiome in children. *Annu Rev Nutr.* (2021) 41:479–510. doi: 10.1146/annurev-nutr-021020-025755

30. Jädert C, Phillipson M, Holm L, Lundberg JO, Borniquel S. Preventive and therapeutic effects of nitrite supplementation in experimental inflammatory bowel disease. *Redox Biol.* (2013) 2:73–81. doi: 10.1016/j.redox.2013.12.012

31. Rivière A, Selak M, Lantin D, Leroy F, De Vuyst L. Bifidobacteria and butyrate-producing colon bacteria: importance and strategies for their stimulation in the human gut. *Front Microbiol.* (2016) 7:979. doi: 10.3389/fmicb.2016.00979

32. Wang XY, Yin JY, Hu JL, Nie SP, Xie MY. Gastroprotective polysaccharide from natural sources: review on structure, mechanism, and structure-activity relationship. *Food Front.* (2022) 172:1–32. doi: 10.1002/fft2.172

33. Korzenik JR, Podolsky DK. Evolving knowledge and therapy of inflammatory bowel disease. *Nat Rev Drug Discov.* (2006) 5:197–209. doi: 10.1038/nrd1986

34. Liu L, Guo ZJ, Lv ZG, Sun Y, Cao W, Zhang R, et al. The beneficial effect of *Rheum tanguticum* polysaccharide on protecting against diarrhea, colonic inflammation and ulceration in rats with TNBS-induced colitis: the role of macrophage mannose receptor in inflammation and immune response. *Int Immunopharmacol.* (2008) 8:1481–92. doi: 10.1016/j.intimp.2008.04.013

35. Wang Y, Zhang NF, Kan J, Zhang X, Wu XN, Sun R, et al. Structural characterization of water-soluble polysaccharide from *Arctium lappa* and its effects on colitis mice. *Carbohydr Polym.* (2019) 213:89–99. doi: 10.1016/j.carbpol.2019.02.090

36. Liu SP, Dong WG, Wu DF, Luo HS, Yu JP. Protective effect of angelica sinensis polysaccharide on experimental immunological colon injury in rats. *World J Gastroenterol.* (2003) 9:2786–90. doi: 10.3748/wjg.v9.i12.2786

37. Lehmann A, Hornby PJ. Intestinal SGLT1 in metabolic health and disease. *Am J Physiol Gastrointest Liver Physiol.* (2016) 310:G887–98. doi: 10.1152/ajpgi.00068.2016

38. Zambrowicz B, Ding ZM, Ogbaa I, Frazier K, Banks P, Turnage A, et al. Effects of LX4211, a dual SGLT1/SGLT2 inhibitor, plus sitagliptin on postprandial active GLP-1 and glycemic control in type 2 diabetes. *Clin Ther.* (2013) 35:273. doi: 10.1016/j.clinthera.2013.01.010

39. Zhang YJ, Xie QT, You LJ, Cheung PC, Zhao ZG. Behavior of non-digestible polysaccharides in gastrointestinal tract: a mechanistic review of its anti-obesity effect. *eFood.* (2021) 2:59–72. doi: 10.2991/efood.k.210310.001

40. Han R, Wang L, Zhao ZG, You LJ, Pedisić S, Kulikouskaya V, et al. Polysaccharide from gracilaria lemaneiformis prevents colitis in Balb/c mice via enhancing intestinal barrier function and attenuating intestinal inflammation. *Food Hydrocolloid.* (2020) 109:106048. doi: 10.1016/j.foodhyd.2020.106048

41. Brown AJ, Goldsworthy SM, Barnes AA, Eilert MM, Tcheang L, Daniels D, et al. The orphan G protein-coupled receptors GPR41 and GPR43 are activated by propionate and other short chain carboxylic acids. *J Biol Chem.* (2003) 278:11312–9. doi: 10.1074/jbc.M211609200

42. Kimura I, Ichimura A, Ohue-Kitano R, Igarashi M. Free fatty acid receptors in health and disease. *Physiol Rev.* (2020) 100:171–210. doi: 10.1152/physrev.00041.2018

43. Kim MH, Kang SG, Park JH, Yanagisawa M, Kim CH. Short-chain fatty acids activate GPR41 and GPR43 on intestinal epithelial cells to promote inflammatory responses in mice. *Gastroenterology.* (2013) 145:e1–10. doi: 10.1053/j.gastro.2013.04.056

44. Saitou M, Fujimoto K, Doi Y, Itoh M, Fujimoto T, Furuse M, et al. Occludin-deficient embryonic stem cells can differentiate into polarized epithelial cells bearing tight junctions. *J Cell Biol.* (1998) 141:397–408. doi: 10.1083/jcb.141.2.397

45. Saitoh Y, Suzuki H, Tani K, Nishikawa K, Irie K, Ogura Y, et al. Tight junctions. Structural insight into tight junction disassembly by *Clostridium perfringens* enterotoxin. *Science.* (2015) 347:775–8. doi: 10.1126/science.1261833

46. Sang TT, Guo CJ, Guo DD, Wu JJ, Wang YJ, Wang Y, et al. Suppression of obesity and inflammation by polysaccharide from sporoderm-broken spore of *Ganoderma lucidum* via gut microbiota regulation. *Carbohydr Polym.* (2021) 256:117594. doi: 10.1016/j.carbpol.2020.117594

frontiers | Frontiers in Nutrition

TYPE Original Research
PUBLISHED 17 November 2022
DOI 10.3389/fnut.2022.1012348

OPEN ACCESS

EDITED BY
Jianhua Xie,
Nanchang University, China

REVIEWED BY
Hua-Min Liu,
Henan University of Technology, China
Kit Leong Cheong,
Shantou University, China
Ying Lan,
Northwest A&F University, China

*CORRESPONDENCE
Guoli Li
liguoli929@163.com
Xudan Guo
guoxudan123@126.com

SPECIALTY SECTION
This article was submitted to Food Chemistry, a section of the journal Frontiers in Nutrition

RECEIVED 05 August 2022
ACCEPTED 25 October 2022
PUBLISHED 17 November 2022

CITATION
Ji X, Wang Z, Hao X, Zhu Y, Lin Y, Li G and Guo X (2022) Structural characterization of a new high molecular weight polysaccharide from jujube fruit.
Front. Nutr. 9:1012348.
doi: 10.3389/fnut.2022.1012348

Structural characterization of a new high molecular weight polysaccharide from jujube fruit

Xiaolong Ji[1], Zhiwen Wang[1,2], Xiyu Hao[3], Yingying Zhu[1], Yan Lin[1], Guoli Li[2]* and Xudan Guo[4]*

[1]College of Food and Bioengineering, Zhengzhou University of Light Industry, Henan Key Laboratory of Cold Chain Food Quality and Safety Control, Henan Collaborative Innovation Center for Food Production and Safety, Zhengzhou, China, [2]Chongqing Key Laboratory of Development and Utilization of Genuine Medicinal Materials in Three Gorges Reservoir Area, Chongqing Three Gorges Medical College, Chongqing, China, [3]Heilongjiang Feihe Dairy Co., Ltd., Beijing, China, [4]Basic Medical College, Hebei University of Chinese Medicine, Hebei Higher Education Institute Applied Technology Research Center on TCM Formula Preparation, Hebei TCM Formula Preparation Technology Innovation Center, Shijiazhuang, China

From *Ziziphus Jujuba* cv. *Muzao* fruit, a new polysaccharide (PZMP3-1) with high molecular weight was isolated. Constructional characterization revealed that PZMP3-1 comprized 2.56 rhamnose, 7.70 arabinoses, 3.73 galactose, and 6.73 galactose, and it has a 241 kDa average molecular weight. The principal structural components of PZMP3-1 were 1,2,4 and 1,4-linked Gal*p*A, 1,4-linked Gal*p*, 1,3 and 1,5-linked Ara*f*, and 1-linked Rha*p* based on methylation and nuclear magnetic resonance spectroscopy (NMR) analyses. X-ray diffraction (XRD), Fourier transforms infrared spectroscopy (FT-IR), atomic force microscopy (AFM), and scanning electron microscopy (SEM) structural analysis of PZMP3-1 revealed a tangled and branching pattern. Overall, these structural results suggested that PZMP3-1 could have unique bioactivities and be widely used in nutritional supplements.

KEYWORDS

jujube, high-molecular-weight polysaccharide, structural characterization, NMR, GC-MS

Introduction

Recent studies have investigated the biological effects of polysaccharides (PZMP3-1) that include their abilities to suppress free radicals and exert anti-bacterial, anti-cancer, anti-tumor, anti-coagulant, anti-viral, and immunological effects, etc., (1, 2). The chemical composition and structural characteristics of polysaccharides could determine their biological effects (3). Numerous studies have demonstrated that sulfation produces excellent physiological effects that support health maintenance and disease prevention (4).

The fruit of *Ziziphus Jujuba* Mill., often known as jujube, is called Jujubae Fructus and is known by the Chinese names Dazao or Hongzao (5, 6). Jujube

has been demonstrated as anti-oxidant, anti-provocative, anti-microbial, anti-cancer, cardiovascular, gastrointestinal protective, anti-HIV, neuroprotective, sedative-hypnotic, anxiolytic, and other bioactivities *in vitro* and *in vivo* technological research, demonstrating the fruit's pharmacological potential (7, 8). Bioactive metabolites are responsible for these actions, containing polysaccharides, oligosaccharides, saponins, cyclopeptide alkaloids, minerals, triterpenoid acids, vitamins, and flavonoids, which are thought to be the distinctive and functional elements of the jujube fruit (9, 10).

The origin of *Z. jujuba* cv. *Muzao* fruit is mainly from Lüliang Shanxi Province and Yulin Shaanxi Province of China (11). Polysaccharides were found in jujube's pharmacological components and have been linked to various health benefits, such as immunomodulation, anti-cancer, anti-oxidation, hypoglycemic, hepatoprotective, and gastrointestinal protection (12, 13). Numerous investigations on low molecular weight polysaccharides have emphasized their structural characteristics and pharmacological activities (14–16). Jujube polysaccharides with molecular weights varying between 10^4 and 10^6 Da have been detected in various experimental conditions, and these polysaccharides demonstrated anti-oxidant activities (2, 17). From *Z. jujuba* cv. *Jinsixiaozao*, the polysaccharides (four fractions) have *Mw* values ranging from 86 to 160 kDa, according to Li et al. (18, 19). However, the higher molecular weight fraction of *Z. jujuba* cv. *Muzao* polysaccharides is not present.

In the current study, from *Z. jujuba*, isolation and purification of a unique polysaccharide with high molecular weight, was given the designation PZMP3-1. The structural conformation and physicochemical properties of PZMP3-1 were detected by model analytical instruments [gas chromatography (GC), high-performance gel permeation chromatography (HPGPC), Fourier transforms infrared spectroscopy (FT-IR), methylation analysis, X-ray diffraction (XRD), nuclear magnetic resonance spectroscopy (NMR), atomic force microscopy (AFM), and scanning electron microscopy (SEM)]. The eventual objective of this research could be to offer a new scientific understanding of the composition of polysaccharides from jujube.

Materials and methods

Materials

Ziziphus Jujuba cv. *Muzao* fruit was donated by Shaanxi Loess Plateau Experimental Orchard (China). GE Healthcare Life Sciences (Piscataway, NJ, USA) provided the Sephacryl S-300 gels and anion-exchange DEAE Sepharose Fast Flow. Sigma-Aldrich Co., Ltd (Sigma, St Louis, MO, USA) provided the standard monosaccharides. The analytical grade was used for all other compounds and reagents.

PZMP3-1's isolation and purification

From *Z. jujuba* cv. *Muzao*, the unprocessed polysaccharides (ZMP) were isolated by water extraction, deproteinized, decolorized, precipitated by ethanol, and freeze-dried, as shown by the method of Ji et al. (20). The dissolved ZMP in deionized water was centrifuged and then filtered the supernatant through a membrane (0.45 μm), a 2.6 × 100 cm diethylaminoethyl (DEAE)-Sepharose Fast Flow column eluted with 0.3 M NaCl was loaded with ZMP. On a 2.6 × 100 cm Sephacryl S-300 column that was equilibrated with distilled water, a separated fraction was pooled, desalted, and further purified. PZMP3-1 and PZMP3-2 were pale yellow powders and derived from the fractions of the prominent peaks collected, concentrated, dialyzed, and lyophilized to get different parts (21). For further structural characterization, the PZMP3-1 fraction was employed.

Analysis of chemical composition

The method (phenol-sulfuric acid) detected the total amount of carbohydrates in PZMP3-1, with glucose serving as the reference (22). Bradford's technique assessed the protein content, with bovine serum albumin as the reference (23). The Folin-Ciocalteu test assessed the total phenolic content (24). At room temperature, the UV-vis spectra of the PZMP3-1 (1.0 mg/ml) in the wavelength (200–400 nm) were captured using a spectrophotometer (25).

Mw determination and monosaccharide analysis

The high-performance liquid chromatography (HPLC) measurement of PZMP3-1's *Mw* was detected on an Agilent instrument (LC 1200, USA) with a 7.8 × 300 mm TSK-gel G3000PWxl column. Using a calibration curve, the *Mw* concerning dextran was calculated (26).

Utilizing a collection of monosaccharides as a standard, the Shimadzu GC (2014 C) with a high-performance capillary column DB-17 (30 ml × 0.25 mm ID; 0.25 μm film thickness, Agilent) measured the various monosaccharide by comparing retention durations and peak regions (27).

FT-IR and NMR analysis

PZMP3-1 was combined with 100 mg of potassium bromide (KBr) powder before being crushed into granules for

infrared spectral measurement between 4,000 and 400 cm^{-1}. A spectrophotometer was used to measure the FT-IR spectra of polysaccharide (VERTEX 70, Bruker, Germany) (28).

To replace exchangeable protons, the freeze-dehydrated PZMP3-1 (50 mg) was dissolved in 2 ml of 99.9% D_2O and freeze-dried three times. A Bruker-600 MHz NMR Spectrometer (Bruker, Rheinstetten, Germany) was used to record the one-dimensional NMR spectra for the ^{1}H and ^{13}C at 25°C. Using the standard Bruker NMR software, data were collected and examined (21).

Methylation analysis

As described in previous studies (29), PZMP3-1 was methylated, followed by hydrolysis, reduction, and acetylation, to analyze glycosyl bonds. The measurement of partially methylated alder aldehyde using gas chromatography/mass spectrometry (GC-MS) requires the use of GCMS-QP2010 Ultra apparatus and a DB-17MS capillary column (60.0 m × 0.25 mm × 0.25 μ m).

Analysis of the molecular structure

PZMP3-1 used the XRD pattern to determine the crystal structure present. The angular range of the diffractometer was 5–50° (2θ), the step size was 0.01°, the scan speed was 15°/min, and tube pressure (40 kV) and tube flow (40 mA) were present. Using an SEM (S-4800, Japan), the morphological characteristics of PZMP3-1 were documented. We used the Cressington 208 HR Sputtering Coater with sputtering gold samples. We dissolved the polysaccharides with distilled water and dried the test samples dripping on the mica carrier surface at ambient pressure of 70°C. A 5500 atomic force microscope (Agilent) was used to create the AFM images (30).

Data analysis

Version 17.0 of SPSS was used for the statistical analysis. The data were reported as mean ± standard deviation (SD), with Duncan's multiple-range test ($p < 0.05$) arriving after the analysis of variance (ANOVA) for each experiment, which was carried out in triplicate.

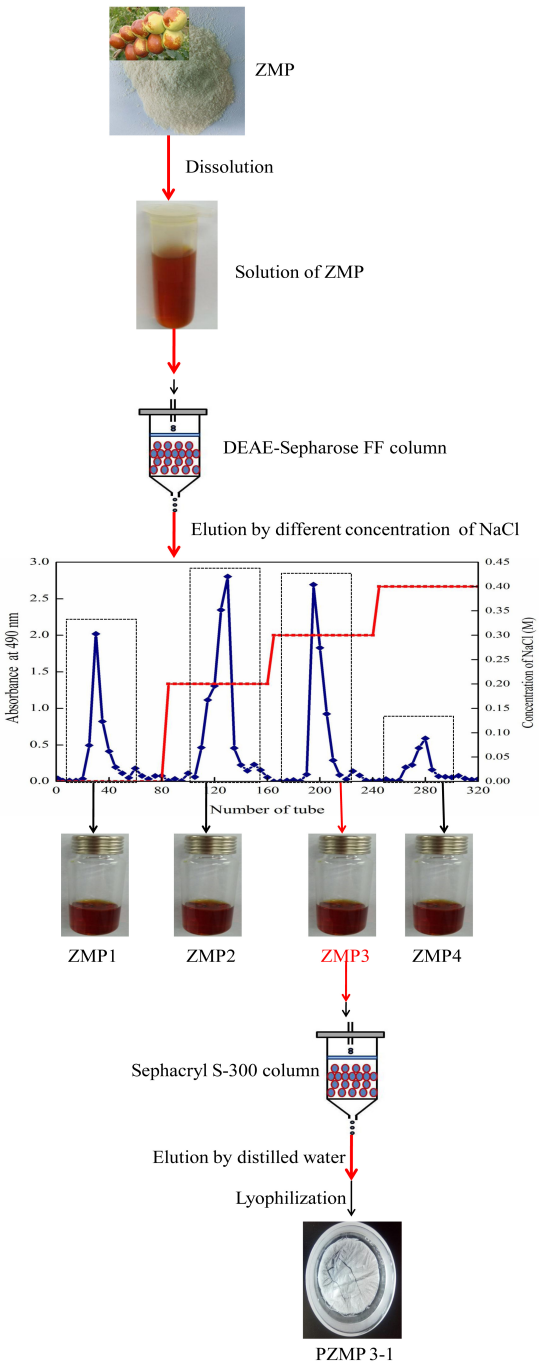

FIGURE 1
The PZMP3-1's separation flow diagram.

Results and discussion

PZMP3-1's extraction and purification

In the current study, the yield of about 3.82% of the fruit of the *Z. jujuba* cv. *Muzao* was used to produce crude ZMP. On a Sepharose Fast Flow column (DEAE), the ZMP was separated using 0.3 M NaCl solution (**Figure 1**). This fraction was then further purified using Sephacryl S-300 columns and yielded 3.04% of PZMP3-1, the same as the neutral polysaccharide PZMP1 from *Z. jujuba* cv. (2.95%) (31).

Characterization of preliminary PZMP3-1

The number of carbohydrates in PZMP3-1, followed by the phenol-sulfuric acid method, was 95.35 ± 1.25%. The result was different with *Z. jujuba* cv. *Hamidazao* polysaccharides which Yang et al. reported that only 0.32% polyphenol and 2.11% protein were found (14). **Figure 2A** demonstrates that the lack of nucleic acids and proteins is shown by PZMP3-1's UV spectrum (there is no absorption at 260–280 nm), which is in line with the research of chemical analysis as previously reported (32).

Determination of Mw and monosaccharide compositions of PZMP3-1

Biological activity depends on the *Mw* distribution of plant polysaccharides (33). The *Mw* of PZMP3-1 was determined to be 241 kDa based on the calibration curve of standards, which corresponded to a retention period of 17.10 min and might indicate a higher molecular weight polysaccharide. Li et al. observed that from *Z. jujuba* cv. *Jinsixiaozao*, the molecular weights of four polysaccharide fractions (ZSP1b, ZSP2, ZSP3c, and ZSP4b) varied between 86 and 160 kDa (19), and Cui et al. showed that Fructus Jujubae polysaccharides consisted mainly of low molecular weight (83.8 and 123.0 kDa) fractions (34). The PZMP3-1 obtained in this study significantly exceeded the polysaccharide *Mw* shown in previous studies. The *Mw* of *Z. jujuba* polysaccharide obtained by each research group was different. This may be due to the variety, extraction, purification process, and test method (13, 35).

The PMP-GC technique was used to examine the monosaccharides content of PZMP3-1. Rhamnose, arabinose, galactose, and galacturonic acid made up most of PZMP3-1, with the molar ratios being 2.56:7.70:3.73:6.73, with arabinose and galacturonic acid making up the most significant amount when compared to other monosaccharides, according to the monosaccharide standards. Previous reports (HJP1, the ratio of mannose to galacturonic acid to rhamnose to galactose to glucose to arabinose, was 1.3:6.7:27.6:13:3.7:47.6 and HJP3 was 0.6:16.7:16:21:6.5:39.2) reported by Wang et al. could be used to confirm the polysaccharide molar ratio and monosaccharide content found in *Z. jujuba* cv. *Dongzao* (36), which had rhamnose, arabinose, galactose, glucose, and xylose ratios of 1.0:3.6:1.0:0.5:0.2 (37) and had results that were distinct from those of PZMP3-1 in this work. The varietals, production conditions, and measurement techniques might play a role in the monosaccharide composition of jujube polysaccharides (13, 14).

FT-IR spectra of PZMP3-1

Detecting distinctive organic groups in polysaccharides using FT-IR spectroscopy is a powerful technique (38, 39). The primary functional groups of plant polysaccharides may be better understood using the FT-IR spectrum. The FT-IR spectra showed that PZMP3-1 contained the typical absorption peaks of plant polysaccharides (**Figure 2B**; 40). Stretching vibration (O-H) caused the characteristic peak at 3,431 cm^{-1}, and stretching vibration (C-H) caused the rise at 2,935 cm^{-1} (41). They were regarded as the defining bands for polymers comprized of plant polysaccharides because of their two significant absorption peaks. Stretching vibrations (carboxylic groups) were connected to the absorption peak at 1,741 cm^{-1} (29). PZMP3-1's absorption peak at 1,616 cm^{-1} showed that symmetrical stretching vibrations (C = O) were present (42). The bands in the 1,415 cm^{-1} likely represented the bending and deformation of C-OH and C-H vibrations, respectively (43). The intense bands at 1,099 and neighboring 1,000 cm^{-1} revealed the pyranose form of galactosyl residues (44).

Methylation analysis of PZMP3-1

Less information about the detailed structure of jujube's high molecular weight polysaccharides is available in the literature, especially the glycosidic bond types. Methylation analysis could determine the kind and number of glycosidic linkages in plant polysaccharide polymers (45). To determine PZMP3-1's glycosidic bond types by GC-MS analysis, it was methylated, hydrolyzed, reduced, and converted into partially methylated alditol acetates (PMAAs) (46). The linkage patterns of PZMP3-1 were compiled, which are shown in **Table 1**, using a spectral database based on the PMAA standard date in the Complex Carbohydrate Research Center (CCRC) spectrum database, retention duration, and relevant literature. Six different methylated sugar derivatives were found, i.e., 1,2,4 and 1,4-linked Gal*p*A, 1,4-linked Gal*p*, 1,3 and 1,5-linked Ara*f*, and 1-linked Rha*p*. The composition of monosaccharides and PZMP3-1 was discovered using methylation analysis (45). NMR spectra provided additional evidence supporting the structure of PZMP3-1.

PZMP3-1's NMR analysis

To understand the structural characteristics of PZMP3-1, ^{1}H and ^{13}C NMR spectra (one-dimensional) were identified and resolved. The five residues of PZMP3-1 that GC-MS isolated were given chemical shifts (**Table 2**) based on 1D spectra (**Figure 3**) and information from the literature. Five anomeric signals were present in the ^{1}H and ^{13}C NMR spectra (**Figures 3A,B**) at 3.70–5.25 ppm and 60–110 ppm,

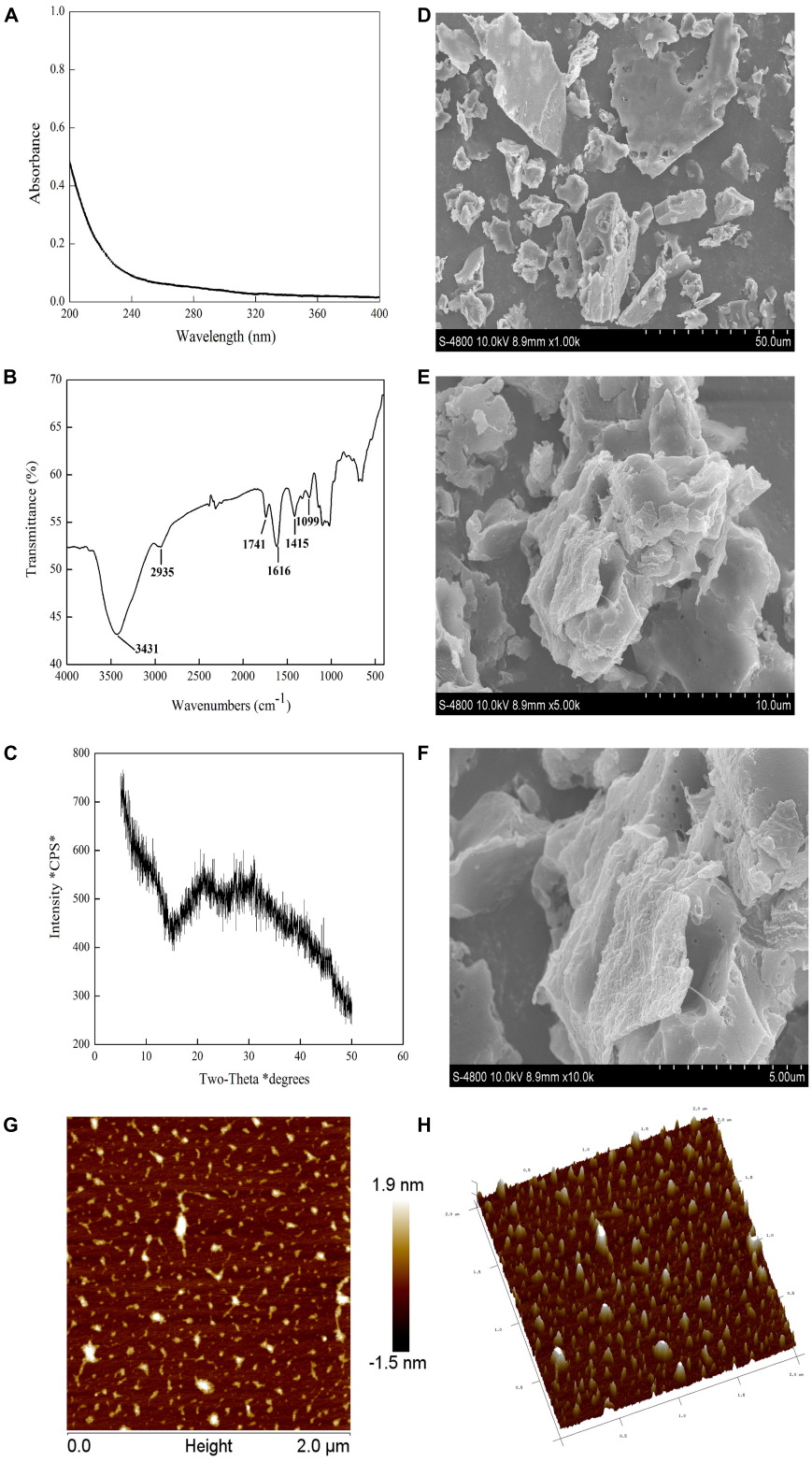

FIGURE 2
PZMP3-1's physicochemical analysis. **(A)** The X-ray diffraction (XRD) pattern. **(B)** The spectrum of UV-vis. **(C)** The spectrum of Fourier transforms infrared spectroscopy (FT-IR). **(D,E)** Scanning electron microscopy (SEM) images [×1,000 in panel **(D)**, ×5,000 in panel **(E)**, and ×10,000 in panel **(F)**]. **(G)** Atomic force microscopy (AFM) images; **(H)** a three-dimensional image of AFM.

TABLE 1 PZMP3-1's methylation analysis results.

Peak no.	Residues	Retention time (min)	Methylated sugars	Linkage patterns	Relative amount (mol%)
1		40.086	2,3,4-Me_3-Rha*p*	Rha*p*-(1→	7.45
2	C	40.245	2,4,5-Me_3-Ara*f*	→3)-Ara*f*-(1→	5.72
3	D	41.437	2,3-Me_2-Ara*f*	→5)-Ara*f*-(1→	39.75
4	E	63.049	2,3,6-Me_3-Gal*p*	→4)-Gal*p*-(1→	16.5
5	A	65.037	2,4,6-Me_3-Gal*p*A	→4)-Gal*p*A-(1→	22.93
6	B	66.250	3,6-Me_2-Gal*p*A	→2,4)-Gal*p*A-(1→	7.65

TABLE 2 PZMP3-1's ^{1}H and ^{13}C nuclear magnetic resonance spectroscopy (NMR) data.

Residues	Linkage		1	2	3	4	5	6
C	→3)-Ara*f*-(1→	C	107.53	82.26	84.04	86.79	63.93	
		H	5.12	4.28	4.18	3.98	3.92	
D	→5)-Ara*f*-(1→	C	109.35	82.26	79.06	86.79	68.34	
		H	5.12	4.28	4.17	3.99	3.93	
E	→4)-Gal*p*-(1→	C	100.52	70.56	80.96	72.01	74.39	63.67
		H	4.94	3.71	4.50	4.07	4.77	3.85
A	→4)-Gal*p*A-(1→	C	103.39	68.08	71.26	81.37	73.49	170.91
		H	5.21	3.77	4.08	4.42	4.80	
B	→2,4)-Gal*p*A-(1→	C	103.39	70.62	71.98	81.37	73.49	171.01
		H	5.21	3.97	4.10	4.42	4.80	

respectively. The primary anomeric proton signals in PZMP3-1 were identified as A, B, C, D, and E in the ^{1}H NMR spectra at 5.21, 5.21, 5.12, 5.12, and 4.94.

In the ^{1}H NMR spectrum, residues C-2, 3, 4, and 5's protons received chemical shifts between 3.7 and 4.28. Five anomeric signals were resonated at 103.39, 103.39, 107.53, 109.35, and 100.52 after labeling the corresponding signal (allogeneic carbon) tagged in the ^{13}C NMR spectra. Based on findings from the literature, Table 2 displays the results; the signals of all the tagged residues in the ^{1}H and ^{13}C NMR spectra are assigned. The heteropoly proton of residue A's chemical shift caused the signal at δH 5.21, and in the heterogeneous carbon, the corresponding signal was seen at δC 103.39. The signals were created by the residue A's C-2, 3, 4, 5, and 6 at δC 68.08/δH 3.77, δC 71.26/δH 4.08, δC 73.49/δH 4.80, and δC 170.91, respectively. According to the NMR data, this residue A's chemical shifts were the same as those of →4)-Gal*p*A-(1→ (17). Similar to how residue B was identified as →2,4)-Gal*p*A-(1→, the signals at δC 2 70.62/δH 2 3.97, δC 3 71.98/δH 3 4.10, and δC 6 171.01 matched the residue B (anomeric carbons and protons) (47).

Ara*f* was initially given credit for the cross-peak in the anomeric area at 107–110 ppm (residues C and D). The chemical shifts of H-1, 2, 3, 4, and 5 were determined from the ^{1}H spectra at 5.12, 4.28, 4.18, 3.98, and 3.92 ppm, respectively (Figure 3A), in agreement with previous reports. From the proton chemical shifts in the C spectra, the carbon chemical shifts of the residue C from C-1, 2, 3, 4, and 5 were found (Table 2). The carbons and anomeric protons of residue D were identified by the signals at δC-1 109.35/δH-1 5.12, δC-3 79.06/δH-3 4.17, and δC-5 68.34/δH-5 3.93. These outcomes corroborated FT-IR and methylation analysis results, demonstrating that residues C/D were (1→3)-linked Ara*f*/(1→5)-linked Ara*f* (29, 31). According to the NMR data, the similar alternate signals for carbon and hydrogen were 100.52 (4.94), 70.56 (3.71), 80.96 (4.50), 72.01 (4.07), 74.39 (4.77), and 63.67 (3.85), this residue's chemical changes were the same as those of 1,4-linked Gal*p* (48, 49).

Morphological properties of PZMP3-1

It is generally known that plant polysaccharides could be crystallized using XRD technology (50). Figure 2C depicts the X-ray diffraction pattern of PZMP3-1. PZMP3-1 had a prominent peak that appeared at around 20 and 30°, and its X-ray diffraction curves were "bun-shaped" (30, 51). The semicrystalline structure we obtained earlier could explain that PZMP3-1 might have some semicrystalline structures (an abundant polysaccharide in galacturonic acid from *Z. jujuba* cv. *Muzao*) (21, 52).

The findings of the SEM analysis of PZMP3-1's surface morphology are shown in Figures 2D–F. PZMP3-1 was formed in an aggregation condition with an unsteady surface. The formation of intermolecular and intramolecular hydrogen bonds between polysaccharides requires the polysaccharide to have a higher molecular weight (30, 53).

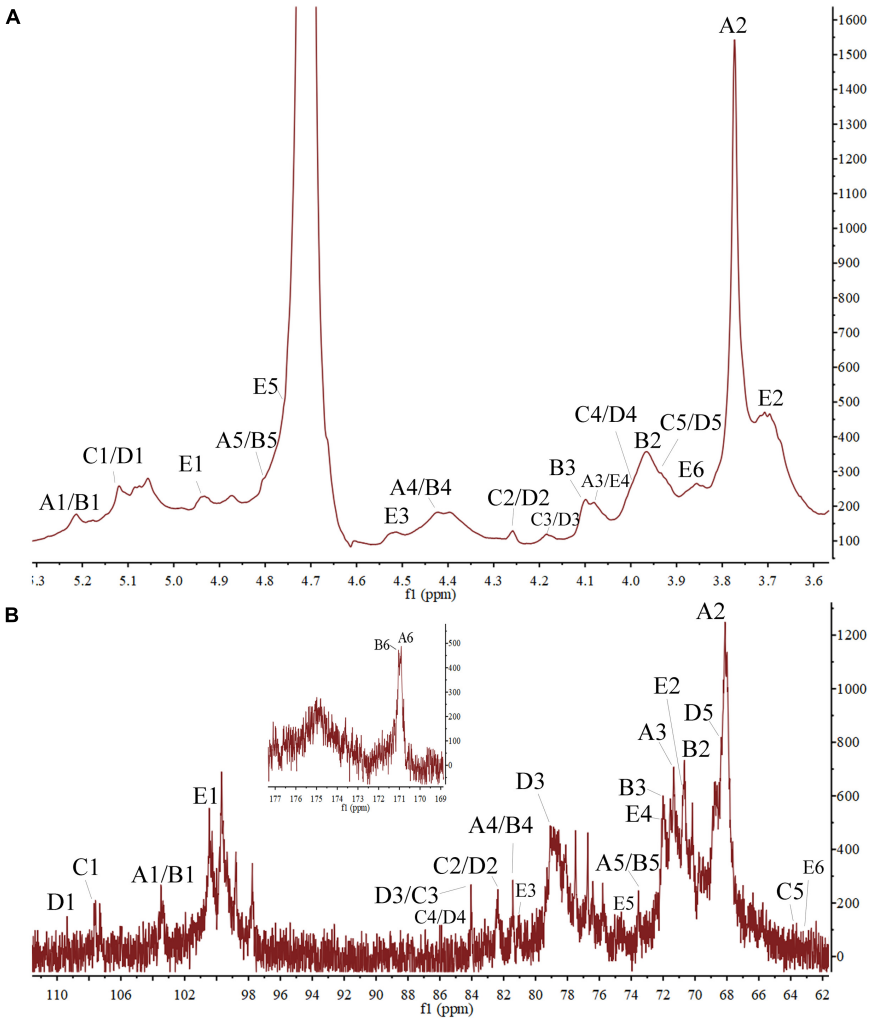

FIGURE 3
The PZMP3-1's nuclear magnetic resonance spectroscopy (NMR) spectra in D_2O. **(A)** ^{1}H spectrum. **(B)** ^{13}C spectrum.

For this reason, PZMP3-1 revealed a tangled structure that is folded with each other.

Observing the three-dimensional structure of biologically active macromolecules requires using AFM and nanoscale microstructures, especially the form of plant polysaccharides (54, 55). PZMP3-1's 3-dimensional and planar AFM pictures are displayed in **Figures 2G,H**, respectively. PZMP3-1 had a linear or branched structure, and the chain of PZMP3-1 featured a helical shape. PZMP3-1 aggregation might be explained by intermolecular and intramolecular hydrogen bonding on its surface, which acted as a catalyst to produce the potent intramolecular and intermolecular connections and the interactions with the water molecule (56, 57). Considering these morphological traits, we could conclude that the entangled and branched structure existed in PZMP3-1 molecules, which could significantly affect the bioactivity, structure, and distribution.

Conclusion

In the current work, *Z. jujuba* cv. *Muzao* fruit was used to create a new polysaccharide PZMP3-1 with high molecular weight, and its characteristics were elucidated through physicochemical and experimental investigations using modern analytical instruments. Rhamnose, galactose, arabinose, and galacturonic acid were the main components of PZMP3-1, which was 241 kDa in weight and had a molar ratio of 2.56:3.73:7.70:6.73. PZMP3-1's primary linkage types included →2,4)-Gal*p*A-(1→, →4)-Gal*p*A-(1→, →4)-Gal*p*-(1→, →5)-Ara*f*-(1→, →3)-Ara*f*-(1→ and Rha*p*-(1→ based on the findings of the methylation and NMR analyses. According to studies on chain conformation, PZMP3-1 was entangled with itself. The biological functions of PZMP3-1 and the links between its structure and activity are the subject of in-depth research.

Data availability statement

The original contributions presented in this study are included in the article/supplementary material, further inquiries can be directed to the corresponding authors.

Author contributions

XJ was involved in the study's idea, design, and funding. ZW and XH set the database into order. YZ and YL wrote the initial draft of the document. XG participated in writing – review and editing. GL provided funding for this manuscript. All authors approved and reviewed the article's submission.

Funding

This work was supported by the National Natural Science Foundation of China (32201969 and 82204668), Hebei Natural Science Foundation (H2022423376), Young and Middle-Aged Top Talent Project in Chongqing Three Georges Medical College, Chongqing Talent Project (cstc2022ycjh-bgzxm0226), Natural Science Foundation of Henan Province (212300410297), the Basic Research Plan of Higher Education School Key Scientific Research Project of Henan Province (21A550014), the Doctoral Research Foundation of Zhengzhou University of Light Industry (2020BSJJ015), and the Science and Technology Research Project of Higher Education in Hebei Province (QN2020233) are all acknowledged.

Conflict of interest

Author XH was employed by company Heilongjiang Feihe Dairy Co., Ltd.

The remaining authors declare that the research was conducted in the absence of any commercial or financial relationships that could be construed as a potential conflict of interest.

Publisher's note

References

1. Kadam SU, Tiwari BK, O'Donnell CP. Extraction, structure and biofunctional activities of laminarin from brown algae. *Int J Food Sci Technol.* (2015) 50:24–31. doi: 10.1111/ijfs.12692

2. Li J, Shang W, Si X, Bu D, Strappe P, Zhou Z, et al. Carboxymethylation of corn bran polysaccharide and its bioactive property. *Int J Food Sci Technol.* (2017) 52:1176–84. doi: 10.1111/ijfs.13382

3. Zong A, Cao H, Wang F. Anticancer polysaccharides from natural resources: a review of recent research. *Carbohydrate Polymers.* (2012) 90:1395–410. doi: 10.1016/j.carbpol.2012.07.026

4. Wang J, Hu S, Nie S, Yu Q, Xie M. Reviews on mechanisms of in vitro antioxidant activity of polysaccharides. *Oxidative Med Cell Longevity.* (2016) 2016:1–13. doi: 10.1155/2016/5692852

5. Liu S, Lv Y, Tang Z, Zhang Y, Xu H, Zhang D, et al. *Ziziphus jujuba* mill., a plant used as medicinal food: a review of its phytochemistry, pharmacology, quality control and future research. *Phytochemistry Rev.* (2021) 2s0:507–41. doi: 10.1007/s11101-020-09709-1

6. Ji X, Hou C, Gao Y, Xue Y, Yan Y, Guo X. Metagenomic analysis of gut microbiota modulatory effects of jujube (*Ziziphus jujuba* mill.) polysaccharides in a colorectal cancer mouse model. *Food Function.* (2020) 11:163–73. doi: 10.1039/C9FO02171J

7. Lu Y, Bao T, Mo J, Ni J, Chen W. Research advances in bioactive components and health benefits of jujube (*Ziziphus jujuba* mill.) fruit. *J Zhejiang Univ Sci B.* (2021) 22:431–49. doi: 10.1631/jzus.B2000594

8. Chen J, Tsim KW. Review of edible jujube, the *Ziziphus jujuba* fruit: a heath food supplement for anemia prevalence. *Front Pharmacol.* (2020) 11:593655. doi: 10.3389/fphar.2020.593655

9. Wang M, Gao Q, Shen J, Wang X, Ji X. The jujube (*Ziziphus jujuba* mill.) fruit: a review of current knowledge of fruit composition and health benefits. *J Agric Food Chem.* (2013) 61:3351–63. doi: 10.1021/jf4007032

10. Rashwan AK, Karim N, Shishir MRI, Bao T, Lu Y, Chen W. Jujube fruit: a potential nutritious fruit for the development of functional food products. *J Funct Foods.* (2020) 75:104205. doi: 10.1016/j.jff.2020.104205

11. Zhang L, Liu X, Wang Y, Liu G, Zhang Z, Zhao Z, et al. In vitro antioxidative and immunological activities of polysaccharides from *Zizyphus jujuba* cv. Muzao. *Int J Biol Macromol.* (2017) 95:1119–25. doi: 10.1016/j.ijbiomac.2016.10.102

12. Xie J, Tang W, Jin M, Li J, Xie M. Recent advances in bioactive polysaccharides from *Lycium barbarum* L., *Zizyphus jujuba* mill, *Plantago* spp., and morus spp.: structures and functionalities. *Food Hydrocolloids.* (2016) 60:148–60. doi: 10.1016/j.foodhyd.2016.03.030

13. Ji X, Peng Q, Yuan Y, Shen J, Xie X, Wang M. Isolation, structures and bioactivities of the polysaccharides from jujube fruit (*Ziziphus jujuba* mill.): a review. *Food Chem.* (2017) 227:349–57. doi: 10.1016/j.foodchem.2017.01.074

14. Yang Y, Qiu Z, Li L, Vidyarthi SK, Zheng Z, Zhang R. Structural characterization and antioxidant activities of one neutral polysaccharide and three acid polysaccharides from *Ziziphus jujuba* cv. hamidazao: a comparison. *Carbohydrate Polymers.* (2021) 261:117879. doi: 10.1016/j.carbpol.2021.117879

15. Zhu Y, He Z, Bao X, Wang M, Yin S, Song L, et al. Purification, in-depth structure analysis and antioxidant stress activity of a novel pectin-type polysaccharide from *Ziziphus Jujuba* cv. Muzao residue. *J Funct Foods.* (2021) 80:104439. doi: 10.1016/j.jff.2021.104439

16. Ji X, Hou C, Yan Y, Shi M, Liu Y. Comparison of structural characterization and antioxidant activity of polysaccharides from jujube (*Ziziphus jujuba* Mill.) fruit. *Int J Biol Macromol.* (2020) 149:1008–18. doi: 10.1016/j.ijbiomac.2020.02.018

17. Ji X, Hou C, Shi M, Yan Y, Liu Y. An insight into the research concerning *Panax ginseng* CA meyer polysaccharides: a review. *Food Rev Int.* (2022) 38:1149–65. doi: 10.1080/87559129.2020.1771363

18. Li J, Fan L, Ding S. Isolation, purification and structure of a new water-soluble polysaccharide from *Zizyphus jujuba* cv. jinsixiaozao. *Carbohydrate Polymers.* (2011) 83:477–82. doi: 10.1016/j.carbpol.2010.08.014

19. Li J, Liu Y, Fan L, Ai L, Shan L. Antioxidant activities of polysaccharides from the fruiting bodies of *Zizyphus jujuba* cv. jinsixiaozao. *Carbohydrate Polymers.* (2011) 84:390–4. doi: 10.1016/j.carbpol.2010.11.051

20. Ji X, Cheng Y, Tian J, Zhang S, Jing Y, Shi M. Structural characterization of polysaccharide from jujube (*Ziziphus jujuba* mill.) fruit. *Chem Biol Technol Agric.* (2021) 8:1–7. doi: 10.1186/s40538-021-00255-2

21. Ji X, Yan Y, Hou C, Shi M, Liu Y. Structural characterization of a galacturonic acid-rich polysaccharide from *Ziziphus jujuba* cv. Muzao. *Int J Biol Macromol.* (2020) 147:844–52. doi: 10.1016/j.ijbiomac.2019.09.244

22. Dubois M, Gilles KA, Hamilton JK, Rebers PAT, Smith F. Colorimetric method for determination of sugars and related substances. *Analy Chem.* (1956) 28:350–6. doi: 10.1021/ac60111a017

23. Bradford MM. A rapid and sensitive method for the quantitation of microgram quantities of protein utilizing the principle of protein-dye binding. *Analy Biochem.* (1976) 72:248–54. doi: 10.1016/0003-2697(76)90527-3

24. Guo Y, Deng G, Xu X, Wu S, Li S, Xia E, et al. Antioxidant capacities, phenolic compounds and polysaccharide contents of 49 edible macro-fungi. *Food Funct.* (2012) 3:1195–205. doi: 10.1039/C2FO30110E

25. He B, Zheng Q, Guo L, Huang J, Yun F, Huang S, et al. Structural characterization and immune-enhancing activity of a novel high-molecular-weight polysaccharide from *Cordyceps militaris*. *Int J Biol Macromol.* (2020) 145:11–20. doi: 10.1016/j.ijbiomac.2019.12.115

26. Liu X, Liu H, Yan Y, Fan L, Yang J, Wang X, et al. Structural characterization and antioxidant activity of polysaccharides extracted from jujube using subcritical water. *LWT Food Sci Technol.* (2020) 117:108645. doi: 10.1016/j.lwt.2019.108645

27. Wang X, Zhang L, Wu J, Xu W, Wang X, Lü X. Improvement of simultaneous determination of neutral monosaccharides and uronic acids by gas chromatography. *Food Chem.* (2017) 220:198–207. doi: 10.1016/j.foodchem.2016.10.008

28. Wang L, Zhao Z, Zhao H, Liu M, Lin C, Li L, et al. Pectin polysaccharide from flos magnoliae (xin yi, magnolia biondii pamp. flower buds): hot-compressed water extraction, purification and partial structural characterization. *Food Hydrocolloids.* (2022) 122:107061. doi: 10.1016/j.foodhyd.2021.107061

29. Ji X, Zhang F, Zhang R, Liu F, Peng Q, Wang M. An acidic polysaccharide from *Ziziphus jujuba* cv. Muzao: purification and structural characterization. *Food Chem.* (2019) 274:494–9. doi: 10.1016/j.foodchem.2018.09.037

30. Tan M, Zhao Q, Zhao B. Physicochemical properties, structural characterization and biological activities of polysaccharides from quinoa (*Chenopodium quinoa* willd.) seeds. *Int J Biol Macromol.* (2021) 193:1635–44. doi: 10.1016/j.ijbiomac.2021.10.226

31. Ji X, Liu F, Peng Q, Wang M. Purification, structural characterization, and hypolipidemic effects of a neutral polysaccharide from *Ziziphus jujuba* cv. Muzao. *Food Chem.* (2018) 245:1124–30. doi: 10.1016/j.foodchem.2017.11.058

32. Jia X, Zhang C, Qiu J, Wang L, Bao J, Wang K, et al. Purification, structural characterization and anticancer activity of the novel polysaccharides from *Rhynchosia minima* root. *Carbohydrate Polymers.* (2015) 132:67–71. doi: 10.1016/j.carbpol.2015.05.059

33. Ji X, Peng B, Ding H, Cui B, Nie H, Yan Y. Purification, structure and biological activity of pumpkin polysaccharides: a review. *Food Rev Int.* (2021) 2021:1–13. doi: 10.1080/87559129.2021.1904973

34. Cui G, Zhang W, Wang Q, Zhang A, Mu H, Bai H, et al. Extraction optimization, characterization and immunity activity of polysaccharides from fructus jujubae. *Carbohydrate Polymers.* (2014) 111:245–55. doi: 10.1016/j.carbpol.2014.04.041

35. Hou C, Yin M, Lan P, Wang H, Nie H, Ji X. Recent progress in the research of angelica sinensis (oliv.) diels polysaccharides: extraction, purification, structure and bioactivities. *Chem Biol Technol Agric.* (2021) 8:1–14. doi: 10.1186/s40538-021-00214-x

36. Wang Y, Liu X, Zhang J, Liu G, Liu Y, Wang K, et al. Structural characterization and in vitro antitumor activity of polysaccharides from *Zizyphus jujuba* cv. Muzao. *RSC Adv.* (2015) 5:7860–7. doi: 10.1039/C4RA13350A

37. Zhao Z, Liu M, Tu P. Characterization of water soluble polysaccharides from organs of Chinese jujube (*Ziziphus jujuba* mill. cv. Dongzao). *Eur Food Res Technol.* (2008) 226:985–9. doi: 10.1007/s00217-007-0620-1

38. He Y, Liu C, Chen Y, Ji A, Shen Z, Xi T, et al. Isolation and structural characterization of a novel polysaccharide prepared from *Arca subcrenata* lischke. *J Biosci Bioeng.* (2007) 104:111–6. doi: 10.1263/jbb.104.111

39. Yang C, He N, Ling X, Ye M, Zhang C, Shao W, et al. The isolation and characterization of polysaccharides from longan pulp. *Separation Purificat Technol.* (2008) 63:226–30. doi: 10.1016/j.seppur.2008.05.004

40. Gao X, Qi J, Ho C, Li B, Xie Y, Chen S, et al. Purification, physicochemical properties, and antioxidant activities of two low-molecular-weight polysaccharides from *Ganoderma leucocontextum* fruiting bodies. *Antioxidants.* (2021) 10:1145. doi: 10.3390/antiox10071145

41. Wang M, Chen G, Chen D, Ye H, Sun Y, Zeng X, et al. Purified fraction of polysaccharides from *Fuzhuan brick* tea modulates the composition and metabolism of gut microbiota in anaerobic fermentation in vitro. *Int J Biol Macromol.* (2019) 140:858–70. doi: 10.1016/j.ijbiomac.2019.08.187

42. Liu Z, Jiao Y, Lu H, Shu X, Chen Q. Chemical characterization, antioxidant properties and anticancer activity of exopolysaccharides from *Floccularia luteovirens*. *Carbohydrate Polymers.* (2020) 229:115432. doi: 10.1016/j.carbpol.2019.115432

43. Zhang J, Chen M, Wen C, Zhou J, Gu J, Duan Y, et al. Structural characterization and immunostimulatory activity of a novel polysaccharide isolated with subcritical water from *Sagittaria sagittifolia* L. *Int J Biol Macromol.* (2019) 133:11–20. doi: 10.1016/j.ijbiomac.2019.04.077

44. Kpodo FM, Agbenorhevi JK, Alba K, Bingham RJ, Oduro IN, Morris GA, et al. Pectin isolation and characterization from six okra genotypes. *Food Hydrocolloids.* (2017) 72:323–30. doi: 10.1016/j.foodhyd.2017.06.014

45. Pei J, Wang Z, Ma H, Yan J. Structural features and antitumor activity of a novel polysaccharide from alkaline extract of *Phellinus linteus* mycelia. *Carbohydrate Polymers.* (2015) 115:472–7. doi: 10.1016/j.carbpol.2014.09.017

46. Yuan Q, Zhao L, Li Z, Harqin C, Peng Y, Liu J. Physicochemical analysis, structural elucidation and bioactivities of a high-molecular-weight polysaccharide from *Phellinus igniarius* mycelia. *Int J Biol Macromol.* (2018) 120:1855–64. doi: 10.1016/j.ijbiomac.2018.09.192

47. Xiong Q, Luo G, Zheng F, Wu K, Yang H, Chen L, et al. Structural characterization and evaluation the elicitors activity of polysaccharides from *Chrysanthemum indicum*. *Carbohydrate Polymers.* (2021) 263:117994. doi: 10.1016/j.carbpol.2021.117994

48. Cheng X, Shi S, Su J, Xu Y, Ordaz-Ortiz JJ, Li N, et al. Structural characterization of a heteropolysaccharide from fruit of *Chaenomelese speciosa* (sweet) nakai and its antitumor activity. *Carbohydrate Polymers.* (2020) 236:116065. doi: 10.1016/j.carbpol.2020.116065

49. Zhang S, An L, Li Z, Wang H, Shi L, Zhang J, et al. An active heteropolysaccharide from the rinds of *Garcinia mangostana* linn.: structural characterization and immunomodulation activity evaluation. *Carbohydrate Polymers.* (2020) 235:115929. doi: 10.1016/j.carbpol.2020.115929

50. Milani A, Jouki M, Rabbani M. Production and characterization of freeze-dried banana slices pretreated with ascorbic acid and quince seed mucilage: physical and functional properties. *Food Sci Nutr.* (2020) 8:3768–76. doi: 10.1002/fsn3.1666

51. Contreras-Jiménez B, Torres-Vargas OL, Rodríguez-García ME. Physicochemical characterization of quinoa (*Chenopodium quinoa*) flour and isolated starch. *Food Chem.* (2019) 298:124982. doi: 10.1016/j.foodchem.2019.124982

52. Qian J, Chen W, Zhang W, Zhang H. Adulteration identification of some fungal polysaccharides with SEM, XRD, IR and optical rotation: a primary approach. *Carbohydrate Polymers.* (2009) 78:620–5. doi: 10.1016/j.carbpol.2009.05.025

53. Chen Z, Zhao Y, Zhang M, Yang X, Yue P, Tang D, et al. Structural characterization and antioxidant activity of a new polysaccharide from *Bletilla striata* fibrous roots. *Carbohydrate Polymers.* (2020) 227:115362. doi: 10.1016/j.carbpol.2019.115362

54. Zhang L, Zhao S, Lai S, Chen F, Yang H. Combined effects of ultrasound and calcium on the chelate-soluble pectin and quality of strawberries during storage. *Carbohydrate Polymers.* (2018) 200:427–35. doi: 10.1016/j.carbpol.2018.08.013

55. Zhang Y, Xu X, Xu J, Zhang L. Dynamic viscoelastic behavior of triple helical lentinan in water: effects of concentration and molecular weight. *Polymer.* (2007) 48:6681–90. doi: 10.1016/j.polymer.2007.09.005

56. Wu Z, Li H, Wang Y, Yang D, Tan H, Zhan Y, et al. Optimization extraction, structural features and antitumor activity of polysaccharides from *Ziziphus jujuba* cv. Ruoqiangzao seeds. *Int J Biol Macromol.* (2019) 135:1151–61. doi: 10.1016/j.ijbiomac.2019.06.020

57. Yao W, Qiu H, Cheong K, Zhong S. Advances in anti-cancer effects and underlying mechanisms of marine algae polysaccharides. *Int J Biol Macromol.* (2022) 221:472–85. doi: 10.1016/j.ijbiomac.2022.09.055

frontiers | Frontiers in Nutrition

TYPE Original Research
PUBLISHED 05 December 2022
DOI 10.3389/fnut.2022.1073368

OPEN ACCESS

EDITED BY
Jianhua Xie,
Nanchang University, China

REVIEWED BY
Xiaolong Ji,
Zhengzhou University of Light Industry, China
Jiangping Ye,
Nanchang University, China

*CORRESPONDENCE
Yanjun Zhang
zhangyanjun0305@163.com
Chongxing Huang
huangcx21@163.com

†These authors have contributed equally to this work and share first authorship

SPECIALTY SECTION
This article was submitted to Food Chemistry, a section of the journal Frontiers in Nutrition

RECEIVED 18 October 2022
ACCEPTED 08 November 2022
PUBLISHED 05 December 2022

CITATION
Li B, Xie B, Liu J, Chen X, Zhang Y, Tan L, Wang Y, Zhu L, Zhu K and Huang C (2022) A study of starch resources with high-amylose content from five Chinese mutant banana species. *Front. Nutr.* 9:1073368. doi: 10.3389/fnut.2022.1073368

A study of starch resources with high-amylose content from five Chinese mutant banana species

Bo Li[1,2,3†], Baoguo Xie[4†], Jin Liu[5†], Xiaoai Chen[1,3†], Yanjun Zhang[1,3*], Lehe Tan[1,3], Yitong Wang[6], Libin Zhu[7], Kexue Zhu[1,3] and Chongxing Huang[2*]

[1]Chinese Academy of Tropical Agricultural Sciences, Spice and Beverage Research Institute, Wanning, Hainan, China, [2]College of Light Industry and Food Engineering, Guangxi University, Nanning, Guangxi, China, [3]Key Laboratory of Processing Suitability and Quality Control of the Special Tropical Crops of Hainan Province, Wanning, Hainan, China, [4]Reproductive Medicine Center, The First Affiliated Hospital of Hainan Medical University, Haikou, China, [5]Women's and Children's Hospital of Wanning, Wanning, Hainan, China, [6]School of Forest, Northeast Forestry University, Haerbing, Heilongjiang, China, [7]College of Food Science, Heilongjiang Bayi Agricultural University, Daqing, Heilongjiang, China

Investigation on staple crop starch of new species has been becoming the research focus of scholars at present. Based on this, the physicochemical properties and microstructural characteristics of starches isolated from Chinese mutant *Musa acuminata* Colla *acuminata* and double *balbisiana* (MA), *Musa* double *acuminata* cv. Pisang Mas (MAM), *Musa acuminata* cv. Pisang Awak (MAA), and *Musa* Basjoo Siebold (MBS), and *Musa* double *acuminata* and *balbisiana*-Prata (MAP) were investigated. Results exhibited that all starches exhibited high content of amylose (34.04–42.59%). According to the particle size, they were divided into medium (MA, MAM) (14.54–17.71 μm) and large (MAA, MBS, MAP) (23.01–23.82 μm) group. The medium group with A-type crystallization showed higher peak viscosity (PV), final viscosity, gel fracturability and gel hardness. For large group with B-type crystallization, the compact particle morphology, higher degree of crystallinity, short range order, gelatinization enthalpy, pasting temperature, lower porosity, water absorption capacity (WAC) and oil absorption capacity were found. In addition, the medium group with higher PV and gel hardness could be used as food thickening or gelling agents. The large group with higher Rc, short-range order, lower porosity and WAC could be potential to become raw material for resistant starch. All results showed the amylose content, had significant effect on the microstructure and physicochemical properties of starch samples. Outcomes in this investigation might provide a basis of theoretical application for industrial food production.

KEYWORDS

high amylose banana starch, new Chinese banana resources, A-or B-type crystallize, physicochemical properties, particle morphology properties, statistical analysis

Introduction

Banana (*Musa* spp.) is a subtropical and tropical giant perennial herb belonging to the Musaceae botanical family originating from Southeast Asia, Malaysia, and China. China is the second largest *Musa* producer after India (1, 2). Due to their low investment, high efficiency, and rapid income, bananas have become the fifth most important crop produced in the world after coffee, cereals, sugar, and cocoa. Banana production is also a source of employment in many developing countries (2). The unripe banana flesh has <1% soluble sugar content, 2 g/100 g fresh weight of fiber, 5.55 mg/100 g of potassium, and 20–23% starch content (wet basis) (3).

Musa is also a climacteric fruit with respiration and fruit ripening is dependent on ethylene production; therefore, it cannot be stored for longer periods (4). Until now, a large number of unsalable bananas decay frequently, resulting in a wastage of resources. Since *Musa* fruit is rich in starch, converting some green (unripe) banana pulps into starch would provide a more stable storage form (1–2 years) and increase its generality and practicality (5). Due to its cyclic regeneration capability and low cost, starch is considered one of the three major nutrient substances in human beings and is widely applied in food products as a green alternative material (6). In addition, the Chinese mutant banana species, a novel potential resource of high amylose content starch, was cultivated in the South Subtropical Crops Research Institute, Chinese Academy of Tropical Agricultural Sciences. However, the physicochemical properties and crystalline characteristics of these new types of Chinese banana starch with a high amylose content have not been reported.

Starch granules are semicrystalline polysaccharides consisting of amylose with (1–4)-linked α-glucan and amylopectin with α-(1–4)-linked α-glucan with α-(1–6) branch points (7). Due to various packing patterns of amylose and amylopectin structures, diverse crystallinity properties and physicochemical properties have been identified (8). Chen et al. (9) found that a high amylose content within the crystalline region confers a high rate of amylose reassociation after gelatinization for jackfruit seed starch, leading to its high retrogradation rate of the crystal nucleus. This phenomenon could lead to a significant change in the quality and nutrition structure of starch-based food products during food processing. Therefore, starch with a high amylose content has become the hot spot of research so that it can be used as potential raw materials for food additives and human staple food. Zou et al. (10) reported that the high amylose content of yam starch resulted in high proportions of a double helix, and compact and ordered crystalline structures, leading to high thermal stability and low digestibility, which demonstrated that a high amylose content of yam starch could be considered the resource of a high-resistant starch content (10). The new type of banana starch with high amylose content in this study needed to be further studied to be utilized as a potential resource of food additives and resistant starch.

Therefore, this study aimed to characterize the crystal structure and physicochemical properties of high-amylose starch from five mutant banana species grown in China: *Musa acuminata* Colla *acuminata* and double *balbisiana* (MA), *Musa* double *acuminata* cv. Pisang Mas (MAM), *Musa acuminata* cv. Pisang Awak (MAA), *Musa Basjoo* Siebold (MBS), and *Musa* double *acuminata* and *balbisiana*-Prata (MAP). The proximate composition, physicochemical properties, and crystal characteristics were measured. Principal component analysis (PCA) was used to determine the correlation between each characteristic parameter. The results obtained from this analysis will contribute to food and non-food applications in the future.

Materials and methods

Materials

Unripe fruits of all banana species were collected from the agricultural land of the South Subtropical Crops Research Institute, Chinese Academy of Tropical Agricultural Sciences (Guangzhou, China). The banana species were obtained in three batches-—29 August 2021, 25 September 2021, and 30 October 2021—and each batch included 20 kg of each banana species.

Starch preparation

The unripe mutant banana pulp was dried in a vacuum freeze dryer (50°C for 48 h) and ground into banana flour. The *Musa* flour (100 g) was mixed with 1 L of distilled water, and the mixed liquor was sieved through a 100-mesh filter cloth. The filtrate was centrifuged (4,000 × g, 15°C, 10 min), the precipitate was dissolved in 1 L of NaOH (0.2% w/v), and the solution was stirred (10 min) to remove soluble fibers. The mixed liquor was centrifuged at 4,000 × g for 10 min, and the supernatant was discarded. Then, the brown skin (exogenous impurities) was removed, and the starch sediment was repeatedly washed with distilled water until neutrality was

Abbreviations: MA, *Musa acuminata* Colla *acuminata* and double *balbisiana*; MAM, *Musa* double *acuminata* cv. Pisang Mas; MAA, *Musa acuminata* cv. Pisang Awak; MBS, *Musa Basjoo* Siebold; MAP, *Musa* double *acuminata* and *balbisiana*-Prata; WAC, water absorption capacity; OAC, oil absorption capacity; Rc, relative crystallinity; PV, peak viscosity; BDV, breakdown viscosity; FV, final viscosity; SBV, back viscosity; TV, trough viscosity; PT, pasting temperature; To, onset temperature; Tp, peak temperature/gelatinization temperature; Tc, conclusion temperature; ΔHg, enthalpy of gelatinization; R, gelatinization range; TPA, textural profile analysis; PCA, principal component analysis.

achieved. The remaining samples were dried at 50°C for 24 h until the moisture content was <13 g/100 g and was then filtered through a 100-mesh sieve (7).

X-ray diffraction analysis

X-ray diffraction (XRD) patterns were analyzed using an X-ray diffractometer (Bede XRD Di System, Durham, United Kingdom). A copper tube was used to measure starch samples (40 kV and 200 mA, Cu Kα radiation at 0.154 nm). The diffraction pattern was measured by a step length of 0.02°, a scattering slit width of 1°, a slit width of 0.02 mm, and scanning from 4 to 40° (2°) at a speed of 4°/min. Each sample was evaluated in triplicate. The relative crystallinity of different starch samples was calculated as described by Barros et al. (5).

Proximate composition of isolated starch

The AOAC Official Methods of Analysis. 18th edn. Association of Official Analytical Chemists; Arlington, VA, USA: 2012 method was used to measure the contents of moisture, total starch, ash, lipid, and protein (11).

Amylose content

The amylose content was quantified as mentioned by Li et al. (12). A measure of 1 ml of ethanol and 9 ml of 1 M NaOH were mixed with a 100 mg of starch sample (dry basis) and then boiled in a water bath. After cooling to 25°C, the mixed solution was diluted to 100 ml. A volume of 2.5 ml of this aliquot was added to 50 ml of 1 M I_2-KI. The absorbance of the obtained mixture was then measured at 620 nm in an ultraviolet spectrophotometer (SPECORD 250 Plus, Analytik Jena AG, Jena, Germany).

Pasting properties

For studying the pasting properties, 3 g of the starch sample was added to 25 ml of deionized water in an RVA container. The solution was stirred at 960 rpm/min for 10 s, followed by 160 rpm/min, and then was analyzed using a Rapid Visco Analyzer (RVA super 4, Newport Scientific, Australia). The corresponding viscosity characteristics was calculated by a Stander 1 program in this instrument (12). The samples were incubated at 50°C for 1 min and then heated to 95C at 6 °C/min. The starch paste was cooled to 50C at 6°C/min, maintained at 95°C for 5 min, and then kept at 50°C for 2 min. All measurements were performed in triplicate.

Morphology and particle size distribution analysis of starch granules

The granule morphology of the starch samples was examined using a scanning electron microscope (SEM) (Phenom ProX, Phenom Company, The Netherlands). The starch samples were applied to a silver plate coated with a thin film of gold (10 nm) and then kept at an accelerating voltage of 15 kV. Then, the samples were examined using a polarized light microscope linked to a CCD camera, using which we observed Maltese crosses (Olympus BX51, Tokyo, Japan).

The size distributions corresponding to granules of the starch were measured using a Malvern Mastersizer 3,000 laser diffraction size analyzer following the method of Barros et al. (5) and Ren et al. (13).

Water and oil absorption capacity

A measure of 1 gram of the starch sample was taken in a centrifuge tube and then 10 ml of distilled water or first-grade peanut oil was added to it, and the mixture was pre-weighed. The solution was mixed for 1 h in a vortex oscillator. The mixture was centrifuged (2,000 × g, 30 min, 25 °C), the supernatant was discarded, and the tube containing the pellet was weighed. The oil and water absorption capacities were expressed as percentages of water or oil absorbed by the starch samples (11).

Bulk, true densities, and porosity

Bulk densities were measured by using the method of Zhang et al. (14), except that 5 g of the starch sample was used. The bulk densities were calculated as the ratio of the weight of the starch sample to the occupied volume. True density (T_d) was measured using the liquid displacement method and calculated as follows:

$$T_d = \frac{WS}{X + W - Y} \quad (1)$$

where W is the weight of the sample, S is the specific gravity of xylene, X is the weight of the bottle and xylene, and Y is the weight of the bottle, xylene, and the sample.

The porosity (P_f) of the starch sample was calculated using the following formula:

$$p_f = \left(1 - \frac{B_d}{T_d}\right) \times 100\% \quad (2)$$

where B_d is the bulk density and T_d is the true density.

Thermal properties

A differential scanning calorimeter (DSC-Q2000 TA Instruments, USA) equipped with a thermal analysis data station (TA Instruments, New Castle, DE, USA) was used to study the gelatinization parameters of thermal properties following the method of Zhang et al. (7). A total of 5 mg of dry sample was mixed with 10 mg of distilled water in a crucible, sealed, incubated at room temperature for 24 h, and then the mixture was heated from 10 to 100°C (10°C /min). Universal Analysis Program (TA Instruments) was used to calculate T_o, the temperature at which the tangential line from the lower temperature side of the peak intersects with the baseline; T_p, the temperature at the tip of the peak; T_c, the temperature at which the tangential line from the high-temperature side of the peak intersects with the baseline; and ΔH_g, the area under the peak bound by the baseline on the graph. Each sample was evaluated in triplicate.

Fourier transform infrared (FTIR) spectrum

The short-range order was analyzed using a Nicolet 6700 Fourier transform near-infrared spectrometer (Thermo Fisher Scientific, USA) linked to a smart ITR attachment. The scanning times and resolution were 64 and 4 cm^{-1}, respectively. The ratio of 1,047/1,022 cm^{-1} was recorded (15).

Gel texture properties of starch

A texture analyzer (TA.XT*Plus*, Texture Technologies Corp., United Kingdom) equipped with a weight sensor (max 50 kg) was used to conduct a texture profile analysis (TPA) of starch gels prepared by the RVA. The Texture Expert Exceed version 1.0 program (Stable Micro Systems software) was used to record and analyze the texture properties of the gel. A P/36R cylinder probe was used to carry out the TPA pattern, and a P/0.5R cylinder probe was used to determine the gel 0.5 pattern according to the methods in the program with 40% strain, a pre-test speed of 1.0 mm/s, a test speed of 2 mm/s, and a post-test speed of 2 mm/s. The hardness, fracturability, adhesiveness, springiness, cohesiveness, gumminess, chewiness, resilience, gel strength, gel rupture strength, gel rupture distance, and gel hardness of the sample were determined (16).

Statistical analysis

Mean, standard deviations, and significant differences between values and correlations between parameters were calculated using SPSS 12.0.1 (SPSS Inc., Chicago, Illinois, USA). Significant differences between the means were determined by using Duncan's multiple range test at a significance level of 0.05. The significant differences, mean values, and standard deviation between values were identified by Duncan's multiple range tests at a significance level of 0.05 (SPSS 20.0., Inc., Chicago, Illinois, US). IBM SPSS 20.0 was used to analyze the principal component analysis (PCA), neural network analysis, and cluster analysis.

Results and discussion

Crystalline structure

The characteristics of crystalline structures and long-range order in the starch granules were analyzed by XRD (Figure 1). The diffraction peaks of MA and MAM occurred at $2\theta = 15$, 17, 18, and 23°, which represent an A-type crystal structure, as mentioned in Jiang et al. (2). The MAA, MBS, and MAP occurred at $2\theta = 15°$, 17°, and 23°, indicating a B-type crystal structure (Figure 1), as describes by Zhang et al. (8). This result was broadly consistent with Utrilla-Coello et al. (17), who also found a B-type crystal structure for Mexico banana starch. The degree of relative crystallinity (R_c) followed the order: MAP (37.06%) > MBS (33.75%) > MAA (32.01%) > MAM (30.95%) > MA (27.36%) (Table 1). A significant difference in the Rc value between banana samples was observed ($p < 0.05$). Based on Zou et al. (10), this diversity might be ascribed to the difference in the Bragg diffraction distance and characteristic size of the crystallite unit. Compared with the B- or C-type crystal structure of banana starch reported in a previous study (5), it was found that the type of the crystal structure and Rc of banana starch in the present study significantly differed. This distinct conclusion might be explained by the difference in the planting genotype, which causes a diversity of banana starch-branching enzyme (BE)IIb, gene-encoding starch synthase (SS)IIa, and granule-bound starch synthase (GBSS)I (15). The R_c of the A-type crystal structure banana starch samples was also higher than that of Enano, Morado, Valery, and Macho banana species starch samples (28–30%) (17). According to Bi et al. (18), a more ordered arrangement of amylopectin double helices in the semicrystalline lamellae is correlated with higher R_c values. Meanwhile, Zhang et al. (16) also reported that higher crystallinity (R_c) is consistent with longer single helices of amylose and greater disruption of double helix crystals.

Composition analysis

The moisture and protein contents of starch from all banana species were below 13 and 1.0%, respectively, in accordance with the food industry of China and Food Chemicals Codex (19), which required that the maximum value of moisture and protein were lower than 18% and 1% for the high purity starch (14). The amylose content of MA, MAM, MAA, MBS, and MAP was in

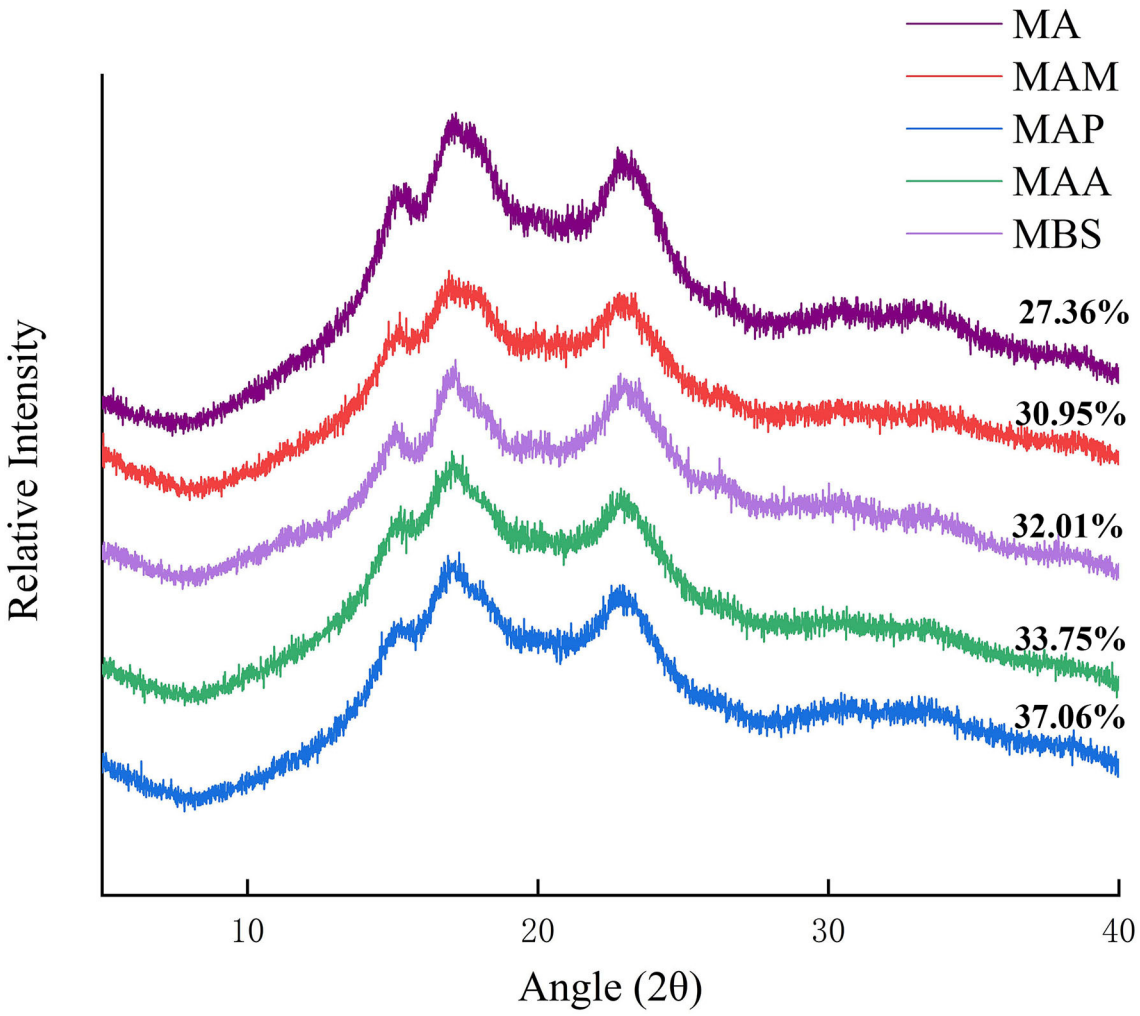

FIGURE 1
X-ray diffraction patterns of starch samples.

the range of 34.04–42.59% (Table 1); therefore, all species tested were regarded as starch with a high amylose content according to published research (8). The amylose content of banana starch was partly higher than that reported by Bi et al. (18), who reported that the amylose content of MAA Cavendish starch was 31.41%. The difference in the amylose content of MAA may be due to various growing conditions. It was suggested that starch with a high amylose content may be used as a water-insoluble dietary fiber for promoting colony-balanced microbiota in the human small intestine (10).

According to Jiang et al. (2), the total starch content in some Chinese banana cultivates is about 92.10%, which is lower than that observed in this study (96.75–99.07%) (Table 1). Significant variations between the species were observed in starch yield, moisture, purity, protein, lipid, and ash amounts. In our study, moisture, protein, and lipid contents of the starch samples were compared with those of Colombian banana species (7.5–7.8%, 0.8–1.1%, and 0.1–0.8%) (20), but the protein content was lower in our study samples. MBS showed the highest ash and lipid content, a relatively high protein content, and the lowest purity and amylose content. Based on Zou et al. (10), the lower starch purity of MBS might be explained by the lower amylose content of MBS than the others, which caused a higher surface tension of MBS resulting in its stronger suction force of nano-surface. This showed that MBS was easily mixed with small bran-containing protein, ash, and lipids and was difficult to completely remove.

Morphology and size distribution

The particle morphologies of MA, MAM, MAA, MBS, and MAP starch samples showed two major shapes: elongated and spherical (Figure 2 left). MA had consistent rod-like shapes with narrower and longer elongations, with a rough appearance

TABLE 1 Chemical composition, granule size and distribution, bulk, true density, porosity, and water and oil absorption capacity of starch samples isolated from five different banana species.

Starch samples	MA	MAM	MAA	MBS	MAP
Starch yields (%)	19.82 ± 0.35^{cd}	23.61 ± 0.68^{a}	21.14 ± 1.44^{bc}	18.70 ± 0.98^{d}	22.45 ± 1.22^{ab}
Moisture (%)	6.67 ± 0.75^{b}	3.88 ± 0.34^{d}	5.94 ± 0.63^{c}	10.28 ± 0.35^{a}	3.51 ± 0.24^{d}
Starch (%, db)	98.94 ± 0.24^{a}	98.56 ± 0.76^{a}	99.14 ± 0.65^{a}	96.75 ± 0.59^{b}	99.07 ± 0.36^{a}
Protein (%, db)	0.39 ± 0.03^{c}	0.54 ± 0.02^{a}	0.22 ± 0.03^{d}	0.47 ± 0.05^{b}	0.44 ± 0.04^{bc}
Lipid (%, db)	0.40 ± 0.05^{c}	0.57 ± 0.03^{b}	0.26 ± 0.02^{c}	2.31 ± 0.16^{a}	0.29 ± 0.03^{c}
Ash (%, db)	0.27 ± 0.07^{cd}	0.32 ± 0.05^{bc}	0.39 ± 0.04^{ab}	0.47 ± 0.04^{a}	0.20 ± 0.03^{d}
Amylose content (%, db)	40.58 ± 0.33^{b}	41.09 ± 0.38^{b}	41.39 ± 0.17^{b}	34.04 ± 0.69^{c}	42.59 ± 0.96^{a}
Rc (%)	27.36 ± 0.18^{e}	30.95 ± 0.47^{d}	32.01 ± 0.40^{c}	33.75 ± 0.56^{b}	37.06 ± 0.71^{a}
D [4,3]-D [3,2] (μm)	4.44 ± 0.55^{b}	3.57 ± 0.52^{b}	3.43 ± 0.76^{b}	4.39 ± 0.69^{b}	8.64 ± 0.71^{a}
Bulk density (g/ml)	0.73 ± 0.04^{d}	0.80 ± 0.03^{cd}	0.88 ± 0.03^{bc}	0.99 ± 0.03^{ab}	1.02 ± 0.04^{a}
True density (g/ml)	1.33 ± 0.08^{b}	1.43 ± 0.06^{b}	1.54 ± 0.08^{ab}	1.70 ± 0.07^{a}	1.71 ± 0.04^{a}
Porosity (%)	45.28 ± 0.61^{a}	44.13 ± 0.45^{b}	42.67 ± 0.55^{c}	41.50 ± 0.52^{d}	40.24 ± 0.41^{e}
Water absorption capacity (%)	88.45 ± 1.54^{a}	83.20 ± 0.63^{b}	80.92 ± 1.06^{c}	77.84 ± 1.21^{d}	74.53 ± 0.92^{e}
Oil absorption capacity (%)	67.66 ± 0.35^{a}	65.49 ± 1.03^{b}	62.19 ± 1.31^{c}	60.39 ± 0.32^{d}	58.85 ± 0.76^{e}

The Dx (10), Dx (50), and Dx (90) are the granule sizes at which 10, 50, and 90% of all the granules by volume are smaller. The D [3,2] and D [4,3] are the area mean diameter and volume mean diameter, respectively. Samples with different letters in the same column are significantly different at $P < 0.05$.

compared with the other samples. Meanwhile, the starch granules of the MAM, MAA, MBS, and MAP species were flattened, and the surfaces were smooth. Our results were different from those of jackfruit seed starch samples, which had oval/bell shapes with a smoother granule surface (11). The differences may be ascribed to differences in amylose content and the type of the X-ray crystal. In addition, previous research (21, 22) revealed that a large number of smaller spherical clusters polymerized by amylopectin nanomodules within semicrystalline lamella could arrange beneath the surface of starch granules. This might have led to the lower root mean square roughness of the starch nanosurface and could also be used to explain the smoother granule surface of the MAM, MAA, MBS, and MAP than that of MA. Typical Maltese crosses (radial organization) were observed in the top position microstructures of all starch granules (Figure 2 right). This study showed that all samples have a semicrystalline structure, which is similar to the findings reported by Tongdang (23). In addition, the size distribution corresponding to the starch particle determined by the SEM is shown in Figure 2. For this part, Dx (10), Dx (50), and Dx (90) represent a starch particle size smaller than the corresponding diameter, which accounted for 10, 50, and 90% of the total amount of the particles, respectively (13). The Dx (10), Dx (50), and Dx (90) of MA, MAM, MAA, MBS, and MAP were in the following range: 8.72–30.47, 10.87–34.87, 15.60–41.45, 14.41–43.72, and 14.76–44.87 μm, respectively. The particle size distribution in this study was consistent with previous studies on banana (7.6–49.6 μm) (24) and yam starch (19.79–32.25 μm) (10). A surface area moment mean diameter (D[3,2]) and volume moment mean diameter (D[4,3]) were 18.98–32.22 μm and 14.54–23.82 μm, respectively, which were significantly different from the size distributions of the five banana starch samples ($p < 0.05$).

According to their significant area mean particle size ($p < 0.05$), the starch samples could be divided into two groups: medium (MA, MAM) and large (MAA, MBS, MAP) (Figure 2). MAP had significantly higher Dx (10), Dx (50), Dx (90), D[3,2], and D[4,3] values (14.76, 25.34, 23.82, 32.22, and 44.87 μm) ($p < 0.05$) than the other starch samples. Meanwhile, MA showed the lowest Dx (10), Dx (50), Dx (90), D [3,2], and D [4,3] values (8.72, 16.05, 30.47, 14.54, and 18.98 μm). A previous report showed that when the amylose content of banana starch increased from 26.54 to 29.01%, the granule sizes increased from 36.58 to 41.88 μm (5). It is suggested the difference in the particle size distribution among MA, MAM, MAA, MBS, and MAP may be due to the varieties of bananas and different plant growth conditions, leading to different amylose contents between each starch sample. Moreover, according to Ao and Jane (21) and Espinosa-Solis et al. (22), the highest particle size distribution for MAP might also be explained by that MAP showing the highest branching degree of amylopectin and the highest value of the degree of polymerization of trans-lamellar amylopectin long chains than the other samples. The difference values in D[4,3]-D[3,2] of MA, MAM, MAA, and MBS were comparable (Table 1), indicating that these starch samples had the highest granule consistency, while MAP had the lowest consistency, which agrees with Zou et al. (10). According to previous studies (5, 21), the surface micro-textures of starch granule including channel pores (extend into the hilum), emulsion bumps, fractal dimension, and roughness could significantly affect the contact area between the exposed hydroxyl group and free water. Therefore, morphology and size distributions are related to the

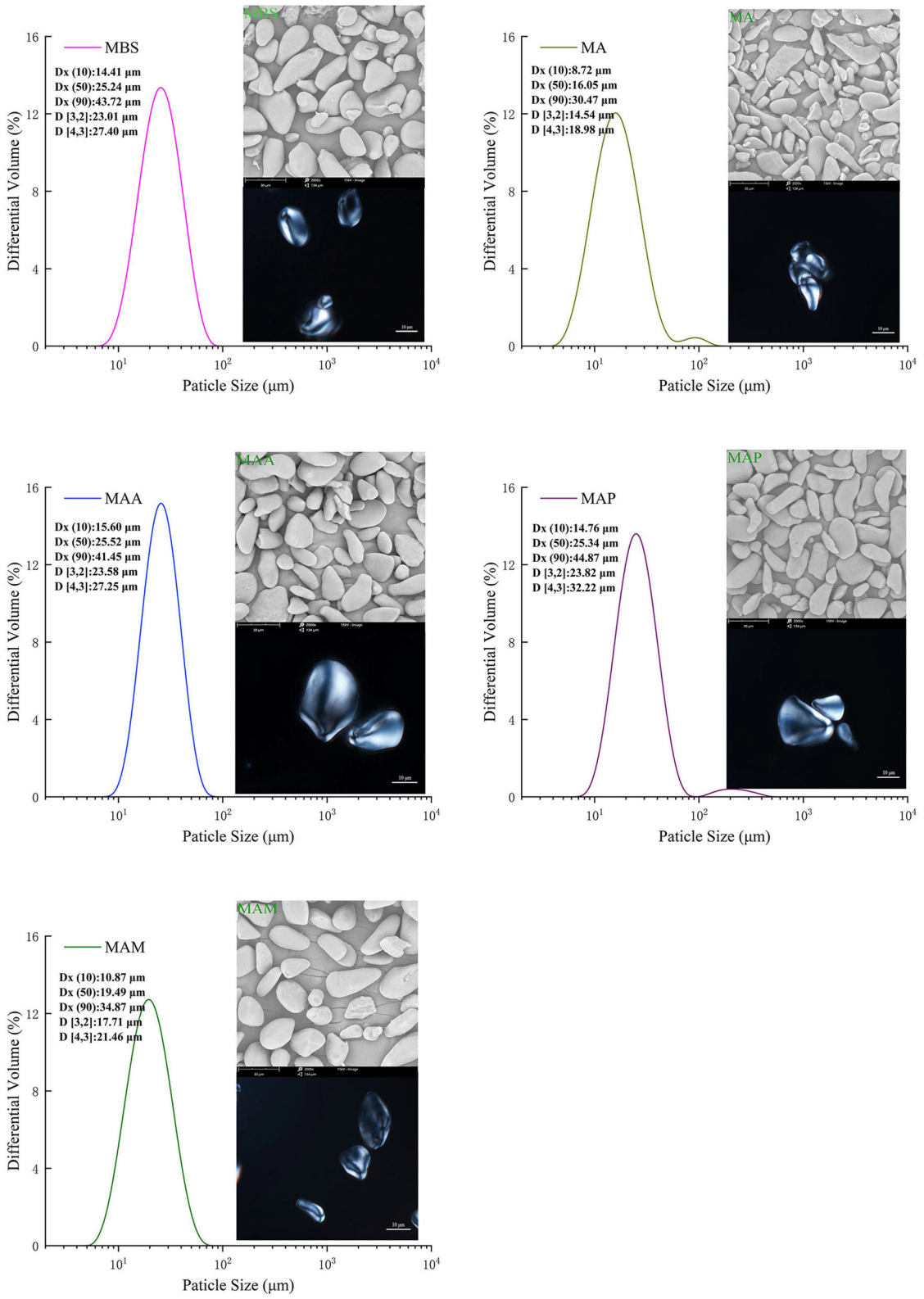

FIGURE 2
Particle size and distribution, and microscopy of starch granules at 2,000 × magnification (SEM) and visualized with a polarized light microscope.

properties of banana starch, and the physicochemical properties were measured as follows.

Bulk, true density, porosity, and water, and oil absorption capacity

The large group (MAA, MBS, and MAP) had a significantly higher bulk density and true density than the medium-sized group (MA and MAM), and significant differences in bulk density were also found between samples in the medium-sized group (Table 1). The true densities of all species were similar to those of different rice starch samples (1.620–1.989 g/ml) (25); however, the bulk densities of all species were higher than those of different rice starch samples (0.633–0.675 g/ml) (26). MA showed the highest porosity (45.28%), followed by MAM (44.13%), MAA (42.67%), and MBS (41.50%), while the lowest porosity was found for MAP (40.24%). All these values were lower than those of different *Colocasia* starch samples (69.7–73.28%) (27). The differences in the density and porosity of the starch samples may be attributed to the particle size and granule morphology, which may be related to differences in starch composition, starch origin, and amylose contents (25, 27).

The water absorption capacity (WAC) and oil absorption capacity (OAC) of the five different samples were ranked as MA (88.45 and 67.66%) > MAM (83.20 and 65.49%) > MAA (80.92 and 62.19%) > MBS (77.84 and 60.39%) > MAP (74.53 and 58.85%) (Table 1), indicating that there was a significant difference between large- and medium-sized groups ($p < 0.05$). MA and MAP showed the highest and the lowest ability to bind water and oil, respectively. This differs from the WAC and OAC values of various rice starch samples (93.73–106.34% and 112.55–151.48%, respectively) (28). The different results between rice and banana starch may be due to distinct internal associative forces of water-binding sites within the starch molecule, according to Bhat and Riar (26). According to Falade & Christopher. (28), the lower water and oil binding ability of MAP particles might be because MAP particles have more ordinal and close-knit molecular structures.

Thermal properties

The significant thermal properties were determined for MA, MAM, MAA, MBS, and MAP ($p < 0.05$). Specifically, the onset temperatures (T_o, 68.74–72.91°C) and conclusion temperatures (T_c, 84.57–91.62°C) of MA, MAM, MAA, MBS, and MAP in this study (Figure 3A, Table 2) were similar to those of cassava starch (60.47and 79.32°C, respectively) (9), while the peak temperatures (T_p, 76.08–82.55°C) and gelatinization enthalpies (ΔH_g, 5.39 11.79 J/g) were consistent with those of Brazilian banana starch (70.58–72.17°C and 9.45–14.73 J/g, respectively) (5). T_p and ΔH depend on the amylose-to-amylopectin ratio and ordering of the double helix structure within crystalline regions (9). Moreover, T_o, T_c, and R remarkably correlated with the homogeneity and size of crystallites units, and the number of double helices and V-type polymorphs (27, 28). Therefore, the highest and lowest T_o, T_p, T_c, R, and ΔH_g values in MAP and MA indicated that these samples showed the highest and lowest quantity of amylose contents and ordered helix structures of the starch crystallites, respectively, which is indicative of their degree of homogeneity and characteristic size.

Pasting properties

Significant variations were found in pasting behaviors among the five starch samples (Figure 3B, Table 2) ($p < 0.05$). The peak viscosity (PV, 3,723–5,399 cP) and breakdown viscosity (BDV, 226–2,383 cP) of banana starch in our study were comparable with those reported in previous studies on cassava, corn, potato, maize, wheat, and rice (PV, 1,852–8,046 cP and BDV, 767–6,717 cP) (12). Similarly, our trough viscosity (TV, 1,962–4,825) was similar to the TV values of different rice starch samples (1,635–3,403 cP) (26). MAM showed the highest PV compared with the other samples, indicating it has the most rigid gel network, which was shown to be formed during starch retrogradation. Meanwhile, MBS had the highest TV, which may have resulted from much lower swelling power and a comparatively smoother particle surface, according to Chen et al. (9). The highest BDV was found in MAA, indicating it has a much lower stability than the other samples under high temperatures and mechanical stirring based on Xia et al. (29).

The setback viscosity (SBV) and final viscosity (FV) of MA, MAM, MAA, MBS, and MAP were 2,661–5,414 cP and 4,623–8,161 cP, respectively (Figure 3B, Table 2), with the MA and MAP samples showing the highest and lowest FV and SBV values, respectively. Our range of values differs from a previous study on potato starch, showing an SBV of 202 cP and an FV of 1622 cP (29). These differences may be due to the length of a shorter amylopectin side chain and the amylose-to-amylopectin ratio (30). According to Chen et al. (9), granules with high FV (MA) have stronger reassociation forces (van der Waals) of amylose molecules during retrogradation. In addition, as described in a previous study (30), the higher SBV of MA than that of MAM, MAA, MBS, and MAP was responsible for its higher strength gel network formation. which involves amylose and amylopectin after gelatinization, which leads to a higher reassociation ability of MA amylopectin chains during cooling.

The peak time (4.93–5.07 min) and pasting temperature (Pt, 82.25to 86.25 °C) of the *Musa* starch samples varied significantly among samples (Figure 3B, Table 2). Our peak times were consistently lower than previous findings with rice starch (5.33–7.23 min), while the pasting temperatures (75.25–87.20°C) were comparable (Bhat & Riar, 2019). MAP showed the highest pasting temperature among the five starch samples, indicating its low porosity and high amylose content (Table 2) may result

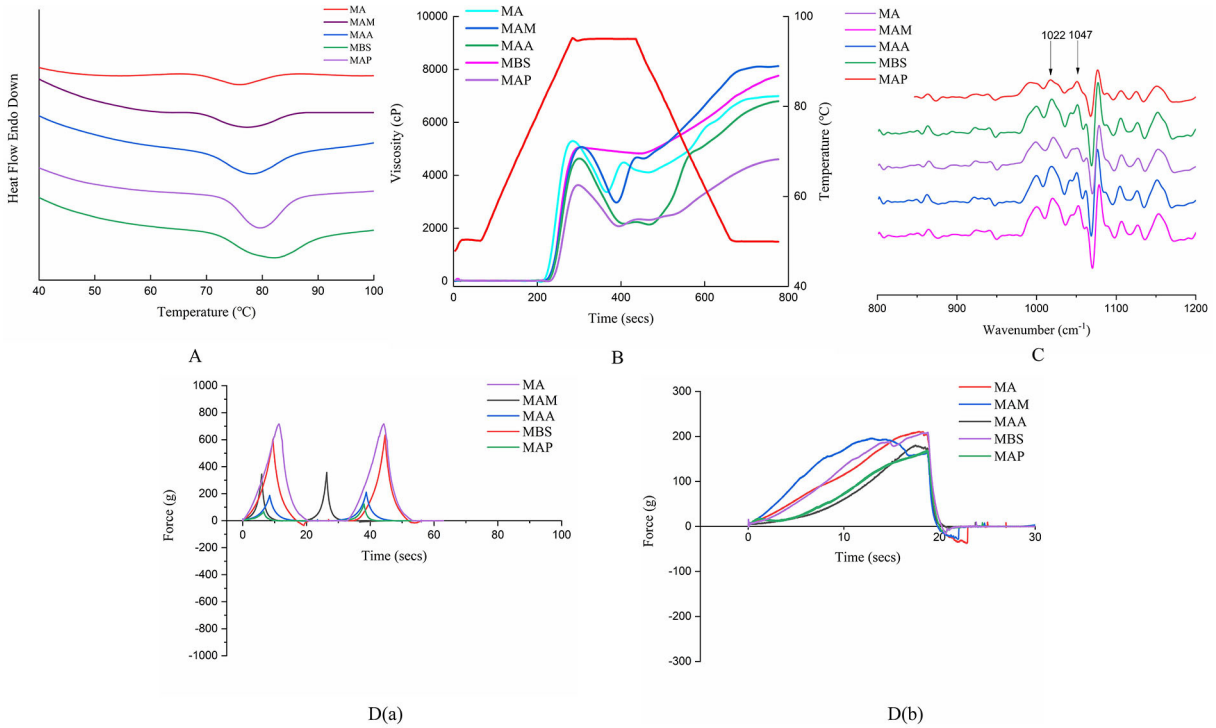

FIGURE 3
Physicochemical property of starch from five Chinese banana species. **(A)** Thermodynamic characteristics of starch samples. **(B)** Pasting profiles of different kinds of starch. **(C)** Deconvoluted FTIR spectra of starch samples. **(D)** Textural properties of starch gels from starch samples. a. Occlusal dynamic curve of TPA pattern. b. Occlusal dynamic curve of gel 0.5 pattern.

in a compact granular structure, attributed to stronger van der Waals forces between the amylose and amylopectin molecules based on the result of Zhang et al. (8).

Short-range order analysis

The short-range order of the starch molecules was analyzed by infrared spectroscopy at 800–1,200 cm^{-1} (Figure 3C) with the absorbance ratios (1,047 cm^{-1}/1,022 cm^{-1}) of the five banana samples ranging from 0.68 to 0.87 (Table 2). A significant difference in short-range order value was observed for the five banana samples ($p < 0.05$). These results are comparable with those obtained for *Amaranthus* starch (0.644) (13). Starch molecules with high-amylose chain length distributions and alternately arranged order between the crystalline lamellae and the amorphous lamellae show a higher short-range order (15, 30). Moreover, the combination of the results of thermal properties and pasting properties suggested that the higher length of a shorter amylopectin side chain, higher amylose chain length distributions, and larger numbers of ordered amylopectin double helices within crystalline lamella might lead to higher short-range orders and compact granular structures (18), which contributed to the higher values of Pt, T_o, T_p, T_c, R, and ΔH_g. However, this resulted in lower FV, PV, and BDV due to the lower stability and strength of the gel network formed by weaker reassociation of amylose and amylopectin chains. These theories could be used to explain the differences in the short-range order, thermal properties, and pasting properties among the banana starch samples. Moreover, for a large size group with B-type crystallization, the overall higher amylose content, Rc, short-range order, and compact and smooth particle morphology could be attributed to higher ΔH_g and Pt. Based on published reports (27, 28), the denser molecular crosslinking network and the lower space distance of the six double helices in a crystal water unit cell led to a higher Rc, short-range order, and Pt, causing the higher RS content. Therefore, compared with a previous report on other banana starch samples, cassava, and rice starch (5, 28), a higher Rc, short-range order, and Pt were found for alarge-particle size group (MAA, MBS, MAP) (Tables 1, 2), which might be suggested the MA and MAM could be used as the potential raw materials of thickening or gelling agents to improve quality and taste during food processing.

TABLE 2 Thermal properties, relative crystallinity, short-range molecular order (1,047 cm^{-1}/1,022 cm^{-1}), pasting properties, and texture profiles of TPA pattern and gel 0.5 pattern of different starch samples.

Starch samples	MA	MAM	MAA	MBS	MAP
To (°C)	68.74 ± 0.53^{d}	69.33 ± 0.60^{cd}	70.61 ± 0.93^{bc}	71.56 ± 0.57^{b}	72.91 ± 0.89^{a}
Tp (°C)	76.08 ± 0.96^{d}	77.53 ± 0.82^{c}	78.39 ± 0.74^{bc}	79.22 ± 0.58^{b}	82.55 ± 0.66^{a}
Tc (°C)	84.57 ± 0.92^{d}	87.78 ± 0.87^{c}	86.91 ± 0.41^{c}	89.86 ± 0.64^{b}	91.62 ± 0.36^{a}
ΔHg (J/g)	5.39 ± 0.37^{a}	8.12 ± 0.43^{c}	7.53 ± 0.21^{c}	10.57 ± 0.35^{b}	11.79 ± 0.49^{a}
R (°C)	15.83 ± 0.72^{c}	18.45 ± 0.73^{b}	16.30 ± 0.67^{c}	19.95 ± 0.77^{a}	20.06 ± 0.53^{a}
I 1047/1022	0.68 ± 0.02^{a}	0.69 ± 0.03^{a}	0.71 ± 0.04^{ab}	0.76 ± 0.03^{b}	0.87 ± 0.03^{c}
Peak viscosity (cP)	5099 ± 1.78^{b}	5399 ± 0.87^{a}	4711 ± 1.55^{d}	5051 ± 1.99^{c}	3723 ± 2.54^{e}
Trough viscosity (cP)	2747 ± 1.45^{c}	3016 ± 1.35^{b}	2027 ± 1.67^{d}	4825 ± 2.44^{a}	1962 ± 2.61^{e}
Breakdown viscosity (cP)	2352 ± 1.27^{c}	2383 ± 1.01^{a}	2684 ± 1.95^{b}	226 ± 2.69^{e}	1761 ± 1.83^{d}
Final viscosity (cP)	8161 ± 2.07^{a}	6967 ± 1.99^{c}	6815 ± 4.89^{d}	7760 ± 9.82^{b}	4623 ± 4.01^{e}
Setback viscosity (cP)	5414 ± 1.39^{a}	3951 ± 2.01^{c}	4788 ± 2.04^{b}	2935 ± 2.09^{d}	2661 ± 2.22^{e}
Peak time (mins)	5.07 ± 0.08^{a}	4.73 ± 0.11^{d}	5.00 ± 0.02^{b}	5.07 ± 0.02^{a}	4.93 ± 0.03^{c}
Pasting temperature	82.25 ± 0.17^{e}	83.55 ± 0.19^{d}	84.00 ± 0.04^{c}	85.15 ± 0.03^{b}	86.25 ± 0.03^{a}
Hardness	434.60 ± 3.39^{a}	288.69 ± 6.54^{c}	209.55 ± 1.98^{d}	357.89 ± 5.17^{b}	122.90 ± 2.33^{e}
Fracturability	8.77 ± 0.29^{b}	10.80 ± 0.22^{a}	8.53 ± 0.03^{c}	8.77 ± 0.10^{b}	7.75 ± 0.05^{d}
Adhesiveness (g.s)	-4.16 ± 0.04^{d}	-13.40 ± 0.03^{e}	-4.47 ± 0.07^{c}	-0.63 ± 0.05^{b}	-0.54 ± 0.03^{a}
Springiness	0.95 ± 0.03^{d}	1.07 ± 0.02^{c}	1.19 ± 0.05^{a}	1.11 ± 0.02^{ab}	1.10 ± 0.02^{ab}
Cohesiveness (g)	0.52 ± 0.05^{e}	1.09 ± 0.01^{b}	1.06 ± 0.03^{bc}	1.44 ± 0.04^{a}	1.02 ± 0.01^{d}
Gumminess (g)	227.26 ± 1.97^{c}	315.25 ± 6.61^{b}	221.99 ± 1.89^{d}	176.67 ± 2.63^{e}	365.38 ± 1.59^{a}
Chewiness (g)	216.57 ± 3.33^{d}	336.17 ± 2.57^{b}	263.34 ± 2.77^{c}	196.11 ± 3.15^{e}	402.11 ± 4.75^{a}
Resilience (g)	0.28 ± 0.02^{e}	0.71 ± 0.01^{b}	0.76 ± 0.04^{ab}	0.42 ± 0.01^{d}	0.64 ± 0.02^{c}
Gel strength (g)	58.40 ± 1.99^{e}	96.83 ± 1.24^{a}	78.20 ± 1.88^{b}	19.49 ± 0.33^{d}	19.96 ± 0.05^{cd}
Gel rupture strength (Hardness) (g)	210.96 ± 5.60^{c}	196.24 ± 2.39^{b}	180.35 ± 7.32^{d}	198.67 ± 3.10^{ab}	169.16 ± 6.37^{e}
Gel Rupture Distance (g)	14.29 ± 0.44^{b}	10.29 ± 0.05^{d}	13.99 ± 0.07^{c}	9.60 ± 0.71^{e}	15.00 ± 0.09^{a}

To, onset temperature; Tp, peak temperature; Tc, conclusion temperature; R, gelatinization temperature range; ΔHg, enthalpy of gelatinization (J/g dry starch). Samples with different letters in the same column are significantly different at $P < 0.05$.

Textural properties

A texture profile analysis has been used to simulate human chewing *in vitro via* double occlusion. The apparent texture property parameter of gelatinous foods was measured by an A P/36R TPA pattern. In general, the internal texture property parameter is determined by using a P/0.5R cylinder probe. TPA using T/36 R and T/0.5 R probes showed consistent results, with the MA and MAP gels being the hardest (434.60 g for T/36R and 210.96 g for T/0.5R) and softest (122.90 g for T/36R and 169.16 g for T/0.5R), respectively, from the five samples [Table 2,Figure 3D (**a, b**)] . This differs from the hardness reported for wheat starch (68.0–131.1 g) (31). There is a positive correlation between gel hardness and the crystallization speed of the amylopectin double helix (31); therefore, the differences may be ascribed to variability in the amylose content and crystal structures of the two different starch sources. It was indicated that MA and MAP had the fastest and slowest amylopectin retrogradation, respectively.

MAP starch gels exhibited the greatest gel adhesiveness (−0.54 g.s), followed by MBS (−0.63 g.s), MA (−4.16 g.s), MAA (−4.47 g.s), and MAM (−13.40 g.s). This was lower than the values obtained for potato starch gel (−26.257 g.s to −81.315 g.s) (32), indicating that green banana starch might have a stronger starch gel network than potato. Previous results showed that gel adhesiveness is linked to R_c since the R_c of jackfruit seed starch increases from 13.29 to 15.87% when the gel adhesiveness increases from 134.38 to 121.31 g.s (16). Our results followed a similar trend, with MAP showing the highest R_c value, while MAM has the second lowest R_c value. Moreover, the lower gel adhesiveness of MAP is correlated with its higher speed of amylose retrogradation than that of the other samples, as reported by Nie et al. (32).

The ranges of fracturability, springiness, cohesiveness, gumminess, chewiness, resilience, cohesiveness, gel strength, gel rupture strength, and gel rupture distance were as follows: 7.75–10.80, 0.95–1.19, 0.52–1.44, 176.67–365.38, 196.11–402.11, 0.28–0.76, 19.49–96.83, 169.16–210.96, and 9.60–15.00 g, respectively [Table 2,Figure 3D (**a, b**)]. Higher fracturability,

springiness, cohesiveness, gumminess, and chewiness but lower resilience of MA, MAM, MAA, MBS, and MAP were determined in this study compared with the earlier reports of wheat, potato, and rice starch (32, 33), indicating that green banana starch samples have stronger particle properties. The significant differences in the TPA between cereal starch and green banana starch samples may be due to the different amylose contents, and variations in true density, WAC, and short-range order. In addition, the medium-size group with A-type crystallization showed higher water absorption capacity and porosity in general, leading to their higher PV, FV, BDV, and gel hardness (Tables 1, 2). Compared with the obvious majority report for potato, wheat, and rice (29, 32, 33), the higher FV and gel hardness for the medium particle-size group (MA and MAM) indicated that MA and MAM could be used as the raw materials of thickening or gelling agents to improve quality and taste during food processing.

Relationship between the physicochemical properties, amylose content, and particle size

Principal component analysis

The interactions among the physicochemical characteristics using PCA showed that the starch samples were widely scattered, indicating that the type of starch markable affected the physicochemical and functional characteristics (Figure 4A). According to a previous study (15), these diversities might be explained by plant origins, climate, and environmental surroundings, leading to the distinct properties of starch self-assembled synthases, including synthase (BE)IIb, synthase (SS) IIa, and synthase I (GBSSI). As displayed in the PCA Figure, a significant positive correlation ($p < 0.05$) could be conjectured when the inclined angle between two components was remarkably smaller than 90°. Furthermore, there might be a positive correlation when the angle between the two components was remarkably higher than 90° ($p < 0.05$), whereas no correlation could be conjectured when the angle between the two components was nearly 90° ($p > 0.05$). The first principal component (PC1) mainly included PV, BDV, porosity, WAC and OAC, hardness, gel rupture strength, and FV. The second principal component (PC2) mainly included amylose content, R_c, T_p, Pt, ΔH_g, R, D[3,2], and 1,047/1,022. A significantly positive correlation was observed between gel adhesiveness, R_c, T_p, Pt, ΔH_g, R, D[3, 2], 1,047/1,022, and amylose content ($p < 0.05$), and among PV, porosity, WAC and OAC, hardness, gel rupture strength, and FV. The PV, BDV, porosity, WAC, and OAC also showed a positive correlation. These findings broadly correlate with the results reported in a study by Utrilla-Coello et al. (17), who found that when the T_p of different types of banana starch samples increased from 70.2 to 78.7°C, the ΔH increased from 10.4 to 15.1 J/g. Also, when the WAC of jackfruit seed starch increased from 88.98% to 112.46, the BDV increased from 174 to 981 cP (11). Overall, the proportions of gel adhesiveness, amylose, R_c, T_p, Pt, ΔH, R, D[3,2], and 1,047/1,022 were significantly negatively correlated with PV, porosity, WAC and OAC, hardness, gel rupture strength, and FV ($p < 0.05$). A similar result using cocoyam starch found that when the FV increased from 189.79 to 252.17 RVU, Pt decreased from 88.75 to 84.83°C (34). The amylose content did not correlate with adhesiveness and ΔH ($p > 0.05$). A proportion of BDV showed a weak correlation with the gel rupture strength, hardness, and FV ($p > 0.05$).

Neural network and cluster analysis

The neural network and cluster analysis based on the Pearson correlation are shown in Figures 4B,C, which could be used to further analyze the interactions among the physicochemical characteristics (8). As shown in Figure 4B, it was found that when the line showed deep red and deep purple between physicochemical characteristic parameters, it represents that there is a significant correlation between them ($p < 0.5$), while lines of other colors represented a less correlation between physicochemical characteristic parameters. In this part, a remarkably positive correlation was shown for Rc, Tp, Pt, ΔHg, R, D[3,2], and 1,047/1,022. Porosity showed a significantly positive correlation with WAC and OAC. FV was positively correlated with hardness, gel rupture strength, and PV and BDV. The amylose content showed a positive correlation with BDV. Rc displayed a negative correlation with WAC and OAC, FV, hardness, gel rupture strength, and PV. Porosity showed a significantly negative correlation with Rc, Tp, 1,047/1,022, and D[3,2]. Tp and 1,047/1,022 showed a negative correlation with WAC and OAC, FV, gel rupture strength, and PV. ΔHg showed a negative correlation with WAC and OAC, and D[3,2] displayed a significantly negative correlation with WAC and OAC, hardness, and gel rupture strength. The results of neural network analysis slightly differed from the results of principal component analysis. Based on Li et al. (12), this diversity might be due to the differences in statistical analysis mechanism. PCA relied on the kernel of optimal scaling and dimension reduction, and the neural network was based on the two-dimensional visualization of the correlation coefficient. Cluster analysis inferred that MAM and MA had relatively similar physicochemical characteristics. MBS, MAA, and MAP had cluster consistency. This conclusion was agreed with the classification for medium-size (MA, MAM) and large-size (MAA, MBS, MAP) size groups in this research. Moreover, four types of cluster trees were obtained. Rc, Tp, ΔHg, R, D[3,2], and 1,047/1,022 were found in one cluster tree. Porosity, WAC, OAC, FV, PV, hardness, and gel rupture strength were found in another cluster tree. PV and BDV appeared in one cluster tree. According to Zhang

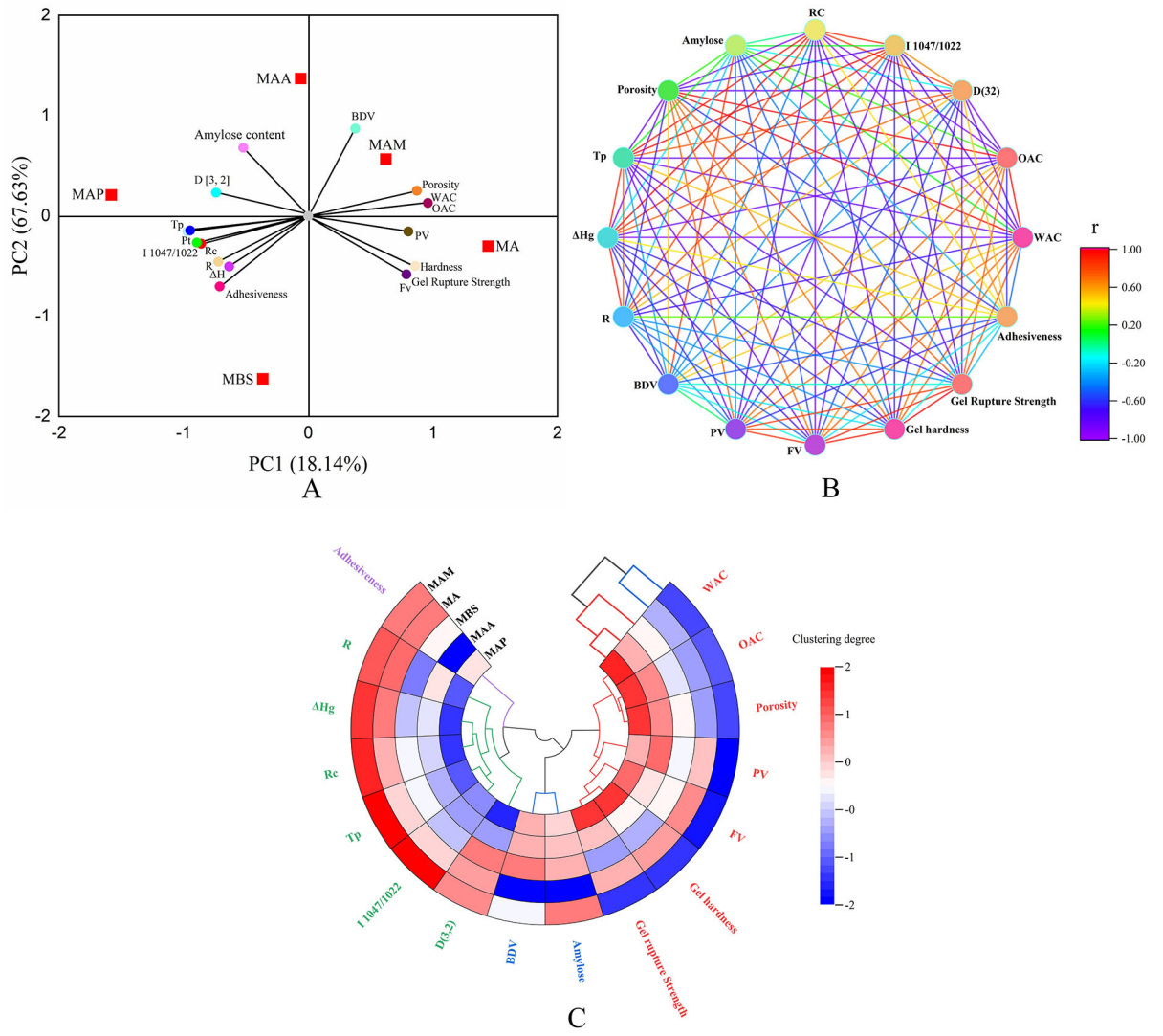

FIGURE 4
Statistical analysis. **(A)** Principal component analysis (PCA) score and loading plot of PC1 and PC2 of starch samples. **(B)** Neural network analysis based on the Pearson method. **(C)** Cluster tree analysis.

et al. (16), these phenomena indicated that these characteristic parameters could interact and affect each other. Adhesiveness showed weaker interactions with others. Zhang et al. (15) found similar results in jackfruit seed starch and reported that when Rc increased from 28.58 to 35.29%, Tp increased from 83.4to 86.2°C and 1,047/1,022 increased from 0.710 to 0.796.

The combination of PCA, neural network, and cluster analysis indicated that the crystalline structure, number of double helices, and double helix order, long-/short-range order (XRD/FTIR), amylose content, and particle size significantly influenced the physicochemical characteristics of A-type crystal green banana starch. Strong hydrogen bonds between the double helix of amylose and amylopectin form a higher long-/short-range order, double helix arrangement order, double helix structure content, and larger and smoother particle morphology (35), which resulted in stronger particle properties (higher R_c, Pt, T_p, and ΔH_g, and lower WAC, FV, PV, gel hardness, and porosity) in MAP than the other banana starch samples, while the opposite particle properties were observed among the other samples. However, Zhang et al. (16) reported that the particle size negatively correlated with R_c, Pt, T_p, and ΔH_g in seed starch of different jackfruit species, indicating that small starch particles have stronger

particle properties. Based on previous reports, the crystalline structure types and winding manner of amylose with single helices have important effects on the particle properties (17, 32, 33), which are likely to be relevant to the study of banana starch. In addition, compared with previous research studies (2, 5, 17, 18, 24), it was found that crystal structure type and amylose content of banana starch in the present study significantly differed, suggesting its higher starch extraction rate, Rc, semicrystalline conformation order, gelatinization enthalpy, gelation temperature, final viscosity, setback viscosity peak viscosity, breakdown viscosity, and gel hardness than banana starch of other species. Therefore, this phenomenon indicated that starch from Chinese mutant banana species might provide a wider range of applications for food or non-food products.

Conclusion

The characteristics of starch from Chinese mutant banana species were investigated, which showed a high-amylose starch content. The crystal structure and physicochemical properties varied among the starch species ($p < 0.05$). Based on diverse starch properties, the starch samples were divided into the medium-size group (MA and MAM) and the large-size group (MAA, MBS, and MAP). The higher amylose content, Rc, short-range molecular order, Pt, Tp, and lower viscous characteristics and gel hardness were shown by the large-size group, and a contrary result was shown by the medium-size group. The A-type structure of banana starch was found in the medium-sized group, and the B-type structure was shown in the other group. Neural network and cluster analyses further showed that gel adhesiveness, R_c, T_p, Pt, ΔH, R, D[3,2], and 1,047/1,022 were significantly positively correlated ($p < 0.05$). A significant positive correlation was also exhibited among PV, porosity, WAC, and OAC; hardness, gel rupture strength, and FV; PV, BDV, porosity, WAC, and OAC. Meanwhile, gel adhesiveness, amylose, R_c, T_p, Pt, ΔH_g, R, D[3,2], and 1,047/1,022 were significantly negatively correlated with PV, porosity, WAC and OAC, gel hardness, gel rupture strength, and FV ($p < 0.05$). These results demonstrated that a higher amylose content, short-range order, double helix arrangement order, double helix structure content, and larger and smoother particle morphology of MAP lead to its higher Pt, Tp, and ΔHg, and lower porosity, WAC, FV, PV, and gel hardness than those of MA, MAM, MAA, and MBS. These findings may be used as a reference to prompt a wider investigation of green banana starch for utilization in the food and non-food industries.

Data availability statement

The original contributions presented in the study are included in the article/supplementary material, further inquiries can be directed to the corresponding author/s.

Author contributions

CH: conceptualization, methodology, software, and validation. BL: formal analysis, investigation, writing—original draft preparation, and data curation. YZ: resources, project administration, funding acquisition, writing—review and editing, visualization, and supervision. All authors have read and agreed to the published version of the manuscript.

Funding

This research was funded by the Key Research and Development Program of Hainan Province (ZDYF2022SHFZ122) and the Chinese Central Public-Interest Scientific Institution Basal Research Fund (1630142022007). This study was financially supported by the College of Light Industry and Food Engineering of Guangxi University and Spice and Beverage Research Institute, the Chinese Academy of Tropical Agricultural Sciences, and the Key Laboratory of Processing Suitability and Quality Control of the Special Tropical Crops of Hainan Province.

Conflict of interest

The authors declare that the research was conducted in the absence of any commercial or financial relationships that could be construed as a potential conflict of interest.

Publisher's note

All claims expressed in this article are solely those of the authors and do not necessarily represent those of their affiliated organizations, or those of the publisher, the editors and the reviewers. Any product that may be evaluated in this article, or claim that may be made by its manufacturer, is not guaranteed or endorsed by the publisher.

References

1. Anyasi TA, Jideani AIO, Mchau GRA. Functional properties and postharvest utilization of commercial and non-commercial banana cultivars. *Compr Rev Food Sci Food Saf.* (2013) 12:509–22. doi: 10.1111/1541-4337.12025

2. Jiang H, Zhang Y, Hong Y, Bi Y, Gu Z, Cheng L, et al. Digestibility and changes to structural characteristics of green banana starch during *invitro* digestion. *Food Hydrocoll.* (2015) 49:192–9. doi: 10.1016/j.foodhyd.2015.03.023

3. Goswami B, Borthakur A. Chemical and biochemical aspects of developing culinary banana (Musa ABB) "Kachkal". *Food Chem.* (1996) 55:169–72. doi: 10.1016/0308-8146(95)00072-0

4. Aurore G, Parfait B, Fahrasmane L. Bananas, raw materials for making processed food products. *Trends Food Sci Technol.* (2009) 20:78–91. doi: 10.1016/j.tifs.2008.10.003

5. Barros Mesquita C, Leonel M, Franco CML, Leonel S, Garcia EL, dos Santos TPR. Characterization of banana starches obtained from cultivars grown in Brazil. *Int J Biol Macromol.* (2016) 89:632–9. doi: 10.1016/j.ijbiomac.2016.05.040

6. Zhao Y, Huang C, Huang X, Huang H, Zhao H, Wang S, et al. Effectiveness of PECVD deposited nano-silicon oxide protective layer for polylactic acid film: Barrier and surface properties. *Food Packag Shelf Life.* (2020) 25:100513. doi: 10.1016/j.fpsl.2020.100513

7. Zhang Y, Liu W, Liu C, Luo S, Li T, Liu Y, et al. Retrogradation behavior of high-amylose rice starch prepared by improved extrusion cooking technology. *Food Chem.* (2014) 158:255–61. doi: 10.1016/j.foodchem.2014.02.072

8. Zhang Y, Li B, Xu F, He S, Zhang Y, Sun L, et al. Jackfruit starch: Composition, structure, functional properties, modifications and applications. *Trends Food Sci Technol.* (2021) 107:268–83. doi: 10.1016/j.tifs.2020.10.041

9. Chen J, Liang Y, Li X, Chen L, Xie F. Supramolecular structure of jackfruit seed starch and its relationship with digestibility and physicochemical properties. *Carbohydr Polym.* (2016) 150:269–77. doi: 10.1016/j.carbpol.2016.05.030

10. Zou J, Xu M, Wen L, Yang B. Structure and physicochemical properties of native starch and resistant starch in Chinese yam (Dioscorea opposita Thunb). *Carbohydr Polym.* (2020) 237:116188. doi: 10.1016/j.carbpol.2020.116188

11. Zhang Y, Zhu K, He S, Tan L, Kong X. Characterizations of high purity starches isolated from five different jackfruit cultivars. *Food Hydrocoll.* (2016) 52:785–94. doi: 10.1016/j.foodhyd.2015.07.037

12. Li B, Wang H, Wang X, Zhang Y, Tan Y, Zhang Y, et al. Prediction of the postprandial blood sugar response estimated by enzymatic kinetics of in vitro digestive and fine molecular structure of artocarpus heterophyllus lam seed starch and several staple crop starches. *Starch/Starke.* (2019) 71:9–10. doi: 10.1002/star.201800351

13. Ren Y, Guo K, Zhang B, Wei C. Comparison of physicochemical properties of very small granule starches from endosperms of dicotyledon plants. *Int J Biol Macromol.* (2020) 154:818–25. doi: 10.1016/j.ijbiomac.2020.03.147

14. Zhao J, Zhang Y, Wu Y, Liu L, Ouyang J. Physicochemical properties and in vitro digestibility of starch from naturally air-dried chestnut. *Int J Biol Macromol.* (2018) 117:1074–80. doi: 10.1016/j.ijbiomac.2018.06.034

15. Zhang Y, Zuo H, Xu F, Zhu K, Tan L, Dong W, et al. The digestion mechanism of jackfruit seed starch using improved extrusion cooking technology. *Food Hydrocoll.* (2021) 110:106154. doi: 10.1016/j.foodhyd.2020.106154

16. Zhang Y, Hu M, Zhu K, Wu G, Tan L. Functional properties and utilization of Artocarpus heterophyllus Lam seed starch from new species in China. *Int J Biol Macromol.* (2018) 107:1395–405. doi: 10.1016/j.ijbiomac.2017.10.001

17. Utrilla-Coello RG, Rodríguez-Huezo ME, Carrillo-Navas H, Hernández-Jaimes C, Vernon-Carter EJ, Alvarez-Ramirez J. In vitro digestibility, physicochemical, thermal and rheological properties of banana starches. *Carbohydr Polym.* (2014) 101:154–62. doi: 10.1016/j.carbpol.2013.09.019

18. Bi Y, Zhang Y, Jiang H, Hong Y, Gu Z, Cheng L, et al. Molecular structure and digestibility of banana flour and starch. *Food Hydrocoll.* (2017) 72:219–27. doi: 10.1016/j.foodhyd.2017.06.003

19. *Committee on Food Chemicals Codex, Food Chemicals Codex (FCC8)*. Natl Academy Pr, ISBN: 9780309088664.

20. Chávez-Salazar A, Bello-Pérez LA, Agama-Acevedo E, Castellanos-Galeano FJ, Álvarez-Barreto CI, Pacheco-Vargas G. Isolation and partial characterization of starch from banana cultivars grown in Colombia. *Int J Biol Macromol.* (2017) 98:240–6. doi: 10.1016/j.ijbiomac.2017.01.024

21. Ao Z, Jane J, Lin. Characterization and modeling of the A- and B-granule starches of wheat, triticale, and barley. *Carbohydr Polym.* (2007) 67:46–55. doi: 10.1016/j.carbpol.2006.04.013

22. Espinosa-Solis V, Sanchez-Ambriz SL, Hamaker BR, Bello-Pérez LA. Fine structural characteristics related to digestion properties of acid-treated fruit starches. *Starch/Staerke.* (2011) 63:717–27. doi: 10.1002/star.201100050

23. Tongdang T. Some properties of starch extracted from three thai aromatic fruit seeds. *Starch/Staerke.* (2008) 60:199–207. doi: 10.1002/star.200800641

24. Peroni-Okita FHG, Simão RA, Cardoso MB, Soares CA, Lajolo FM, Cordenunsi BR. In vivo degradation of banana starch: structural characterization of the degradation process. *Carbohydr Polym.* (2010) 81:291–9. doi: 10.1016/j.carbpol.2010.02.022

25. Das AB, Goud V, Das C. Microencapsulation of anthocyanin extract from purple rice bran using modified rice starch and its effect on rice dough rheology. *Int J Biol Macromol.* (2019) 124:573–81. doi: 10.1016/j.ijbiomac.2018.11.247

26. Bhat FM, Riar CS. Effect of chemical composition, granule structure and crystalline form of pigmented rice starches on their functional characteristics. *Food Chem.* (2019) 297:124984. doi: 10.1016/j.foodchem.2019.124984

27. Deepika V, Jayaram Kumar K, Anima P. Isolation and partial characterization of delayed releasing starches of Colocasia species from Jharkhand, India. *Carbohydr Polym.* (2013) 96:253–8. doi: 10.1016/j.carbpol.2013.04.002

28. Falade KO, Christopher AS. Physical, functional, pasting and thermal properties of flours and starches of six Nigerian rice cultivars. *Food Hydrocoll.* (2015) 44:478–90. doi: 10.1016/j.foodhyd.2014.10.005

29. Xia T, Gou M, Zhang G, Li W, Jiang H. Physical and structural properties of potato starch modified by dielectric treatment with different moisture content. *Int J Biol Macromol.* (2018) 118:1455–62. doi: 10.1016/j.ijbiomac.2018.06.149

30. Sandeep S, Singh N, Isono N, Noda T. Relationship of granule size distribution and amylopectin structure with pasting, thermal, and retrogradation properties in wheat starch. *J Agric Food Chem.* (2010) 58:1180–8. doi: 10.1021/jf902753f

31. Sandhu KS, Kaur M, Mukesh. Studies on noodle quality of potato and rice starches and their blends in relation to their physicochemical, pasting and gel textural properties. *LWT - Food Sci Technol.* (2010) 43:1289–93. doi: 10.1016/j.lwt.2010.03.003

32. Nie H, Li C, Liu PH, Lei CY, Li J, Bin. Retrogradation, gel texture properties, intrinsic viscosity and degradation mechanism of potato starch paste under ultrasonic irradiation. *Food Hydrocoll.* (2019) 95:590–600. doi: 10.1016/j.foodhyd.2017.08.035

33. Choi SG, Kerr WL. Water mobility and textural properties of native and hydroxypropylated wheat starch gels. *Carbohydr Polym.* (2003) 51:1–8. doi: 10.1016/S0144-8617(02)00083-8

34. Falade KO, Okafor CA. Physicochemical properties of five cocoyam (*Colocasia esculenta* and *Xanthosoma sagittifolium*) starches. *Food Hydrocoll.* (2013) 30:173–81. doi: 10.1016/j.foodhyd.2012.05.006

35. Ji X, Yin M, Hao L, Shi M, Liu H, Liu Y. Effect of inulin on pasting, thermal, rheological properties and *in vitro* digestibility of pea starch gel. *Int J Biol Macromol.* (2021) 193:1669–75. doi: 10.1016/j.ijbiomac.2021.11.004

frontiers | Frontiers in Nutrition

TYPE Original Research
PUBLISHED 05 May 2023
DOI 10.3389/fnut.2023.1157015

OPEN ACCESS

EDITED BY
Jianhua Xie,
Nanchang University, China

REVIEWED BY
Jie Tu,
Jiangsu University of Science and Technology, China
Yingbin Shen,
Guangzhou University, China
Xu Chen,
Dongguan University of Technology, China

*CORRESPONDENCE
LongKui Cao
caolongkui2013@163.com

†These authors have contributed equally to this work

RECEIVED 02 February 2023
ACCEPTED 19 April 2023
PUBLISHED 05 May 2023

CITATION
Wang Y, Wang W, Wu Y, JiLiu J, Hu X, Wei M and Cao L (2023) Characterization of manganized soluble dietary fiber complexes from tigernut meal and study of the suppressive activity of digestive enzymes *in vitro*.
Front. Nutr. 10:1157015.
doi: 10.3389/fnut.2023.1157015

Characterization of manganized soluble dietary fiber complexes from tigernut meal and study of the suppressive activity of digestive enzymes *in vitro*

Yifei Wang[1†], Weihao Wang[1,2†], Yunjiao Wu[1], Junlan JiLiu[1], Xin Hu[1], Mingzhi Wei[1] and LongKui Cao[1,2*]

[1]College of Food Science, Heilongjiang Bayi Agricultural University, Daqing, China, [2]National Coarse Cereals Engineering Research Center, Heilongjiang Bayi Agricultural University, Daqing, China

In this study, manganized soluble dietary fiber (SDF–Mn(II)) was prepared from tigernut meal using a microwave solid-phase synthesis method with SDF. Microscopic morphological and structural analyses of SDF–Mn(II) were carried out using scanning electron microscopy, Fourier infrared spectroscopy, UV full-band scanning, X-ray diffraction, a thermal analyzer, gel permeation chromatography, and nuclear magnetic resonance, and its *in vitro* hypoglycemic activity was initially investigated. The results of these analyses revealed that the reaction of Mn(II) with SDF mainly involved hydroxyl and carbonyl groups, with the Nuclear magnetic resonance (NMR) analysis showing that specific covalent binding was produced and substitution was mainly carried out at the C_6 position. Moreover, compared with SDF, the SDF–Mn(II) complex exhibited a porous structure, red-shifted, and color-enhancing effects on the UV characteristic peaks, significantly increased crystallinity and decreased molecular weight, and improved thermal stability; in addition, SDF–Mn(II) afforded significantly enhanced inhibition of α-amylase and α-glucosidase and possesses good *in vitro* digestive enzyme inhibition activity.

KEYWORDS

soluble dietary fiber, manganese, structural characterization, α-amylase, α-glucosidase

1. Introduction

Tigernuts (*Cyperus esculentus* L.) are widely distributed throughout the world, mainly as a snack in tropical and Mediterranean regions. They are often used in the food industry for the production of flavored beverages (1, 2). They have the ability to tolerate drought and sandy and acidic environments and are now widely grown in the northern regions of China (3), where they are cultivated with great ability and high yield. Because of its high oil content and ease of cultivation, it has potential value for the development of edible oil resources in China. Tigernut meal, a by-product of the processing of tigernuts, is rich in dietary fiber and a good source of high-quality dietary fiber.

The intake of dietary fiber is inversely proportional to the level of blood glucose values, and many studies have shown that a moderate intake of dietary fiber can prevent the development of diabetes and alleviate the manifestations of the disease, to some extent, in these patients (4). Dietary fiber lowers blood glucose mainly by improving insulin resistance, regulating disorders of glucolipid metabolism, improving oxidative stress and the inflammatory response, and regulating the intestinal flora; furthermore, it stabilizes postprandial blood glucose by inhibiting

the activity of digestive enzymes and delaying glucose absorption in the intestine (5).

Manganese is an essential trace element that is mainly taken up through food and water, digested and absorbed through the gastrointestinal tract, and transported to mitochondria-rich organs (especially the liver, pancreas, and pituitary gland), where it exerts its biological effects (6). Manganese is involved in the synthesis and activation of various enzymes in the body, aids in glucose and lipid metabolism, regulates endocrine disorders, and improves immune function (7). Manganese supplementation also increases insulin secretion, improves glucose tolerance under conditions of dietary stress, and prevents type II diabetes and its complications (8). A moderate intake of organic trace elements can improve animal productivity and immunity, with the advantage of being able to reduce antagonistic effects among trace elements (9). Previous studies have shown that heavy metals can denature enzymes, resulting in a decrease in enzymatic activity (10).

α-amylase and α-glucosidase are important enzymes in the catabolism of starch, glycogen, and disaccharides in the gastrointestinal tract. Because of the reduced rate of intestinal carbohydrate metabolism, inhibition of the activity of these enzymes is commonly used to control blood glucose levels (11). α-Glucosidase plays an important role in the regulation of postprandial blood glucose levels in humans (12), and its inhibitors block postprandial hyperglycemia and are commonly used to prevent or treat type II diabetes (13). α-amylase acts as a catalyst in reactions involving α-1,4-glycosidic bonds, to hydrolyze branched-chain starch, straight-chain starch glycogen, and many maltodextrins, thus acting as a catalyst in the reactions responsible for starch digestion (14).

Tigernut meal is a by-product of the processing of tigernuts, and there is no report on the inhibition of *in vitro* enzyme activity by chelation of SDF from tigernut meal with metal ions. In this study, the method of solid-state microwave synthesis is adopted, an SDF–Mn(II) complex was prepared by introducing Mn^{2+} (which is a factor that can increase insulin secretion) onto SDF (which has an anti-glycemic effect) using the latter as the raw material. The particle morphology, structural characterization, relative molecular mass, and thermal properties of SDF and SDF–Mn(II) were determined using scanning electron microscopy, Fourier transform infrared spectroscopy, ultraviolet spectroscopy, X-ray diffraction, NMR, gel permeation chromatography, and a thermal analyzer; moreover, their *in vitro* digestive-enzyme inhibitory activities were investigated to provide a new direction for controlling blood glucose levels and slowing down blood glucose elevation.

2. Materials and methods

2.1. Materials

Commercially available tigernut meal was used. α-amylase (enzymatic activity, 50 U/mg) and α-glucosidase (enzymatic activity, 40–80 U/mg) were purchased from Sigma, United States. Manganese chloride was from Tianjin Damao Chemical Reagent Factory. The remaining chemicals and reagents were of analytical grade.

2.2. Extraction of SDF from tigernut meal

The preparation of SDF from defatted tigernut meal was carried out according to the method of Shen et al. (15), with slight modification. The SDF was extracted from the supernatant by centrifugation, concentrated by rotary evaporation, subjected to alcoholic sedimentation in 95% ethanol for 12 h, and freeze dried after centrifugation for 8 h. The purified SDF was obtained by dialysis and deproteinization (16).

2.3. Synthesis of SDF–Mn(II) complexes

SDF–Mn(II) was synthesized according to the method of Xu Lockping (17). SDF and $MnCl_2$ were weighed according to the mass ratio of 1:0.8, followed by the addition of 150% (relative to the mass of SDF) anhydrous ethanol; the solution was mixed well and placed in a microwave solid-phase synthesis extractor (Xianghu Technology Development Co., Ltd., Beijing, China), with the microwave time set to 3 min and its power set to 210 W for the coordination reaction. The precipitate was dried in a hot-air drying oven (55°C) to a constant weight, to obtain SDF–Mn(II).

2.4. Determination of manganese content and fit rate in SDF–Mn(II)

The obtained samples were dissolved and the content of manganese (II) was determined using a spectrophotometric method (540 nm) (18). The equation of the manganese standard curve was as follows: $y = 0.0343x + 0.002$, with a linear correlation coefficient of $R^2 = 0.9998$, where y is the manganese content and x is the absorbance in μg/g. The manganese content of the SDF–Mn(II) prepared in this experiment was 71.89 μg/g, with a fit ratio of 41.60%.

2.5. Scanning electron microscopy (SEM) analysis

The microstructure of SDF and SDF–Mn(II) was observed using SEM (Type-SU1510 Hitachi microscope; HITACHI Inc., Japan) (19). The samples were dried and processed, and a specific amount was collected and bonded using conductive tape; the samples were then gold-plated and observed.

2.6. Fourier transform infrared (FT-IR) spectroscopy

FT-IR (Tensor 27 instrument; Bruker Daltonics Inc., Bremen, Germany) was used for the determination the sample (20). The sample was mixed with potassium bromide powder in the ratio of 1:100 and fully ground in a mortar, to homogenize the mixture, which was then poured into a compression device and finally scanned on the machine (4,000–400 cm^{-1}).

2.7. UV spectroscopy

This experiment was performed using an ultraviolet generalizable spectrophotometer (T6 series; Yuan Analysis Instrument Co., Ltd., Shanghai, China). The sample solution was prepared at a mass

concentration of 2 mg/ml, and distilled water was used as a blank control. The sample to be measured was aspirated using a syringe, filtered through a pinhole filter, and scanned in the wavelength range of 190–400 nm with a scan interval of 1 nm (21).

2.8. X-ray diffraction (XRD) pattern analysis

Measurements were performed using an X-ray diffractometer (Type D/MAX2000V, Neo-Confucianism Manufacturing Company, Japan). The dried and delicate samples were uniformly dispersed in the plate frame and compacted, so that the sample surface was smooth and flat, and the sample frame was fixed and tested. The diffraction test conditions were as follows: tube current, 40 mA; tube voltage, 40 kV; Cu target wavelength, 1.5406 Å; Co target wavelength, 1.79026 Å; scan rate, 7°/min; and measurement range, 2θ from 5° to 70° (22).

2.9. Molecular weight determination

A narrowly distributed polyethylene glycol (PEO) was used as the standard curve for the relative calibration method and as the standard sample group in the detection using a differential refractive index detector (RID-20, Shimadzu, Japan). The precipitate was washed twice with anhydrous ethanol, air dried, dissolved by adding a solution of 0.1 mol/l $NaNO_3$ and 0.06% NaN_3, reacted at 121°C for 20 min, and centrifuged at 5000 r/min for 10 min; subsequently, 20 µl of the sample was collected. The detection conditions were as follows: flow rate, 0.6 ml/min, and column temperature, 35°C.

2.10. Nuclear magnetic resonance (NMR) measurements

The samples were dissolved in D_2O and shaken well to achieve complete dissolution, followed by 1D-NMR (1H-NMR, 13C-NMR) measurements using a 600 MHz NMR instrument (Bruker AVANCE III, Brooke, Inc., Germany) (23).

2.11. Thermal stability analysis

These measurements were performed using a thermogravimetric analyzer (TGA 550; TA Instruments, New Castle, DE, United States) (24). A 20.0 mg sample was placed in an alumina crucible and heated in the temperature range of 25°C–600°C at a rate of 10°C/min under a nitrogen atmosphere, to obtain TGA and DSC curves.

2.12. *In vitro* enzymatic activity inhibition study

2.12.1. Inhibition of α-glucosidase by SDF and SDF–Mn(II)

α-Glucosidase was diluted with 0.1 mol/l (pH = 6.8) phosphate-buffered solution to 1 U/ml. For the assay, 50 µl of the sample solution and 50 µl of the pNPG solution were simultaneously added to a 96-well plate. Incubate at 37°C for 10 min, and then 100 µl of the α-glucosidase solution was added and incubated for 45 min at 37°C. The reaction was terminated by adding 50 µl of Na_2CO_3 solution at a concentration of 0.2 mol/l. The absorbance at 405 nm was measured using an enzyme standardizer for the calculation of the enzyme inhibition rate (25).

2.12.2. Inhibition of α-amylase by SDF and SDF–Mn(II)

A buffer solution was used to prepare porcine α-amylase at a concentration of 2 U/ml. The sample solution at different concentration gradients was mixed with 40 µl of α-amylase and incubated at 37°C for 30 min. A 40 µl of soluble starch was then added and incubated for 10 min, followed by the addition of 160 µl of DNS and boiling for 5 min, for color development. The absorbance of the inhibited group was measured at 540 nm; control, background, and blank groups were also used in this experiment (26).

2.12.3. Data statistics and analysis

Data were processed using the SPSS 22 software, and the statistical analysis of the data was performed using the Excel 2019 software, whereas plotting was performed using the Origin 96 software. Three groups of parallel experiments were set up for all experiments.

3. Results

3.1. SEM analysis

The results of the SEM analysis of SDF and SDF–Mn(II) are reported in Figure 1. From the figure, we can clearly see that SDF is in the form of a sheet structure, with a dense structure and fewer holes. However, SDF-Mn (II) structure presents a cellular

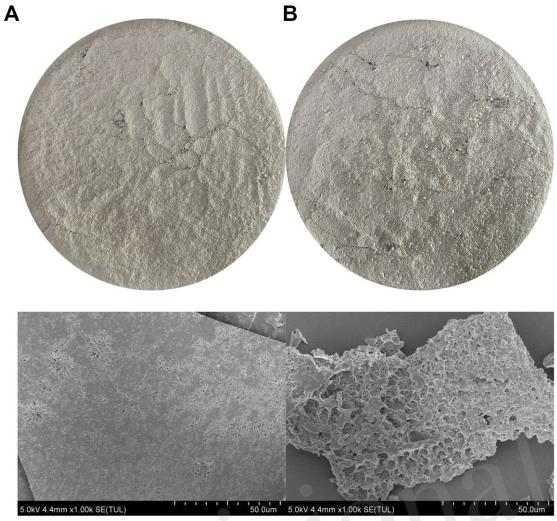

FIGURE 1
The SEM diagram of SDF **(A)**, SDF-Mn(II) **(B)**.

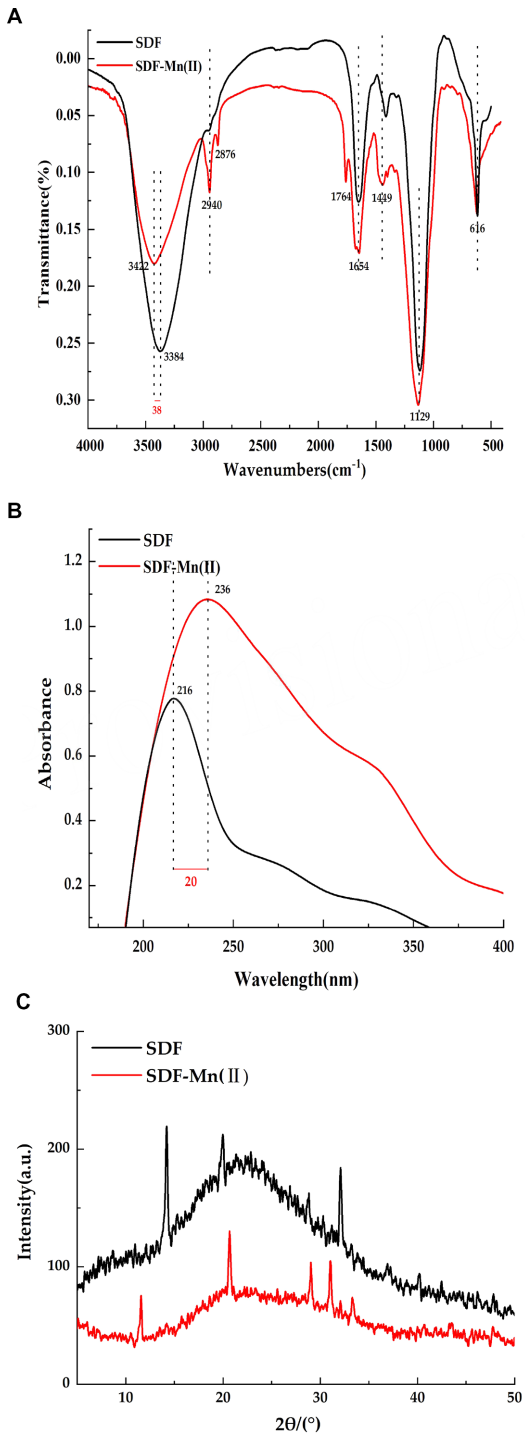

FIGURE 2
FT-IR spectrum diagram **(A)**, UV spectra **(B)**, X-ray diffraction plot **(C)**.

structure with obvious fragmentation trend, which increases the relative surface area and may lead to changes in its physical and chemical properties. After microwave treatment, the internal structure, morphology, and polymerization mode were altered, and the wrapped groups were exposed, which laid the structural foundation for the full completion of the subsequent chelation reaction.

3.2. FT-IR analysis

The Fourier transform infrared spectra of SDF and SDF–Mn(II) are shown in Figure 2A. SDF showed a characteristic absorption peak of O-H at 3,384 cm^{-1} (27), while the O-H characteristic absorption peak in the absorption spectrum of SDF-Mn(II) was red-shifted to 3,422 cm^{-1}. The intensity of the SDF-Mn(II) absorption peak becomes weaker, which may be due to the chelation reaction consuming part of the O-H in SDF. The absorption peak detected at 2,940 cm^{-1} may be attributed to the C-H stretching vibration of the -CH_2 group (28). In turn, the peak near 1,764 cm^{-1} in the SDF–Mn(II) spectrum may be attributed to the stretching vibration of the carbonyl group, which is not present in SDF (29); thus, the carbonyl group may be involved in the chelation reaction. SDF has a strong absorption peak near 1,654 cm^{-1} for the carboxyl group (30). The peak here in SDF-Mn(II) was not significantly shifted, but the peak strength weakened, indicating that the carboxyl group may be involved in the chelation reaction. The presence of an absorption peak near 1,449 cm^{-1} indicated the existence of a pyranoside functional group (31). The appearance of the absorption peak at 1,129 cm^{-1} was mainly attributed to the coupling valence vibration of the C=O bond and the deformation vibration of the C–H bond (32). Most of the characteristic peaks of SDF did not significantly change between before and after the modification, indicating that the basic skeleton of SDF remained unchanged. Finally, the IR spectrograms showed that the hydroxyl and carbonyl groups were mainly involved in the chelation reaction.

3.3. UV spectroscopy

The UV spectra of SDF and SDF–Mn(II) are provided in Figure 2B. There was no obvious absorption peak between 260 and 280 nm, indicating a negligible amount of protein in the sample (33). It can be seen from the figure that SDF shows a strong absorption peak at 216 nm, while SDF-Mn(II) shows a strong absorption peak at 236 nm. SDF–Mn(II) is a complex comprising several components. Mn^{2+} is an oxidation state transition metal ion with a half-full d orbital (an electron acceptor), and SDF is an organic compound with a conjugated π-electron system (an electron donor). Therefore, SDF–Mn(II) belongs to the spectral ligand-to-metal charge transfer, a process equivalent to the reduction of metals. With the enhancement of the metal cation reduction ability, the wavelength shifts toward the long wave direction, producing a red-shift effect. In turn, with the enhancement of the cation oxidation ability, the color deepens, producing a color-enhancing effect. Because the main chromogenic group present in SDF is the carbonyl group and the co-color group is the hydroxyl group (34), as can be seen from the figure, the absorption of SDF-Mn(II) in the UV region is significantly higher than that of SDF, thus indicating that mainly the carbonyl and hydroxyl groups are involved in the coordination reaction, which results in a change in the UV absorption intensity. It may also be due to the conjugation of several chromogenic groups to produce a new conjugated absorption band.

3.4. XRD analysis

The XRD analysis of SDF and SDF–Mn(II) is reported in Figure 2C. From the figure, we can see that both SDF and

TABLE 1 Relative molecular mass of SDF, SDF-Mn(II).

Index	SDF	SDF–Mn(II)
Mn(Da)	$(2.25 \pm 0.56) \times 10^2$	$(6.05 \pm 1.23) \times 10^2$
Mw(Da)	$(5.776 \pm 1.21) \times 10^3$	$(2.567 \pm 1.57) \times 10^3$
Mw/Mn	25.72 ± 0.23	4.25 ± 0.44

Mn, Number Average Molecular Weight; Mw, Weight Average Molecular Weight.

SDF-Mn(II) show broad diffraction peaks, which are typical for polymers, and the broad peaks indicate low crystallinity in the structure, which may be due to the fact that the extracted SDF is a mixed polysaccharide (35). Which are typical of polymers; moreover, wide peaks indicate a lower crystallinity in the structure, which may be attributed to the fact that the extracted SDF is a mixed polysaccharide. Furthermore, the figure shows that the peak dispersion of SDF was lower than that of SDF–Mn(II) and the calculated crystallinity of SDF was 23.48%, whereas that of SDF–Mn(II) was 33.82%, which may be attributed to the disruption of macromolecular chains after treatment, resulting in the higher crystallinity of SDF–Mn(II) (36, 37). The XRD results were very different, further confirming the formation of SDF–Mn(II).

3.5. Molecular weight analysis

The relative molecular masses of SDF and SDF–Mn(II) are provided in Table 1, from which it can be seen that the Mw of SDF was 5,776, with a dispersion coefficient of 25.72, whereas the Mw of SDF–Mn(II) was 2,567, with a dispersion coefficient of 4.25. The data included in the table revealed that the Mw and dispersion coefficient of SDF were increased and the molecular weight distribution broadened, whereas those of SDF–Mn(II) Mw were significantly reduced, probably because the molecular chains were opened after microwave treatment, resulting in a decrease in the molecular weight of the modified SDF; in contrast, the dispersion coefficient was also significantly reduced, which suggests that the modified SDF system is more homogeneous and simpler in composition (38).

3.6. NMR analysis

The SDF and SDF–Mn(II) NMR ^{1}H spectra are shown in Figure 3. The chemical shifts were affected by the sugar type, bond type, substitution, and modifications. It was previously shown that the chemical shifts are lower than 5.0×10^{-6} for β-configuration pyranosides and higher than 5.0×10^{-6} for α-configuration pyranosides, which can be used to distinguish the types of sugar rings (39). In the range of heteroheaded hydrogen proton signals, SDF exhibited three peaks at 1.830, 2.293, and 3.656×10^{-6}, indicating that it belongs to the group of β-configuration pyranosides (40). In contrast, SDF–Mn(II) had two signal peaks at 3.219 and 4.350×10^{-6}, indicating that the conformation of SDF did not significantly change after treatment and the reduced signal peak of SDF–Mn(II) may be attributed to the shortening of the ligand relaxation time that occurs upon binding of SDF to Mn^{2+}; moreover, the large width of the signal range precluded the detection of the signal around paramagnetic Mn^{2+}, thus forming a high-spin blind region with Mn^{2+} as the core (41).

The SDF and SDF–Mn(II) NMR ^{13}C spectra are provided in Figure 4. The signal detected at 60.208×10^{-6} was attributed to the C_6 glycosidic bond. The spectrum of SDF–Mn(II) became more complex because the carbon directly attached to the electron-absorbing group shifted to a lower field position, whereas the carbon indirectly attached to the electron-absorbing group shifted to a higher field position (42). Moreover, the signal peak of SDF–Mn(II) detected at 60.208×10^{-6} disappeared; this may be attributed to the highest -OH activity at the C_6 position, which was replaced by the Mn^{2+} group. The C_1 signal splits if the -OH on C_2 is substituted, and this splitting correlates well with the degree of substitution on the C_2 atom (43). In Figure 4B, At $90–100 \times 10^{-6}$, the signal exhibited multiple splits, which may have been caused by the substitution of the hydroxyl group on C_2 by the Mn^{2+} group (44), because the -OH activity at the C_2 position was second only to that at C_6.

3.7. Thermal characterization

Thermal stability plays an important role in food industry applications (45); therefore, the thermal properties of SDF before and after modification were characterized using TGA and DSC. Figure 5A shows that the decomposition temperature of SDF is 161°C, while the decomposition temperature of SDF-Mn(II) is 162°C, The two decomposition temperatures are similar, so the ease of dehydration is similar for both When the temperature increased from the decomposition temperature to 500°C, the weights of both samples started to significantly decrease because of the violent thermal degradation of the galacturonic acid chains in the samples, followed by decarboxylation of the acidic side groups in the rings and the carbon, which eventually produced different gaseous products, to form solid carbon (46, 47). Furthermore, the final residual mass of SDF (37.36%) was lower than that of SDF–Mn(II) (43.35%), suggesting that the thermal stability of SDF–Mn(II) is stronger than that of SDF. The curves of DSC presented in Figure 5B demonstrated that SDF had two exothermic peaks, at 105°C and 500°C, whereas SDF–Mn(II) exhibited one exothermic peak at 102°C. The appearance of two exothermic peaks for SDF may be related to the inhomogeneity of the composition, with SDF–Mn(II) becoming one peak, which suggests that the composition of SDF–Mn(II) is more homogeneous, in agreement with the results of the relative molecular mass analysis.

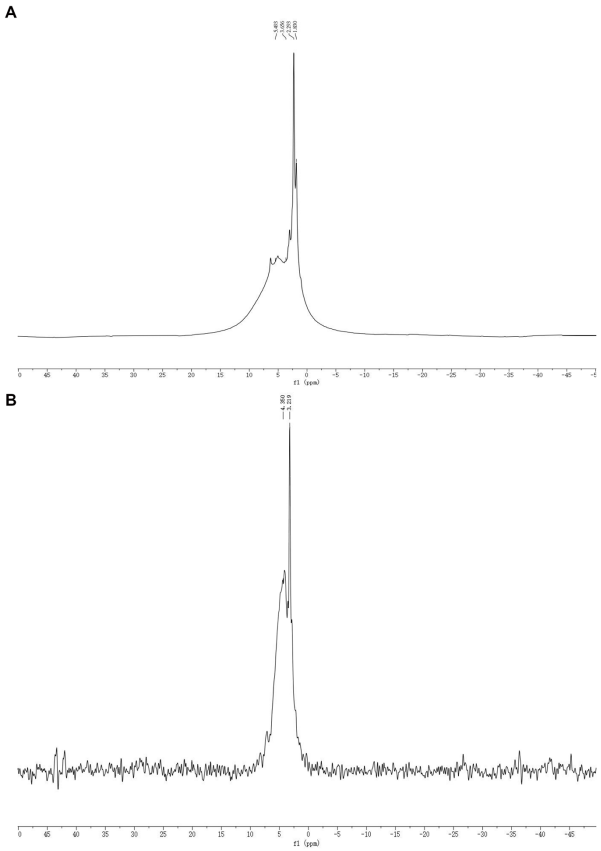

FIGURE 3
SDF **(A)**, SDF-Mn(II) **(B)** NMR ^{1}H diagram.

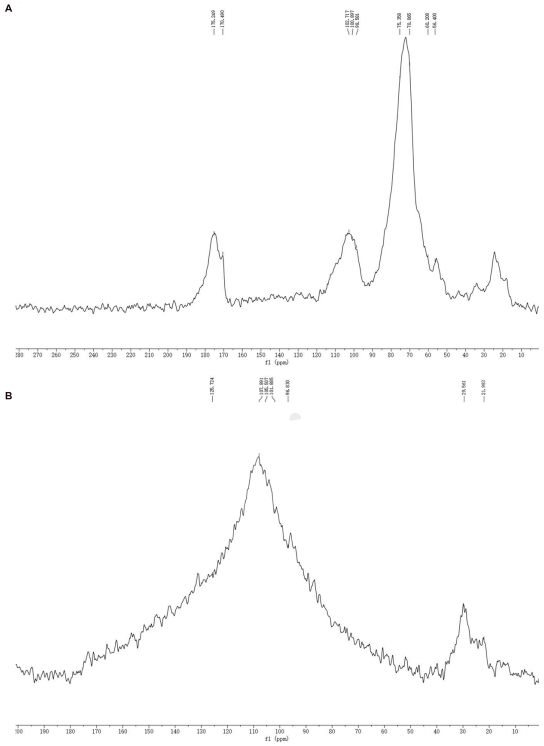

FIGURE 4
SDF **(A)**, SDF-Mn(II) **(B)** NMR ^{13}C diagram.

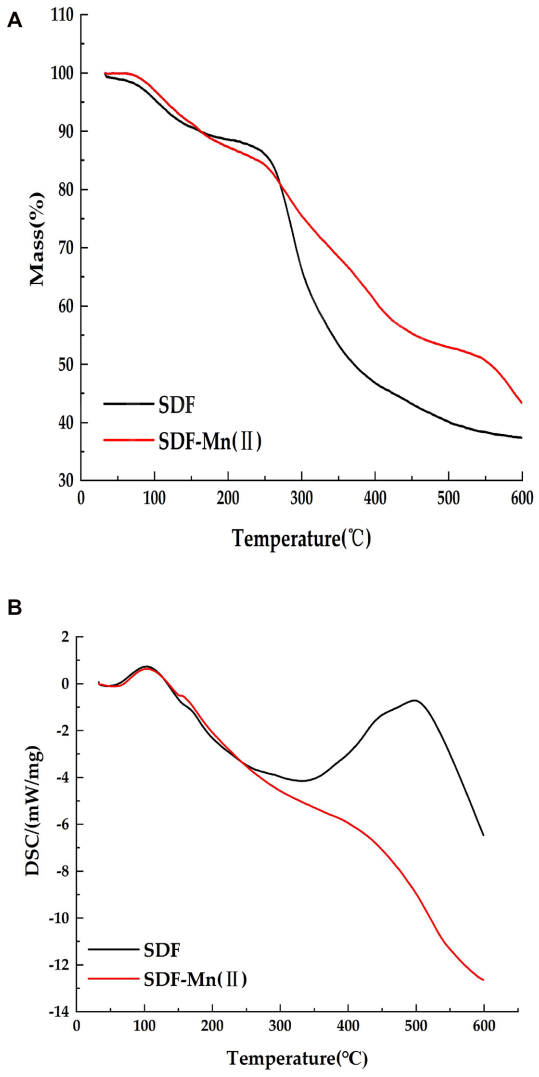

FIGURE 5
Thermal characteristics analysis of SDF, SDF–Mn(II). **(A)** The mass loss of SDF and SDF-Mn (II). **(B)** The changes in SDF and SDF-Mn (II) DSC.

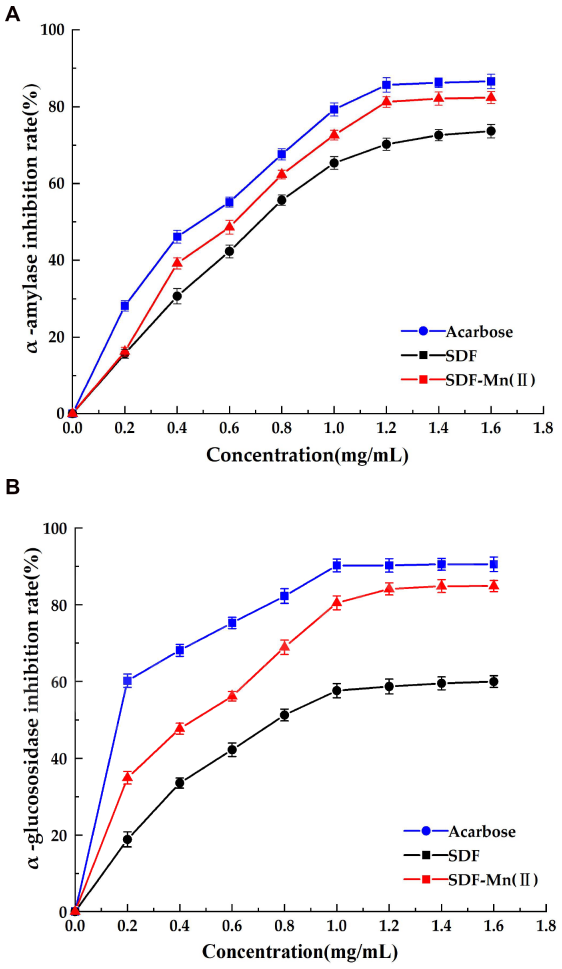

FIGURE 6
Effect of SDF and SDF-Mn(II) inhibition on α-amylase **(A)** and α-glucosidase **(B)**.

3.8. Inhibitory effect of SDF and SDF–Mn(II) on enzymatic activity *in vitro*

SDF has inhibitory activity against sugar hydrolases, including α-amylase and α-glucosidase; thus, it has the potential to replace commercial hypoglycemic drugs, such as acarbose and voglibose (48). The inhibition of α-amylase by SDF occurs via binding interactions between SDF and the active site of the enzymes as a result of hydrogen bonding and hydrophobic forces (44). The structure of SDF determines, to a large extent, its binding affinity to the enzymes. Figure 6 shows the inhibitory activities of SDF and SDF–Mn(II) toward α-amylase and α-glucosidase. Figure 6A shows the rate of inhibition of α-amylase, which gradually increases with increasing sample concentration (0–1.8 mg/ml); moreover, the inhibition rate of SDF–Mn(II) was stronger than that of SDF. When the sample concentration was greater than 1.2 mg/ml, the inhibitory effect no longer linearly increased, with the IC_{50} values of SDF and SDF–Mn(II) being 0.87 and 0.729 mg/ml, respectively. Figure 6B shows the rate of inhibition of α-glucosidase, which was similar to the results reported for α-amylase, with the SDF and SDF–Mn(II) IC_{50} values being 1.025 and 0.583 mg/ml, respectively. The figure demonstrated that there was a significant increase in the inhibitory rate of SDF–Mn(II) for both enzymes (49), which may be attributed to the microwave treatment, as it reduced the molecular weight of SDF–Mn(II) and facilitated binding to the active site of the enzyme, leading to an enhanced inhibition (50, 51); alternatively, the manganese element was introduced to denature the enzyme, leading to a decrease in enzymatic activity. The higher inhibitory activity of SDF–Mn(II) toward α-amylase and α-glucosidase may delay the absorption of dietary carbohydrates, which may contribute to the control of postprandial blood glucose levels.

4. Conclusion

This study reported the structural characterization and enzyme activity inhibition analysis of SDF and SDF–Mn(II). The experiments showed that SDF–Mn(II) exhibited a porous surface structure with a more obvious fragmentation trend, without obvious changes in the

basic skeleton, as well as red-shifting and color-enhancing effects in the UV characteristic peaks, increased crystallinity, and decreased relative molecular mass. NMR revealed that SDF-Mn(II) mainly underwent a substitution reaction on C_6. SDF-Mn(II) has better structural and thermal properties and has better inhibition of *in vitro* digestive enzymes, providing a good theoretical basis for further studies of SDF-Mn(II).

Data availability statement

The original contributions presented in the study are included in the article/supplementary material, further inquiries can be directed to the corresponding author.

Author contributions

WW and YuW: data curation. YiW, WW, YuW, and JJ: formal analysis. LC: funding acquisition. YiW and WW: investigation, methodology, and writing—original draft. YiW and JJ: validation. YiW, XH, MW, and LC: writing—review and editing. All authors contributed to the article and approved the submitted version.

Funding

This work was supported by the Technology Major Program of Heilongjiang Province of Department of Science and Technology (2021ZX12B06), the National Key R&D Program of China (2021YFD2100902).

Conflict of interest

The authors declare that the research was conducted in the absence of any commercial or financial relationships that could be construed as a potential conflict of interest.

Publisher's note

All claims expressed in this article are solely those of the authors and do not necessarily represent those of their affiliated organizations, or those of the publisher, the editors and the reviewers. Any product that may be evaluated in this article, or claim that may be made by its manufacturer, is not guaranteed or endorsed by the publisher.

References

1. Sánchez-Zapata E, Fernández-López J, Pérez-Alvarez JA. Tiger nut(*Cyperus esculentus*)commercialization: health aspects, composition, properties, and food applications. *Compr Rev Food Sci Food Saf*. (2012) 11:366–77. doi: 10.1111/j.1541-4337.2012.00190.x

2. Roselló-Soto E, Poojary MM, Barba FJ, Lorenzo JM, Mañes J, Moltó JC. Tiger nut and its by-products valorization: from extraction of oil and valuable compounds to development of new healthy products. *Innov Food Sci Emerg Technol*. (2018) 45:306–12. doi: 10.1016/j.ifset.2017.11.016

3. Wang RY, Wang XS, Xiang H. A multi-purpose novel oil crop——Cyperus beans. *Chinese oil*. (2019) 44:1–4. doi: 10.3390/plants11091127

4. Li YD. *Study on hypoglycemic effect of a compound seaweed dietary fiber*. Huaqiao University (2014).

5. Wang YF, Yang XH, Cao JH, Qu CF, Zhang LP, Liao JL. Progress in the regulation of dietary fiber regulating blood glucose in type 2 diabetes. *Food Mach*. (2020) 36:6–11+17. doi: 10.13652/j.issn.1003-5788.2020.10.002

6. Qi D, Jing L, Qing L, Kangcheng C, Zhenfang L, Yuefei S, et al. Interaction of occupational manganese exposure and alcohol drinking aggravates the increase of liver enzyme concentrations from a cross-sectional study in China. *Environ Health*. (2013) 12:1–6. doi: 10.1186/1476-069X-12-30

7. Aschner JL, Aschner M. Nutritional aspects of manganese homeostasis. *Mol Asp Med*. (2005) 26:353–62. doi: 10.1016/j.mam.2005.07.003

8. Soh-Hyun L, Jouihan Hani A, Cooksey Robert C, Deborah J, Hyung KJ, Dennis WR, et al. Manganese supplementation protects against diet-induced diabetes in wild type mice by enhancing insulin secretion. *Endocrinology*. (2013) 154:1029–38. doi: 10.1210/en.2012-1445

9. Kincaid RL, Chew BP, Cronrath JD. Zinc oxide and amino acids as sources of dietary zinc for calves: effects on uptake and immunity. *J Dairy Sci*. (1997) 80:1381–8. doi: 10.3168/jds.S0022-0302(97)76067-3

10. Zhou R, Liu H, Hou G, Ju L, Liu C. Multi-spectral and thermodynamic analysis of the interaction mechanism between Cu^{2+} and α-amylase and impact on sludge hydrolysis. *Environ Sci Pollut Res*. (2017) 24:9428–36. doi: 10.1007/s11356-017-8570-z

11. Chhatbar MU, Meena R, Prasad K, Chejara DR, Siddhanta AK. Microwave-induced facile synthesis of water-soluble fluorogenic alginic acid derivatives. *Carbohydr Res*. (2011) 346:527–33. doi: 10.1016/j.carres.2011.01.002

12. Azad SB, Ansari P, Azam S, Hossain SM, Shahid MI-B, Hasan M, et al. Anti-hyperglycaemic activity of *Moringa oleifera* is partly mediated by carbohydrase inhibition and glucose-fibre binding. *Biosci Rep*. (2017) 37:BSR20170059. doi: 10.1042/BSR20170059

13. Carmen C, Reyes A, Rafael G. Beneficial effects of green tea--a review. *J Am Coll Nutr*. (2006) 25:79–99. doi: 10.1080/07315724.2006.10719518

14. van de Laar FA, Lucassen PL, Akkermans RP, van de Lisdonk EH, Rutten GE, van Weel C. α-Glucosidase inhibitors for patients with type 2 diabetes: results from a Cochrane systematic review and meta-analysis. *Diabetes Care*. (2005) 28:154–63. doi: 10.2337/diacare.28.1.154

15. Yang CY, Yen YY, Hung KC, Hsu SW, Lan SJ, Lin HC. Inhibitory effects of pu-erh tea on alpha glucosidase and alpha amylase: a systemic review. *Nutr Diabetes*. (2019) 9:1–6. doi: 10.1038/s41387-019-0092-y

16. Shen M, Kang ZY, Ge YF, Xia TT, Ning DF, Kou F. Research of enzymatic modification on the extraction and properties of soluble dietary Fiber from black bean hulls. *Nat Prod Res Dev*. (2018) 30:1046–1053+1084. doi: 10.16333/j.1001-6880.2018.6.021

17. Xie JH. *Molecular modification of polysaccharide from Cyclocarya paliurrus and their biological activity*. Nanchang University (2014).

18. Xu SP. *Study on the microwave solid state synthesis and antibacterial activities of cu, co, Ni, Zn, Mn complexes*. China Mining University (2013).

19. Wang J, Sun H M, Gu E, et al. Determination of manganese content in organic matter including feed and feed additives by spectrophotometry. 2010 Shandong Feed Science and Technology Exchange Conference Proceedings. (2010) 49–51.

20. Gan JP, Huang ZY, Yu Q, Peng G, Chen Y, Xie J, et al. Microwave assisted extraction with three modifications on structural and functional properties of soluble dietary fibers from grapefruit peel. *Food Hydrocoll*. (2020) 101:105549. doi: 10.1016/j.foodhyd.2019.105549

21. Cong Z, Mao H, Ri H, Hongman C. Preparation of a *Momordica charantia* L. polysaccharide-chromium (III) complex and its anti-hyperglycemic activity in mice with streptozotocin-induced diabetes. *Int J Biol Macromol*. (2019) 122:619–27. doi: 10.1016/j.ijbiomac.2018.10.200

22. Zhao ST, Wang WH, Quan ZG, Wang J, Liu DZ, Wang YF, et al. Preparation, structure characterization and inhibition kinetics of mung bean RS4·se(IV). *Food Sci*. (2022) 43:53–62. doi: 10.7506/spkx1002-6630-20210907-089

23. González M, Vernon-Carter EJ, Alvarez-Ramirez J, Carrera-Tarela Y. Effects of dry heat treatment temperature on the structure of wheat flour and starch *in vitro* digestibility of bread. *Int J Biol Macromol*. (2021) 166:1439–47. doi: 10.1016/j.ijbiomac.2020.11.023

24. Li M, Ndiaye C, Corbin S, Foegeding EA, Ferruzzi MG. Starch-phenolic complexes are built on physical CH-π interactions and can persist after hydrothermal treatments altering hydrodynamic radius and digestibility of model starch-based foods. *Food Chem*. (2020) 308:125577. doi: 10.1016/j.foodchem.2019.125577

25. Zhao M, Bai J, Bu X, Yin Y, Wang L, Yang Y, et al. Characterization of selenized polysaccharides from *Ribes nigrum* L. and its inhibitory effects on α-amylase and α-glucosidase. *Carbohydr Polym*. (2021) 259:117729. doi: 10.1016/j.carbpol.2021.117729

26. Wang H, Wang J, Liu YJ, Ji Y, Guo Y, Zhao J. Interaction mechanism of carnosic acid against glycosidase (α-amylase and α-glucosidase). *Int J Biol Macromol*. (2019) 138:846–53. doi: 10.1016/j.ijbiomac.2019.07.179

27. Sangilimuthu AY, Sivaraman T, Chandrasekaran R, Sundaram KM, Ekambaram G. Screening chemical inhibitors for alpha-amylase from leaves extracts of *Murraya koenigii* (Linn.) and *Aegle marmelos* L. *J Complement Integr Med*. (2020) 18:51–7. doi: 10.1515/jcim-2019-0345

28. Wang J, Yang W, Wang J, Wang X, Wu F, Yao J, et al. Regioselective sulfation of Artemisia sphaerocephala polysaccharide: characterization of chemical structure. *Carbohydr Polym*. (2015) 133:320–7. doi: 10.1016/j.carbpol.2015.07.030

29. Meidong G, Fang H, Gao Y, Tan S, Yuge N, Liangli Y(L). Characterization of enzymatic modified soluble dietary fiber from tomato peels with high release of lycopene. *Food Hydrocoll*. (2020) 99:105321. doi: 10.1016/j.foodhyd.2019.105321

30. Ren Y, Zheng G, You L, Wen L, Li C, Fu X, et al. Structural characterization and macrophage immunomodulatory activity of a polysaccharide isolated from *Gracilaria lemaneiformis*. *J Funct Foods*. (2017) 33:286–96. doi: 10.1016/j.jff.2017.03.062

31. Zhu M, Jinggang M, ChangSheng H, Haiping X, Ning M, Caijiao W. Extraction, characterization of polysaccharides from lycium barbarum and its effect on bone gene expression in rats. *Carbohydr Polym*. (2010) 80:672–6. doi: 10.1016/j.carbpol.2009.11.038

32. Ma X, Li C, Qi W, Li X, Wang S, Cao X, et al. Protective effect of extracellular polysaccharides from Grifola frondosa mycelium on CCl4-injured liver *in vitro*. *Bioact Carbohydr Diet Fibre*. (2015) 6:7–14. doi: 10.1016/j.bcdf.2015.06.001

33. Cao Y-Y, Ji Y-H, Liao A-M, Huang J-H, Thakur K, Li X-L, et al. Effects of sulfated, phosphorylated and carboxymethylated modifications on the antioxidant activities in-vitro of polysaccharides sequentially extracted from Amana edulis. *Int J Biol Macromol*. (2020) 146:887–96. doi: 10.1016/j.ijbiomac.2019.09.211

34. Wang J, Chen H, Wang Y, Xing L. Synthesis and characterization of a new Inonotus obliquus polysaccharide-iron (III) complex. *Int J Biol Macromol*. (2015) 75:210–7. doi: 10.1016/j.ijbiomac.2015.01.041

35. Kianpour S, Ebrahiminezhad A, Mohkam M, Tamaddon AM, Dehshahri A, Heidari R, et al. Physicochemical and biological characteristics of the nanostructured polysaccharide-iron hydrogel produced by microorganism *Klebsiella oxytoca*. *J Basic Microbiol*. (2017) 57:132–40. doi: 10.1002/jobm.201600417

36. Wang H. *Synthesis study of jujube polysaccharide iron (III) complex*. Northwest University (2009).

37. Jeddou KB, Chaari F, Maktouf S, Nouri-Ellouz O, Helbert CB, Ghorbel RE. Structural, functional, and antioxidant properties of water-soluble polysaccharides from potatoes peels. *Food Chem*. (2016) 205:97–105. doi: 10.1016/j.foodchem.2016.02.108

38. Mokni Ghribi A, Sila A, Maklouf Gafsi I, Blecker C, Danthine S, Attia H, et al. Structural, functional, and ACE inhibitory properties of water-soluble polysaccharides from chickpea flours. *Int J Biol Macromol*. (2015) 75:276–82. doi: 10.1016/j.ijbiomac.2015.01.037

39. Wlga B, Min C, Wlp A, Qing Z, Jia-Xin X, Yi-Chen L, et al. Hypoglycemic and hypolipidemic mechanism of organic chromium derived from chelation of Grifola frondosa polysaccharide-chromium (III) and its modulation of intestinal microflora in high fat-diet and STZ-induced diabetic mice. *Int J Biol Macromol*. (2020) 145:1208–18. doi: 10.1016/j.ijbiomac.2019.09.206

40. Liu W, Lv X, Huang W, Yao W, Gao X. Characterization and hypoglycemic effect of a neutral polysaccharide extracted from the residue of *Codonopsis Pilosula*. *Carbohydr Polym*. (2018) 197:215–26. doi: 10.1016/j.carbpol.2018.05.067

41. Zhu M, Huang R, Wen P, Song Y, He B, Tan J, et al. Structural characterization and immunological activity of pectin polysaccharide from kiwano (*Cucumis metuliferus*) peels. *Carbohydr Polym*. (2021) 254:117371. doi: 10.1016/j.carbpol.2020.117371

42. Li L, Xu JX, Cao YJ, Lin YC, Guo WL, Liu JY, et al. Preparation of *Ganoderma lucidum* polysaccharide-chromium (III) complex and its hypoglycemic and hypolipidemic activities in high-fat and high-fructose diet-induced pre-diabetic mice. *Int J Biol Macromol*. (2019) 140:782–93. doi: 10.1016/j.ijbiomac.2019.08.072

43. Richter A, Wagenknecht W. Synthesis of amylose acetates and amylose sulfates with high structural uniformity. *Carbohydr Res*. (2003) 338:1397–401. doi: 10.1016/S0008-6215(03)00179-4

44. Miao M, Jiang B, Jiang H, Zhang T, Li X. Interaction mechanism between green tea extract and human α-amylase for reducing starch digestion. *Food Chem*. (2015) 186:20–5. doi: 10.1016/j.foodchem.2015.02.049

45. Yang Y, Lei Z, Zhao M, Wu C, Wang L, Xu Y. Microwave-assisted extraction of an acidic polysaccharide from *Ribes nigrum* L.: structural characteristics and biological activities. *Ind Crop Prod*. (2020) 147:112249. doi: 10.1016/j.indcrop.2020.112249

46. Gao P, Bian J, Xu S, Liu C, Sun Y, Zhang G, et al. Structural features, selenization modification, antioxidant and anti-tumor effects of polysaccharides from alfalfa roots. *Int J Biol Macromol*. (2020) 149:207–14. doi: 10.1016/j.ijbiomac.2020.01.239

47. Wang W, Ma X, Jiang P, Hu L, Zhi Z, Chen J, et al. Characterization of pectin from grapefruit peel: a comparison of ultrasound-assisted and conventional heating extractions. *Food Hydrocoll*. (2016) 61:730–9. doi: 10.1016/j.foodhyd.2016.06.019

48. Zheng Y, Liu S, Xie J, Chen Y, Dong R, Zhang X, et al. Antioxidant, α-amylase and α-glucosidase inhibitory activities of bound polyphenols extracted from mung bean skin dietary fiber. *Lwt*. (2020) 132:109943. doi: 10.1016/j.lwt.2020.109943

49. Wang ZL, Wang X, Han Y, et al. Preparation of sweet corn cob and its inhibition on amylase. *Packag Eng*. (2021) 42:33–41. doi: 10.19554/j.cnki.1001-3563.2021.21.005

50. Xiao H, Fu X, Cao C, Chao L, Chun C, Qiang H, et al. Sulfated modification, characterization, antioxidant and hypoglycemic activities of polysaccharides from *Sargassum pallidum*. *Int J Biol Macromol*. (2018) 121:407–14. doi: 10.1016/j.ijbiomac.2018.09.197

51. Xu Y, Guo Y, Gao Y, Niu X, Wang L, Li X, et al. Seperation, characterization and inhibition on α-glucosidase, α-amylase and glycation of a polysaccharide from blackcurrant fruits. *Lwt*. (2018) 93:16–23. doi: 10.1016/j.lwt.2018.03.023

Frontiers in Nutrition

Explores what and how we eat in the context of health, sustainability and 21st century food science

A multidisciplinary journal that integrates research on dietary behavior, agronomy and 21st century food science with a focus on human health.

Discover the latest Research Topics

See more →

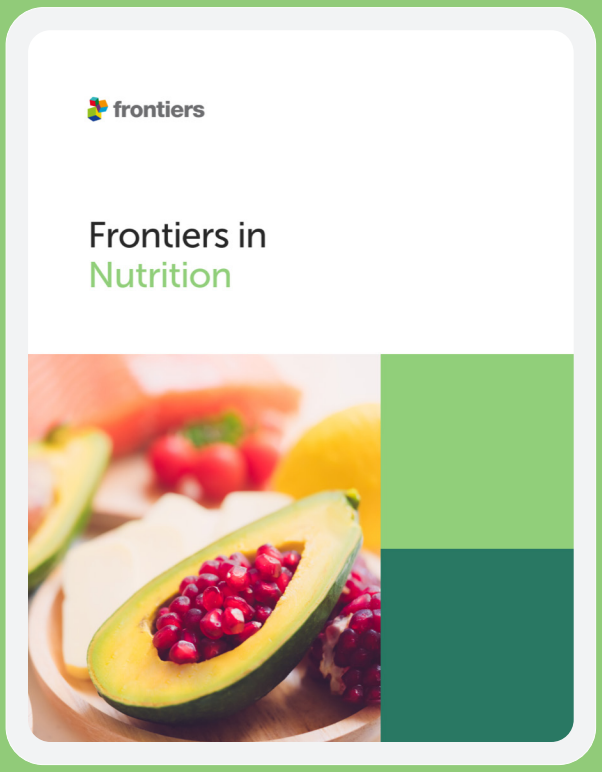

Frontiers

Avenue du Tribunal-Fédéral 34
1005 Lausanne, Switzerland
frontiersin.org

Contact us

+41 (0)21 510 17 00
frontiersin.org/about/contact